Technische Universität München

Fakultät für Chemie

Design of Supramolecular Nanocatalysts for the Biphasic Epoxidation of Olefins

Fabian Schmidt

Vollständiger Abdruck der von der Fakultät für Chemie der Technischen Universität München zur Erlangung des akademischen Grades eines

Doktors der Naturwissenschaften (Dr. rer. nat.)

genehmigten Dissertation.

Vorsitzender:	Prof. Dr. Dr. h.c. Bernhard Rieger
Prüfer der Dissertation:	1. Prof. Dr. Dr. h.c. Roland A. Fischer
	2. Prof. Dr.-Ing. Andreas Jess

Die Dissertation wurde am 12.01.2022 bei der Technischen Universität München eingereicht und durch die Fakultät für Chemie am 10.03.2022 angenommen.

Die vorliegende Arbeit wurde am Lehrstuhl für Anorganische und Metallorganische Chemie der Technischen Universität München im Zeitraum von September 2017 bis Dezember 2021 erstellt.

„Die bloße Empirie erschöpft und wiederholt sich,
die Wissenschaft führt zu einem stetigen Fortschritt,
und ihr gehört die Zukunft“

− Max von Pettenkofer

Bayerischer Chemiker und Deutschlands erster Ordinarius für Hygiene

Danksagung

Mein besonderer Dank gilt meinem Doktorvater

Prof. Dr. Roland A. Fischer

für die herzliche und bereitwillige Aufnahme in Ihrem Lehrstuhl und die Betreuung im Zuge des Habilitationsverfahrens von Dr. Mirza Cokoja. Ich bin Ihnen für dieses hochprofessionelle und angenehme Arbeitsumfeld sowie für die großartige Lehrstuhlleitung äußert dankbar.

Darüber hinaus gebührt mein herzlichster Dank meinem Betreuer

Dr. Mirza Cokoja

für die großartige Möglichkeit, Doktorand am AMC-Lehrstuhl und Teil des Teams „Mizellare Katalyse“ sein zu dürfen, die ständigen Freiheiten, die Du mir eingeräumt hast und für das Vertrauen, welches Du mir stets entgegengebracht hast.

Vielen Dank für die zahlreichen Gespräche, Anekdoten und Ratschläge, die mich im Leben sicherlich nicht nur fachlich weiterbringen werden. Außerdem danke ich Dir für das freundschaftliche Verhältnis, das der Betreuung stets zugrunde lag.

Des Weiteren bedanke ich mich bei meinem Kooperationspartner

Prof. Dr.-Ing. Andreas Jess

für die Übernahme der Mentorenschaft meines Promotionsvorhabens sowie die herzlichen Einladungen an den Lehrstuhl für chemische Verfahrenstechnik der Universität Bayreuth im Rahmen des Kooperationsprojektes „Mizellare Katalyse“. In diesem Zuge gilt mein weiterer Dank den weiteren “Bayreuthern“ **Dr. Wolfgang Korth** und **Bastian Zehner** für die äußert erfolgreiche Bearbeitung des DFG-Projekts, die exzellente Zusammenarbeit und Kommunikation sowie die äußert produktiven Projekttreffen, die mir sicherlich lange in Erinnerung bleiben werden und vermutlich weder menschlich noch fachlich zu toppen sind.

Für die bereitwillige Übernahme des Prüfungsvorsitzes danke ich **Prof. Dr. Bernhard Rieger**.

For the outstanding advanced spectroscopy lesson, the professional advice and the plurality of spectroscopic measurements and evaluations, I am thankful to

Prof. Dr. János Mink

It was a great pleasure to learn from your skills and expertise! Without you, we would never have been able to identify those mechanistic pathways. I am deeply grateful to you for your efforts and discoveries!

Im Besonderen danke ich

Dr. Markus Drees

da Du stets ein offenes Ohr für Fragen aller Art -egal ob fachlich, persönlich oder administrativ- hast und über die Jahre Dein Beitrag durch die Vielzahl an DFT Rechnungen für viele meiner Teilprojekte maßgeblich zur Publikation der Ergebnisse beigetragen hat.

Dr. Gabriele Raudaschl-Sieber, Dr. Christan Gemel, **Dr. Gregor Kieslich** und **Dr. Alexander Pöthig** danke ich für die vielen netten Unterhaltungen, die wissenschaftlichen Ratschläge und dass Ihr den Doktoranden immer mit Rat und Tat zur Seite steht.

Dass der Lehrstuhl so hervorragend rund läuft, ist unter anderem dem Sekretariat mit den Beschäftigten **Dr. Dana Weiß** und **Martin Schellerer** zu verdanken, die stets verfügbar sind und bei allen Angelegenheiten zur Seite stehen. Insbesondere Martin danke ich für die zahlreichen und vielseitigen Hilfen zur Bewältigung der Hochschulbürokratie bei Verträgen, Dienstreisen und Auslagen.

Dr. Eliza Gemel danke ich für die Organisation der CRC-Zentralanalytik im 3. Stock und der NMR-Spektroskopie, die uns oft zu langwierigen, aber netten und produktiven Gesprächen zusammenbrachte. Für das mir entgegengebrachte Vertrauen in der Wartung und Zuständigkeit für diverse Geräte bin ich sehr dankbar.

Dr. Carsten Peters bin ich dankbar für die vielen aussagekräftigen Cryo-TEM Messungen, die uns viele gemeinsame Stunden am Mikroskop in „Kälte und Finsternis“ beschert haben.

Maria Matthews danke ich für die Einweisung und Hilfe am „Spezialexperimente“-NMR und im Besonderen für die Hilfe beim Optimieren und Einrichten der Wolfram-Experimente. Gleicher Dank gilt **Jürgen Kudermann** für die außerordentlich gute Wartung und Organisation der CRC-Analytik im 4. Stock und die akribische Unterweisung in die weite Welt der Gaschromatographie. **Ulrike Ammari** vom mikroanalytischen Labor des CRCs danke ich für die vielen elementaranalytischen Messungen, die Ratschläge zur Probenvorbereitung sowie die ständige Bereitschaft und Freundlichkeit.

Des Weiteren danke ich meinen fleißigen Forschungspraktikanten **Lilla Koser**, **Melanie Strauss**, **Antonia Seitz, Kathrin Kollmannsberger, Karina Hemmer** und **Florian Tschernuth** für die unglaublich vielen und beeindruckenden Ergebnisse, die ihr produziert habt. Euch zu betreuen hat mir unglaublich viel Freude bereitet und ich hoffe ihr konntet einiges für euren weiteren Bildungsweg mitnehmen.

Ich danke dem gesamten **AMC-Lehrstuhl** für die großartige Atmosphäre, die Offenheit in Angelegenheiten privater und fachlicher Natur sowie die den vielen Gesprächen, sei es am Mittagstisch oder am späten Abend.

Insbesondere danke ich meinen Freunden von der „Neufahrn-Connection“ **Sebi, Pati, Karina, Margit, Silva, Kathi und Alex** für die vielen gemeinsamen Unternehmungen. Ihr habt maßgeblich dazu beigetragen, den Uni-Alltag abwechslungsreicher und locker zu gestalten.

Auch bei meinen langjährigen Studiums- und Promotions-Begleitern und „Althasen“ **Lena, Stefan, Tom und Marc** möchte ich mich für die vielen Kaffeerunden, die ständige Hilfsbereitschaft und die fachliche Unterstützung im Labor-Alltag bedanken. Egal wohin es euch auch verschlagen wird, ich hoffe, dass diese jahrelange Freundschaft weiterhin Bestand haben wird.

Zu guter Letzt danke ich **meinen Eltern** für den Rückhalt und dass sie mir stets alle Freiheiten gelassen haben.

Abstract

In this project, supramolecular catalysts are developed to investigate the application of nano-sized aggregates in biphasic reactions with special regard to catalyst recycling. The epoxidation of hydrophobic olefins using hydrogen peroxide as environmentally benign oxidant is the ideal object of investigation since the role of the catalyst is multifunctional: it should solubilize the substrate in water and operate in the aqueous phase without itself being soluble in the organic phase for the sake of recyclability and the activation of hydrogen peroxide.

By a targeted design of the catalyst structure, the phase behavior as well as the aggregation characteristics are optimized to achieve a high substrate solubility in water and allow for a facile catalyst separation from the organic product. Ionic catalysts with hydrophobic motifs show a pronounced interaction with hydrogen peroxide as well as the substrate molecule, both essential premises for epoxidation in water using hydrogen peroxide. The choice of surface-active imidazolium ionic liquids is based on their ability to form aggregates in water, their widely tuneable polarity, and their stability under oxidative conditions. The study of the aggregation behavior and the olefin solubilization of the catalyst is important to understand the crucial factors of substrate transport into the aqueous phase. It can be shown that the substitution pattern of the imidazolium cation is a significant parameter for the formation of a micellar system and the interaction with the substrate molecules. The respective counterions are selected to be hydrophilic oxo-anions, which serve for H_2O_2 activation. The dynamic immobilization of these anions on the micellar surface by electrostatic forces leads to unpredicted reactivities, hence allowing for an investigation of promising, metal-based as well as metal-free oxo-anions with the general formula $[EO_x]^{z-}$ for hydrogen peroxide activation. So far, the expensive perrhenate anion has been shown to be able to activate hydrogen peroxide in micellar systems for olefin epoxidation. Hence, this concept is transferred to more abundant anions within this work.

Micellar imidazolium tungstates show to be highly active in olefin epoxidation in the aqueous phase. Mechanistic studies reveal that peroxo-tungstates are formed upon contact with hydrogen peroxide which effectively epoxidize the substrate solubilized inside the micelles. In contrast, metal-free imidazolium nitrates activate hydrogen peroxide according to the ‘outer-sphere’ hydrogen bond mechanism in analogy to the perrhenate anion. Hence, the central nitrogen atom is not actively involved in bond formation as elaborate mechanistic studies suggest. The nitrate anion activates hydrogen peroxide in micellar systems exclusively, while homogeneously dissolved nitrate salts do not interact with hydrogen peroxide sufficiently, which is due to the partial loss of the hydration shell of the nitrate by the hydrophobic effect of the micelle.

Depending on the requirements, supramolecular concepts can be exploited to change the phase of reaction. The sulfate anion $[SO_4]^{2-}$ is not active in micellar epoxidation due to the comparably stronger hydratization. Thus, an inverse solubilization approach, the transfer of the hydrophilic sulfate into the organic phase is investigated. It could be shown that tailored organic receptor molecules form supramolecular ion pairs with the ability to effectively solubilize the anions in the organic phase. The formed peroxomonosulfate is shown to be the active species which unfolds its reactivity towards the olefin in the organic phase.

In general, metal-oxo-based catalysts are highly reactive and allow for a full conversion of the olefin within a few minutes to hours. The lower activity of the metal-free derivatives can be compensated by operation in a continuous process as the micellar catalysts are easily separated from the organic phase and perfectly stable. This is highly attractive for the production of epoxides, which can be withdrawn purely from the process, and is supported by the great scalability of catalyst synthesis and application. The effect of the accumulating water is tackled by a further catalyst optimization, which involves a structural solubility-switch for catalyst precipitation, triggered by the external stimulus temperature. The introduction of a polyfluorinated substituent, provided by the great functionalizability of the imidazolium cation, results in an increased cation interaction, limiting the catalyst solubility in the cold aqueous phase below reaction temperature while excluding a solubility in the organic phase.

In conclusion, biphasic supramolecular catalysis using environmentally benign hydrogen peroxide as oxidant can be regarded as both an ecologically and economically promising approach for the epoxidation of hydrophobic olefins. This is further supported by the choice of water as solvent, the great recyclability of the catalysts, and the facile catalyst synthesis.

Zusammenfassung

In dieser Arbeit werden supramolekulare Katalysatoren entwickelt und optimiert, um den Einsatz von nanoskaligen Aggregaten in Zweiphasenkatalysen mit besonderem Fokus auf Katalysatorrecycling zu untersuchen. Aufgrund der Multifunktionalität der Katalysatoren erweist sich die Epoxidation von hydrophoben Olefinen als das ideale Untersuchungsfeld, da einerseits eine gute Solubilisierung des Substrats in der wässrigen Phase, ohne im Hinblick auf die Rezyklierbarkeit selbst in der Organik löslich zu sein, als auch die Aktivierung des Wasserstoffperoxids gefordert wird.

Durch gezieltes Design der Katalysatorstruktur können sowohl das Phasen- als auch das Aggregationsverhalten in Lösung für eine hohe Solubilisierungsrate gesteuert und eine effiziente Katalysatorabtrennung erreicht werden. Besonders ionische Katalysatoren mit hydrophoben Strukturmerkmalen sind aufgrund der starken Wechselwirkung mit Wasserstoffperoxid als auch mit dem Substrat für die katalytische Zweiphasenepoxidation geeignet. Die Wahl von grenzflächenaktiven Imidazolium-basierten ionischen Flüssigkeiten ergibt sich aus deren Fähigkeit, Aggregate in wässrigen Lösungen zu bilden, deren synthetischen Zugang zur Anpassung der Polarität, sowie deren hervorragenden Stabilität unter oxidativen Bedingungen. Die Untersuchung des Aggregationsverhaltens und der Substratsolubilisierung ist entscheidend für das Verständnis der zugrundeliegenden Transportphänomene. Es kann gezeigt werden, dass das Substitutionsmuster des Imidazoliumkations ausschlaggebend für die Bildung von Mizellen und die Substratinteraktion ist. Die entsprechenden Gegenionen sind hydrophile Oxo-Anionen, welche für die Aktivierung des Wasserstoffperoxids zuständig sind. Die dynamische Immobilisierung der Anionen auf der kationischen Mizelloberfläche durch elektrostatische Wechselwirkung führt zu ungeahnten Reaktivitäten, welche in einem klassischen homogenen System nicht erreicht werden. Bisher wurde das teure Perrhenat für die mizellare Aktivierung von Wasserstoffperoxid untersucht, weswegen das Ziel dieser Arbeit ist, dieses Konzept auf ubiquitäre und metallfreie Anionen auszuweiten.

Mizellare Imidazoliumwolframate erweisen sich als ausgesprochen aktiv in der Epoxidation von hydrophoben Olefinen in der wässrigen Phase. Zugrundeliegende mechanistische Untersuchungen zeigen, dass Peroxy-Wolframate bei Kontakt mit Wasserstoffperoxid gebildet werden, die das in den Mizellen solubilisierte Substrat effizient epoxidieren. Im Vergleich dazu aktivieren Imidazoliumnitrate das Wasserstoffperoxid mechanistisch in Analogie zum Perrhenat mittels Wasserstoffbrückenbindungen, wie tiefgehende mechanistische Untersuchungen zeigen. Das zentrale Stickstoffatom ist somit nicht direkt an der Bindungsbildung beteiligt. Für die Aktivierung von Wasserstoffperoxid benötigen die

Nitrationen eine mizellare Umgebung, während homogen gelöste Nitratsalze keine Reaktivität aufweisen. Dies ist auf die Abschwächung der Hydratisierung durch den hydrophoben Effekt der Mizellen zu erklären, der eine stärkere Interaktion des Nitrats mit dem Wasserstoffperoxidmolekül zulässt.

Abhängig von den Anforderungen erlauben supramolekulare Ansätze ebenso den Wechsel der Reaktionsphase von der wässrigen zur organischen Phase. Im Falle des Sulfations ist eine mizellare Aktivierung von Wasserstoffperoxid aufgrund der sehr starken Hydratisierung nicht möglich, weswegen die Reaktivität des Sulfations in der organischen Phase untersucht wird. Mittels geeigneter Rezeptormoleküle werden supramolekulare Ionenpaare gebildet, die das Sulfation $[SO_4]^{2-}$ in die organischen Substratphase transferieren. Dort ist das entstehende Peroxymonosulfat in der Lage, das Olefin direkt zu epoxidieren.

Allgemein sind metallhaltige supramolekulare Katalysatoren reaktiver als die nichtmetallischen Pendants und epoxidieren das Olefin quantitativ innerhalb von Minuten oder wenigen Stunden. Die niedrigere Aktivität der metallfreien Katalysatoren kann in einem kontinuierlichen Prozess kompensiert werden, da mizellaren Katalysatoren einfach von der organischen Phase zu trennen sind und aufgrund der ausgezeichneten Stabilität eine hohe Rezyklierbarkeit besitzen. Der Einsatz in einem kontinuierlichen Prozess ist aufgrund der guten Skalierbarkeit der Katalysatorsynthese als auch des Reaktionsansatzes hochgradig attraktiv für die Epoxidierung von hydrophoben Olefinen mit Wasserstoffperoxid. Der Nachteil des sich anreichernden Wassers wird mithilfe einer weiteren Katalysatoroptimierung überwindet. Die Funktionalisierung des Imidazoliumkations mit polyfluorierten aromatischen Substituenten führt zu einem temperatursensitiven Katalysator, dessen Löslichkeit in der kalten wässrigen Phase aufgrund der starken Kationinteraktion vernachlässigbar ist. Bei erhöhter Temperatur bilden sich reversibel Mizellen, während der Katalysator in der Organik gänzlich unlöslich bleibt.

Zusammenfassend kann die supramolekulare Zweiphasenkatalyse aufgrund des Einsatzes umweltfreundlichen Wasserstoffperoxids für die Epoxidation von Olefinen im Lösungsmittel Wasser sowohl als ökologisch als auch ökonomisch als sehr attraktiv betitelt werden. Dies wird durch die hervorragende Rezyklierbarkeit der Katalysatoren und die gute Skalierbarkeit der Synthese und Katalyse bekräftigt.

Table of Contents

List of Abbreviations and Unit Symbols

Å	Ångström [10^{-10} m]
AIBN	Azobis(isobutyronitrile)
B.P.	Boiling Point
BA	Benzamide
BINOL	[1,1'-Binaphthalene]-2,2'-diol
BMIM	1-Butyl-3-methylimidazolium
Bn	Benzyl
^{F}Bn	2',3',4',5',6'-Pentafluorobenzyl
Bu	*n*-Butyl
γ	Surface Tension [mN/m]
Γ	Gibbs Excess Concentration [mol/m²]
CAC	Critical Aggregation Concentration [mol/L]
CMC	Critical Micelle Concentration [mol/L]
CP	Cetylpyridinium
δ	Chemical Shift (NMR) [ppm]
d	Day
DCM	Dichloromethane
De	*n*-Decyl
DEEP	Diethylethylphosphonate
DeMIM	1-Decyl-3-methylimidazolium
DFT	Density Functional Theory
DHA	Dihexylammonium
DLS	Dynamic Light Scattering
DNA	Deoxyribonucleic Acid
DODA	Dioctadecyldimethylammonium
DSC	Differential Scanning Calorimetry
Do	*n*-Dodecyl
DoMIM	1-Dodecyl-3-methylimidazolium
DoMMIM	1-Dodecyl-2,3-dimethylimidazolium
DOSY	Diffusion Ordered Spectroscopy
DSC	Differential Scanning Calorimetry
E	Element
E_A	Activation Energy [KJ/mol]
EPA	Ethylphosphonic Acid
Eq.	Equivalent
ESI	Electrospray Ionization
Et	Ethyl
FID	GC: Flame Ionization Detector NMR: Free Induction Decay
G	Gibbs free Energy [KJ/mol]
GC	Gas Chromatography
H	Enthalpy [KJ/mol]
h	Hour

HFIP	Hexafluoroisopropanol
HPPO	Hydrogen Peroxide to Propylene Oxide
IL	Ionic Liquid
^{i}Pr	*iso*-Propyl
IR	Infrared
k	Reaction Constant
L	Liter
M.P.	Melting Point
Me	Methyl
MeOPh	*para*-Methoxyphenyl
min	Minute
MMIM	1,3-Dimethylimidazolium
MS	Mass Spectrometry
$\tilde{\nu}$	Wavenumber [cm^{-1}]
NBS	*N*-Bromosuccinimide
NMR	Nuclear Magnetic Resonance
NTF_2^-	Bis(trifluoromethylsulfonyl)imide
Oct	*n*-Octyl
OMIM	1-Octyl-3-methylimidazolium
OMMIM	1-Octyl-2,3-dimethylimidazolium
POM	Polyoxometalate
PPA	Phenylphosphonic Acid
PPM	Parts Per Million
PTC	Phase-Transfer-Catalysis
R	In Chemical Formula: Organic Residue
	In Physical Formula: Universal Gas Constant
r	Reaction Rate
rpm	Revolutions per Minute [min^{-1}]
RT	Room Temperature
RTIL	Room Temperature Ionic Liquid
S	Entropy [J/(K·mol)]
SAIL	Surface-Active Ionic Liquid
SAXS	Small-Angle X-Ray Scattering
SC-XRD	Single Crystal X-Ray Diffraction
SIP	Supramolecular Ion Pair
T	Temperature [°C or K]
t	Time [min or h]
*t*Bu	*tert*-Butyl
TEM	Transmission Electron Microscopy
TFE	2,2,2-Trifluoroethanol
TGA	Thermogravimetric Analysis
THF	Tetrahydrofuran
TLC	Thin Layer Chromatography
TMA	3,5,5-Trimethylhexanamide
TUM	Technical University of Munich
UV	Ultraviolet
VT	Variable Temperature
XRD	X-Ray Diffraction

1 Introduction

1.1 Supramolecular Chemistry

The term “Supramolecular Chemistry” was first coined by Jean Marie Lehn in 1978[1] for the field of chemistry which deals with molecular assembly formation via non-covalent interactions.[2] These weak interactions result in a dynamic aggregation process, which optimizes the assembly structure by association and dissociation of subunits towards the overall energetic minimum.[3][4] The correct choice of the small subunits is fundamental for the integrity of the supramolecular assembly and can mostly not be designed a priori due to the versatility and fluctuation of the dynamic structures in solution. Hence, supramolecular concepts must be studied and optimized elaborately as the vast choice of subunits and hence the multiple possibilities of assemblies for specific tasks are literally infinite. Due to the nano-scale dimension of these assemblies, supramolecular chemistry can be accounted as a noteworthy contribution to nanotechnology nowadays.[5][6]

Despite of the 50th anniversary of supramolecular chemistry in 2017,[7] the fundamental principles of assembly formation have been described before and date decades back to e.g. discoveries of ‘Supramolecules’ in solution by Wolf in 1937[8] or the helix structure of DNA by Wilson and Crick in 1953.[9] Since the emergence of modern supramolecular chemistry in the late 20th century, the majority of approaches have been developed for applications in ion reception upon formation of specific host/guest complexes.[10] Mostly, multidentate organic ligands form coordination bonds to *Lewis*-acidic metal ions. Especially the work on crown ethers[11] and cryptands[12] must be highlighted, which form a complex −by choice of the right size− with a specific cation. Concepts like these allow for the extraction of the metal ions into organic media and can be exploited for the treatment of radioactive waste water by removal of radioactive caesium or technetium ions.[13][14] Further developments on the field of supramolecular chemistry gave rise to sensing of specific inorganic species in solution. Mostly, guest-specific functional groups bind to the respective ion selectively and shift the wavelength absorption maximum of covalently linked chromophores. Accordingly, structural combinations of azo dyes and crown ethers allow for the colorimetric determination of specific metal cations by a color shift of the solution arising from the formation of a guest/host assembly.[15] Regarding the sensing of neutral species, it is somewhat intricate to design a selective receptor and is rather restricted to detection of carbohydrates in solution. These form covalent boronic acid esters which shift the adsorption maxima of adjacent chromophores.[16]

Supramolecular assemblies are not necessarily limited to complexation of the host molecule or ion for a respective purpose. It is rather considered to be the holy grail of supramolecular chemistry to mimic natures' concepts of enzymatic conversion of organic substrates.[17] One major factor in this field is the selective molecular recognition of the substrate and its consequent catalytic conversion. As this is the most difficult aspect of supramolecular catalysis to be tackled, examples are very rare and rather restricted to simple acid catalyzed ester hydrolyzations exploiting functionalized cyclodextrins as enzyme models.[18][19]

The difference of metabolic to industrial processes is the shear infinite variety of organic compounds mixed in cell and body fluids, requiring a high enzymatic substrate selectivity, while catalytic processes are mostly conducted with one distinct substrate. Hence, a high activity and product selectivity is sufficient for supramolecular catalysts. These should therefore be designed in a fashion to convert the substrate selectively and facilitate the reaction by attracting it close to the catalytic active center of the assembly. Micellar concepts are among the most prominent fields of supramolecular catalysis as they can be exploited for the conversion of hydrophobic substrates in water. Micelles are supramolecular assemblies which are formed by weak intermolecular forces in-between surface-active compounds. The resulting micellar spheres can rather be described as soft and undefined surfactant aggregates which are highly sensitive towards their chemical and physical environment.[20][21] Still, these nano-sized assemblies are exploited for their unique physical and chemical properties due to the hydrophobic core surrounded by a polar shell. The micelles are useful for catalytic conversions of hydrocarbons in aqueous media and are therefore a convenient method to phase-mediate in-between an organic substrate layer and an aqueous reactant phase.

Micellar catalysis can be divided into two major approaches; 1) the micelles solubilize the substrate as well as the catalyst and 2) the micelle catalyzes the reaction by direct participation of the assembled surfactant molecules in bond formation (Figure 1).[22] The first concept is rather exploited for the substitution of organic solvents by water in order to render catalytic reactions more sustainable according to the twelve principles of green chemistry.[23] In recent years, this nanoreactor approach received wide interest in late transition metal catalysis, especially C-C cross-coupling reactions due to the possibility to replace toxic solvents.[24] However, the used catalysts are identical to those developed for operation in organic solvents and the micelles allow for the use of conventional catalysts in water without the need to adjust the catalyst's properties.[25]

The second approach, micellar catalysts formed by surfactants bearing catalytically active groups can be divided into two subgroups; 2a) the catalytically active motif is an essential structural part of the surfactant for the micelle formation, e.g. directing the surfactant assembly

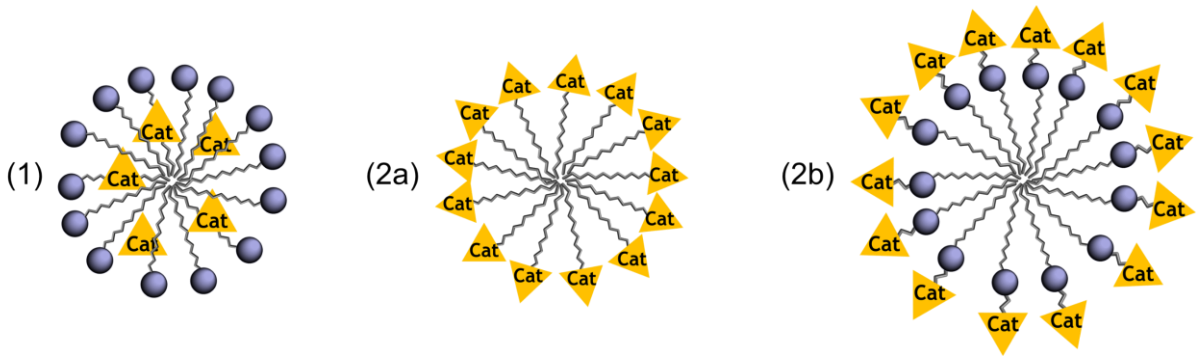

Figure 1: Schematic representation of micelles for catalytic applications.

by the high polarity of the catalytically active polar moiety or 2b) the catalyst is covalently bound to the surfactant molecule (Figure 1, middle and right). The design of micelles for catalytic purposes is one of the fundamental contributions to supramolecular catalysis. These concepts have the unique potential to replace organic solvents in most chemical reactions by water. Moreover, new catalytic mechanisms facilitated by the micelle allow for substrate conversion under mild conditions with unforeseen reactivities. These prospects contribute to a green future of synthetic chemistry.

In order to be able to design supramolecular catalysts, a fundamental understanding of the assembly process, and the influence of the surfactant's structural composition on the micelle formation is required.

1.2 Surfactant Aggregation in Aqueous Solutions

The word '*Surfactant*' is a blend of the term *surface-active agent* and was introduced to classify all compounds that show a certain affinity to surfaces and interfacial boundaries with respect to the change of the physical properties. In most cases, surfactants are amphiphiles which consist of covalently connected structural motives bearing polar, hydrophilic and non-polar, hydrophobic properties. Upon dissolution in aqueous media, the polar section, also defined as the head group, is hydrated by the water molecules and interacts attractively with its surrounding by H-bonds, while the hydrophobic part is repulsed. This leads to an accumulation of the compound at the water/air interphase with the hydrophobic section pushed into the air, resulting in widely changed surface parameters. All surfactant molecules have the same structural motif in common, a long linear alkyl chain which acts as the hydrophobic section of the surfactant. The only structural parameter which is altered is the number of methylene units in the alkyl chain, hence affecting its length and the respective weight compared to the head group. The size of the hydrophobic section in ratio to the whole molecule defines its strength of surface-adsorption and the physical properties of the surface. In case it is too small, the molecule is completely hydrated in the aqueous phase and lacks surface-activity. If it is too

large, the hydrophobic character dominates and it is therefore insoluble in water, both cases limiting the surface adsorption. The alkyl chain is covalently bound to the polar head group, which can be chosen from a large portfolio of different classes. Primarily, these can either be of ionic or non-ionic nature. The first class has an intrinsically high hydrophilicity due to the presence of the electrostatic field of the head group charge and the respective counterion. Industrial relevant representatives are sodium dodecylsulfate (SDS) and cetyltrimethylammonium bromide (CTAB). Non-ionic surfactants require larger polar domains to be sufficiently hydrated. In most cases, a sequence of oligomeric ethoxylate units meet the requirements for this task (Figure 2).

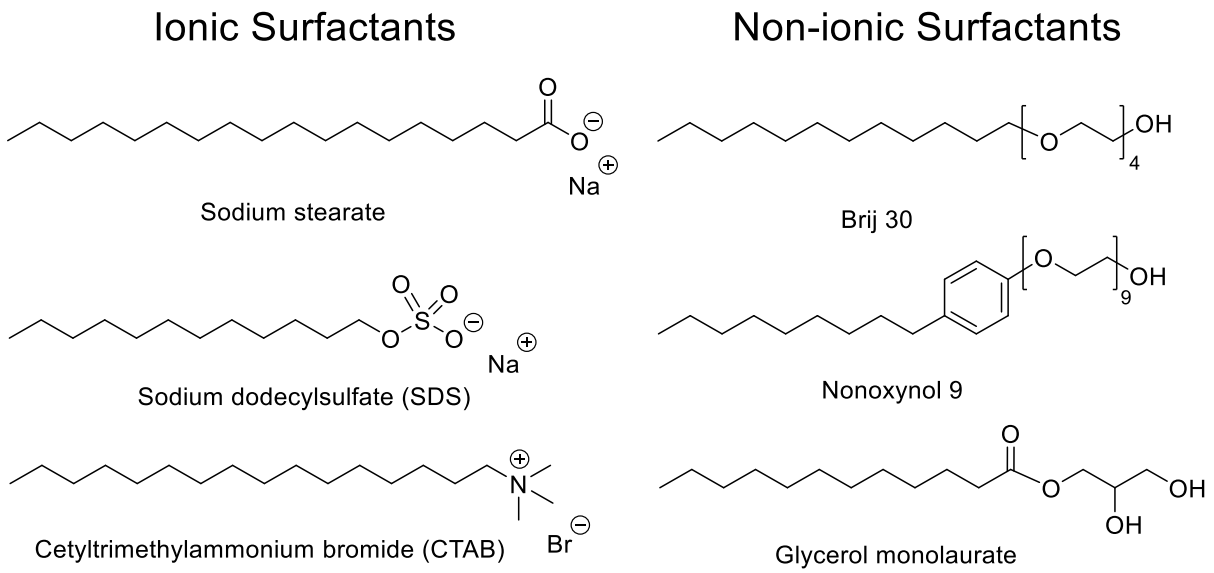

Figure 2: Examples of industrially relevant surfactants.

The most prominent solvent property to be affected by dissolution of surfactants is the surface tension. In the bulk of a pure solvent, all forces are omnidirectional and well-balanced. On the surface, the solvent molecules experience an attractive force towards the bulk medium, which cannot be compensated by the weakly interacting air molecules (Figure 3). This renders the medium into limiting its surface area to the possible minimum. This surface tension is specific for the strength of the intermolecular interactions within the liquid. Hence, this value is rather high for the polar medium water and low for non-polar *n*-hexane with 72 and 18 mN/m, respectively.[26]

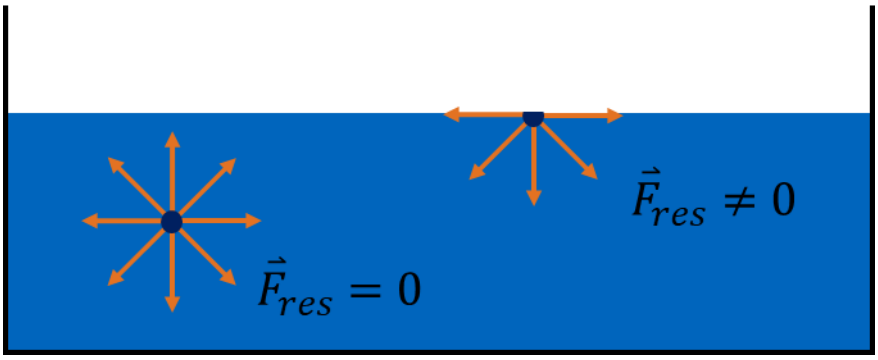

Figure 3: Schematic representation of the intermolecular forces within a solvent in bulk and on the surface.

Regarding an aqueous surfactant solution, the surface-adsorption of amphiphiles leads to an osmotic uptake of water molecules into the surfactant layer on the surface due to the hydration of the polar groups.[27] In case of ionic surfactants, the electrostatic repulsion of the charged head groups plays the major role. These forces lead to a maximum spreading of the surfactant molecules over the whole surface available, analogous to the homogenous ion distribution of a dissolved salt. The spreading pressure π is contrary in effective direction to the surface tension γ and therefore reduces the initial surface tension of the solvent.

$$\gamma = \gamma_0 - \pi$$

The reduced surface tension is a direct measure of the surface-activity of the surfactant and can conveniently be investigated by tensiometry. The most prominent methods used in literature to determine surface tensions are the du Noüy ring and the Wilhelmy plate method.[28][29] While the first requires an instrument-dependent empirical correction factor, the latter one can be used to directly calculate the surface tension from the used plate geometry. There, a platinum or glass plate connected to a forcemeter levitates over the solution surface and is slowly lowered. Upon contact with the liquid, it is wetted, and a solvent meniscus is formed (Figure 4). This additional force pulling on the plate is measured and can easily be converted to the surface tension via the equation:

$$\gamma = \frac{F}{2l \cdot \cos\Theta}$$

Usually, the contact angle of the water θ to materials such as glass or platinum is 0° or close to, so the cosine term equals one or can be neglected. This fast-measuring approach can be utilized to study the change of the surface tension with varying amount of surfactant dissolved.

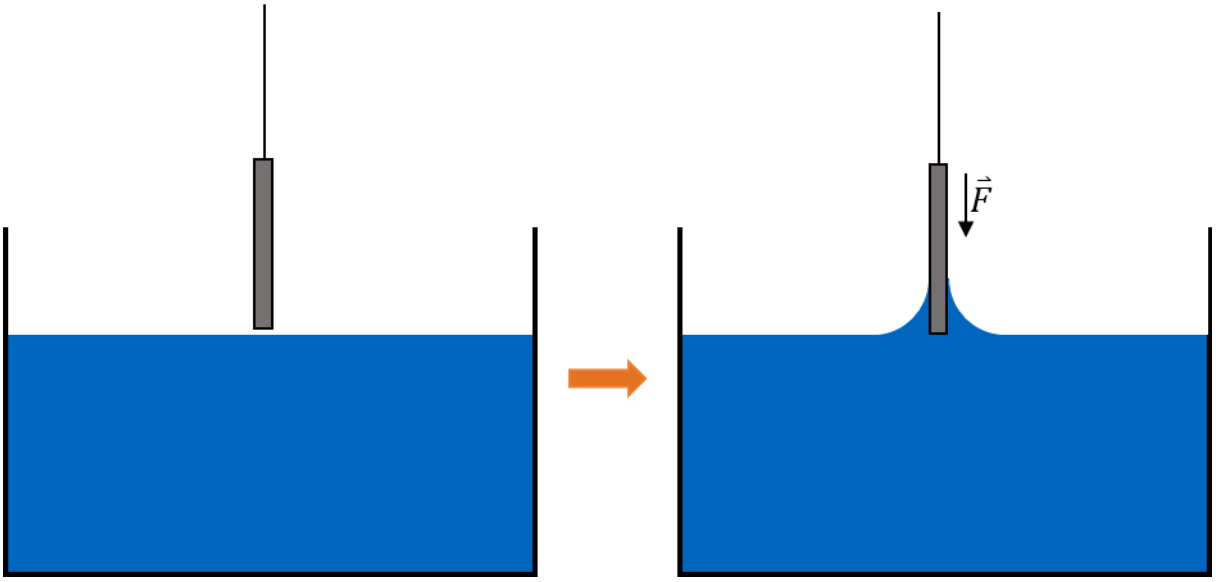

Figure 4: Schematic representation of the Wilhelmy plate method to measure the surface tension.

The information received by tensiometry is not limited to the surfactant-dependent surface tension. It also gives insights into the minimum surface area demand of the surfactant molecules, accordingly the size of the hydrated polar head group. Upon addition of the surfactant to an aqueous medium, it is adsorbed on the surface and distributes homogeneously. With increasing surfactant concentration, the spreading pressure rises due to the repulsion of the surfactant molecules, which in turn is the force that reduces the surface tension. From this surface tension-concentration dependency, the minimum surfactant area can be calculated. The exploited Gibbs adsorption equation is based on the dividing surface model and correlates the change of surface tension with the changes in surface chemical potential.

$$-d\gamma = \Gamma \, d\mu$$

Γ is the Gibbs surface excess and describes the surfactant surface concentration. The surface chemical potential μ can further be defined as sum of the standard chemical potential μ_0 and the surfactant-activity *a*, which can be approximated by the surfactant concentration c.

$$\mu = \mu_0 + RT \ln a = \mu_0 + RT \ln c$$

Differentiation of the expression results in loss of the constant value μ_0:

$$d\mu = RT \, d \ln c$$

Resolving the term above towards Γ results in the Gibbs adsorption isotherm:

$$\Gamma = -\frac{1}{RT}\left(\frac{d\gamma}{d \ln c}\right) = -\frac{1}{2.303\,RT}\left(\frac{d\gamma}{d \log c}\right)$$

With this formula, it is comprehensible that the slope of the tensiometry curve at various points can be used to calculate the demanded surfactant area. A third-degree polynomial fit to the tensiometric curve is sufficiently accurate to calculate the respective slopes by differentiation. The derived curve is then plotted against the surfactant concentration, which results in a plateau at a distinct surfactant concentration. This is the maximum surfactant concentration on the surface (Figure 5) and can further be converted to the molecular surfactant area demand.[30]

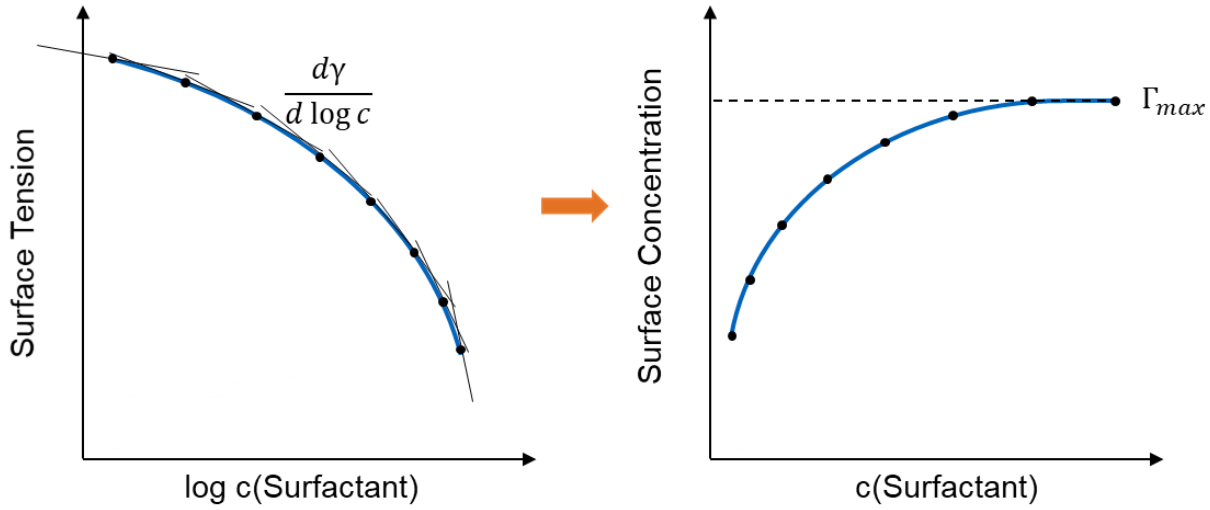

Figure 5: Schematic semi-logarithmic surfactant-concentration vs. surface tension plot (left) and the derived surfactant surface concentration vs. surfactant solution concentration (right).

The reduction of the surface tension by addition of surfactants ultimately reaches a limit in case of a saturation of both, the surface of the solvent and the solvent bulk phase. At this point, the concentration reaches a certain value, at which the intermolecular interaction of the hydrophobic parts comes into play. The van-der-Waals interactions dominate and lead to an aggregation of the surfactants for overcoming the enthalpically unfavoured hydrophobic hydration (vide infra). Upon further addition of the amphiphile, the so-called *critical aggregation concentration* (CAC) is exceeded, and surfactant aggregation occurs. A microscopically heterogenous system and quasi-homogenous solution with unique physical parameters is obtained. The surface saturation is maximized at this point and is not further affected, so that the CAC can be elucidated from tensiometric trendlines as aggregates are not formed on the surface but in the bulk solution exclusively. The concentration at which the physical surface properties (e.g., the surface tension) does not change upon further addition of surfactant is the CAC. Schematic trendlines with the corresponding CAC are presented in Figure 6. In case of contamination of the instrument or solutions with foreign surface-active compounds, the surface tension decreases faster than usual but equilibrates at the corresponding final surface tension γ_{CAC} at higher surfactant concentrations. The reason for this trend is the uptake of the impurities from the surface into the aggregates in the bulk solution.

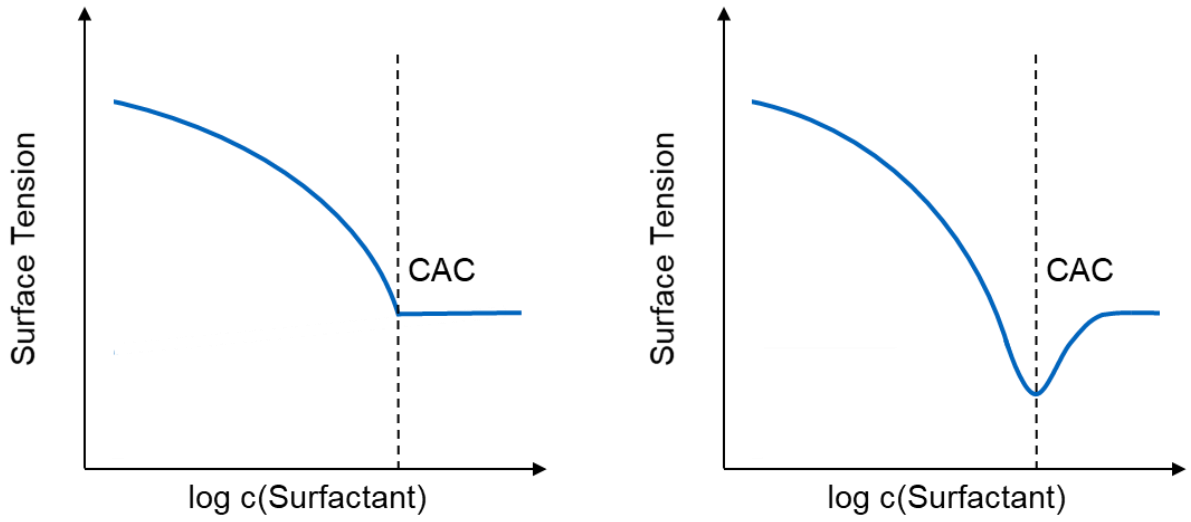

Figure 6: Schematic semi-logarithmic surfactant-concentration vs. surface tension plots for a pure surfactant solution (left) and a contaminated surfactant solution (right).

The constitution and shape of the aggregates formed above the CAC is widely dependent on the surfactant concentration and the molecular structure of the surfactants. In most cases, spherical micelles are formed but there are exceptions, such as vesicles, bilayer sheets or even more complex lyotropic phases. Of all those classes, micelles are by far the most occurring aggregates formed by surfactants. A micelle is ideally a spherical aggregate of multiple surfactant molecules with a polar surface, dominated by the polar surfactant head group and an inner hydrophobic core consisting of the surfactant alkyl chain. Regarding the aggregation of surfactants to micelles, the CAC is called *critical micelle concentration* (CMC).

In case of ionic surfactants, below their CMC, the ions are dissociated and distributed homogenously in the aqueous phase. Upon exceeding the CMC, surfactant molecules aggregate, and the charged head groups form the micellar surface. This high local charge density creates a strong radial electrostatic field, which is compensated by the surfactant's counterions. The Stern-theory can be exploited to describe the molecular constitution of the micellar interface.[31] The charged head groups are surrounded by a layer of anions, which are attracted strongly by the electrostatic interactions (Figure 7). This headgroup/counterion layer is the so-called Stern-layer and can be considered as rather rigid due to the strong ionic interactions. At this Stern-plane, the majority of the electrostatic potential is compensated, and marks the transition to the diffuse layer, from which the residual micellar potential is compensated by randomly distributed counterions and dissolved, non-aggregated surfactant molecules. The result of this constitution is a high ion density on the micellar surface, compared to homogeneously distributed electrolytes. This constitution is prone for the utilization of aggregated surfactant cations with catalytically active counterions, due to the high ion density on the micellar surface.

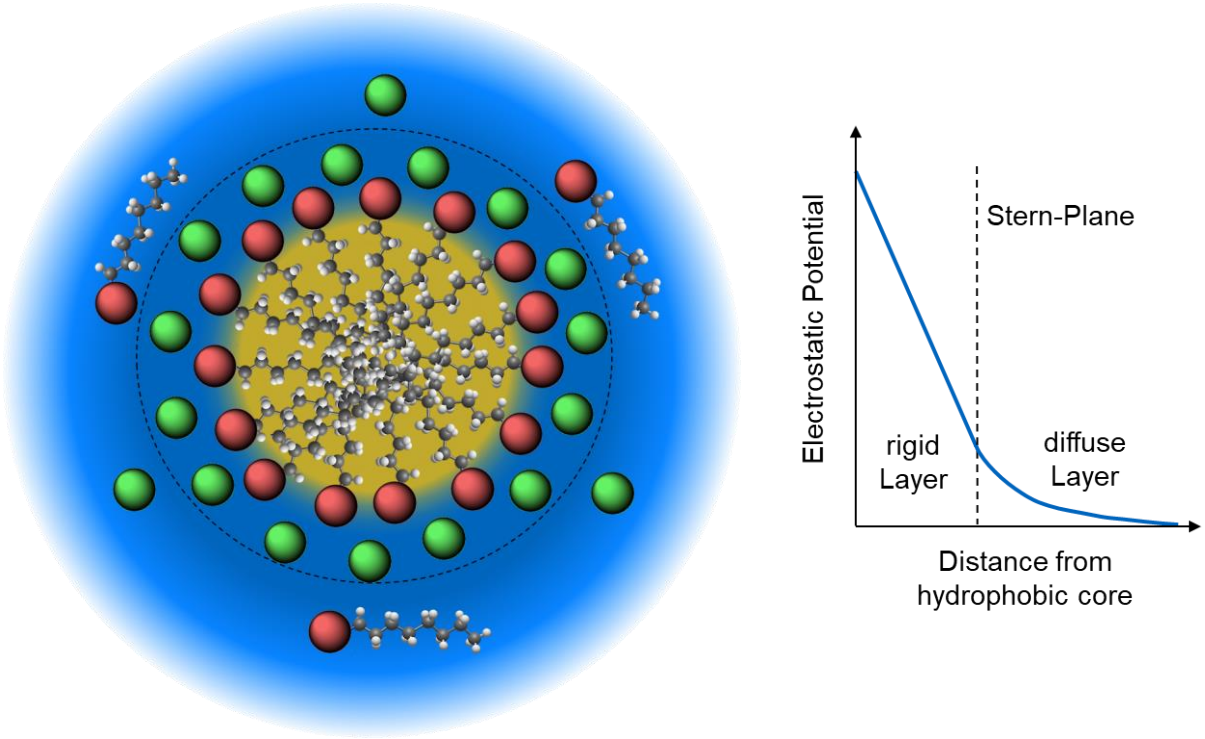

Figure 7: Schematic cutaway view of a micelle (left) and the corresponding Stern-potential from the head group plane (right).

Besides the ionic interactions, the micelle is stabilized by H-bonds in the head group interphase with the polar solvent as well as the van-der-Waals interactions inside the core among the hydrophobic parts. Despite the vast reduction of the entropy upon micellization from single dissolved molecules, the negative enthalpy contribution of the head group hydratization enthalpy and the alkyl chain van-der-Waals interaction lead to a negative Gibbs free energy difference in the range of −5 to −25 kJ/mol, indicating an exergonic and thermodynamically favoured process, greatly impacted by the alkyl chain length.[32] This is the essential premise for micellization to form ordered structures from monomeric units contrary to maximize entropy. However, micelles cannot be regarded as stable particles as the micellar cohesion forces are rather weak and therefore dynamically break and reform. The micelles are in constant equilibrium with surface-adsorbed and dissolved surfactant units, ultimately leading to a polydisperse micelle size distribution.[33]

To find the optimal structural composition of the surfactant for micellization, a geometrical approach can be exploited. As the desired aggregation form is the spherical micelle with the superficial head group on the voluminous hydrophobic core, it is possible to calculate the optimal structure of the monomeric unit. The count of surfactant molecules forming the micelle is the aggregation number n_{agg} and is equal to the quotient of the volume of the core and the individual volume of the surfactant's hydrophobic tail.

$$n_{agg} = \frac{V_{core}}{V_{tail}} = \frac{\frac{4}{3}\pi r^3}{V_{tail}}$$

Similarly, the aggregation number is equal to the total micellar surface area divided by the individual head group area demand.

$$n_{agg} = \frac{A_{micelle}}{A_{head}} = \frac{4\pi r^2}{A_{head}}$$

Equalization of both equations and substitution of the micellar radius with the length of the alkyl tail group ($l_{tail} \leq r$) results in the expression:

$$P = \frac{V_{tail}}{A_{head} \cdot l_{tail}} \leq \frac{1}{3}$$

P is the packing factor of a surfactant molecule and is for spherical micelles ideally ⅓. This results ultimately in a cone-shaped surfactant molecule. Surfactants with higher packing factors tend to form non-spherical micelles, bilayers up to the geometrical inversion towards inverse micelles.[10] Figure 8 gives an overview on possible surfactant shapes and the preferred aggregate shape.

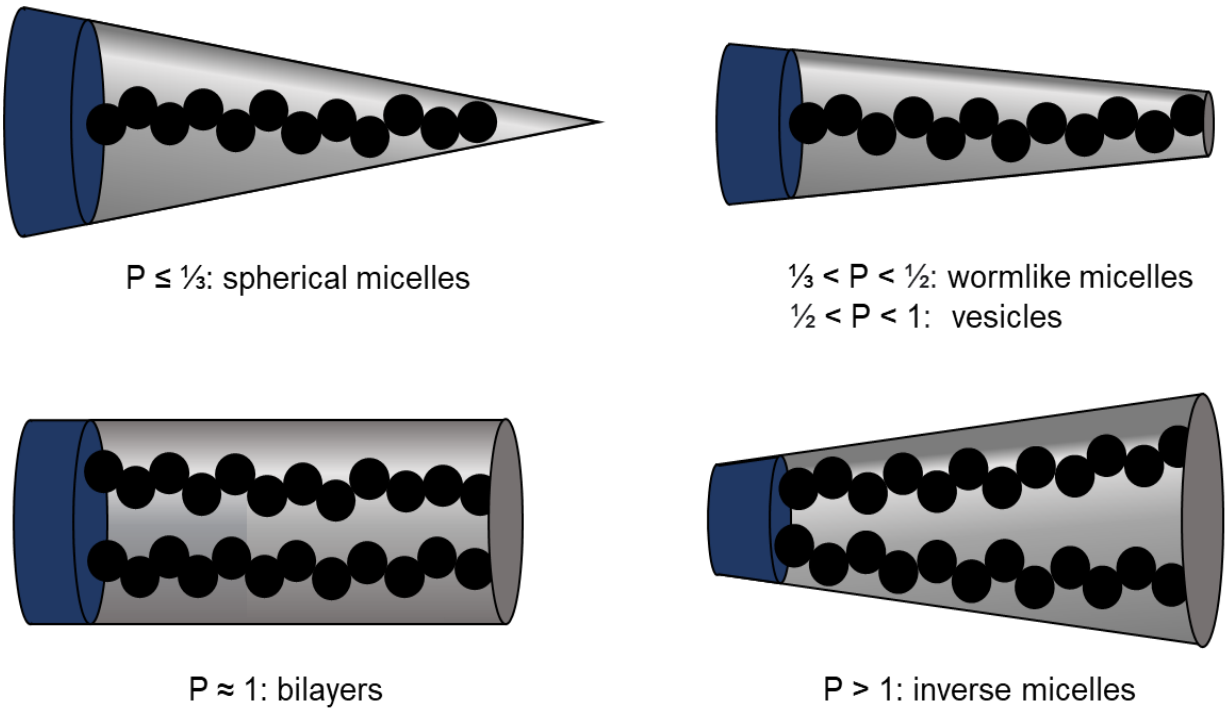

Figure 8: Schematic representation of the packing factor of various surfactant motifs. Blue: area demand of hydrophilic head group; grey: space demand of the hydrophobic alkyl chains.

To design a surfactant for a spherical micelle, it is therefore required to calculate the packing factor a priori. Tandford developed equations for the calculation of the volume and length of alkyl chains of surfactant molecules:[34]

$$V_{tail} = (27.4 + 26.9 \cdot n_C)\ \text{Å}^3$$

$$l_{tail} = (1.5 + 1.265 \cdot n_C)\ \text{Å}$$

Where n_C is the numbers of carbon atoms of the alkyl chain. However, it is recommended to not take the first carbon atom of the alkyl chain into account, as it is significantly hydrated and can therefore be more attributed to the polar head group.[35]

$$V_{tail} = (27.4 + 26.9 \cdot (n_C - 1))\ \text{Å}^3$$

$$l_{tail} = (1.5 + 1.265 \cdot (n_C - 1))\ \text{Å}$$

Regarding the head group area demand it is not reasonable to take the molecular size, but rather the minimum micellar surface area demand into account. This value can be elucidated from tensiometric measurements exploiting the Gibbs adsorption isotherm (vide supra). For example, the typical 1-octyl-3-methylimidazolium tetrafluoroborate surface-active ionic liquid [OMIM] [BF_4], has a minimum surface area demand of the head group of 56 Å^2,[36] which results in the packing parameter of P = 0.364, considering the volume of the octyl group. This is very close to the ideal value of ⅓ for spherical micelles. Hence, 1-alkyl-3-methylimidazolium ILs can be considered to be the ideal surfactant class for the formation of spherical micelles in aqueous solutions.[37] Moreover, the substitution of the imidazolium motif allows for a virtually unlimited functionalizability of the surfactant, allowing for a tailoring of the formed micelle.[38] The sizes of the formed micelles are in the nanometer regime,[39][40] hence excluding a direct observation by light microscopy.[41] More sophisticated methods have to be exploited to determine the micellar size distribution and thus provide the confirmation of presence of micelles besides tensiometry and conductometry. As the micelles are highly dynamic aggregates, the change of the environment may have an impact on the micelle sizes. Hence, *in situ* methods should be the method of choice. Here, dynamic light scattering (DLS)[42] as well as small angle X-ray scattering (SAXS)[43] have shown to be suitable for the determination of micellar size distributions under application conditions. Moreover, the responsiveness of the micelles on external stimuli such as the temperature as well as the interaction with additives can be investigated. This is of particular importance for the investigation of the solubilization of hydrophobic compounds inside the micelles.

1.3 Solubilization of Hydrocarbons in Aqueous Solutions

It is commonly known that non-polar hydrocarbons (e.g., oil, gasoline, etc.) and water are immiscible and do not mix spontaneously. Upon vigorous stirring or shaking an emulsion can be created but with an immediate phase separation to the initial situation. As easy as the negligible solubility of one in another can be explained by the polarity of the substances like hydrophobic and hydrophilic properties, the thermodynamic background of hydrocarbon solvation in water is much more difficult. Theoretic investigations suggest that the water molecules surrounding the hydrophobic hydrocarbon chain require a reorientation and reorganization called hydrophobic hydration. This is entropically unfavoured as it disrupts the continuous water phase. As example, the Gibbs free energy ΔG of the hydration of *n*-butane at room temperature can be separated into the enthalpic and entropic term. While ΔH is negative with −4.3 kJ/mol, speaking for an exothermic process, the entropic term −TΔS is more than six time larger and positive with +28.7 kJ/mol, rendering the hydration unfavourable and strongly endergonic.[44]

Microscopically, the emulsification phenomenon upon vigorous shaking of a biphasic oil/water mixture relies on the formation of plenty of small droplets and not solubilization of single molecules. To describe this process, surface and interfacial thermodynamics must be addressed. The formation of an emulsion causes the area of boundary surfaces to rise proportionally with the number of droplets and to the power of three with their size. Energetically, the additionally formed boundary area has to be multiplied with the boundary surface tension to calculate the total energy demand of the emulsion process:

$$\Delta G_{emul} = \gamma \cdot \Delta A$$

This inevitably positive free energy demand is responsible for the instability of binary emulsions and the driving force towards demulsification. Furthermore, the curved droplet surface creates an internal pressure due to the surface tension according to the Young-Laplace equation for spherical bodies:

$$\Delta P = \frac{2\gamma}{r}$$

This simple-looking but meaningful equation describes the behavior of the non-stabilized emulsion. For a hypothetical droplet of the size 0.5 µm and a typical interfacial tension of oil/water systems of 12.5 mN/m, an additional pressure of 100 kPa, one atmosphere, is contained within the particle.[45] Hence, the droplets tend to overcome this high internal pressure by increasing the droplet radius, leading to particle aggregation to larger domains until the emulsion is, so-called, '*broken*'. This process occurs primarily by droplet collisions due

to Brownian or buoyancy motions and can be supported by shear forces, e.g., gentile stirring or swivelling.

The droplet surface tension is a proportional parameter in both equations and therefore plays a major role in emulsification processes and stabilities. Among other effects, surfactant molecules decrease the surface tension drastically, thus increasing the stability of the emulsion. Upon addition of surfactants beyond their critical micelle concentration (CMC), the formed supramolecular aggregates with large interior hydrophobic domains can interact with hydrophobic hydrocarbons. Especially for non-ionic surfactants, the phase distribution is difficult to predict and cannot be explained by the packing factor exclusively. Due to the less polar and much larger head group, the surfactant may be soluble in either one or both, the aqueous or the organic phase. The surfactant phase distribution and the micellar phase can be distinguished by Bancroft's rule, named after him for his initial investigations on the theory of emulsifications:[46][47]

'The phase in which an emulsifier is more soluble constitutes the continuous phase.'[48]

It can be stated that ionic surfactant species with well-hydrated counterions such as 1-alkyl-3-methylimidazolium halides and element oxides are exclusively forming micelles in the aqueous phase. Hence, besides the high anion and accordingly catalyst concentration on the micellar surface, the focus of micellar oxidation catalysis should lie on the use of ionic surfactants to ensure the operation in the aqueous phase. The micellar inner core, composed of the hydrophobic alkyl chain tails of the aggregated surfactant molecules is the domain of the van-der-Waals interactions and behaves liquid-like due to the rotational flexibility of the methylene units in the alkyl chains. It is not of great surprise that non-polar compounds interact vigorously with those alkyl moieties, resulting in their uptake into the micelle and therefore in a micelle swelling. It is anticipated that the swelling is further assisted by the direct interaction of the surfactant alkyl chain with the organic compound. It spreads the alkyl moieties further apart, resulting a higher geometrical packing factor *P* (see Figure 8).[49] Thus, larger micelles are formed which in turn may take up more substrate molecules.

Early results by Klevens show that the solubilization of ethylbenzene inside micelles of a homologous series of potassium alkanoates is widely depended on the alkyl chain length of the surfactant, with solubilities reaching more than one mole of substrate per mole surfactant at room temperature for the long-chained hexadecanoate.[50] The overall trend shows that the shorter the surfactant's alkyl chains, the less ethylbenzene is solubilized in the aqueous solution. These findings must be considered for the design of a surfactant, however, this influence on the concentration of the substrate inside the micelle is still not predictable.

McBain and Richards investigated the influence of the alkane size on their solubility inside micelles formed by 0.1 M sodium oleate.[51] While *n*-heptane shows a solubility of as high as 0.5 moles per mole surfactant, the amount decreases rapidly to 0.05 for *n*-dodecane. These results can be explained by the dynamic liquid-like interior of the micelle as small substrates are more easily distributed between the micellar alkyl tail groups. This fact is less important for the micelle formation itself, however, it should be kept in mind that low solubility rates of large olefins could be met by using a surfactant with a longer alkyl chain.

From the point of mass transportation, micelles can be exploited to drastically accelerate the reaction of a non-polar hydrocarbon with an aqueous reactant.[52] In absence of the micelles, the small oil/water interphase does not allow for noteworthy substrate conversion. The addition of surfactants beyond their CMC will ultimately accelerate the reaction rate due to vast increase of interphase area. There, the micelles can be regarded as shuttles which transfer the olefin into the organic phase without necessarily contributing to the reaction mechanism, hence not acting as a 'true' catalyst. The micellar surface represents a micellar pseudophase in between the aqueous bulk phase and the hydrophobic micellar inner core. Both reactants will react upon contact in the pseudophase for which a reaction constant k_{pseudo} must be formulated. Mostly, this constant is identical to the reaction constant of the aqueous phase k_{aq} with the difference in reaction rate originating from the different reactant concentrations.[53] In some cases, the reaction rate is even smaller in the presence of micelles due to the uptake of organic substrate from the aqueous phase into the micelle, shielding it from the other reactant.[54]

From the point of micellar catalysis, the activation of the reactants is the rate limiting factor as micelles can be regarded as the ideal shuttles for non-polar substrate molecules into water.[55] In order to investigate micellar catalysis from the point of structural optimization of supramolecular subunits, a catalytic reaction requiring a bifunctional catalyst for the activation of reactants and the transfer of hydrocarbon substrates into water is desirable. Among industrial relevant catalytic processes, the epoxidation of non-polar olefins with hydrogen peroxide is very intricate as it requires large amounts of polar organic solvents and expensive catalysts. Hence, the biphasic epoxidation of olefins using hydrogen peroxide is the ideal model reaction for the development of supramolecular catalyst strategies. Moreover, this reactions allows for the development of a recycling strategy, exploiting the biphasic nature of the system and the 'immobilization' of the catalyst in the aqueous phase. A huge industrial and academic research field is the epoxidation of hydrophobic olefins with inorganic oxidants, which are considered sustainable.

1.4 Aspects of Sustainable Catalytic Olefin Epoxidations

Epoxides are a class of organic compounds which bear the oxirane ring moiety and are mostly produced from olefins upon oxidation of the C=C double bond. This class of compounds is exploited for their high reactivity towards nucleophiles due to the high ring strain of the three-membered ring.[56] Upon nucleophilic attack of a *Lewis*-base, the ring opens and yields a *trans*-1-X-2-hydroxyethane derivative, depending on the nature of the nucleophile X^- and the substitution pattern of the two carbon atoms (Scheme 1). Due to this versatility, epoxides are convenient organic building blocks for chemical specialities, pharmaceutical drug precursors and polymers.[57] The high demand of epoxide compounds requires them to be affordable and easy to produce on a large scale, preferably in an economically favourable continuous process. The great majority of the annual production of epoxides is attributed to ethylene oxide with expected capacities of 32 megatons in 2023[58] and is synthesized from ethylene and molecular oxygen with a heterogeneous silver catalyst in a continuous process.[59] The second most important epoxide, propylene oxide, is produced from propylene and hydrogen peroxide by various classical and catalytic approaches. For this epoxide, the hydrogen peroxide to propylene oxide (HPPO) process with a titanosilicate-based catalyst is the most convenient catalytic synthesis procedure in industry.[60]

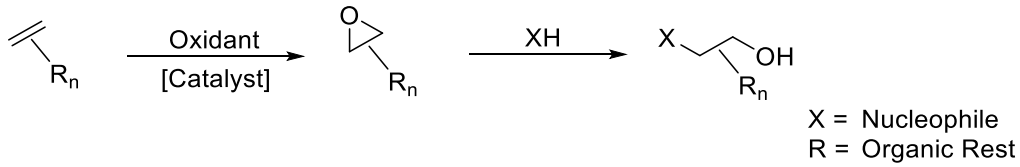

Scheme 1: Synthesis and use of epoxides (middle structure).

In contrast to the rather simple substrates ethylene and propylene, structurally more demanding olefins cannot be epoxidized under such heterogeneous conditions as the low tolerance towards functional groups of these catalysts results in side reactions and hence in a low epoxide yield.[61] Due to the complexity and the synthetic effort of the respective precursor, high epoxide selectivities are pursued, which do not meet with the characteristics of heterogeneous epoxidation processes. Thus, sophisticated catalytic approaches with a high tolerance to functional groups are required. Commonly, transition-metal based catalysis procedures are employed, which also offer the possibility to introduce chirality upon epoxidation of a C=C double bond.[62] 'Hydrocarbon-only' liquid olefins are epoxidized on a far smaller scale than ethylene or propylene, concluding that continuous processes are not economically promising. Despite their simplicity, these olefins are mostly epoxidized using environmentally concerning oxidants with expensive and non-recyclable catalysts, creating large amounts of chemical waste. This renders the price of the epoxides enormously high and

is ecologically questionable. Moreover, high quantities of concerning organic solvents are required to dilute the reaction mixture. The used stoichiometric oxidants are predominately peroxomonosulfate, *tert*-butyl hydroperoxide, percarbonic acids or hypochlorites, inevitably producing environmentally concerning by-products which must be regenerated or disposed (Figure 9). Molecular oxygen is by far the most affordable and abundant oxidant with an active oxygen content of theoretically 100%. However, in heterogeneous processes the oxidant efficiency is somewhat smaller due to some overoxidation of the olefin to CO_2 or aldehydes.[63] In homogenous catalysis with molecular metal complexes, only one oxygen atom can be transferred to the substrate while the other has to be removed from the catalyst by reducing agents in order to restore the catalytically active complex.[64] This leads to a drastically reduced atom efficiency, hence hampering a sustainable epoxide production.

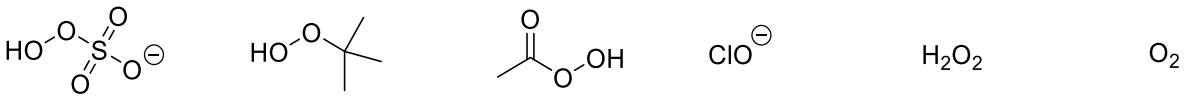

Figure 9: Common oxidants for the production of epoxides in uprising order of their active oxygen content by mass.

Hydrogen peroxide with an active oxygen content of 47% is the most atom-economic oxidant besides molecular oxygen and can be considered environmentally friendly as it releases water as only by-product. The production of hydrogen peroxide is conveniently performed by the anthraquinone process from equimolar amounts of hydrogen and oxygen in a two-step process (Scheme 2). First, anthraquinone is reduced over a heterogeneous palladium catalyst to anthrahydroquinone. In the next step, this intermediate is autoxidized with molecular oxygen to release hydrogen peroxide and regain the anthraquinone, re-entering the process. The H_2O_2 is then extracted with water.[65] H_2O_2 is commercially available in aqueous solutions up to 70 wt.% and considered stable in water at low temperatures. The major drawback of the aqueous hydrogen peroxide oxidant in organic reactions is the immiscibility with non-polar hydrocarbons, preventing desirable high reaction rates due to phase transfer limitations. Moreover, the environmental benign oxidant hydrogen peroxide requires a catalyst for its activation, whereas other oxidants provide sufficient reactivity by themselves. Hence, the use of hydrogen peroxide for the epoxidation of non-polar olefins with hydrogen peroxide requires a catalyst that i) facilitates the phase mediation beyond the interphase to overcome mass transfer limitations and ii) activates hydrogen peroxide for its use as oxidant.

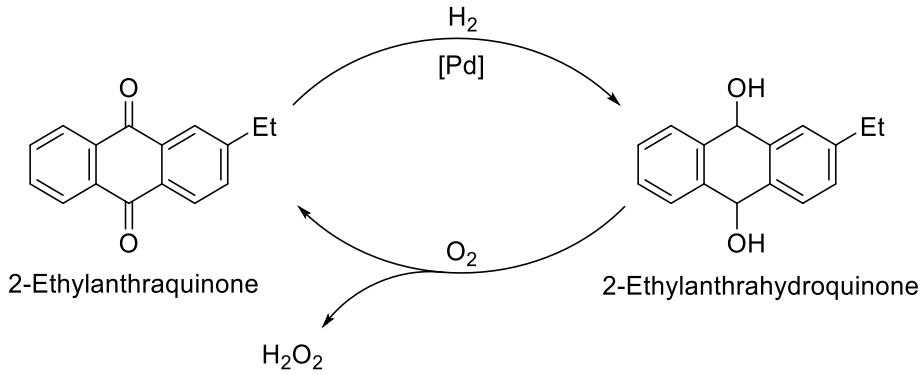

Scheme 2: Anthraquinone process for the indirect production of H_2O_2 from hydrogen and oxygen.

To not diminish the ‘green’ advantages of the use of hydrogen peroxide, the catalyst should ideally be recoverable and stable for its use over multiple runs. Especially biphasic reaction setups have been shown to be superior to single-phase approaches involving large amounts of organic solvents. The catalyst can easily be recovered in case that the aqueous oxidant and organic substrate/product phase are separated.

The design of sustainable concepts for the biphasic epoxidation of olefins is of utmost importance under the aspects of green chemistry. The historical developments and most recent advances on tackling of the issues with special regard to recyclability is evaluated in the following chapter.

1.5 Catalytic Biphasic Epoxidation using Hydrogen Peroxide

1.5.1 Overview

Most catalytic olefin epoxidations using hydrogen peroxide as oxidant are performed in monophasic systems and hence require large amounts of polar solvents such as acetonitrile, methanol or hexafluoroisopropanol.[66] Besides their high toxicities, the solvent complicates the product separation and catalyst recovery. The product is required to be extracted with even larger solvent quantities and to be further purified by distillation or chromatography for catalyst removal. As a result, the catalyst is decomposed or disposed in order to obtain a high purity product. This limited focus on the product avoids large-scale catalytic epoxidations beyond the laboratory scale. Moreover, due to the catalyst loss, it would be necessary to synthesize the catalyst in large quantities.

A recent review article by this author is published in the journal *Green Chemistry* and focuses on the supramolecular approaches towards catalyst recycling in biphasic epoxidations.[67]

In recent years, it has been shown that a biphasic system consisting of a substrate phase and aqueous hydrogen peroxide phase is advantageous for catalyst recycling due to the phase separation, ideally with the catalyst and the substrate present in different phases.[68] Transition metal oxides based on Nb, Mo or W gained wide interest in biphasic liquid/liquid oxidation reactions using hydrogen peroxide as oxidant.[69][70] In combination with suitable organic cations mediating their solubility in the organic phase, high catalytic activities were reported.[71] As the metalates are of an anionic nature, the charge compensation by organic cations leads to supramolecular assemblies in solution. Depending on the bulkiness and hydrophilic/lipophilic ratio of the cation, micellar aggregates are formed, which are either of classic constitution with a hydrophobic core (oil-in-water micelles) or contain the polar metalate inside a hydrophilic core in an inverse fashion (water-in-oil micelles) (Figure 10). This way, the phase behavior can be directed by the choice of the cation, enabling the solubilization of the substrate in the aqueous phase or the solubilization of the catalyst and oxidant in the substrate phase. Moreover, the solubility and hence the catalytic activity is greatly tuneable by the choice of the anion/cation and the combination thereof.

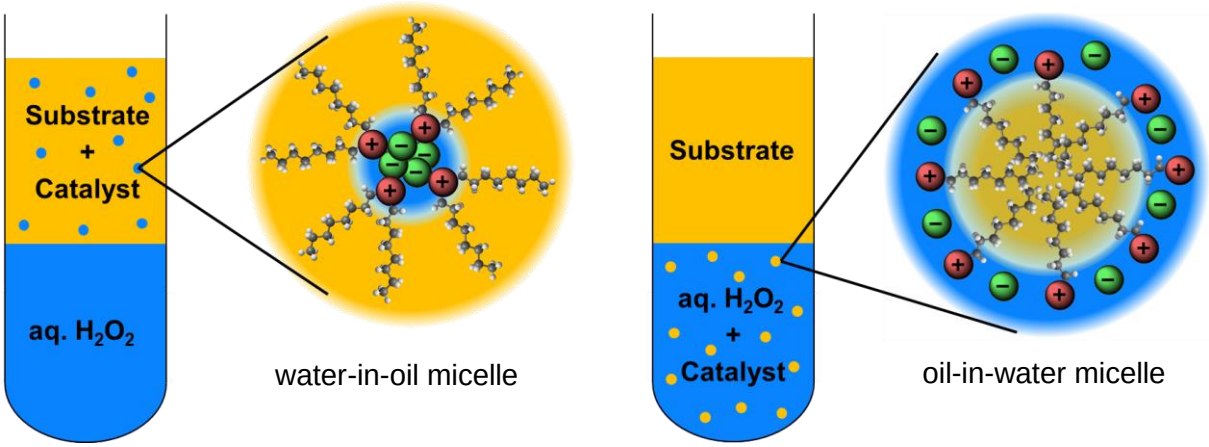

Figure 10: Schematic representation of the supramolecular biphasic epoxidation strategies. Left: transfer of H_2O_2 and the catalyst into the organic phase. Right: solubilization of the olefin in the aqueous phase by micelles.

1.5.2 Epoxidation in the Organic Phase

Most reports on in the last decades focused on the epoxidation of the olefin in the organic phase. Here, the focus was rarely set on the catalyst recycling but rather high catalytic activities were in the spotlight of research. The transfer of the anion into the organic phase increases its reactivity as polar interactions, required for the activation of H_2O_2 and the transfer of an oxygen to the olefin, are generally intensified in a hydrophobic environment. Depending on the nature and size of the cation and the charges to be compensated, the active center is completely encapsulated in a hydrophobic nano-environment.[72] Due the interactions of the organic shell

with the substrate, the catalytic performance may be enhanced, as the hydrophobic olefins interact more intensively with the hydrophobic environment than the respective more polar epoxides.[73] This creates a driving force for the substrate to be attracted to the supramolecular assembly, and a repulsion of the product. Due to the plurality of negative charges to be compensated by organic cations, polyoxometalates (POMs) gained wide interest in the design of catalytically active catalysts. Most catalytic epoxidations involving POMs are based on the initial concepts by Venturello et al.[74] Tungstic acid and phosphoric acid form the two-component POM $[PO_4(WO(O_2)_2)_4]^{3-}$ in aqueous hydrogen peroxide. At first, it was exploited as a highly reactive stoichiometric oxidant in olefin epoxidation reactions. In combination with a suitable quaternary ammonium salt like the esteemed phase-transfer agents trioctylmethylammonium (Aliquat® 336), di(hexadecyl)dimethylammonium (Aliquat® 206) or di(hexadecyl)ammonium chloride (Arquad® 2HT), the POM is transferred to the organic substrate phase, where the epoxidation reaction takes place. Investigations by X-ray diffraction analysis revealed that the active species consists of a phosphate center connecting the four tungstate groups carrying two side-on peroxo groups each.[75] This peroxide is of sufficient reactivity to transfer an oxygen atom to the substrate until all peroxo-groups are consumed. It was soon found that the active species can be regenerated *in situ* upon addition of fresh H_2O_2, enabling a catalytic application of the Venturello-anion $[PO_4(WO_3)_4]^{3-}$ under biphasic conditions. A variety of olefins were reported to be successfully epoxidized under mild conditions using large quantities of 1,2-dichloroethane or benzene as solvents to dilute the organic phase.[76]

In 1988, Ishii et al. discovered that phosphatododecametalates $[PM_{12}O_{40}]^{3-}$ (M = Mo, W) can be used similarly as catalysts for the biphasic olefin epoxidation in combination with surface-active cetylpyridinium (CP) counterions.[77] Initial investigations on the isolation of the corresponding peroxo-Keggin-type POM $[CP]_3[PMo_{12}O_{34}(O_2)_6]$, showed that it can also be used as a stoichiometric oxidant for the epoxidation of olefins,[78] but soon it was found that the oxidant precursor $[CP]_3[PMo_{12}O_{40}]$ is able to operate as a catalyst under biphasic conditions using H_2O_2 as well. Upon *in situ* formation of the peroxo-POM in the aqueous hydrogen peroxide phase, the aggregate is expected to be transferred to the organic phase, but spectroscopic investigations on the active species have shown that not the whole peroxo-Keggin-type POM itself is transferred to the organic medium, but rather fragments thereof like the smaller Venturello-anion.[79][80] Under the influence of hydrogen peroxide, the catalytically active species are formed by a disassembly of the original PW_{12}-POM, responsible for the epoxidation of the olefin in the organic phase. Spectroscopic investigations by means of Raman, ^{31}P- and ^{183}W-NMR-spectroscopy of the Ishii-system showed that the catalyst $[CP]_3[PW_{12}O_{40}]$ not only disassembles during the reaction, but also reassembles to $[PW_{12}O_{40}]^{3-}$ and its derivative $[PW_{11}O_{39}]^{7-}$ by formation of W-O-W bonds after catalysis upon consumption

of the H_2O_2.[81] The so-called Venturello-Ishii-system for olefin epoxidation was exploited as a model for further improvements and in further studies, especially the problematic and difficult recycling of the catalyst due its solubility in both, the organic and aqueous phase, was tackled.

One of the most prominent aims of catalyst recycling is its convenient separation by purely mechanical techniques, e.g., filtration of a precipitated catalyst. For example, a **temperature-controlled** recycling approach was presented by Neumann et al. in 2003.[82] Polyfluorinated quaternary ammonium ions $[CF_3(CF_2)_7(CH_2)_3]_3CH_3N^+$ as counterparts of the highly active sandwich-type POM $[WZnMn_2(H_2O)_2(ZnW_9O_{34})_2]^{12-}$ were applied in the biphasic epoxidation of various olefins using hydrogen peroxide and a toluene/substrate overlayer. In the beginning, the catalyst is insoluble but upon a temperature increase to 60-80 °C, the catalyst gets fully soluble in the organic phase. After full conversion, the cooling of the reaction mixture results in the desired catalyst precipitation, enabling its simple separation from the reaction mixture by filtration. Another example for temperature-controlled precipitation was presented by Ikegami et al., exploiting the lower critical solution temperature of a cationic poly(*N*-isopropylacrylamide)-based polymer with the Keggin-type POM $[PW_{12}O_{40}]^{3-}$.[83] The polymer dissolves in aqueous hydrogen peroxide at elevated temperature and emulsifies the organic substrate and the oxidant phase. Upon cooling, the emulsion separates quickly and allows for a recovery of the polymeric catalyst. Hou et al. synthesized a derived polymeric catalyst based on the lacunary POM $[PW_{11}O_{39}]^{7-}$.[84] The combination with quaternary PEG-functionalized ammonium cations as counterions have been shown to result in an active catalyst for the epoxidation of cyclooctene in a biphasic mixture of 30 wt.% H_2O_2/EtOAc. Despite the self-precipitation of the catalyst at 0 °C after the reaction, the authors observed a leaching of tungstate, decreasing the recyclability of the catalyst. After three consecutive catalytic runs, the activity in cyclooctene conversion reduced noticeable and dropped significantly after six catalytic runs. Concluding, the rare number of examples for temperature-controlled catalyst precipitation underlines the difficulty to design such catalysts.

Apart from the catalyst separation by the stimulus temperature, numerous studies focused on the catalyst separation by **reaction-controlled** precipitation. Upon formation of side-on peroxo groups on POMs in presence of hydrogen peroxide, the catalyst solubility increases in non-polar media such as the substrate due to the higher coordination number of the tungsten atom and the weakened intermolecular interactions. This effect was first exploited by Zuwei et al. in 2001.[85] There, a reaction-controlled recycling driven by the different organic solubility of the Venturello-derived catalyst $[CP]_3[PO_4(WO_3)_4]$ and its corresponding activated peroxo-counterpart $[CP]_3[PO_4(WO_2(O_2))_4]$ was reported. Upon full conversion of the H_2O_2, consequently only the insoluble species is present and precipitates from the mixture. With this approach it is possible to epoxidize cyclohexene and 1-hexene using aqueous H_2O_2 with

selectivities over 87% at full conversion with respect to the reaction-limiting hydrogen peroxide stoichiometry (olefin:H_2O_2 = 3:1). The authors also studied the influence of the organic cation by their size on the catalyst performance and the recycling. Application of tetrapropylammonium counterions result in an insoluble catalyst, limiting the conversion of the substrate. Octadecyl-benzyldimethylammonium cations provide a perfectly good soluble catalyst with great catalytic performance, however, it does not precipitate after complete H_2O_2 consumption. These comparisons show that the stimuli-responsiveness of the catalyst has to be tailored and the cation has to be aligned to the anion in order to obtain a reaction-controlled precipitating catalyst. Hence, the simple and "old reliable" Venturello-Ishii epoxidation still provides room for optimizations as the impact of the organic cation has not been considered besides the phase-transfer into the organic phase. Therefore, the cation must be tailored to the catalytically active anion to allow for sustainable recycling procedures.

The transfer of the POMs into the organic phase upon formation of inverse micelles by several phase transfer catalysts was postulated to be a major contribution to the high reaction rate.[86] Neumann and Khenkin suggested in 1994 the existence of inverse (water-in-oil) micelles formed by cetyltrimethylammonium (CTA) cations with microscopic techniques.[87] They used an organic, water-soluble dye and investigated the 1,2-dichloroethane layer. Small, colored droplets of the size of 5 µm which turned out to be inverse micelles formed by the long-chain quaternary ammonium cations incorporate aqueous hydrogen peroxide and are likewise responsible for the transfer of the catalytic active anion into the organic phase. The use of tetrahexylammonium chloride as surfactant did not lead to an inverse micellar environment and explains a drastically decreased reaction rate for the epoxidation of 1-octene with the Venturello-anion $[PO_4(WO_3)_4]^{3-}$. Comparison of the activities of different quaternary ammonium cations in the biphasic epoxidation of olefins shows that the reaction rate is dependent on the number of carbon atoms of the counterion. Aliquat® 336 (trioctylmethylammonium chloride) has shown to be superior to the cetyltrimethylammonium and tetrabutylammonium cations in terms of catalytic performance.[88]

The right choice of the cation is also crucial for the recycling strategy, which should be designed as simple as possible. Non-suitable cations might indeed yield higher reactivities but do not necessarily allow for a green recycling procedure. For example, Mizuno et al. combined the highly active silicodecatungstate $[\gamma\text{-}SiW_{10}O_{34}(H_2O)_2]^{4-}$ with tetrabutylammonium counterions for the epoxidation of terminal olefins using acetonitrile to create a homogeneous mixture.[89] The catalyst recycling was performed unsustainably by evaporation of all volatile components followed by washing with *n*-hexane, retaining the catalyst in >95% yield. In contrast, Ding et al. applied the related silicotungstate POM $[SiO_4H(WO(O_2)_2)_3]^{3-}$ for a reaction-controlled catalytic epoxidation allowing for the use of the more suitable dioctadecyl dimethyl

ammonium (DODA) cations.[90] The catalyst itself emulsifies both phases under the influence of aqueous H_2O_2 at elevated temperature and precipitates after the reaction, enabling an efficient recycling by filtration or centrifugation. These examples emphasize the importance of the correct cation choice for the anionic catalyst species and the impact on recyclability.

Completely surfactant-encapsulated clusters were first presented in 2000 by Kurth et al., when they covered the heteropolymolybdate $[H_3Mo_{57}V_6(NO)_6O_{183}(H_2O)_{18}]^{21-}$ with 20 dioctadecyldimethylammonium (DODA) cations.[91] Presumably, there are no catalytic applications due to the high grade of isolation of the potentially active POM core and there would be detrimental mass transport limitations. However, upon the use of the beforementioned smaller Keggin type POMs $[PW_{12}O_{40}]^{3-}$ (M = Mo, W), only three negative charges must be compensated by DODA cations and therefore yielding a less shielded POM. This aggregate shows a remarkably tendency towards self-assembly to supramolecular POM nanocones, visualized by optical and electronic microscopy techniques.[92] These structures are active in sulphide and alcohol oxidation as well as epoxidation of alkenes with excellent selectivities and high to moderate yields using aqueous H_2O_2.[93] The authors assume that the Keggin type POM known from the Ishii epoxidation does not disassemble to the Venturello anion upon peroxo-formation but rather stays intact due to the confined space within the DODA capsule. The major advantage of these nanocones in contrast to the bare Keggin type catalysts is the possibility to incorporate Fe_3O_4 nanocrystals in hydrophobic pockets of the assembled DODA cations. This enables a steering of the cones in an external magnetic field and paves the way for a magnetic recovery and recycling of the nanocones. A further Keggin-type silicotungstates-DODA assembly $(DODA)_4SiW_{12}O_{40}$ has been reported to form onion-like layered inverted vesicles, however, catalytic activities were not investigated but anticipated.[94]

Besides the casual catalyst separation by simple filtration, further sophisticated mechanical catalyst separations were presented without the need of a catalyst precipitation. An approach by nanofiltration has been investigated by Witte et al. They used the POM-based catalyst $[MeOct_3N]_{12}[WZn_3(ZnW_9O_{34})_2]$[95] for the epoxidation of cyclooctene and presented a strategy for the catalyst recycling by nanofiltration using a 5 nm pore γ-alumina membrane.[96] The organic layer of the biphasic mixture containing the catalyst, product and toluene was separated and pressurized in a nanofiltration cell, retaining >99% of the catalyst. Consecutive reactions were performed by dissolution of the retentate in toluene upon addition of H_2O_2 and cyclooctene, showing no loss of activity over six runs, but surprisingly an increased activity. The authors state that this might be explained by the removal of chloride anions from excess Aliquat® 336 ($[MeOct_3N]$ Cl) interfering with the reaction. Nevertheless, all above-mentioned catalytic systems require an organic solvent for an effective biphasic epoxidation of olefins

diminishing the environmental advantages of using the green oxidant hydrogen peroxide. Therefore, solvent-free systems are of high interest.

A solvent-free emulsification approach by exploitation of the surface-activity of a protic dodecylimidazolium ditungstate catalyst was presented by Huang et al.[97] The catalyst emulsifies the aqueous H_2O_2 and the cyclooctene phase without any need of further solvents. After the reaction, the catalyst conveniently precipitates and can be recovered and reused for three runs, however, with noticeable loss of activity. Another solvent-free epoxidation creating a microemulsion has been presented by Kozhevnikov et al. in 2003.[98] A non-ionic surfactant (Brij 30) in combination with the Venturello-anion were added to the biphasic reaction mixture of 1-octene and H_2O_2 (with a ratio of olefin/oxidant = 27:4) to form a one-phase microemulsion. The reaction rates are comparable with standard tungstate-based PTC systems,[99] but disadvantageous is the small conversion of the olefin as the hydrogen peroxide is the limiting component, enabling a maximum yield of 15% epoxide at full H_2O_2 conversion. An increase in the amount of oxidant results in the break of the microemulsion as presented by a phase diagram. The quantitative epoxidation of the 1-octene would result in a much higher polarity of the system, which cannot be stabilized by the microemulsion. Nevertheless, upon addition of new substrate and hydrogen peroxide, the reaction restarts and the accumulating water problem was tackled by ultrafiltration, retaining >90% of the catalyst. The filtrate composing of substrate/epoxide and water can be purified by energy-intensive distillation.

The recycling of dissolved ionic catalysts proves to be rather difficult to design, for which reason the immobilization of the cationic counterions on an inorganic silica support have been investigated. Due to the electrostatic interactions, the catalytically active POM is similarly immobilized on the surface of the solid support, in theory allowing for a facile catalyst recycling. However, this opens up to other problems such as mass transport limitations and still the catalyst leaching cannot be completely avoided by these immobilization approaches.[100][101][102] Ionic liquids (ILs) can be exploited as a reaction medium to dissolve and immobilize the catalyst therein, which allows for the catalyst recovery by phase separation. The ILs can further stabilize the molecular catalysts and prevent their decomposition. Moreover, different mechanistic pathways may be supported which allow for unique new catalyst reactivities.[103] Cokoja et al. discovered the activation of hydrogen peroxide by the simple perrhenate anion in ILs. Perrhenate has been considered inactive in oxidation catalysis and rather a dead end of the highly active homogeneous methyltrioxorhenium epoxidation catalyst.[104] In ionic environments, the activation of hydrogen peroxide is achieved via an outer-sphere mechanism by H-bond interaction of the perrhenates' oxo-groups with the H_2O_2 hydrogen atoms, sufficiently strong enough for alkene epoxidations at elevated temperature.[105] This was investigated by several spectroscopic techniques and is supported by DFT calculations. The

reactivity of perrhenate salts towards H_2O_2 in ionic liquids was exploited to epoxidize cyclooctene with good activities in the ILs 1-octyl-3-methylimidazolium tetrafluoroborates [OMIM] [BF_4] or bis(trifluoromethylsulfonyl)imide [OMIM] [NTf_2]. Upon synthesis of the single-component catalyst [OMIM] [ReO_4], excellent olefin conversions and epoxide selectivities were achieved within 4 h.

The perrhenate was also found to not be exclusively active in ILs but also as components of a supramolecular ion pair (SIP). These assemblies based on amidoammonium salts were initially developed by Tasker, Sole et al. for extraction of halidometalates into the organic phase by formation of host-guest complexes.[106][107] This concept was adapted by Cokoja, Love et al. for catalytic biphasic epoxidations using aqueous H_2O_2 with the perrhenate anion as catalytically active species.[108] Perrhenate as part of a SIP is transferred into the solvent-free substrate phase and due to the ionic and polar interactions inside of the SIP capsule, the perrhenate anion activates hydrogen peroxide via the H-bond outer-sphere mechanism resulting in high olefin conversions at mild conditions within 8 h at 70 °C. Supplementary DOSY-NMR studies confirm that the SIPs are formed in the organic phase and can be regarded as rather stable assemblies.

Besides the perrhenate anion, metal-free compounds such as alcohols were reported for the activation of hydrogen peroxide. Jacobs et al. discovered that phenol applied as solvent in the epoxidation of olefins is able to activate hydrogen peroxide for a metal-free epoxidation of non-polar olefins.[109] Detrimental for a large-scale process is the toxicity of the large quantities of phenol required and the very intricate separation of the epoxide from the catalyst. Neumann et al. discovered that fluorinated alcohols are likewise able to activate hydrogen peroxide via H-bonds.[110] 1,1,1,3,3,3-hexafluoroisopropanol (HFIP) and 2,2,2-trifluoroethanol (TFE) used as solvents achieve high olefin conversions. For a better understanding of the requirements for a successful H_2O_2 activation by these solvents, Berkessel investigated the fundamental mechanism by DFT and found that a multiple H-bond network is responsible for the activation of H_2O_2.[111] Deeper investigations by molecular dynamics studies reveal that intrinsically the activity arises from the formation of a micro-heterogeneous system with small substrate domains inside a fluorinated alcohol capsule in aqueous H_2O_2.[112] Small-angle X-ray scattering experiments support these findings. The major drawbacks of this H_2O_2 activation are the requirement of large equivalents of the fluorinated alcohol, which is harmful to the environment. Based on the fluoroalcohol activity in H_2O_2-activation, a metal-free dendritic catalyst has been presented by Berkessel et al.[113] A high concentration of fluorine groups in proximity to hydroxyl groups on the dendrimers surface enabled for the first time the use of catalytic amounts of fluoroalcohols and a catalyst recovery by ultrafiltration. Upon twofold reuse, the activity was

maintained and this shows the potential to replace ecologically harmful and expensive solvents for H_2O_2-activation by designed supramolecular catalysts.

1.5.3 Epoxidation in the Aqueous Phase

In general, the catalyst activity in olefin epoxidation is strongly dependent on the reaction medium. The catalytic epoxidation taking place in the organic phase benefits from a high concentration of both, substrate and catalyst, resulting in an enormously high activity. Despite the facilitated product and catalyst separation, epoxidations in the aqueous oxidant phase are somewhat lower in activity. Still, a perfect catalyst recyclability could compensate for the low reactivity, especially in a continuous process, where the product phase is free of solvent and catalyst. The approach to separate the catalyst and to yield a catalyst-free product without intricate work-up is rather simple when the catalyst remains in the aqueous oxidant phase. The substate is required to be solubilized therein, achieved by supramolecular aggregates which transfer the olefin from the supernatant organic phase. In terms of recycling, it is advantageous to use this biphasic approach to 'immobilize' the catalyst in the aqueous oxidant phase while the substrate/product phase forms a supernatant organic overlayer, which can easily be removed by decantation. However, the catalytic epoxidation of olefins in the aqueous phase is investigated to a far smaller extend.[70] In first reports, olefins were epoxidized in aqueous solutions with manganoporphyrin-based catalysts in micelles formed by commercially available surfactants such as CTAB or Brij 35. The catalyst as well as the olefin are solubilized inside the micelles, exploited as nanoreactors.[114] Soon it was found that the reactivity could be increased by tailoring the porphyrin ligand to be more attracted to the ionic micellar interphase by derivatization with cationic quaternary ammonium groups. The ionic interaction leads to a repulsion from the hydrophobic core and the catalyst shows a higher affinity to the micellar surface, where it is more likely to interact with the oxidant hypochlorite.[115] Heijnen et al. were able to render the micellar catalysis with manganoporphyrin catalysts 'greener' by use of hydrogen peroxide, releasing water as only by-product.[116] A greater progress is achieved with another micellar approach, exploiting the assembled surfactants as catalysts themselves.[117] The successful design of a single-component surface-active catalyst with the ability to both, micelle-formation and oxidant activation, is highly challenging. A covalently bound catalytically active motif to the surfactant molecule turned out to yield superior catalysts in terms of both activity and recyclability. In this case, the catalysts are immobilized on the micellar surface. This has the advantage of a major acceleration of the reaction rate, as the catalyst is not trapped inside the micelle but in the micellar pseudo-phase, where the reaction is expected to occur (vide supra).

Based on the abovementioned H_2O_2-activation by perrhenate in ionic liquids[105] and supramolecular ion pairs,[108] Cokoja et al. investigated the catalytic performance of several micellar imidazolium perrhenate ionic liquids in aqueous hydrogen peroxide.[118] Catalytic application of 5 mol-% of the imidazolium perrhenates revealed the formation of micelles in aqueous hydrogen peroxide with the ability to dissolve the model substrate *cis*-cyclooctene (COE) therein, with simultaneous H_2O_2 activation by the perrhenate anion in this micellar environment under mild conditions (full conversion after 8 h at 70 °C). The surface-active perrhenate catalysts were prepared in a one-step anion exchange procedure from the corresponding imidazolium bromides, but the question arose if it is possible to use a commercially available ionic liquid and add a perrhenate salt to achieve an *in situ* anion equilibrium to form catalytically active micelles. Therefore, [OMIM] [BF_4], which does not show any significant catalytic activity but micelle formation, was added with equimolar amounts of $KReO_4$ (5 mol%) to a biphasic mixture of cyclooctene and aqueous hydrogen peroxide. Remarkably, the catalytic activity is higher for the salt/IL mixture than for the pure synthesized [OMIM] [ReO_4] catalyst.[119] The surface-active imidazolium perrhenate catalysts show an remarkably high recyclability over ten runs without any loss of activity, but the high costs of the perrhenate limits their use beyond the laboratory scale. Nevertheless, it was shown that the catalytic activity clearly correlates with the IL's tendency to form micelles as the CMC decreases with the length of the imidazolium alkyl chain group, resulting in a higher micelle concentration and less dissolved surfactant molecules.[120] The knowledge of the respective catalyst's CMC is crucial to predict the catalytic performance. The CMC of several imidazolium ionic liquids in 50 wt.% aqueous hydrogen peroxide were investigated by Jess et al.[121] The results show that the CMCs are approximately factor five lower compared to water at the same temperature, which can be attributed to the difference in solvation of the surfactant molecules by the respective media.

Besides the excellent micelle formation, imidazolium ionic liquids have been shown to highly interact with organic molecules in aqueous systems. Kragl et al. investigated the complex formation of 1-butyl-3-methylimidazolium ionic liquids and acetophenone in water.[122] Its solubility in water was increased by the factor of 10 compared to the absence of IL. Great solubilization effects can be achieved using surface-active imidazolium ionic liquids beyond their CMC. Hupka et al. investigated the uptake of aromatic compounds into micelles formed by 1-alkyl-3-methylimidazolium chlorides [RMIM] Cl.[123] It could be shown that this class of surfactants is superior in solubilization compared to other commercial ionic surfactants such as sodium dodecylsulfate (SDS) or cetyltrimethylammonium bromide (CTAB). Still, the question arises, if these simple commodity surfactants might be used in combination with catalytically active salts to allow for the epoxidation of olefins in aqueous hydrogen peroxide. This simple approach sounds promising; however, it is worth to keep in mind that anionic

micelles formed by SDS or similar will electrostatically repulse the negatively charged catalyst ions from the micellar interface. Moreover, the dodecylsulfate anion hydrolyzes in slightly acidic media, which hydrogen peroxide certainly is, to 1-dodecanol and hydrogensulfate.[124] This will ultimately result in an even higher acidity, negatively affecting the epoxide selectivity due to ring-opening side reactions. In contrast, the cationic surfactant CTAB is stable and shows a high affinity to anions but unfortunately is not compatible with hydrogen peroxide as halide anions decompose H_2O_2 violently at elevated temperatures in the reactivity order (I^- > Br^- > Cl^-).

Therefore, it is required to synthesize the desired catalyst as a combination of suitable surface-active cations and the catalytically active anions. Surface-active 1-alkyl-3-methylimidazolium salts are known for the excellent micelle formation in aqueous media and the wide functionalizability of the imidazolium head group to allow for a fine tuning of the micellar structure and the anion interactions.[125][126][127] The respective imidazolium bromide precursors are easily synthesized by reaction of 1-methylimidazole with the equimolar amounts of the corresponding alkyl bromide under solvent-free conditions. Simple purification in vacuo and a consecutive anion exchange procedure allows for the synthesis of surface-active catalysts with any water-soluble anion upon application of its corresponding *Brønsted*-acid.

In summary, surface-active imidazolium ionic liquids are the perfect candidates as surfactants for micellar catalysis in aqueous hydrogen peroxide. They are simple to synthesize with respect to the cation functionalization and the choice of the anion, they are stable under oxidative conditions and form micelles, which solubilize large quantities of non-polar compounds in the aqueous phase. The cationic micelles formed by the imidazolium cations bear a layer of anions to compensate the electrostatic field. By combination of the imidazolium with a catalytically active anion, a high catalyst concentration at the oil/water interface is obtained. This could lead to high reaction rates which might render this micellar epoxidation approach superior to epoxidations in the organic phase. Moreover, the catalyst remains in the aqueous phase and is therefore easily separated from the product and recovered. This paves the way for a continuous process, which is highly attractive for the epoxidation of liquid, non-polar olefins.

2 Motivation and Goals of the Thesis

The goal of the thesis is the design of supramolecular catalysts for the conversion of hydrophobic substrates with polar reactants in water. A bifunctional catalyst design is required to i) overcome phase transfer limitations due to the immiscibility and ii) activate the reactants. The epoxidation of 'hydrocarbon-only' olefins with hydrogen peroxide will be exploited as a model reaction to investigate the supramolecular concepts for catalytic applications. The biphasic epoxidation is of great industrial and academic interest due to the possibility to substitute toxic organic solvents by water, and environmentally concerning oxidants by hydrogen peroxide. This approach requires the solubilization of olefins in water, as well as the activation of hydrogen peroxide for its use as oxidant. Most important, the catalyst should be perfectly stable and quantitatively recoverable by simple techniques. This could previously not be achieved in homogeneous epoxidation as the catalyst is decomposed upon separation of the valuable epoxide from the one-phase reaction mixture. Hence, retaining the catalyst in the aqueous phase facilitates the separation of the solvent-free product phase and opens the opportunity to recover the catalyst for further runs. The variety of supramolecular concepts allows for a targeted catalyst design addressing task-specific applications and fundamental requirements. Among the most prominent approaches towards the solubilization of non-polar substances in water is the use of micellar solutions. Micelles are supramolecular assemblies of surfactants with a hydrophobic interior and a polar shell. This constitution allows for an uptake of olefins into the micellar interior, while being solubilized in the aqueous phase. The integration of a catalytically active structural motif into the surfactant molecule results in a bifunctional catalyst, meeting both essential premises for biphasic catalysis.

Recent investigations have shown that surface-active imidazolium perrhenates assemble to micelles in aqueous hydrogen peroxide and effectively solubilize the olefin therein. Most important is the activation of H_2O_2 by the perrhenate anion, which was considered inactive in oxidation catalysis, but is able to activate hydrogen peroxide in ionic environments.[118] DFT calculations support the spectroscopically found evidence that the transfer of the oxygen to the olefin occurs via an outer-spere H-bond mechanism.[105] The central rhenium atom is not directly involved in bond formation, but electronically and structurally affects the oxo-ligands.

At this point, several questions arise and are answered in the following chapters of this thesis. One of the most important question towards the anion's reactivity is:

"Can the concept of H_2O_2-activation by perrhenate in biphasic mixtures be transferred to other element-oxo-anions?"

Several promising metal-based and metal-free oxo-anions will be investigated for the activation of hydrogen peroxide in combination with surface-active imidazolium or supramolecular receptor cations. In each case, the fundamental mechanism of the H_2O_2-activation will be studied by analytic methods such as ESI-MS, NMR- or IR-spectroscopy. The catalyst activity is investigated by kinetic investigations of the epoxidation of the model olefin *cis*-cyclooctene. A major contribution to the potential of the catalyst is the solubilization of the olefin in the aqueous phase. Hence, besides the catalytic activity of the anion, the question regarding the structural influence of the cation must be addressed:

"What is the influence of the cation's substitution pattern and the cation-anion-combination on the assembly formation and the olefin interaction?"

The structural effects of the micelle-forming imidazolium and supramolecular receptor cations on the phase-behavior, aggregate size and olefin uptake of the supramolecular assembles is investigated by means of TEM, DLS and solubility measurements. A structure-property relationship investigation by alteration of decisive substituents must lead to a general conclusion of the optimal cation structure. Moreover, the limits of the functionalizability must be elucidated. Here, the solubility in the organic phase as well as the critical surfactant properties for the assembly process are required for a targeted design of the supramolecular catalysts. The assembly formation as well as the phase solubilities will determine the catalyst presence during and after the completed reaction. To round the green character of the developed catalysts off, a perfect stability and recovery of the catalyst is required, paving the way for an industrial application. The corresponding question is addressed to all catalysts developed in this project:

"Do the supramolecular catalysts allow for a simple recycling procedure and how can the catalyst constitution facilitate this process?"

For the micellar catalysts operating in the aqueous phase, a recycling strategy will be investigated, which is based on the facile separation of the organic phase by decantation. The residual micellar solution is investigated for further catalytic uses by evaporation of the water and addition of fresh hydrogen peroxide. The conclusions of the structure-property studies, especially on the phase and solubility behavior, might provide a basis to exploit the change of the chemical environment for a targeted collapse of the micelles at the end of the reaction, in absence of substrate or at a somewhat lower hydrogen peroxide concentration. Moreover, the influence of the temperature on the surfactant aggregation should be exploited to control the micelle formation.

3 Results and Discussion

3.1 Olefin Epoxidation with Micellar Imidazolium Tungstates

3.1.1 Publication Details and Author Contributions

Major results of this chapter have been published in the article “Ionic liquid surfactants as multitasking micellar catalysts for epoxidations in water” in *Catalysis Science & Technology* **2020**, volume 10, issue 13, pages 4448-4457.[128] The manuscript was submitted on April 3rd 2020 and accepted on June 9th 2020.

Dr. Carsten Peters is thanked for the recording of the cryo-TEM images and development of a blotting procedure for aqueous hydrogen peroxide. Bastian Zehner conducted the tensiometry measurements. The help of Maria Matthews in optimizing the ^{183}W-NMR pulse sequence is acknowledged.

3.1.2 Introduction

The epoxidation of olefins with molecular catalysts is reported for a variety of transition metals and complexes thereof.[129][130] Suitable oxidants are for instance molecular oxygen, *tert*-butylhydroperoxide, hypochlorites or hydrogen peroxide. Under the aspect of sustainability, only hydrogen peroxide with water as side product can be considered ‘green’ as the other oxidants require sacrificial organic reducing agents (e.g., aldehydes for the reaction of O_2’s second oxygen) or release waste compounds as by-products. Hydrogen peroxide is most conveniently activated by transition metals, preferably by group 6 metal oxides.[70] The epoxidation of olefins with molybdates and tungstates using hydrogen peroxide has been widely investigated and reported.[131] These simple oxides do not require sophisticated organic ligands, are stable under catalytic conditions, and dissolve in the polar aqueous hydrogen peroxide phase. There, the metalates react to (peroxo)metalate species with hydrogen peroxide and are then transferred to the organic substrate phase by aid of surface-active cations forming supramolecular assemblies. The peroxo groups show a high reactivity towards olefins in the non-polar organic environment by transfer of the active oxygen atom to the substrate. The ‘used’ catalyst is then transferred back and regenerated in the aqueous phase. However, this phase transfer catalysis approach requires large amounts of organic solvents to dilute the organic phase and to buffer the strong polarity change upon substrate epoxidation affecting the catalyst solubility. Despite the simple phase separation, the product phase has to be purified by distillation to obtain the epoxide, inevitably leading to catalyst loss.

The epoxidation of olefins by the highly active tungstate anion in aqueous hydrogen peroxide is of high interest but has not been reported to date. To avoid the catalyst operation in the organic phase the micellar catalysis approach exploiting the olefin transfer into water by surface-active cations as counterions of the tungstate anions is investigated. Due to the electrostatic immobilization of the tungstate anions on the cationic micellar surface and the high local concentration of catalyst in the micellar pseudophase, a high reactivity is expected. Hence, the micelle formation, substrate solubilization and epoxidation kinetics of olefins by imidazolium tungstates with varying alkyl chain length is investigated by means of tensiometry, cryo-TEM and kinetic catalysis experiments. Furthermore, the mechanistic nature of the tungstate anions and the influence of boosting phosphonate additives are investigated by ^{183}W-NMR spectroscopy and ESI-MS measurements.

3.1.3 Results and Discussion

Synthesis of surface-active imidazolium tungstates

Several imidazolium tungstate ionic liquids with varying alkyl chain lengths of the general formular $[RMIM]_2[WO_4]$ (R = Bu, Oct, De, Do) were synthesized according to an adapted anion exchange procedure, which has proven to be suitable for ionic liquids.[132] Dilute aqueous solutions of the corresponding imidazolium bromide precursors [RMIM] Br are slowly rinsed over freshly regenerated anion exchange resin Amberlite® IRA 402, a slight excess of tungstic acid is added to the eluated imidazolium hydroxide solution, and is stirred for several hours at room temperature. This approach is enormously efficient and atom-economic as tungstic acid does not dissolve in neutral media but exclusively in basic solutions. Therefore, the hydroxides are neutralized till pH = 7 is reached, standing for full conversion to the desired imidazolium tungstates. The excess solid tungstic acid can be filtered off and recovered. Removal of the water in vacuo results in liquid colorless oils which are further dried overnight using a turbomolecular pump (final vacuum 10^{-6} mbar) to remove residual water. Due to the high hygroscopicity, the obtained wax-like solids are stored under a purified argon atmosphere until further use. ^{1}H- and ^{13}C-NMR spectroscopy in heavy water shows the excellent purity of the ionic liquids and the desired constitution of the 1-alkyl-3-methylimidazolium cation. ^{183}W-NMR spectra confirm the mononuclear nature of the tungstate anion. This aspect is of special importance due to the absence of formation of polyoxotungstates, which aqueous solutions of tungstate salts are well-known for. These species would easily be transferred to the organic phase by formation of inverse micelles due to the multianionic nature. The success of the quantitative bromide to tungstate exchange is confirmed by elemental analysis by results of the products perfectly matching to the calculated values.

Surfactant Characteristics

The imidazolium tungstates are fully miscible with water in all proportions and show a moderate solubility in chlorinated solvents such as dichloromethane and chloroform. The immiscibility with aliphatic and aromatic hydrocarbons is prone for a biphasic epoxidation in aqueous phase. Micelle formation by surface-active imidazolium ionic liquids is reported,[133][134] but still an analytic proof of surfactant aggregation in aqueous hydrogen peroxide has to be provided. Tensiometry and conductivity measurements of the IL solutions in 50 wt.% H_2O_2 show the desired surfactant aggregation for the octyl-, decyl-, and dodecyl derivatives with decreasing CMC (Table 1). Both methods are in good agreement and show the drastic influence of the alkyl chain length on the aggregation behavior. $[BMIM]_2[WO]_4$ does not show micelle formation up to an investigated concentration limit of 500 mmol/L. [BMIM]-based ILs are considered to aggregate at somewhat higher concentrations above 2 mol/L without formation of micelles.[135]

Table 1: CMCs of $[RMIM]_2[WO_4]$ ILs in 50 wt.% H_2O_2 at 50 °C with R = Oct, De, Do.

Catalyst	CMC [mmol/L] by tensiometry	CMC [mmol/L] by conductometry
$[OMIM]_2[WO_4]$	31.9	31.1
$[DeMIM]_2[WO_4]$	5.4	5.1
$[DoMIM]_2[WO_4]$	1.9	2.1

Both techniques confirm the aggregation of the ionic liquid surfactant to supramolecular structures, but not necessarily the formation of spherical micelles. To investigate the microscopically heterogenous solution with expected assembly sizes smaller than 100 nm, transmission electron microscopy (TEM) was exploited. Investigations of molecular and biologic assemblies in aqueous systems are routinely performed in various fields of biology with TEM techniques.[136] There, the matrix of the sample is stained using a heavy metal salt solution, likely uranyl acetate. The molecular light-weight assemblies could then be observed as bright dots detected by the CCD-sensor. In the case of the imidazolium tungstates, the counterion is sufficiently heavy to show the micelles as dark spots on a bright background, making the staining procedure redundant. However, the evaporation of the solvent in the required high vacuum leads to a collapse of the micelles as the surfactant concentration is gradually increased until exclusively the non-volatile IL remains. Due to this circumstance and the dynamic behavior of the surfactant assemblies, the special technique cryo-TEM is exploited to freeze the diffusion and motion of all compounds in their equilibrium state. The sample solution is transferred onto a copper mesh TEM-grid and automatically blotted with filter paper to obtain a thin film. This procedure is conducted under humidity >80% to avoid water evaporation and at 50 °C to achieve the assembly equilibrium state of the micelles at

elevated temperature. The film is frozen onto the grid by rapid immersion of the sample into liquid ethane at below −180 °C within milliseconds. The grid is then transferred into liquid nitrogen and kept below −150 °C during transfer, microscope evacuation and imaging. The absence of disturbing water crystals formed during the freezing procedure nicely shows that aqueous hydrogen peroxide is superior to commonly used water, providing an excellent homogeneous matrix.

Solutions of $[OMIM]_2[WO_4]$ and $[DoMIM]_2[WO]_4$ in 50 wt.% H_2O_2 are chosen to image the supramolecular micelle formation and swelling of the assemblies in presence of hydrocarbons. Concentrations of 178 and 357 mmol/L were investigated as these are above the CMC and represent catalyst loadings of 2.5 and 5.0 mol-% (vide infra). The cryo-TEM images of $[OMIM]_2[WO_4]$ of the concentration 178 mmol/L in aqueous H_2O_2 nicely show that spherical micelles are formed upon surfactant assembly. Upon saturation of the micelles with the model substrate *cis*-cyclooctene (COE), the micelles grow in size due to the olefin uptake (Figure 11, left and right, respectively). The anion monolayer on the micellar surface gives sufficient contrast to investigate the particle size distribution and quantify the volumetric swelling of the micelles upon uptake of COE. The diameter of 200 randomly chosen micelles was measured for both cases and show a rather disperse size distribution, supporting the dynamic behavior of the micellar aggregates (Figure 12). From initially 16 ± 5 nm, the micelles swell to 21 ± 6 nm upon saturation of the aqueous phase with COE. To quantify the solubilization of COE in the aqueous phase by uptake into the micelle, the space occupied by the olefin is calculated. Since the micelles are not rigid structures but very dynamic in behavior, there is no void in the ‘empty’ micelles to be filled.

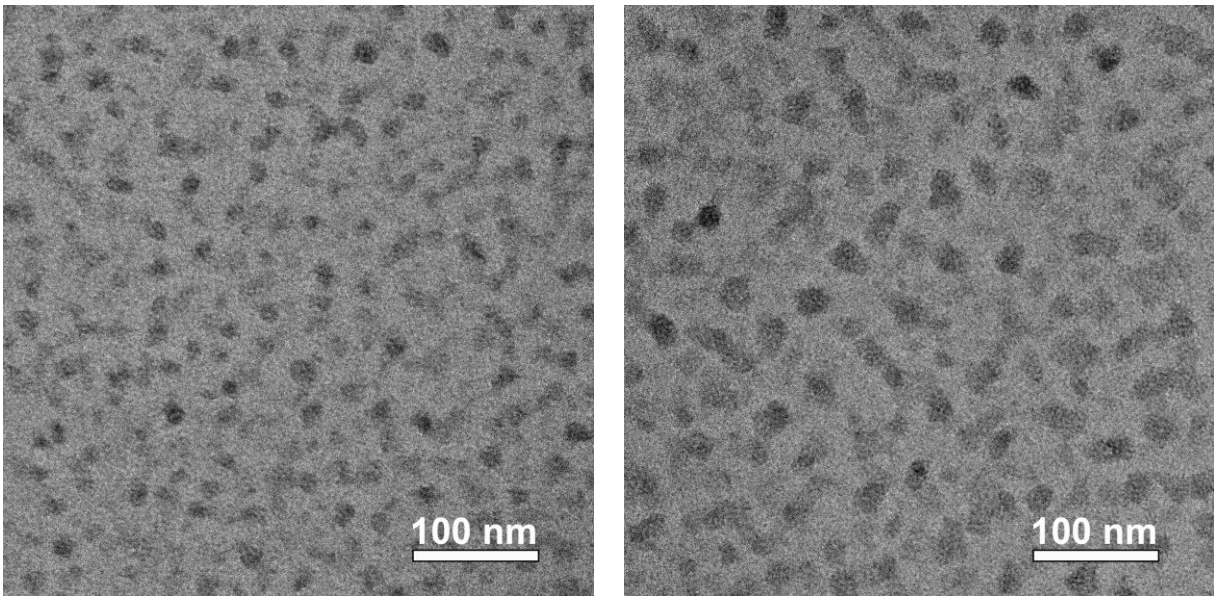

Figure 11: Cut-outs of cryo-TEM images of 178 mmol/L $[OMIM]_2[WO_4]$ in 50 wt.% H_2O_2. Left: Prior to addition of COE; right: saturated with COE.

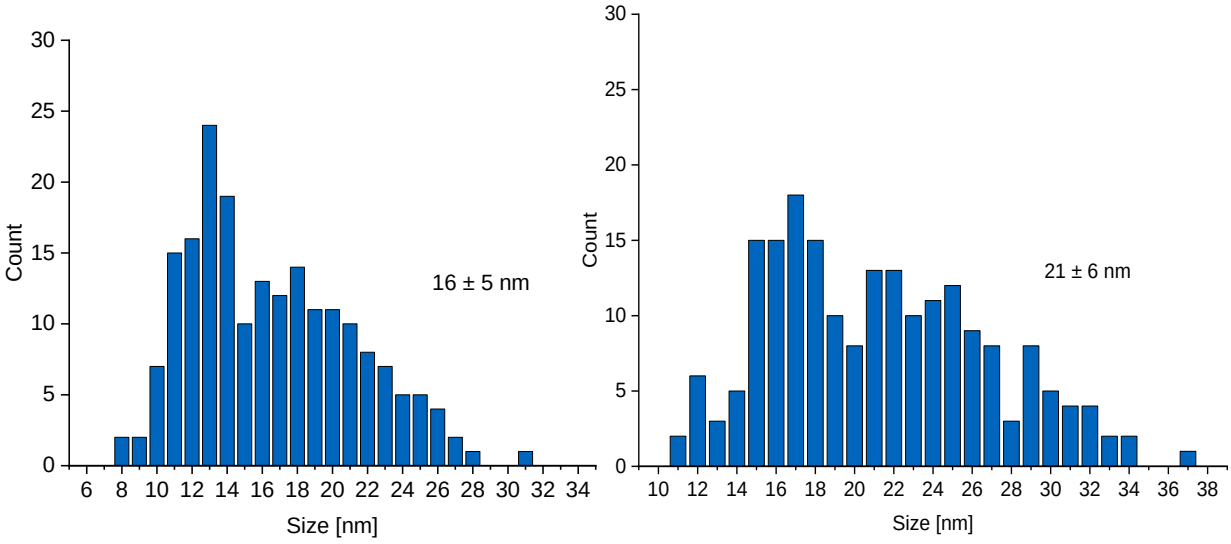

Figure 12: Micelle diameter analysis of 'empty' micelles (left) and micelles saturated with COE (right).

The micelles swell due to the interaction of the hydrophobic alkyl chains with the olefin which pushes the surfactant's alkyl chains apart. For the structural integrity of the micelle, the density of the polar head groups on the micellar surface has to be constant, independent on the micelle size. Hence, with increasing micellar sizes, the surfactant aggregation number has to rise likewise, which in turn, increases the volumetric share of the alkyl chains in the hydrophobic core. The surface density of the head groups can be elucidated by tensiometry measurements and the respective compressibility of the surfactant layer. The Gibbs surface excess *Γ*, which is the molar concentration of the surfactant on the surface is described by the Gibbs-adsorption isotherm:

$$\Gamma = \frac{n}{A} = -\frac{1}{RT} \cdot \frac{d\gamma}{d \ln c}$$

Taking the values T = 323 K for the measurement at 50 °C and −6.255 from the slope of the tensiometric experiment for $\frac{d\gamma}{d \ln c}$ (see Figure 13) into the formula results in an excess-concentration of 2.33 µmol/m² or 1.4 surfactant moieties per nm², standing for 2.8 $[OMIM]^+$ cations per nm². The slope of the Gibbs isotherm is independent on the presence of olefin as the investigated surfactant concentration range is below the CMC. Therefore, the average number of surfactant molecules N per micelle is calculated by:

$$N = \Gamma \cdot A_{micelle} \cdot N_A = \Gamma \cdot 4\pi r^2 \cdot N_A$$

Hence, the aggregation number of $[OMIM]_2[WO_4]$ cations is 606 ± 321 for the 'empty' micelle and 988 ± 522 for the swollen micelles (see Table 2). The total micelle volume of 2394 ± 1903 nm³ divided by the first aggregation number results in a spatial requirement of approximately 3.95 nm³ per $[OMIM]_2[WO_4]$.

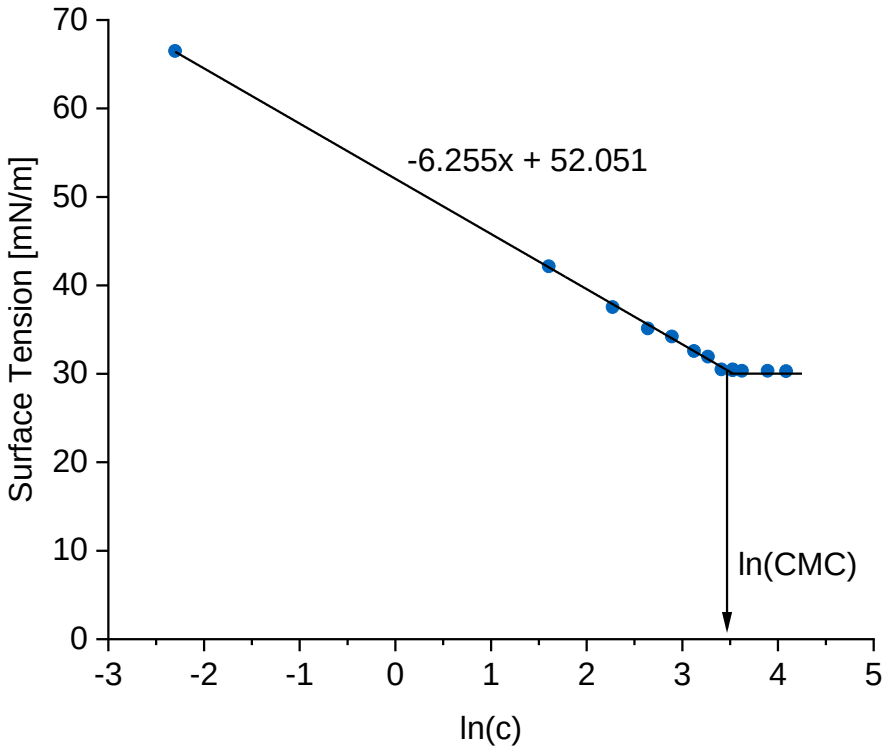

Figure 13: Tensiometric measurement of $[OMIM]_2[WO_4]$ at 50 °C in 50 wt.% aq. H_2O_2 with linear trendline for the sub-CMC region.

The average surface area of the COE-saturated micelles is greater by a factor of 1.63 compared to the 'empty' micelles. The spatial demand of the 988 ± 522 surfactant molecules of the swollen micelles is 3902 ± 2061 nm³, resulting in an average volume difference of 1083 nm³ to the observed micellar volume of 4989 ± 1897 nm³. This average void of 1083 nm³, is the space inside the micelle occupied by the uptaken COE. Taking the molecular volume of 0.21 nm³ per COE into account, the number of COE molecules inside the swollen micelle is on average 5017. This means that each catalyst moiety on average dissolves 2.54 molecules of COE in the aqueous phase (1.27 molecules of COE per $[OMIM]^+$ cation). The large uncertainty due to the disperse size distribution increases vastly as consequence of the potentiation of the radius for the calculation of the micellar surface area and volume. Nevertheless, the calculated results give insights into the molecular constitution of the micelle formed by hundreds of surfactant molecules and provide a hint towards olefin solubilization inside the micelles.

Table 2: Calculated micelle parameters from the elucidated micelle size distribution by cryo-TEM images of 178 mmol/L $[OMIM]_2[WO_4]$ before and after saturation of the aqueous phase with COE.

Micelle parameter	Without COE	With COE
$N_{[OMIM]2[WO4]}$	606 ± 321	988 ± 522
r	8.3 ± 2.2 nm	10.6 ± 2.8 nm
A	865 ± 459 nm²	1411 ± 745 nm²
V	2394 ± 1903 nm³	4989 ± 1897 nm³

This calculation is in very good agreement with the experimental quantification of COE solubilization by ^{1}H-NMR spectroscopy. Here, the concentration of surfactant not taking part in micelle formation, the CMC, is subtracted from the total concentration of 178 mmol/L, leading to a solubilization of 1.10 molecules of COE per $[OMIM]^+$ cation and is only slightly lower than the error-prone calculation from the cryo-TEM images. Upon doubling of the surfactant concentration to 357 mmol/L, the micellar surfactant concentration increases to 325 mmol/L and the higher micelle density results in an overlapping and preventing a size distribution analysis (Figure 14). Still, a remarkable micellar size increase upon uptake of COE size can be observed. The solubility of COE in the micellar phase decreases slightly to 0.94 molecules of COE per $[OMM]^+$ cation, likely due to a high dynamic intermicellar interaction or the formation of deformed spherical micelles. In contrast to the spherical micelles formed by $[OMIM]_2[WO_4]$, the dodecyl-derivative $[DoMIM]_2[WO_4]$ shows the formation of wormlike-micelles (Figure 15, left image). The major difference to $[OMIM]_2[WO_4]$ is the increased alkyl chain length by unchanged head group area demand. This leads to a higher packing parameter of the surfactant molecule which is in the optimal range in between ⅓ and ½ for wormlike micelles. This small structural difference is responsible for the surfactant molecules to the avoid formation of spherical assemblies but rather form less curved cylindrical shapes. Nevertheless, these assemblies show a huge swelling upon treatment with cyclooctene (Figure 15, left image). The empiric solubility of COE determined by ^{1}H-NMR spectroscopy is 1.79 molecules of COE per $[DoMIM]^+$ cation. The solubilization in these types of micelles is higher than these formed by $[OMIM]_2[WO_4]$, likely due to an increased interaction of the substrate with the longer alkyl chain. This difference in-between octyl- and dodecyl derivatives of 1-alkyl-3-methylimidazolium chlorides was reported for the solubilization of aromatic compounds.[123]

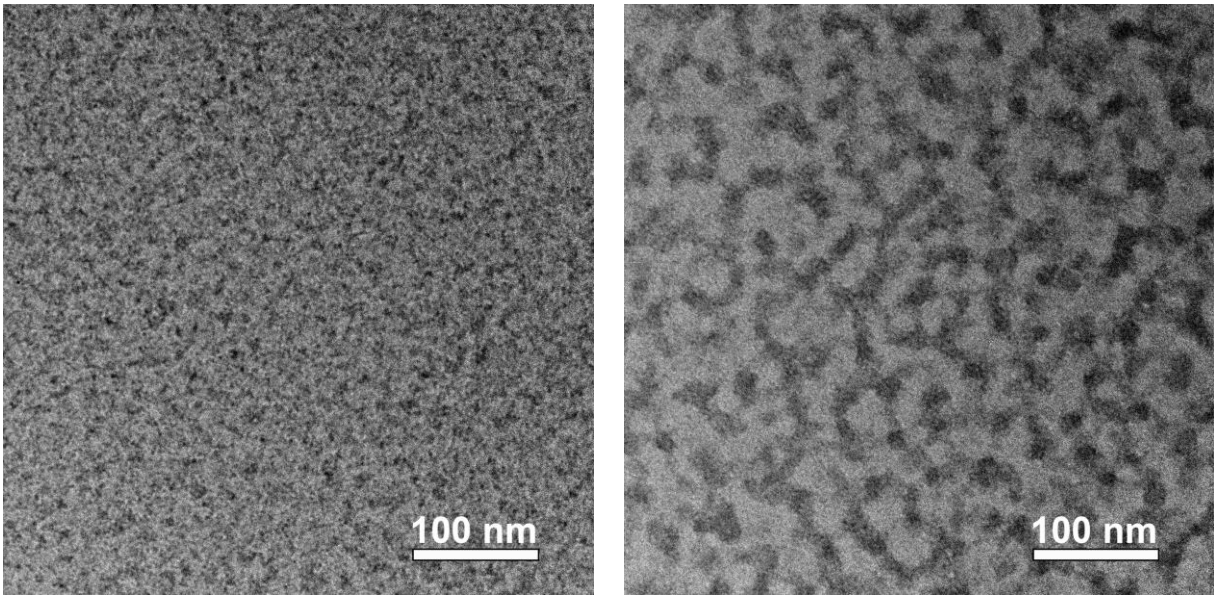

Figure 14: Cut-outs of cryo-TEM images of 357 mmol/L $[OMIM]_2[WO_4]$ in 50 wt.% H_2O_2. Left: Prior to addition of COE; right: saturated with COE.

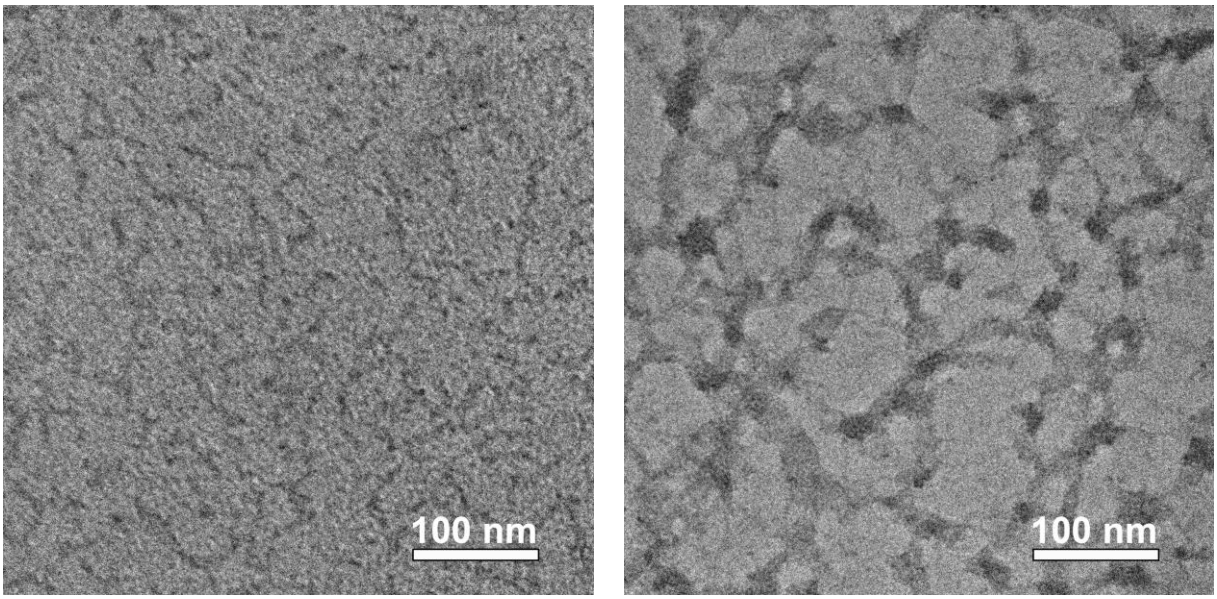

Figure 15: Cryo-TEM images of 178 mmol/L $[DoMIM]_2[WO_4]$ in 50 wt.% H_2O_2. Left: Prior to addition of COE; right: saturated with COE.

Catalytic epoxidation of cis-cyclooctene

To investigate the catalytic activity of the imidazolium tungstates and the influence of the alkyl chain length, the epoxidation of cyclooctene in 2.5 eq. 50 wt.% hydrogen peroxide was carried out at 50 °C. (Scheme 3). Catalyst loadings of 2.5 and 5.0 mol-% vs. COE were applied, standing for a catalyst concentration in the aqueous phase of 178 and 357 mmol/L, respectively. After certain time intervals, aliquots were taken from the organic phase and subjected to ^{1}H NMR spectroscopy after dilution with deuterated chloroform. Conversion of COE and yield of COO were determined by integration of the respective signal areas relative to the mesitylene internal standard.

First, the reactivity of a simple tungstate salt towards COE was investigated. Sodium tungstate was found to show a negligible conversion of COE after eight hours of reaction. Despite a vigorous stirring, the phases do not emulsify, leaving no possibility for the substrate molecules to be transferred to the other phase. Under equal conditions, the imidazolium tungstate ionic liquids are investigated towards their catalytic activity. The results present a strong dependency of the alkyl chain length, hence the micelle formation and the substrate solubilization, on the conversion of COE.

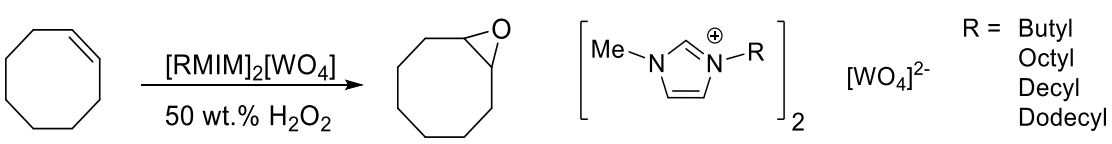

Scheme 3: Catalytic epoxidation of *cis*-cyclooctene (COE) to cyclooctene oxide (COO) with imidazolium tungstate ionic liquids in aqueous hydrogen peroxide.

Table 3: Epoxidation of COE with tungstate catalysts using 50 wt.% H_2O_2. Conditions: $[WO_4]^{2-}$:COE:H_2O_2 = 2.5:100:250, 80 °C, 8h.

Entry	Catalyst	Conc. [mol%]	Conc. [mmol/L]	Micelle conc. [mmol/L][a]	Conv. [%] (8h)	Sel. [%] (8h)
1	$Na_2[WO_4]$	2.5	178	0	4	80
2	$[BMIM]_2[WO_4]$	2.5	178	0	9	69
3	$[OMIM]_2[WO_4]$	2.5	178	146	48	94
4	$[DeMIM]_2[WO_4]$	2.5	178	173	72	96
5	$[DoMIM]_2[WO_4]$	2.5	178	176	77	96
6	$[OMIM]_2[WO_4]$	5.0	357	325	81	99

a: Applied catalyst concentration subtracted by the CMC.

$[BMIM]_2[WO_4]$ was found to not form micelles in the presented concentration range up to 178 mmol/L and rather shows a low COE conversion after eight hours and is comparably low in activity as sodium tungstate (Table 3, Entries 2 and 1). In contrast, the micelle forming long-chain derivatives show reasonable conversions and selectivities towards cyclooctene oxide (Table 3, Entries 3-5). This proofs that the presence of the micelles is the essential premise for the epoxidation in aqueous phase. The conversion of $[OMIM]_2[WO_4]$ is somewhat smaller compared to the decyl- and dodecyl-derivatives. This effect can be explained by the higher CMC of the octyl derivative, resulting in more surfactant molecules passively dissolved in

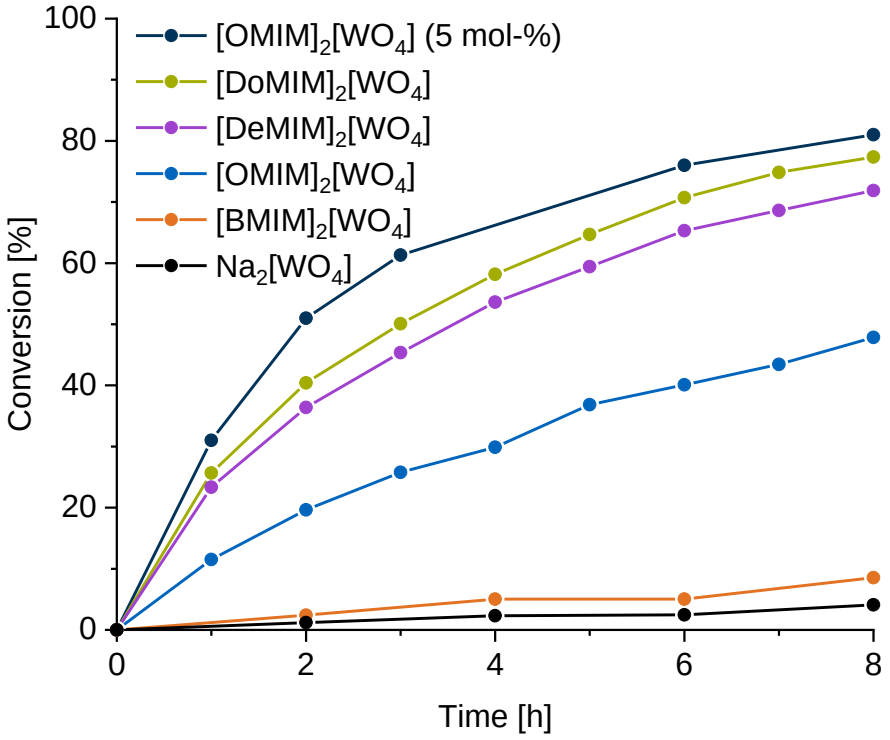

Figure 16: Conversion of COE with 2.5 mol-% tungstate catalysts at 50 °C using 50 wt.% H_2O_2. Conditions: $[WO_4]^{2-}$:COE:H_2O_2 = 2.5:100:250.

solution without aggregation. A further aspect might be the different solubilization rates of COE in the aqueous phase. This is supported by the non-proportional conversion of COE upon doubling of the $[OMIM]_2[WO_4]$ concentration to 5.0 mol-% (Table 3, Entries 3 and 6) as the relative COE solubilization is decreased from 1.10 to 0.94 per $[OMIM]^+$ moiety. However, the kinetic plots show that the activity is indeed proportional with the catalyst loading (Figure 16). For a comprehensive understanding of the molecular mechanisms apart from micelle formation, the catalytically active tungstate species was investigated. A diluted solution of $[OMIM]_2[WO_4]$ in 50 wt.% H_2O_2 was subjected to negative mode ESI-MS revealing all possible combinations of mononuclear (peroxo)tungstate species of the general formula $H[WO_{4-n}(O_2)_n]^-$ (n = 0-4) to be present (Figure 17). This distribution in a large excess of 50 wt.% hydrogen peroxide is highly doubtful and likely caused by decomposition in the gas phase. Similar decompositions of peroxotungstates upon ESI has been reported to be a serious issue.[137] Hence, the reliability on the determination of the true nature of the peroxotungstate species is not provided. Therefore, ^{183}W-NMR as a spectroscopic *in situ* technique to analyze the nature of the tungstate species in is natural environment was exploited. ^{183}W-NMR spectroscopy is an esteemed technique for the investigation of tungstate and its polyoxoclusters as the ^{183}W isotope has a moderately high natural abundancy of 14.3%, a beneficial nuclear spin of ½ and a wide chemical shift range over several thousand ppm.[138] The spectrum of 1 M $[OMIM]_2[WO_4]$ in D_2O shows the presence of a single tungstate species at −6.02 ppm, close to chemical shift of the reference substance Na_2WO_4 at 0.0 ppm (Figure 18, top).

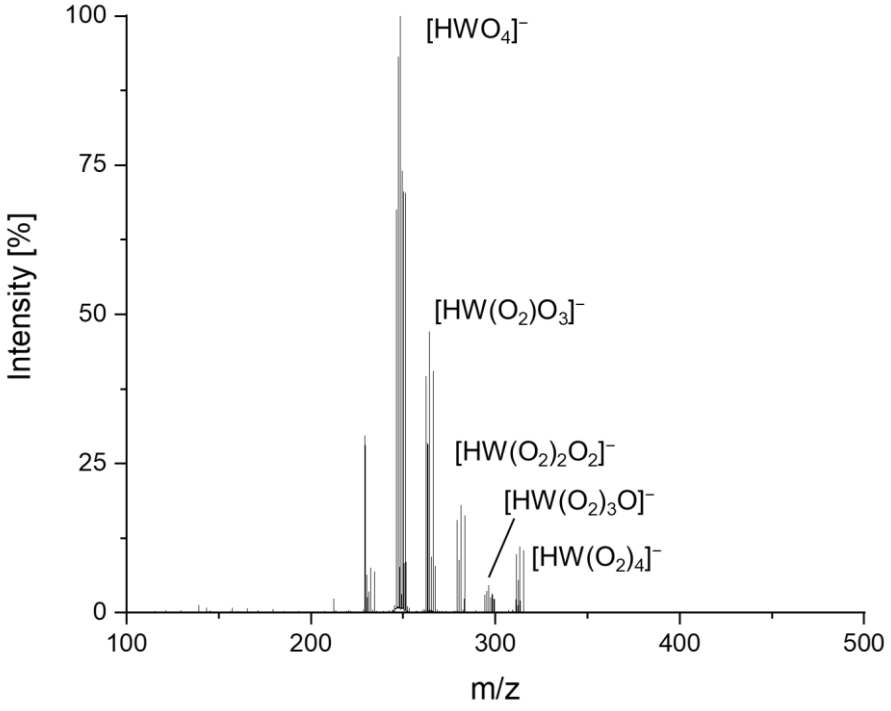

Figure 17: Negative-mode ESI-MS mass spectrum of a diluted solution of $[OMIM]_2[WO_4]$ in 50 wt.% H_2O_2 using water as carrier.

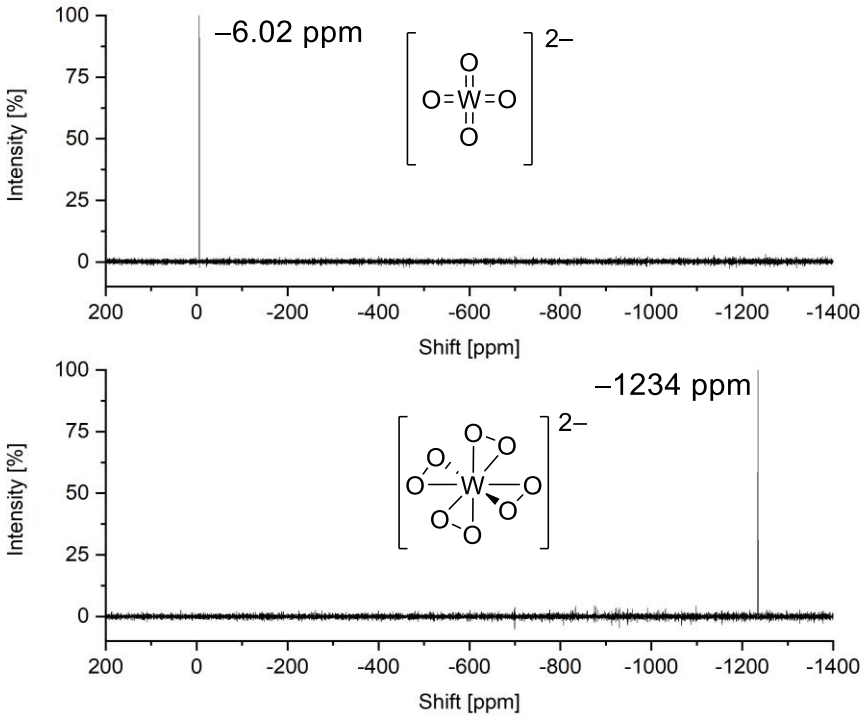

Figure 18: ^{183}W-NMR spectrum of 1 M $[OMIM]_2[WO_4]$ in D_2O before (top) and after (bottom) addition of 5 eq. of 50 wt.% H_2O_2.

Upon addition of as less as 5 eq. of H_2O_2, one single species evolves at −1234 ppm (Figure 18, bottom). This is extraordinarily close to the literature reported value for aqueous solutions of $Na_2[W(O_2)_4]$ at −1247 ppm.[139] The small difference in chemical shift to the literature-values arises from the interaction of the anions with the imidazolium cations in the quasi-homogenous environment. In conclusion, the only present and therefore catalytically active species is 1-octyl-3-methylimidazolium tetraperoxotungstate $[OMIM]_2[W(O_2)_4]$.Tetraperoxotungstate salts, if isolated, are reported to be stable towards decomposition in the long term but explode under mechanical stress under evolution of oxygen gas.[140] However, the kinetic stabilization of the anion due to the high symmetry (compare with the perchlorate anion) might suppress decomposition in solution and more important, decrease the catalytic activity. Noyori et al. reported on the addition of various phosphonic acids to the catalytic epoxidation with tungstate in the organic phase.[141] The proposed formation of a phosphonate-(peroxo)tungstate adduct is observed to boost the rate by a factor of 70-100. Initially, aminomethylphosphonic acid has been investigated as additive and is rather known as the biologically active component of Glyphosate® but was able to vastly accelerate the reaction rate, despite its low stability and full oxidation to phosphoric acid till the full conversion of the olefin.[99] In search of an effective, not potentially carcinogenic and stable additive which boosts the tungstate's reactivity, several organic phosphorus oxide compounds were catalytically investigated as additives (Table 4).

Table 4: Epoxidation of COE with tungstate catalysts and P-containing additives using 50 wt.% H_2O_2 at 50 °C. Catalyst:Additive:COE:H_2O_2 = 2.5:5:100:250.

Entry	Catalyst	Additive	Conv. [%] (1h)	Sel. [%] (1h)
1	$[OMIM]_2[WO_4]$	---	12	>99
2	$[OMIM]_2[WO_4]$	Diethyl ethylphosphonate (DEEP)	8	69
3	$[OMIM]_2[WO_4]$	Diphenylphosphinic acid	15	96
4	$[OMIM]_2[WO_4]$	Phenylphosphonic acid (PPA)	100	>99
5	$[OMIM]_2[WO_4]$	Ethylphosphonic acid (EPA)	92	>99
6	$Na_2[WO_4]$	[OMIM] $[Me_2PO_4]$	10	87
7	$H_2[WO_4]$	[OMIM] $[Me_2PO_4]$	11	93
8	$Na_2[WO_4]$	Octylphosphonic acid	5	>99

The study shows that the phosphorus-oxo-species has to be negative in charge to form a sufficiently strong P-O-W adduct with the tungstate anion. The use of diethyl ethylphosphonate has, compared to the experiment without an additive, a negative effect on both, conversion and selectivity and is therefore obstructive (Table 4, Entries 1 and 2). While diphenylphosphinic acid has little positive effect on the epoxidation rate, phenylphosphonic acid (PPA) boosts the reaction vastly (Table 4, Entries 3 and 4). It has to be noted that both aromatic phosphorus-containing acids are stable towards oxidation under these conditions. In contrast, ethylphosphonic acid, with a little smaller boosting effect than its phenyl derivative, shows partial oxidation to phosphate at the end of the reaction and can therefore not be considered stable and sustainable as it would require constant addition of this additive to a catalytic process. Nevertheless, these findings confirm the enormous influence of organophosphonic acids on tungstate epoxidation catalysis with hydrogen peroxide. Another approach was studied by using the additive as surfactant itself, simplifying the setup by use of the prominent micelle-forming IL [OMIM] $[Me_2PO_4]$ and the addition of sodium tungstate, which are both commercially available in large scales for reasonable prices. Unfortunately, this setup does not increase the reaction rate and rather shows the same activity as the basic $[OMIM]_2[WO_4]$ catalyst. This is likely due to the ion scrambling in solution, leading to the *in situ* formation of the native $[OMIM]_2[WO_4]$ catalyst. Hence, a boosting effect cannot be attributed to the $[Me_2PO_4]^-$ anion. The major difference to the previous experiments is the acidity of the system, as all added P-additives are neutral in charge and deprotonate to yield an anionic species and decrease the pH value of the aqueous phase. For an equal proton count, instead of sodium tungstate, tungstic acid $H_2[WO_4]$ was added as catalytically active component to [OMIM] $[Me_2PO_4]$. However, the similar results show that the acidity of the aqueous solution does not have an impact on the catalytic activity (Table 4, Entries 6 and 7). A further promising approach is the combination of the effects surface-activity and catalytic boost in one compound. Therefore, octylphosphonic acid was synthesized and tested with $Na_2[WO_4]$

towards the activity in COE epoxidation. From a catalytic point of view, the phosphonic acid functional group is identical to EPA and should influence the activity similarly. Unfortunately, the result is not convincing as it reduces the activity drastically compared the original catalyst without additive (Entry 8). This is an indication that the imidazolium structural motif plays an essential role in the epoxidation with tungstate anions.

In conclusion, phenylphosphonic acid (PPA) has been found to be the most promising additive, as it is commercially available, non-toxic, and stable towards oxidation. Due to the enormous impact of the phosphonic acid additive on the reaction rate, a detailed kinetic investigation with various amounts of PPA was conducted to find the optimum PPA:$[WO_4]^{2-}$ ratio. The results show that already after 30 minutes the olefin is completely converted to the epoxide with initially two equivalents PPA per catalyst (Figure 19). This stands for an astonishing boost of the reaction rate by a factor of >90 for the first 50% conversion of COE. The initially chosen ratio of 2 equivalents additive per tungstate anion is found to be the optimal ratio. One equivalent PPA decreases the reaction rate by factor of ½ and three equivalents negatively influence the reaction rate as well as the selectivity, which drops from >99% towards COO to 92% upon acid-catalyzed epoxide ring hydrolyzation to *trans*-1,2-cyclooctanediol. Deeper investigations on the nature of the phenylphosphonic acid additive were conducted by variation of the substitution pattern of the phenyl ring (Figure 20). The effect of an electron-pushing methyl group and an electron-withdrawing fluoride group in *para*-position are expected to have an

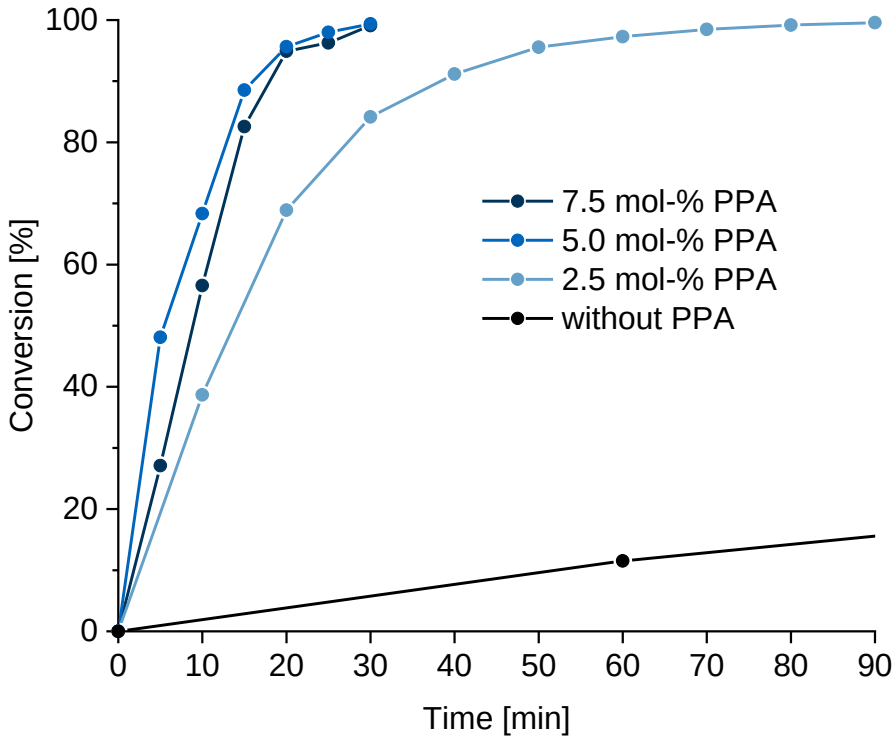

Figure 19: Conversion of COE with 2.5 mol-% $[OMIM]_2[WO_4]$ and various amounts of PPA at 50 °C using 50 wt.% H_2O_2. Conditions: Catalyst:COE:H_2O_2 = 2.5:100:250.

influence on the electronic situation of the phosphonate group, affecting the bond formation and binding strength to the tungstate anion. The kinetic curves show that the *para* substitution pattern of phenyl ring does not have any influence on the catalytic activity as the kinetic curves are identical within the limits of accuracy (Figure 20). For an acidic *p*-hydroxy substituent, the reactivity is significantly decreased. This is presumably due to the deprotonation to a phenolate species, which may compete with the phosphonate group on the coordination to the tungstate anion.[142] The nature of the tungstate species under catalysis conditions was attempted to be investigated with ^{183}W-NMR spectroscopy similar to the additive-free approach (Figure 18). Due to the high required catalyst concentration of 1 M and the corresponding high reactivity, the evolution of oxygen gas by decomposition of H_2O_2 was observed, preventing a spectroscopic analysis at this high required concentration. This phenomenon was not observed under catalytic conditions involving a 178 mmol/L catalyst concentration. The H_2O_2 decomposition could be excluded by a catalytic experiment using an olefin to oxidant ratio of 1:1. This run shows a COE conversion of >99% after four hours, standing for an excellent oxidant efficiency of >99% and the absence of H_2O_2 decomposition. As the ^{183}W-NMR spectroscopy experiments failed due to the high required concentrations, ^{31}P-NMR was exploited to investigate the adduct formation as this nucleus has a better sensitivity by several orders of magnitude. The investigation shows that approximately one third of the added phenylphosphonic acid (with 2 eq. PPA to $[WO_4]^{2-}$) is strongly interacting with tungstate,

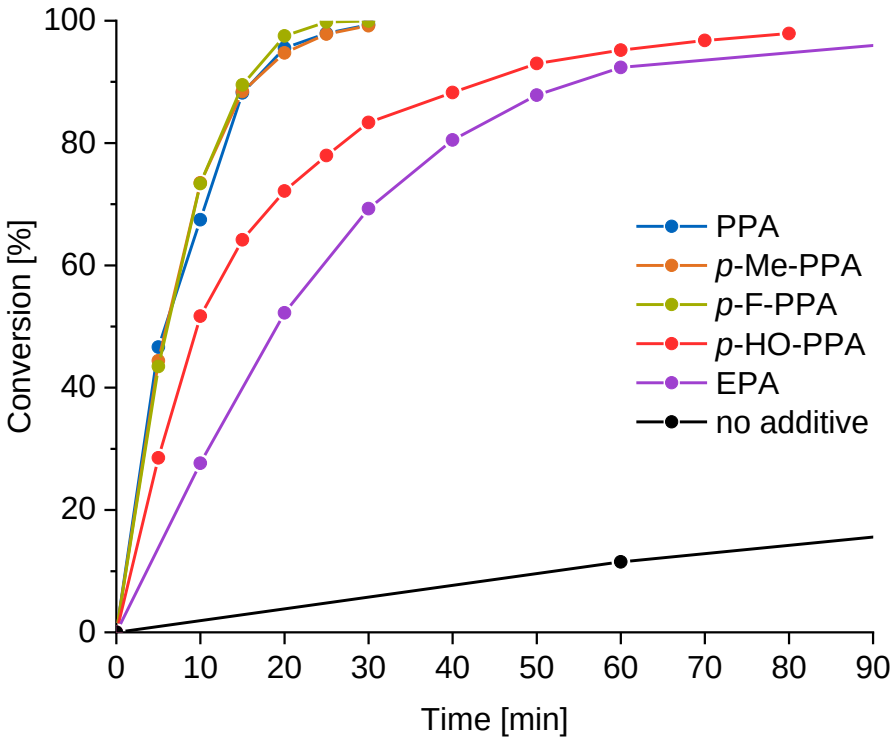

Figure 20: Conversion of COE with 2.5 mol-% $[OMIM]_2[WO_4]$ and 5 mol-% organophosphonic acid (PA) 50 °C using 50 wt.% H_2O_2. Conditions: Catalyst:PA:COE:H_2O_2 = 2.5:5:100:250. Selectivities >99%.

due to a downfield phosphorus shift by 1.38 ppm compared to the “free” PPA at 13.41 ppm (Figure 21). This stands for a complex formation of PPA with 66% of the tungstate ions. The nature of the complex was further investigated by the shape of the phosphorus peak due to its satellite peak formation. 15% of the total peak area is split into two satellite signals with 16.9 Hz symmetrically aside the main signal. The natural abundancy of the only NMR-active nucleus ^{183}W is 14.3% and $^{2}J_{P\text{-}W}$ coupling of phenylphosphonate to tungstate species for a moiety is in the prominent range of 15 to 30 Hz.[143] Hence, the formation of a PPA-tungstate complex is evident. Due to the proton decoupling and the low natural abundancy of ^{13}C, a coupling with other nuclei can be excluded. To further analyze the constitution of the formed complexes, diluted samples of the tungstate/PPA catalyst in hydrogen peroxide were subjected to ESI-MS measurements. This analytical method has been shown to be suitable for the investigation of adduct formation of tungstates and coordinating organic ligands.[144] Besides the two major intense signals of PPA and $H[WO_4]^-$, the formation of a PPA-tungstate adduct is observed. Unfortunately, this species does not bear peroxo-groups, likely due to decomposition in the gas phase, but formation of a catalytically active phenylphosphonate-peroxo-tungstate species during the reaction is postulated (Figure 22). In case of the EPA additive, traces of an additional species bearing two peroxo-groups are detected (Figure 23).

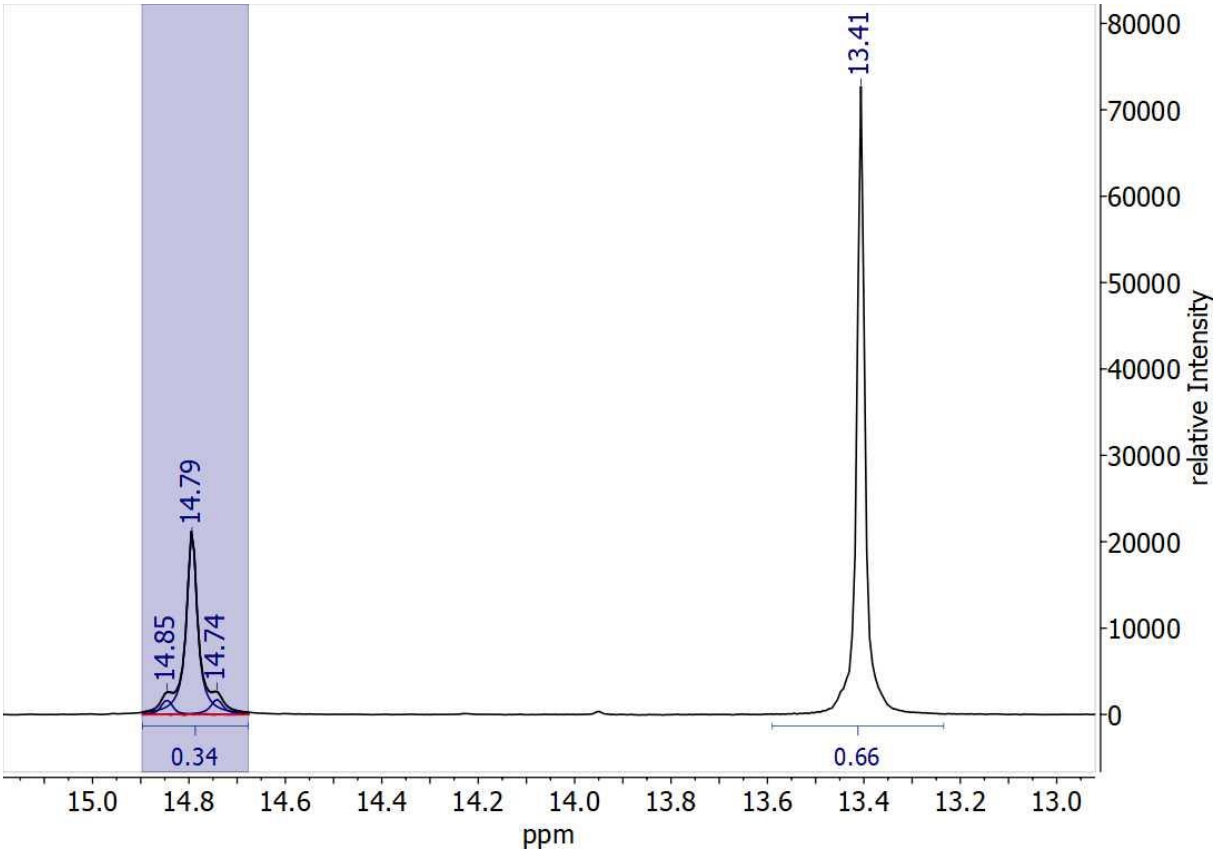

Figure 21: ^{31}P-NMR spectrum of a solution of $[OMIM]_2[WO_4]$ and 2 eq. PPA in 50 wt.% H_2O_2. The blue peak area is deconvoluted (isolated blue peaks) to resolve the two satellite signals originating from the ^{2}J coupling to ^{183}W.

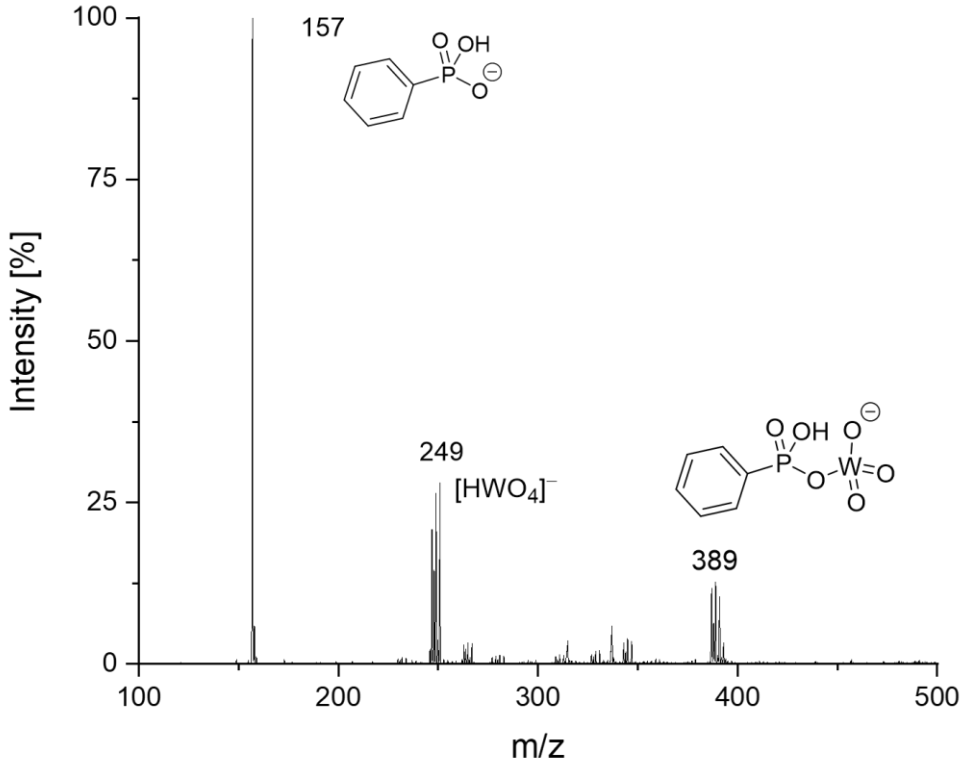

Figure 22: Negative mode ESI-MS spectrum of a dilute solution of $[OMIM]_2[WO_4]$ and PPA (ratio 1:2) in 50 wt.% H_2O_2. Ionization at 50 °C using water as carrier.

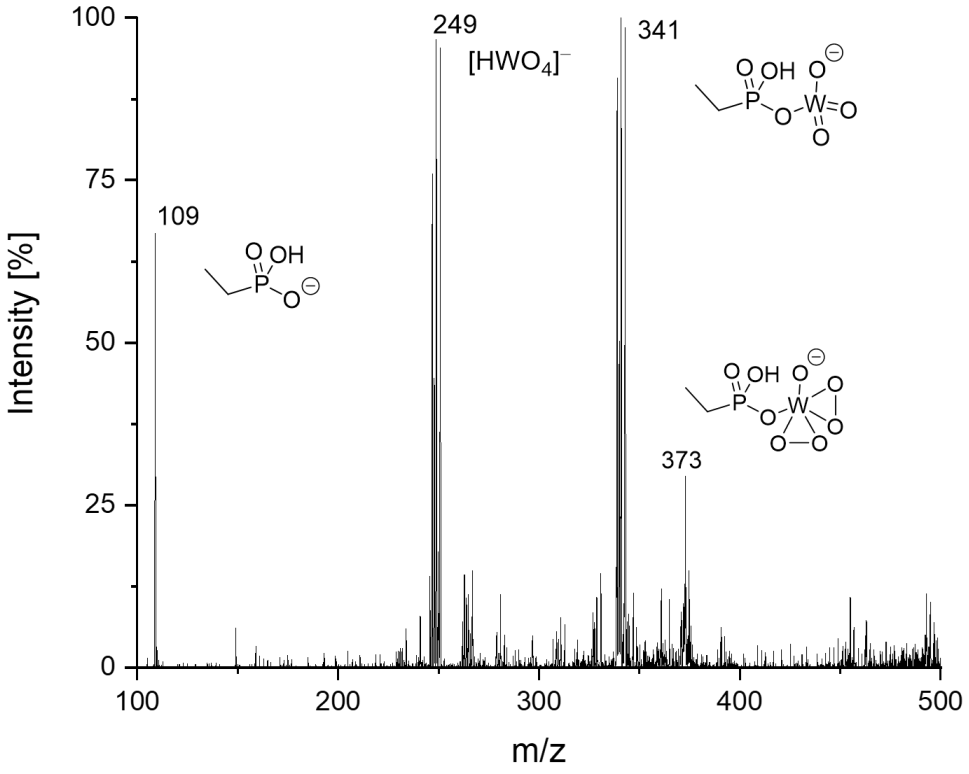

Figure 23: Negative mode ESI-MS spectrum of a dilute solution of $[OMIM]_2[WO_4]$ and EPA (ratio 1:2) in 50 wt.% H_2O_2. Ionization at 50 °C using water as carrier.

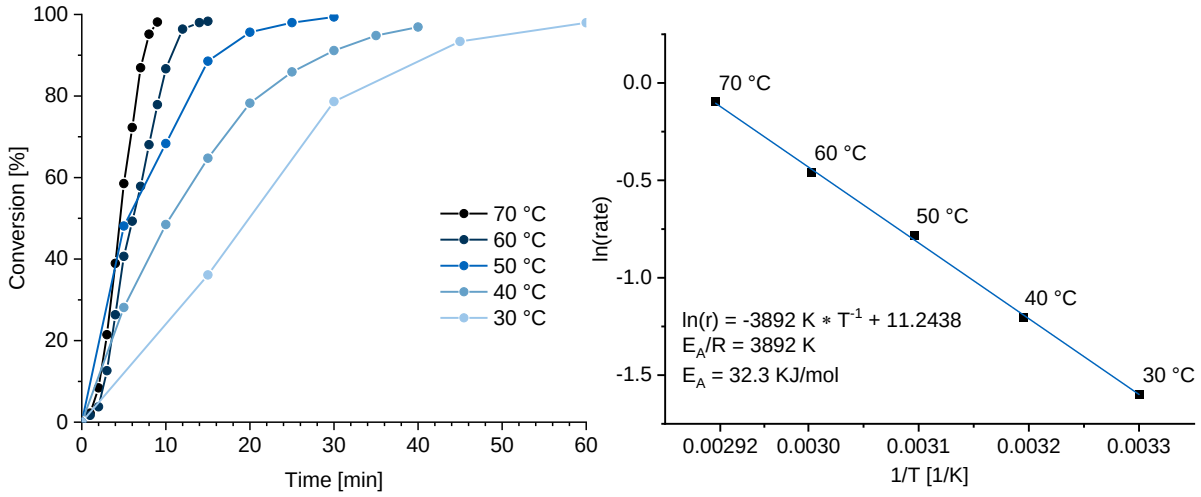

Figure 24: Kinetic plots of the epoxidation of COE with 5 mol-% $[OMIM]_2[WO_4]$ and 10 mol-% PPA at various temperatures (left) and Arrhenius plot of the respective maximum reaction rates (right).

The different mechanism originating from the more reactive covalent phosphonate-tungstate species is further supported by the vastly decreased activation energy of 32 kJ/mol for $[OMIM]_2[WO_4]$ with 2.0 eq. PPA (Supplementary Figure 1) in contrast to 48 kJ/mol for $[OMIM]_2[WO_4]$ without boosting additives (Figure 24, right). These values were calculated by an Arrhenius-plot from the initial reaction rates of the catalysis runs in the temperature range of 30 °C to 70 °C, where it could also be shown that 50 °C is indeed the optimal reaction temperature in terms of reaction rate and a perfect selectivity towards COO.

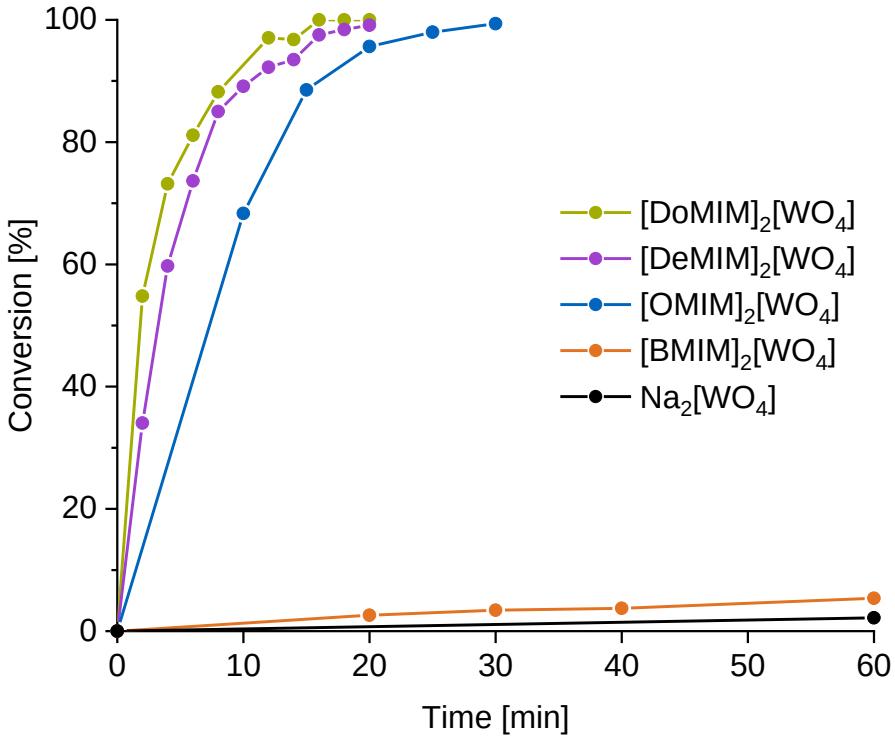

Figure 25: Conversion of COE with tungstate catalysts and the additive PPA at 50 °C using 50 wt.% H_2O_2. Conditions: $[WO_4]^{2-}$:PPA:COE:H_2O_2 = 2.5:5:100:250.

Kinetic investigations for all previously presented imidazolium tungstate catalysts with varying alkyl chain length from butyl to dodecyl were performed with the activity-boosting additive PPA (Figure 25). Here, the effects of the micelles and the substrate solubilization play an even more pronounced role. While $[BMIM]_2[WO_4]$ yields negligible conversions like Na_2WO_4, the micelle forming derivatives show a drastically increased reactivity. The difference of activity arises from the respective CMC and the amount of catalyst aggregated to micelles. For $[DoMIM]_2[WO_4]$, 99% of the total catalyst in solution is taking part in micelle formation, while it is 97% for $[DeMIM]_2[WO_4]$ and only 82% for $[OMIM]_2[WO_4]$. Hence, it is most efficient to use the long-chain derivatives for fast catalysis reactions, but shorter chained imidazolium cations for the investigation of fundamental micelle processes. Hence, the proposed lack of activity for non-aggregated surfactants can be investigated by variation of the catalyst concentration. Figure 26 shows on the one side that the catalyst activity is proportional to the catalyst loading, so non-linear micellar concentration effects can be excluded. On the other side, the extrapolation of the linear trend line of the kinetic data points to the abscissa leads to a 'zero-activity' catalyst concentration of 0.037 mmol/L which is very close to the CMC of $[OMIM]_2[WO_4]$ at 0.032 mmol/L. This proofs that a catalyst concentration below the CMC does not show activity (like $[BMIM]_2[WO_4]$) and that the CMC is the concentration of catalyst which is not active in catalysis. This underlines the necessity to determine the CMC of a respective catalyst in a certain solvent at a temperature to be able to predict and explain the catalytic behavior of the biphasic system.

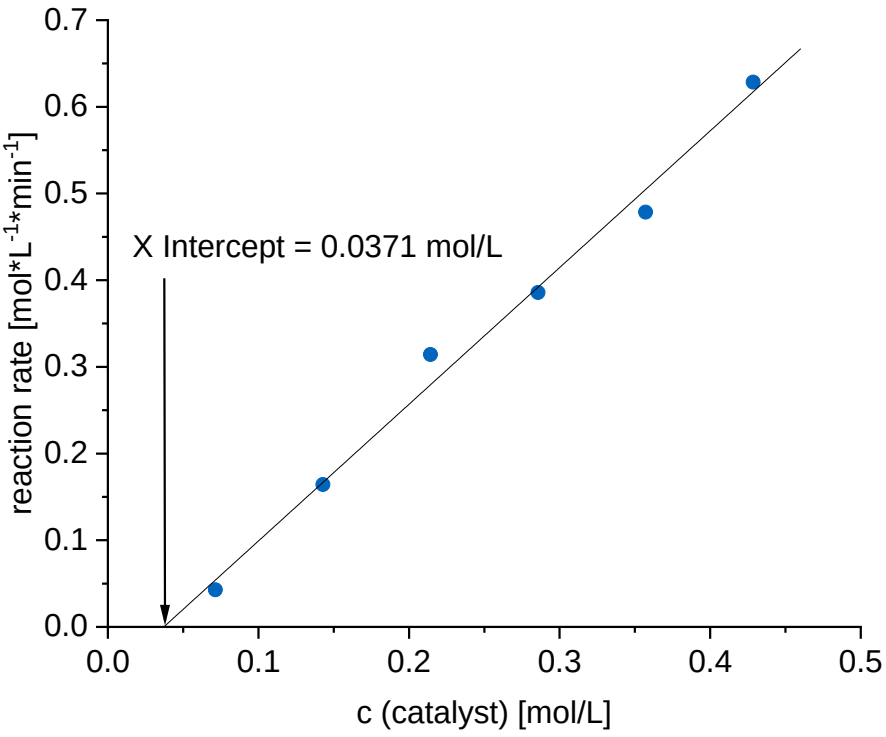

Figure 26: Rates of $[OMIM]_2[WO_4]$ and PPA catalyzed epoxidations of COE in 50 wt.% H_2O_2 plottet against the catalyst concentration.

According to tensiometry measurements by Bastian Zehner, the addition of PPA does not influence the CMC of the catalyst in 50 wt.% aqueous hydrogen peroxide. A solubility measurement of COE in the aqueous phase in presence of PPA supports this observation, as the amount of COE per $[OMIM]^+$ moiety is just little increased from 1.10 to 1.38. This might be due to the additional hydrophobic effects of the PPA additive on the micelle formation potentially promoting an increased micellar swelling. The swelling of $[OMIM]_2[WO_4]$ micelles by COE in presence of 2.0 eq. of PPA (vs. $[WO_4]^{2-}$) is investigated by cryo-TEM. In contrast to the images presented previously, the investigated emulsion lacks contrast and the micelles are barely visible (Figure 27). However, the aggregates are very familiar with those for the PPA-free system. The missing contrast of the supramolecular structures is expected to arise from a rather homogenous distribution of the tungstate anions over the whole aqueous phase. This is caused by an anion scrambling on the cationic micellar surface, where phenylphosphonate exchanges with tungstate in an equilibrium with the majority of the heavy metal content dissolved in the continuous phase. The inactivity of these homogeneously distributed tungstate ions can be elucidated from Figure 24. Further, the use of an additional equivalent of $Na_2[WO_4]$ to $[OMIM]_2[WO_4]$ and 2 eq. PPA results in the exact same activity as without the extra tungstate salt. This can be explained by the complete insolubility of COE in aqueous H_2O_2 but solubilization inside the micelles formed by $[OMIM]_2[WO_4]$. For a fast catalytic reaction, the immobilization of the catalytically active species on the micellar surface would be advantageous.

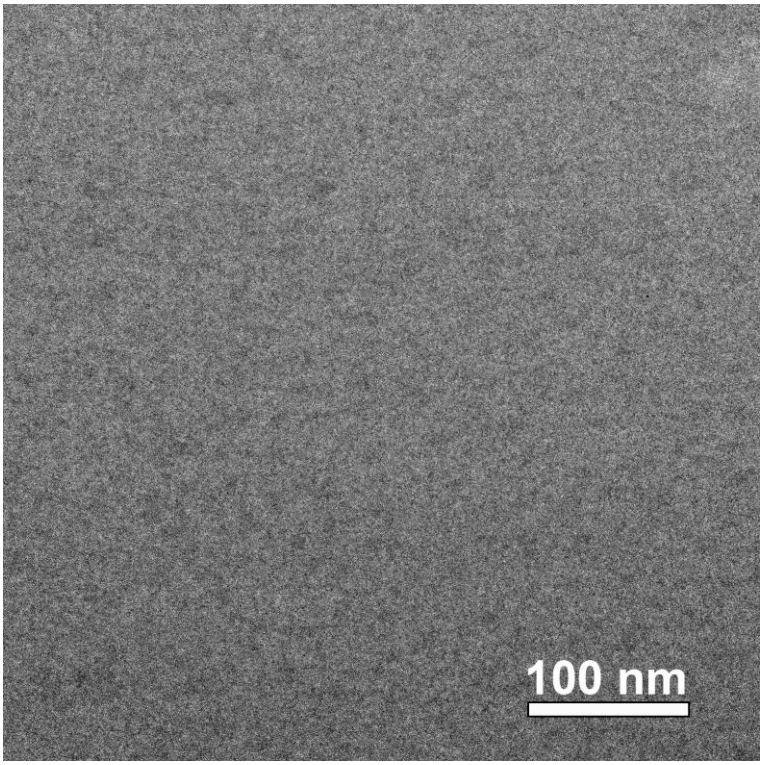

Figure 27: Cryo-TEM images of 178 mmol/L $[OMIM]_2[WO_4]$ and 357 mmol/L PPA in 50 wt.% H_2O_2 saturated with COE. The micelles are barely visible due to a loss of contrast to the matrix.

As the ‘electrostatic immobilization’ of the tungstate to the micellar surface fails for the addition of phosphonic acid additives, it is self-evident that a covalent linkage of the additive to the micelle-forming imidazolium cation, which in turn binds covalently to the tungstate, leads to an increased reaction rate. Thus, for further catalyst optimizations, the reactivity boosting phenylphosphonate motif was connected by a methylene bridge to the imidazolium cation to have a short linker in-between and electronically separate the aromatic systems. The *para*-substitution of the phenylphosphonate is shown to not have an impact on the catalytic activity (Figure 20).

The synthesis was carried out by *N*-alkylation of 1-octylimidazole with diethyl *p*-(bromomethyl)phenylphosphonate (Scheme 4). Next, the resulting ionic liquid is deprotected by acidic cleavage of the ethyl groups. Upon alkaline aqueous workup, the resulting zwitterion-**1** is obtained. Unfortunately, the compound contains a parasitic equivalent of sodium bromide, which would decompose hydrogen peroxide during catalysis. The interaction of zwitterions with salts is rather strong and hence intricate to isolate the single components.[145][146] A chromatographic separation turned out to be successful to remove the concomitant sodium bromide. The zwitterion containing the sodium bromide is slowly eluated in methanol over silica. The salt is washed out and the retained zwitterion can be collected in NaBr-free fractions. The success of the separation is tested by mixing of aliquots thereof with aqueous silver nitrate by absence of a precipitation of silver bromide. The obtained designer-surfactant zwitterion-**1** is then tested towards catalytic activity with tungstate in the epoxidation of cyclooctene. To a great surprise, the catalytic activity is identical to that of pure $[OMIM]_2[WO_4]$ without any additive (Figure 28, red and black curve). Hence, the approach of activity boost by immobilization of the phosphonate to the micellar surface turns out to be unsuccessful. This is further supported by ESI-MS measurements not showing any adduct formation with tungstate (Figure 29). It is anticipated that this is caused by the rigidity of the surfactant and the size of spacer between the imidazolium and the phosphonate groups.

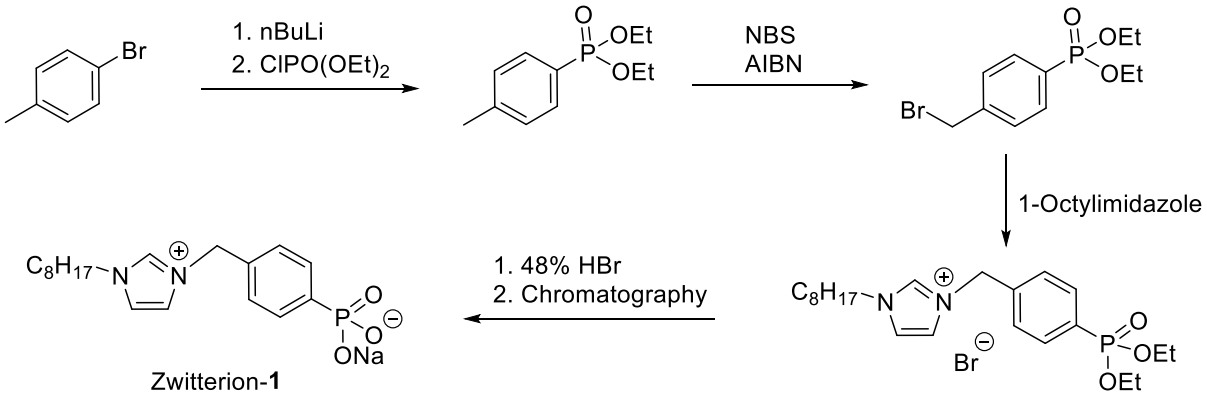

Scheme 4: Synthesis procedure towards zwitterion-**1**.

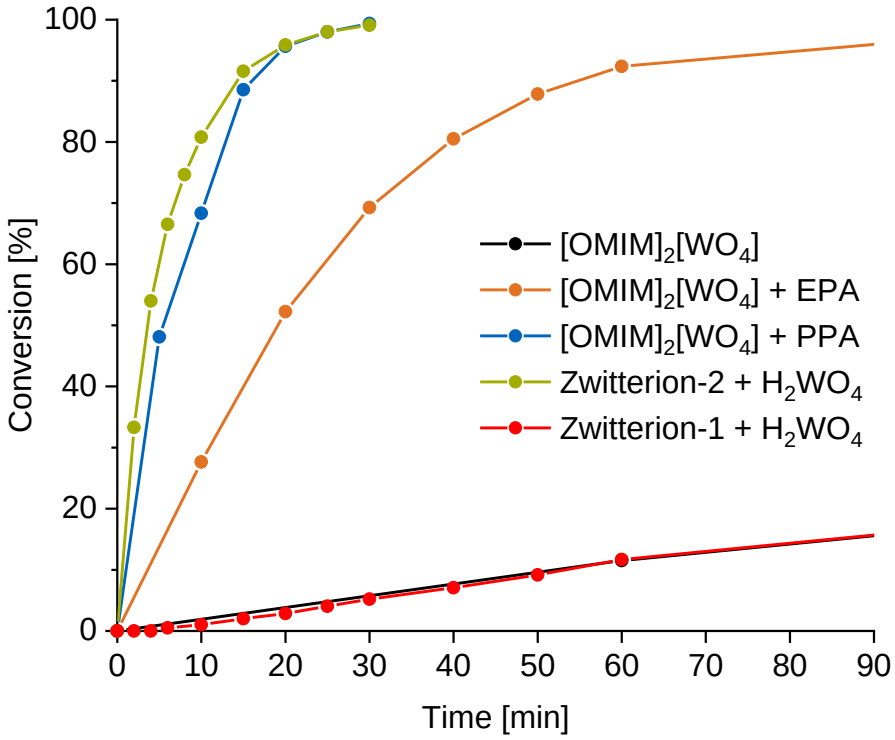

Figure 28: Catalytic epoxidation of COE with tungstate catalysts using 2.5 eq. 50 wt.% H_2O_2 at 50 °C. 2.5 mol-% tungstate vs. COE was added.

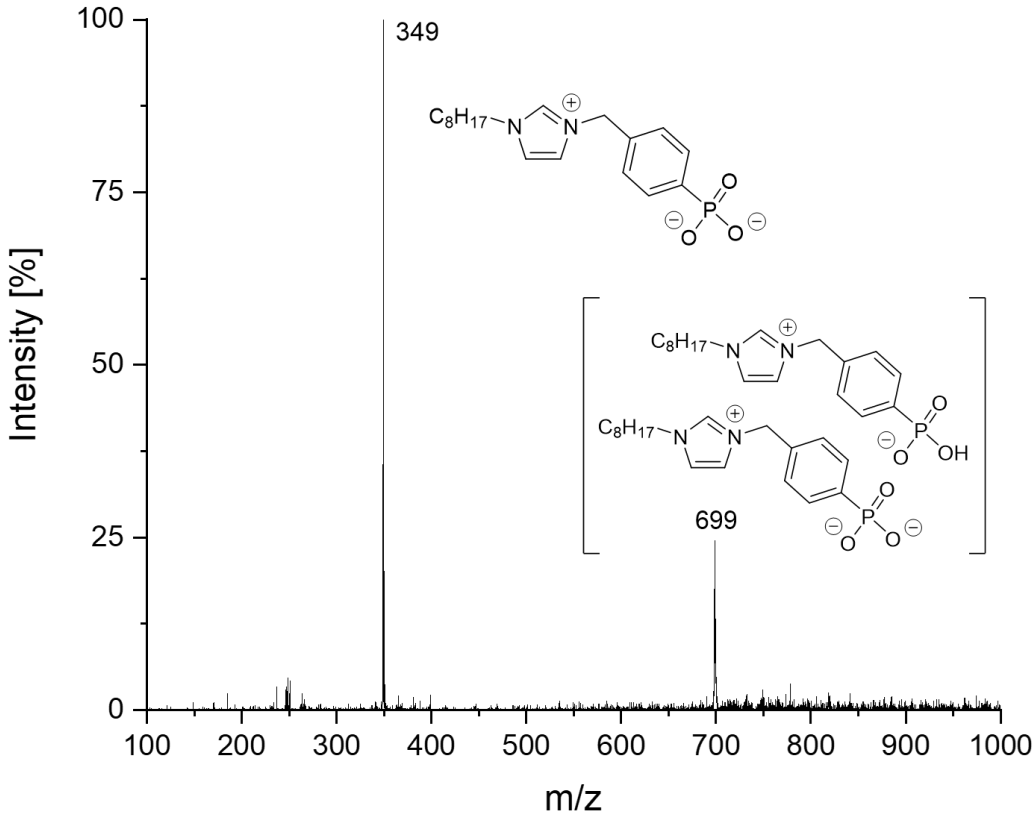

Figure 29: Negative mode ESI-MS spectrum of a dilute solution of zwitterion-**1** and $H_2[WO_4]$ (ratio 1:1) in 50 wt.% H_2O_2. Ionization at 50 °C and water as carrier.

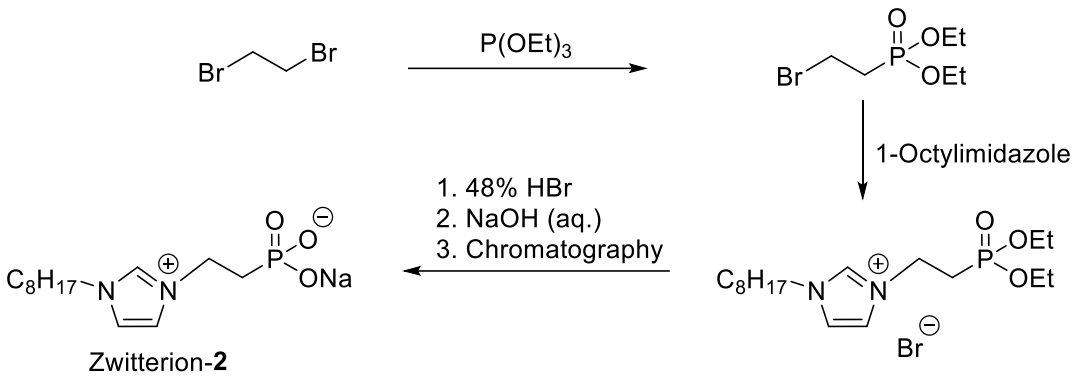

Scheme 5: Synthesis procedure towards zwitterion-**2**.

Hence, the coordinated tungstate is in a too far distance from the hydrophobic core containing the olefin. This prevents a direct interaction of the tungstate's peroxo-groups with the unsaturated double bond. A more flexible and smaller ethylene linker was introduced by an analogous synthetic procedure but using diethyl (2-bromoethyl)phosphonate as precursor (Scheme 5). The resulting designer-surfactant zwitterion-**2** shows a surprisingly high conversion with an acceleration of activity with a factor of 5 compared to its originating $[OMIM]_2[WO_4]$/EPA system.

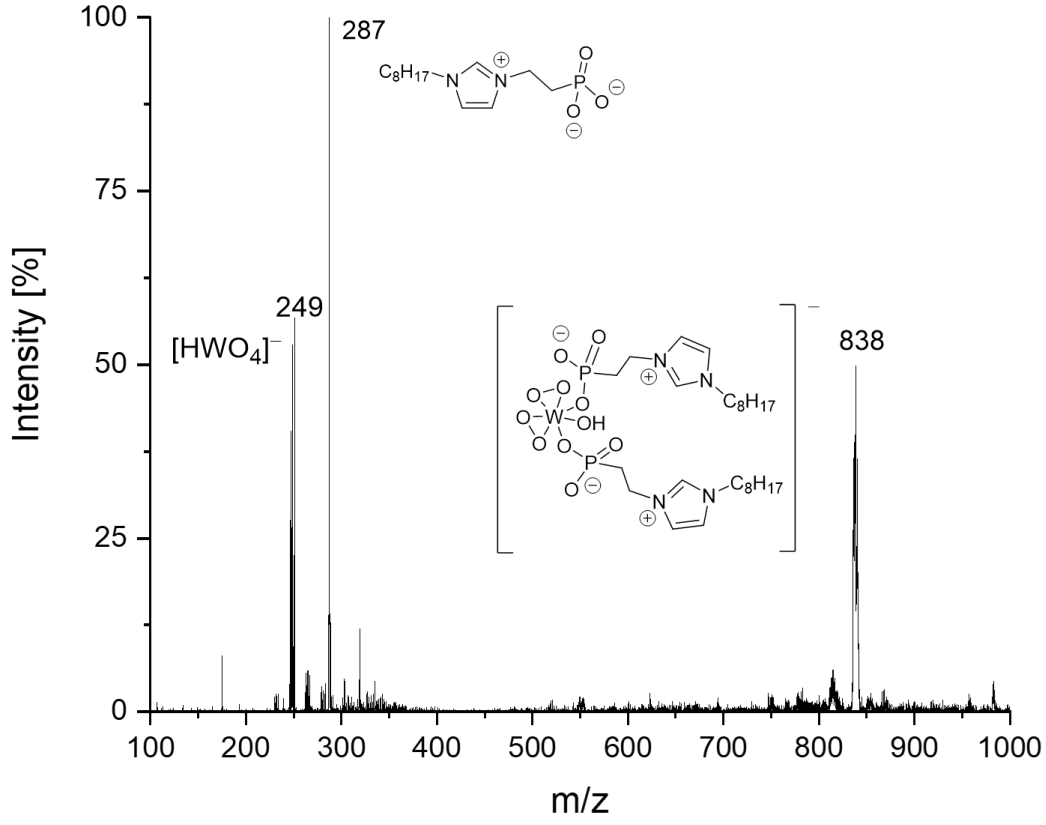

Figure 30: Negative mode ESI-MS spectrum of a dilute solution of zwitterion-**2** and $H_2[WO_4]$ (ratio 1:1) in 50 wt.% H_2O_2. Ionization at 50 °C using water as carrier.

Noteworthy, it is even more active than the catalysis experiment involving the PPA additive. ESI-MS measurements support the formation of a zwitterion-tungstate complex bearing two peroxo-groups (Figure 30). It can be shown that the immobilization of the covalent immobilization of the phosphonate to the micellar surface and hence the 'electrostatic immobilization' of the tungstate anion is superior to the additive approach. The developed multi-task catalyst has to be designed carefully as the linker in-between the functional groups must not be too large, negatively affecting the catalytic activity.

For a sustainable catalytic process, the catalyst must be recover- and recyclable. The exclusive catalyst presence in the aqueous phase allows for a simple product separation by decantation. Moreover, the product is free of solvent or traces of catalyst and can therefore be used without further purification. However, the micelles in the aqueous phase still contain more than 5% of the total olefin, which is intricate to separate by purely mechanical techniques. Hence, the product has to be extracted by organic solvents for a complete separation. Kinetic investigations by Bastian Zehner show that the micelles dissolve preferably the substrate COE, while the product COO is released to the supernatant organic phase.[147] This is further supported by an TEM-image of a completed COE epoxidation with $[OMIM]_2[WO_4]$ (Figure 31). The micelles are shrunk to the average diameter without any substrate solubilized, supporting this observation on a microscopic level. Some residual micelles are still swollen, and this might arise from the 5% cyclooctane content of the substrate COE.

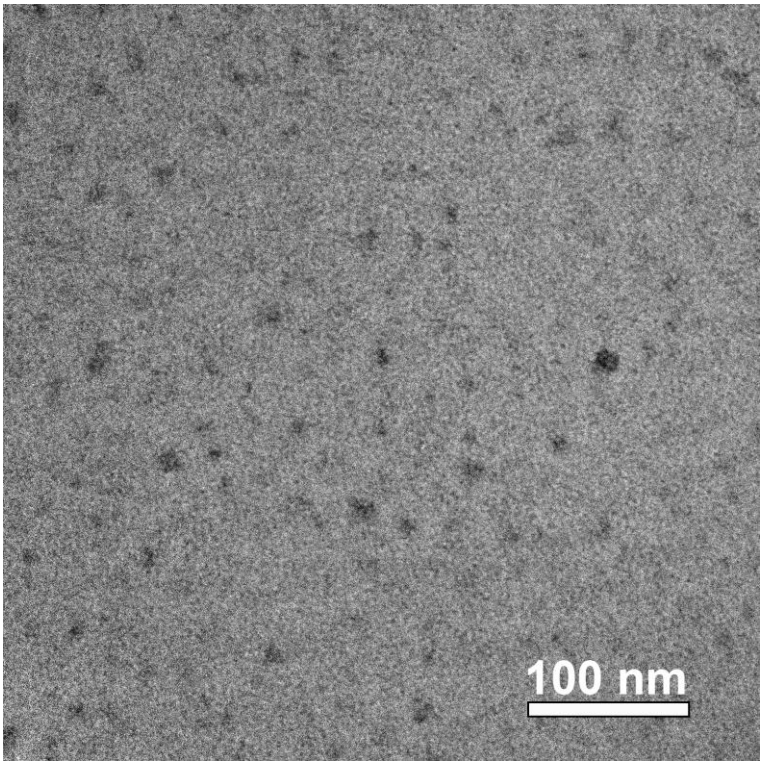

Figure 31: Cryo-TEM image of the aqueous phase of a catalysis experiment with 178 mmol/L $[OMIM]_2[WO_4]$ after full conversion of COE. Catalytic conditions: $[OMIM]_2[WO_4]$:PPA: COE: H_2O_2 = 2.5:5:100:250.

The only significant contaminant inside the micelles at the end of the reaction is cyclooctane which is considered inert during the course of the reaction. Therefore, the aqueous solution could be used as obtained after decantation of the organic phase. However, the accumulating water problem is not tackled, as the addition of fresh H_2O_2 further dilutes the aqueous phase. Hence, for a catalyst stability and activity study over several runs, the residual H_2O_2 is removed. After the end of each run, conversion and selectivity are determined and the catalyst separated by decantation. To avoid the accumulation of cyclooctane, the aqueous phase is extracted with hexane in advance. The residual oxidant is then decomposed using a platinum wire and evaporated, leaving the ionic liquid catalyst and the additive. The recycling strategy of $[OMIM]_2[WO_4]$/PPA shows great success over 10 runs without any loss of activity and selectivity, paving the way for a sustainable continuous process. The catalysis study involving zwitterion-**2** shows constant activity for four recycling runs but then drops in activity due the slow oxidation of the phosphonate group for which alkylphosphonates are prone to (Figure 32).

Cyclooctene has been used as a model substrate exclusively so far. In order to investigate the profitableness of the micellar epoxidation with imidazolium tungstates for industrial relevant olefins, a substrate variation study was conducted. The advantageous $[OMIM]_2[WO_4]$/PPA catalyst has been chosen to epoxidize various olefins (Table 5). Terminal olefins such as 1-octene and 1-dodecene are found to be drastically less reactive towards epoxidation.

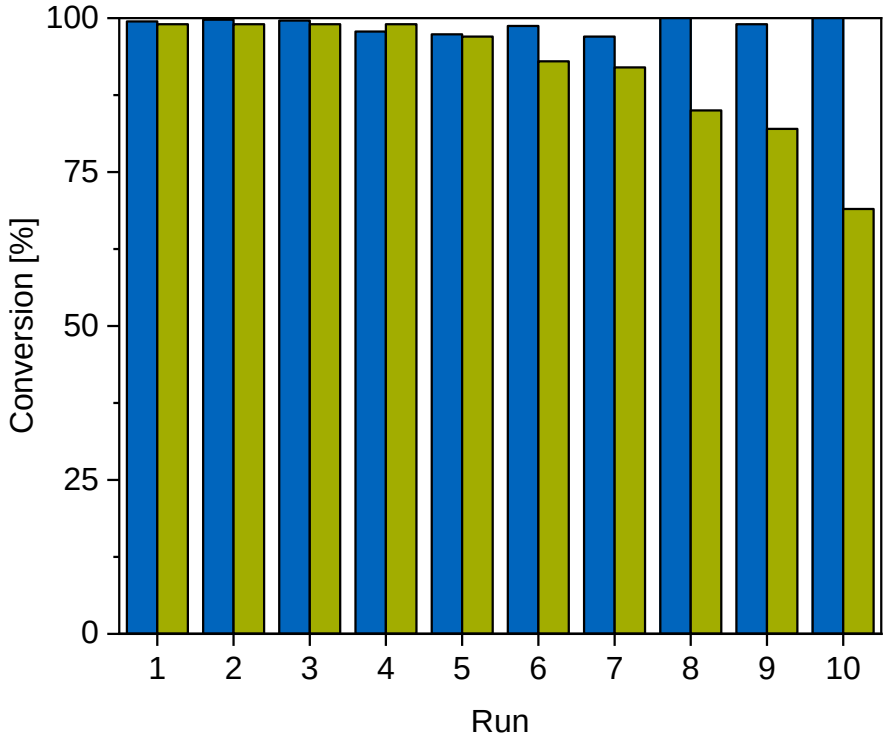

Figure 32: Conversions of the recycling experiments after 30 min each for $[OMIM]_2[WO_4]$ (blue) and zwitterion-**2**/$H_2[WO_4]$ (green).

Table 5: Epoxidation of various olefins with $[OMIM]_2[WO_4]$ using 50 wt.% H_2O_2. Molar ratio catalyst:PPA:COE:H_2O_2 = 2.5:5:100:250.

Entry	Substrate	T [°C]	Conversion [%] (time)	Selectivity [%] (time)
1	*cis*-Cyclooctene	50	100 (30 min)	>99 (30 min)
2	1-Octene	50	81 (7h)	46 (7h)
3	1-Octene	70	95 (4h)	58 (4h)
4	1-Dodecene	70	86 (4h)	70 (4h)
5	*cis*-2-Octene	50	100 (1h)	84 (1h)
6	*trans*-2-Octene	70	92 (1h)	77 (1h)
7	Allyl alcohol	50	83 (30 min)	80 (30 min)
8	Allyl alcohol with $Na_2[WO_4]$	50	91 (30 min)	34 (30 min)

Moreover, the selectivity is decreased as primary epoxides are more prone towards nucleophilic attack by water leading to ring opening reactions to 1,2-diols. Upon increase of the temperature to 70 °C, higher conversions and better selectivities, due to the shorter reaction times are observed. 1-Dodecene shows a higher selectivity at 70 °C compared to the homologue 1-octene but a slightly decreased reactivity, likely due to the lower content of unsaturated carbon atoms in the substrate molecule. The reactivity of internal olefins depends on the configuration of the C=C double bond. The *cis* configuration as it is present in COE shows a higher reactivity than the trans isomers. Likewise, *cis*-2-octene requires drastically shorter reaction times at lower temperatures for similar conversions compared to *trans*-2-octene (Table 5, Entries 5 and 6). Additionally, the epoxidation of the water-soluble olefin allyl alcohol was conducted. Despite the monophasic setup, the micelles are still present and catalyze the epoxidation. Compared to the identical experiment with sodium tungstate as catalyst, the conversion is slightly lower for the micellar system, but the selectivity is vastly increased. The difference in activity is expected to arise from mass transfer limitation due to the presence of the micelles. The beneficial effect of the micelles on the selectivity can be explained by the mechanistic nature of the side-reaction, the epoxide hydrolyzation. In order to be attacked by the rather bad nucleophile water, a partial polarization of the epoxide oxygen by a proton is required. The micelles may shield this acidic interaction from the product due to electrostatic repulsion with the cationic micellar surface.

3.1.4 Conclusion

The obtained data shows that the tungstate anion can successfully be used as a catalyst for the epoxidation of olefins in aqueous phase as part of a cationic micelle. This is the first report on the tungstate catalyzed epoxidation of non-polar olefins in water. The surface-active imidazolium cations aggregate to micelles and take up the olefin internally. These phenomena are conveniently shown by cryo-TEM due to the heavy metal tungstate counterion 'immobilized' on the micellar surface. The operation in the aqueous phase with the olefin solubilization therein has several advantages over the transfer of the catalyst into the organic phase. From the perspective of an efficient catalyst recycling, it is favourable to keep the metal oxide anion in the aqueous phase and solubilize the non-polar substrate therein by aid of micelles. This concept has been investigated herein and found to be suitable for the epoxidation of olefins without any additional solvents besides water. It was revealed that the micellar approach offers several advantages, such as catalyst recycling, pure product separation by decantation, and sufficiently high intrinsic reactivities. The addition of phosphonic acids further boost the reactivity by suppression of the formation of a tetra(peroxo)tungstate in favour of a much more reactive di(peroxo)tungstate-phosphonate complex as ESI-MS measurements suggest. The covalent linkage of the phosphonate group to the cation further boosts the reactivity of the tungstate anion, due to the coordination to the micellar surface. This applies as long as the linker is flexible and allows for a structural degree of freedom. Hence, the ethylene linker is a suitable connector while the benzyl bridge is too rigid.

In contrast to the previously reported perrhenate catalysts, the tungstate anion has proven to be more active in micellar catalysis. This is likely due to the different mode of H_2O_2 activation. The tungstate anion forms peroxo-species as ^{183}W-NMR and ESI-mass spectra present. The epoxidation occurs via an inner-sphere mechanism with the tungsten atom being directly involved in bond formation. The perrhenate anion activates hydrogen peroxide via H-bonds exclusively.[105] The rhenium atom does not play a direct role in bond formation and therefore solely directs the geometry and the electron density of the oxo ligands. Therefore, a more abundant element oxo-anion could similarly or even stronger activate hydrogen peroxide by H-bonds.

3.2 Activation of Hydrogen Peroxide by Micellar Imidazolium Nitrates

3.2.1 Publication Details and Author Contributions

Major results of this chapter have been published in the article “Activation of hydrogen peroxide by the nitrate anion in micellar media” in *Green Chemistry* **2021**, volume 23, issue 5, pages 1965-1971.[148] The manuscript was submitted on October 16th 2020 and accepted on February 12th 2021.

M Sc. Bastian Zehner is thanked for the tensiometry and conductivity measurements. Dr. Markus Drees performed all DFT calculations, and Prof. Dr. János Mink conducted the vibrational spectroscopy experiments.

3.2.2 Introduction

The micellar epoxidation of olefins with surface-active imidazolium tungstates has shown that catalyst operation in the aqueous phase is superior to the reaction conducted in the organic phase, as no additional solvents are required. Moreover, the product can easily be separated and is free of any contaminations. The catalyst can easily be recovered and reused, paving the way for a continuous process. Especially imidazolium surfactants are suitable for micellar catalysis due to the pronounced olefin uptake and the broad functionalizability of the head group. Tungstate profits form the ionic interaction with the imidazolium motif which further boosts the reactivity compared to anionic surfactants such as octylphosphonic acid. However, the tungstate activity depends primarily on the substrate solubilization in the aqueous phase.

This can be considered as widely different for the formerly investigated perrhenate anion, which was reported to be inactive in epoxidation catalysis and the dead-end of an alkyltrioxorhenium oxidation catalyst upon decomposition.[149][150] Besides perrhenic acid,[151] the perrhenate anion does not show reactivity in hydrogen peroxide with inorganic cations towards olefins. Investigations by Cokoja et al. have shown that the perrhenate anion is able to activate hydrogen peroxide sufficiently to be used as oxidant in epoxidation reactions in ionic liquid solvents.[105] NMR-spectroscopic investigations find that isotopically labelled $[Re^{17}O_4]^-$ does not transfer ^{17}O to the olefin in aqueous hydrogen peroxide, hinting towards a mechanism without formation of an intermediate $Re(O_2)$-species. This is further supported by calculations by Genest and Rösch suggesting that an H-bond activation of H_2O_2 is energetically preferred over an inner-sphere mechanism with direct involvement of the rhenium atom in bond formation. The final evidence for the epoxidation by an outer-sphere mechanism was found by János Mink who recorded high resolution IR- and Raman-spectra, suggesting the formation of a $[ReO_4]^{-}\cdots H_2O_2$ adduct by change of the perrhenate symmetry from T_d to C_{2v}, in accordance

with DFT calculations. Hence, the question arises if other oxoanions can activate hydrogen peroxide apart from a direct peroxoanion formation. The respective candidate has to be stable in aqueous H_2O_2 and must not catalyze its decomposition. The possible choice of anions that meet these premises is rather limited, and especially among the abundant anions only a few candidates remain. Of great interest is the nitrate anion, which is cheap, abundant, and stable under oxidative conditions. The Olin® process uses molten nitrate salts for the epoxidation of propylene upon nitrate reduction to nitrite, which is reoxidized with air.[152] So far, a catalytic application of the nitrate anion has not been reported. It can be considered inactive in aqueous phase due to the high hydration enthalpy and the subsequent large hydration shell, preventing interactions with molecules besides water. With focus on the unique properties of micelles, nitrate might be similarly active in olefin epoxidation as the perrhenate anion in a micellar environment. Hence, dialkylimidazolium nitrates have been synthesized and investigated towards micelle formation and the activation of hydrogen peroxide by H-bonds for its catalytic use in epoxidation reactions.

3.2.3 Results and Discussion

Synthesis strategy and compound properties

Several surface-active 1-alkyl-2-R'-3-methylimidazolium nitrates of the general formula [RR'MIM] [NO_3] (R = octyl, dodecyl; R' = H, Me) have been synthesized via the reliable anion exchange procedure using an anion exchange resin (Scheme 6). In contrast to tungstic acid used for the synthesis of the derived imidazolium tungstates, nitric acid is fully miscible with water in all proportions and therefore the neutralization of the basic imidazolium hydroxide eluate has to be monitored thoroughly. By aid of a calibrated pH-meter, pH = 7.0 has to be adjusted prior to evaporation of the water for the targeted perfect imidazolium to nitrate ratio of 1:1.

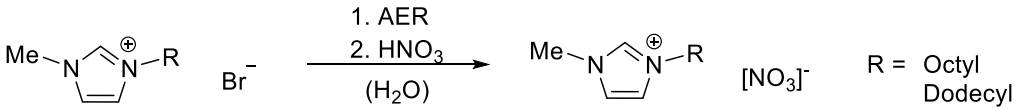

Scheme 6: Synthesis of 1-alkyl-3-methylimidazolium nitrates from 1-alkyl-3-methylimidazolium bromides using an anion exchange resin.

The synthesized imidazolium nitrate ILs show perfect purity by means of NMR spectroscopy and elemental analysis and are colorless in appearance. The absence of residual bromide contaminations by incomplete ion exchange was confirmed by Mohr's titration down to a detection limit of 13 ppm.[153] To remove all traces of water, these compounds have to be dried under high vacuum (10^{-6} mbar) at 80 °C for several hours. Due to the high hygroscopy, all substances were stored under an inert gas atmosphere. All four imidazolium nitrates have a

melting point below 100 °C and can therefore be considered as ionic liquids. [OMIM] [NO_3] is liquid at room temperature and therefore by definition a RTIL. The compounds are immiscible with non-polar organic solvents (and slightly soluble in chlorinated hydrocarbons such as $CDCl_3$ for NMR-spectroscopy), paving the way for biphasic catalysis with water.

Investigations on the surfactant aggregation

In pursuit of a micellar catalyst for the metal-free epoxidation of olefins in hydrogen peroxide, the surface-activity and the micellization of the imidazolium nitrates were investigated by tensiometry by Bastian Zehner. The measurements were performed at 80 °C for [OMIM] [NO_3] and [DoMIM] [NO_3] in 50 wt.% aqueous hydrogen peroxide (Scheme 7) as reactivity towards hydrogen peroxide is expected at elevated temperature, which is also the case for micellar perrhenate catalysts. The elucidated CMCs confirm the formation of supramolecular aggregates from [RMIM] [NO_3] surfactants at 115 and 4.7 mmol/L for R = octyl and dodecyl, respectively. Cryo-TEM has been attempted to visualize the nano-scale assemblies, but due to the lack of contrast by the light-weight elements to the surrounding H_2O/H_2O_2 matrix, no aggregates can be observed (Figure 33). Due to the unsuccessful imaging via electron microscopy, dynamic light scattering (DLS) has been exploited to determine the size of the aggregates. This method is reported to suitable for the measurement of micellar aggregates in aqueous solution.[154]

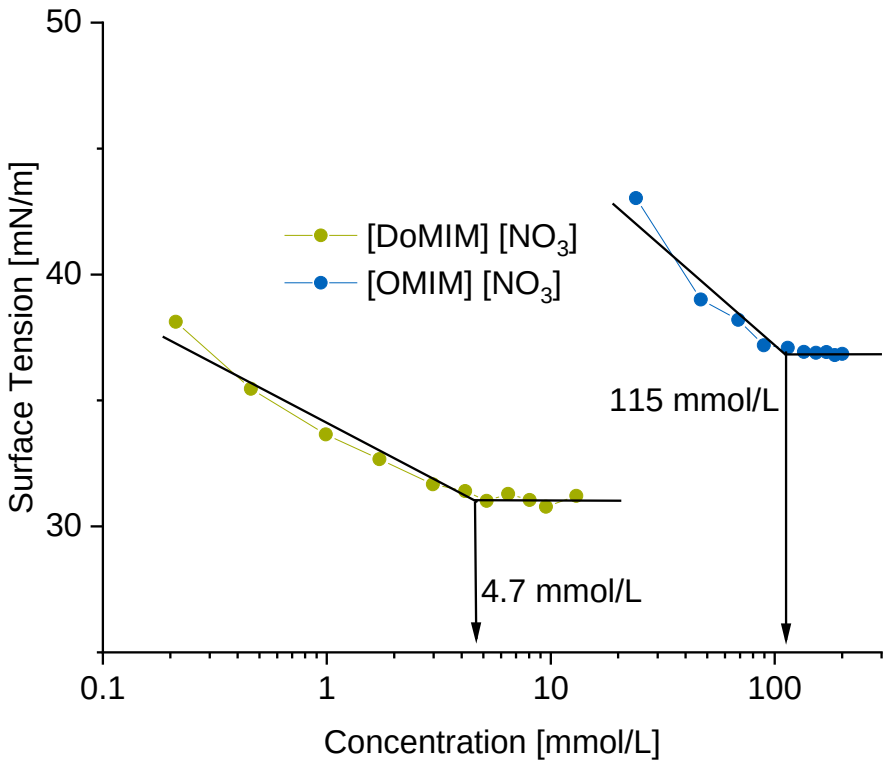

Scheme 7: Tensiometric measurements of [OMIM] [NO_3] (blue) and [DoMIM] [NO_3] (green) at 80 °C in 50 wt.% aqueous H_2O_2.

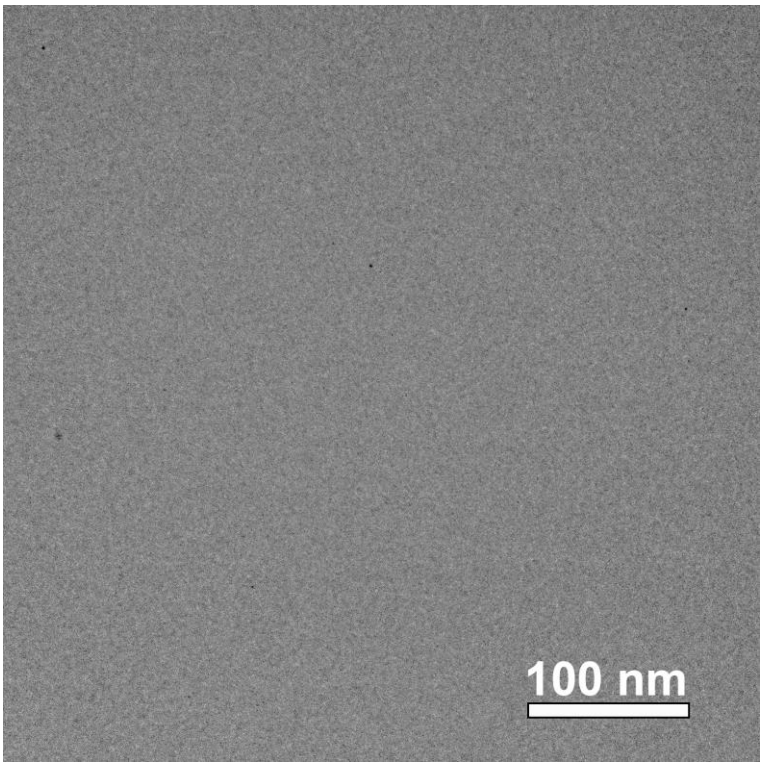

Figure 33: Cryo-TEM image of 357 mmol/L [OMIM] [NO_3] in 50 wt.% H_2O_2. Micelles cannot be identified.

Usual surfactant assemblies are in the range of a few nanometers and hence prone to scatter photons.[155] In contrast to multi-angle static light scattering (MALS), mostly exploited to determine polymer chain lengths, DLS traces the intensity fluctuations of the scattered light for a certain period of time. This course is then transformed to a correlation factor and the time required for this value to equal 1, standing for an averaging of the fluctuation intensity, gives the diffusion coefficient of the assemblies. Via the Stokes-Einstein equation, the hydrodynamic radius can be calculated. This easy approach is also the greatest disadvantage of the technique. The hydrodynamic radius does not contain any information on the shape of the aggregates but rather the size of hypothetical spheric assemblies with the equivalent scattering characteristics. Fortunately, the slope of the correlation curve gives insight into the particle size distribution due vastly increased scattering intensity for larger particles.

A further advantage of DLS is the *operando* observation of the micelle behavior affected by the external stimulus temperature. The required viscosity of 50 wt.% hydrogen peroxide at temperatures other than room temperature has not been reported before and hence was determined by capillary viscometry to be 1.17 mPas and 0.485 mPas at 20 °C and 80 °C, respectively. Solutions of 357 mmol/L imidazolium nitrate (standing for 5 mol-% catalyst loading, vide infra) in 50 wt.% aq. H_2O_2have been investigated by DLS before and after addition of excess *cis*-cyclooctene, a model substrate. Small supramolecular aggregates in the range of 1 nm with a narrow size distribution have been detected for pure [RMIM] [NO_3] ILs. Thus, such small assemblies of light-weight element constitution are impossible to detect by cryo-

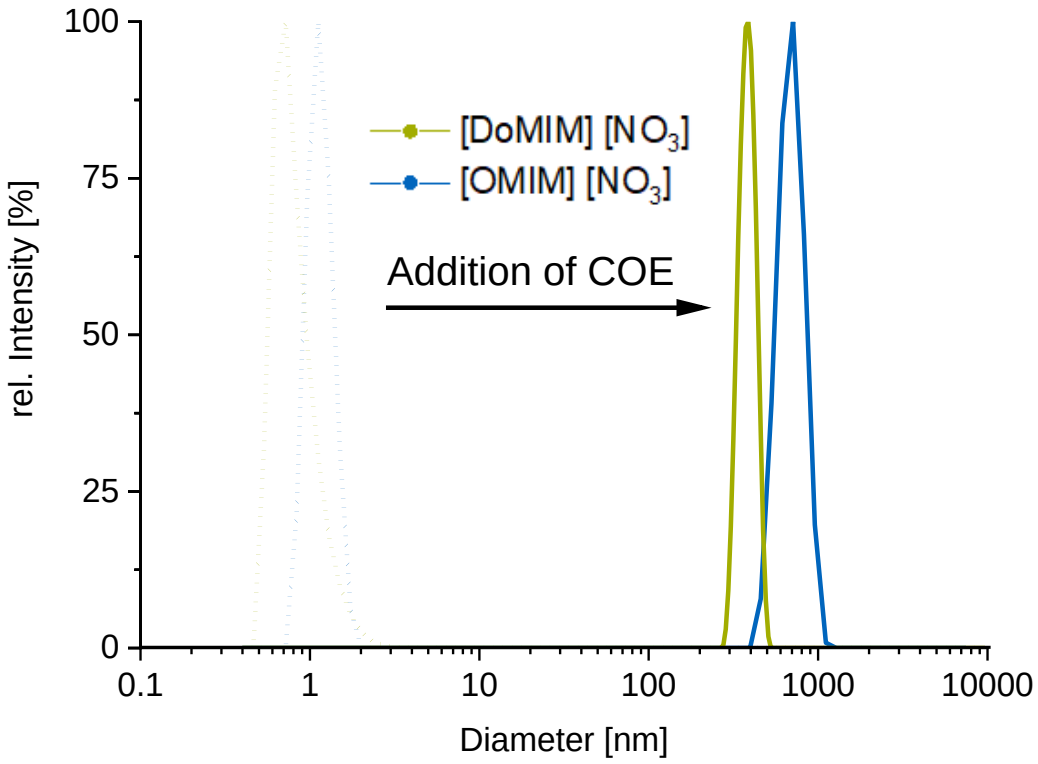

Figure 34: DLS measurement of 357 mmol/L [DoMIM] [NO_3] (green) and [OMIM] [NO_3] (blue) in 50 wt.% H_2O_2 at 80 °C. Dashed line: before addition of COE. Bold line: Aqueous phase saturated with COE.

TEM and therefore not visible (vide supra, Figure 33). Solutions of [DoMIM]-ILs form smaller aggregates than the [OMIM]-ILs, which has been observed and reported before.[156] At 20 °C, the addition of COE leads to a negligible micelle swelling by uptake of a few molecules (Table 6). In contrast, an enormous increase of the average micelle diameter by factor >600 and >450 for [OMIM] [NO_3] and [DoMIM] [NO_3] is observed at 80 °C (Figure 34). This massive swelling is further supported by solubilization measurements. At room temperature, both ionic liquids solubilize negligible amounts of COE in the aqueous phase, while at 80 °C, more than two molecules COE per imidazolium nitrate are solubilized. Hence, a high temperature is required to solubilize the substrate in the aqueous phase.

Table 6: Micellar sizes by DLS and COE uptake of solutions of 357 mmol/L [OMIM] [NO_3] and [DoMIM] [NO_3] in 50 wt.% H_2O_2 at 20 and 80 °C.

Catalyst	T [°C]	DLS without COE [nm]	DLS with COE [nm]	Uptake of COE per catalyst
[OMIM] [NO_3]	20	1.33 ± 0.52	1.61 ± 0.34	traces
[OMIM] [NO_3]	80	1.15 ± 0.20	697 ± 121	2.2
[DoMIM] [NO_3]	20	0.83 ± 0.26	0.98 ± 0.19	<0.2
[DoMIM] [NO_3]	80	0.84 ± 0.28	383 ± 43	2.6

For a potential catalytic application, one of the essential premises, the substrate solubilization is fulfilled. Still, the activation of hydrogen peroxide by nitrate is ambiguous. Hence, vibrational spectroscopy was exploited to analyze the effect of micelles formed by [OMIM] [NO_3] on the H-bond situation. In detail, vibrational changes upon adduct formation were investigated for the nitrate anion and the hydrogen peroxide molecule coordinated to nitrate. A pronounced interaction of the imidazolium C2-H and the nitrate anion is expected from spectra of neat solutions, which might occur and promote the activation of H_2O_2 in aqueous solution. Therefore, the IL derivative [OMMIM] [NO_3] is synthesized and investigated similarly towards the influence of the imidazolium C2-substituent by methylation on the H-bonding to the nitrate anion.

Spectroscopic investigations of the imidazolium nitrates

It is of great interest to investigate the chemical environment of the nitrate anion for its use in catalysis. The theoretically 'isolated' four-atom nitrate anion belongs to the D_{3h} symmetry group and has therefore six vibrational modes, of which two are double degenerate.[157] In the case that the nitrate anion is introduced into a chemical environment, out of the four detectable vibrational frequencies, the double degenerate modes split up. It has been shown, that the intense IR-active asymmetric stretching modes ν_3 (ca. 1340 cm^{-1}) of the nitrate anion are very sensitive to their chemical environment in terms of band splitting (Figure 35).[158]. The peak splitting can be elucidated from the IR spectrum and used as a tool to estimate the strength of the H-bonding of the nitrate anion to its surrounding. First, IR-spectra of solutions of KNO_3 in H_2O and KNO_3 in 50 wt.% H_2O_2 were recorded and the ν_3 band splitting evaluated upon subtraction of the respective pure solvent spectra. For a precise determination of the band positions, the second derivative of the difference spectra were calculated and reveal the multiple frequency bands overlapping in the normal spectrum.

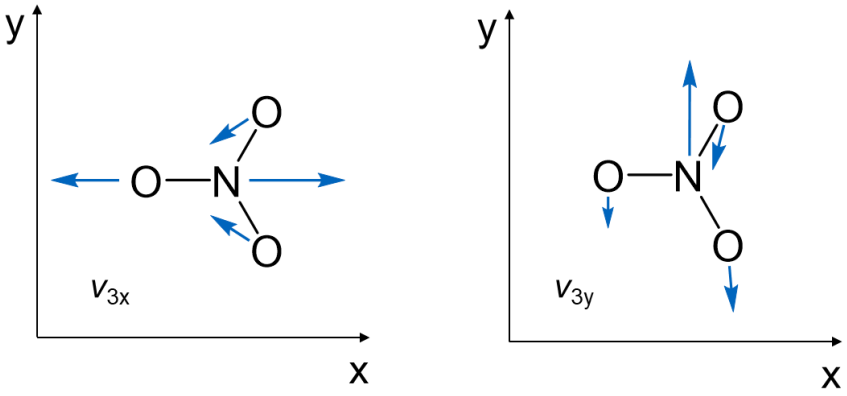

Figure 35: The double degenerate nitrate in-plane asymmetric stretch mode ν_3 at ca. 1340 cm^{-1}. Here, x and y are defined by the direction the nitrogen atom oscillates.

This deconvolution approach is a common procedure for resolution enhancement of vibrational investigations of weak interactions such as H-bonds.[159][160] Both second derivative spectra of KNO_3 show a strong band splitting of 55 and 58 cm^{-1} for H_2O and H_2O/H_2O_2, respectively. Hence, the hydratization of the nitrate anion is very similar in both solvents and an influence of the hydrogen peroxide cannot be elucidated. It is expected that the primary solvent shell of the nitrate anion is formed by water exclusively, due to its higher polarity compared to the hydrogen peroxide molecule. For the micellar solutions of [OMIM] [NO_3] and [OMMIM] [NO_3] with 42 cm^{-1} and 44 cm^{-1}in 50 wt.% H_2O_2, the splitting effect is appreciably smaller than for the KNO_3 solution. Hence, the chemical surrounding of the anion has changed equally for both systems in terms of nitrate hydratization. For comparison, the pure ionic liquid in absence of any traces of water gives a nitrate splitting of 31 and 10 cm^{-1} for [OMIM] [NO_3] and [OMMIM] [NO_3], respectively. The difference arises from the substitution of the slightly acidic hydrogen atom of the C-2 position of the imidazolium cation by a methyl group. Here, a much weaker cation-anion H-bond interaction is observed.[161][162] These nitrate v_3 vibration mode investigations show that the reactivity of the nitrate anion can be influenced by its chemical environment. The micellar-bonded nitrate is less exposed to the strongly binding water molecules than homogeneously dissolved nitrate salts. This may be the reason for the inactivity of the hydrogen peroxide activation with simple nitrate salts as H-bonds to water are preferred over bonds to H_2O_2 (vide infra). Despite that the nitrate v_3 band splitting is a good hint towards the strength of interaction of nitrate with water, it does not provide any information on the activation of hydrogen peroxide for its use as oxidant. Therefore, the changes of the hydrogen peroxide vibrational frequencies are investigated. All six modes are IR active and hence in theory feasible for spectroscopic investigations (Figure 36).[163] Practically, this applies mostly to gaseous H_2O_2 as most of the modes are rather weak in solution.

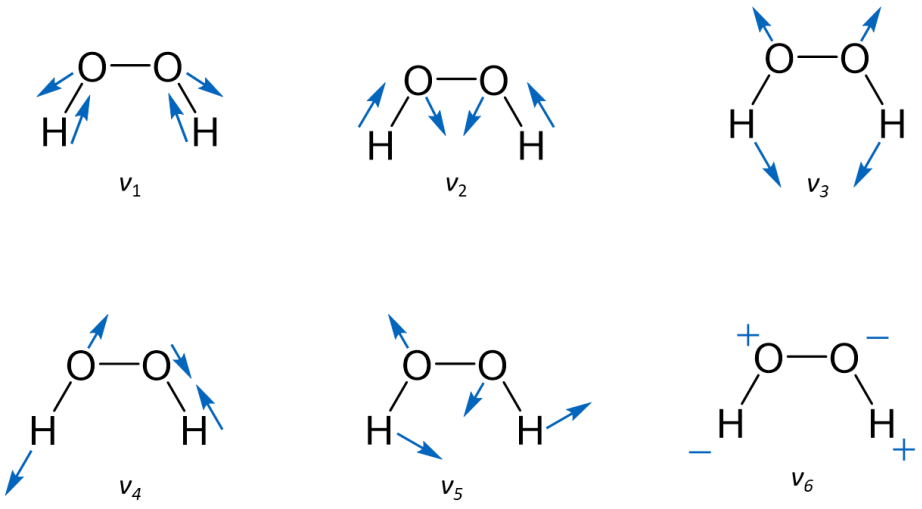

Figure 36: Overview of all six vibrational modes of H_2O_2. For v_6, '+' and '–' denotes up and down perpendicular to the paper plane.

The mechanistically promising ν_5 asymmetric deformation is weak and can unfortunately not be investigated. Still, the activation of hydrogen peroxide can be evaluated by the changes of the O-H dominant vibrational modes. Especially the IR-intense H_2O_2 asymmetric stretching mode ν_4 allows for the investigation of the activation of the molecule by nitrate due to the H-bonding towards the nitrate's oxo groups. This interaction decreases the H-OOH binding strength and thereby also the frequency of the ν_4 vibrational mode. Hence, the comparison of the ν_4 frequency shift is the ideal method to determine the influence of the imidazolium cations on the nitrate counterions compared to homogeneously dissolved inorganic nitrate salts. The spectroscopic investigation of the hydrogen peroxide activation requires high resolution instruments as the aqueous hydrogen peroxide solvent is catalytically used in 50-fold excess to the nitrate salt ($[NO_3]^-$:H_2O_2 = 1:50). The maximum ratio of activated hydrogen peroxide to 'uninvolved' hydrogen peroxide is one to 49. The corresponding peaks in the IR-spectra were identified as follows: Several spectra of imidazolium nitrate salts have been recorded in the OH- vibration region 3400-2800 cm^{-1}. For determination of the corresponding nitrate activated H_2O_2 peak, the spectrum of pure aqueous hydrogen peroxide was subtracted from a KNO_3 solution in aqueous hydrogen peroxide. The second derivative of the difference spectrum contains three dominant species, of which two belong to a water-nitrate adduct and one to the $H_2O_2\cdots[NO_3]^-$ signal. The first two species were assigned by subtraction of the spectrum of pure water from a spectrum of KNO_3 in pure water. There, the first two signals appeared, and one did not show up. Consequentially, the one additional signal at 3129 cm^{-1} of the hydrogen peroxide solution was assigned to the $H_2O_2\cdots[NO_3]^-$ band. This procedure was repeated for solutions of [OMIM] $[NO_3]$ and [OMMIM] $[NO_3]$ resulting in peaks at 3118 and 3115 cm^{-1} for the respective H_2O_2 asymmetric stretching frequency (Figure 37). The signals of the imidazolium nitrate solutions are notably shifted compared to the band of the KNO_3 solution, supporting the postulation that the presence of micelles allows for a stronger nitrate H-bonding to hydrogen peroxide, in contrast to the nitrate-protecting water shell for KNO_3 solutions (Table 7).

Table 7: Summary of the results of the spectroscopic investigation.

Parameter	Description	Gaseous H_2O_2 [164]	KNO_3/ H_2O_2	[OMIM] $[NO_3]$/ H_2O_2	[OMMIM] $[NO_3]$/ H_2O_2	Unit
ν_3 ($[NO_3]^-$)	$[NO_3]^-$ band splitting	---	58	42	44	cm^{-1}
ν_4 (H_2O_2)	H_2O_2 frequency for $[NO_3]^-$ adduct	---	3129	3118	3115	cm^{-1}
n(OH) [a]	O-H bond order	1.00	0.722	0.715	0.714	-
n(OO) [a]	O-O bond order	1.00	1.045	1.037	1.037	-

a: The bond orders have been calculated by Wilson's GF matrix method[165] by Janos Mink using his developed computer software[166]

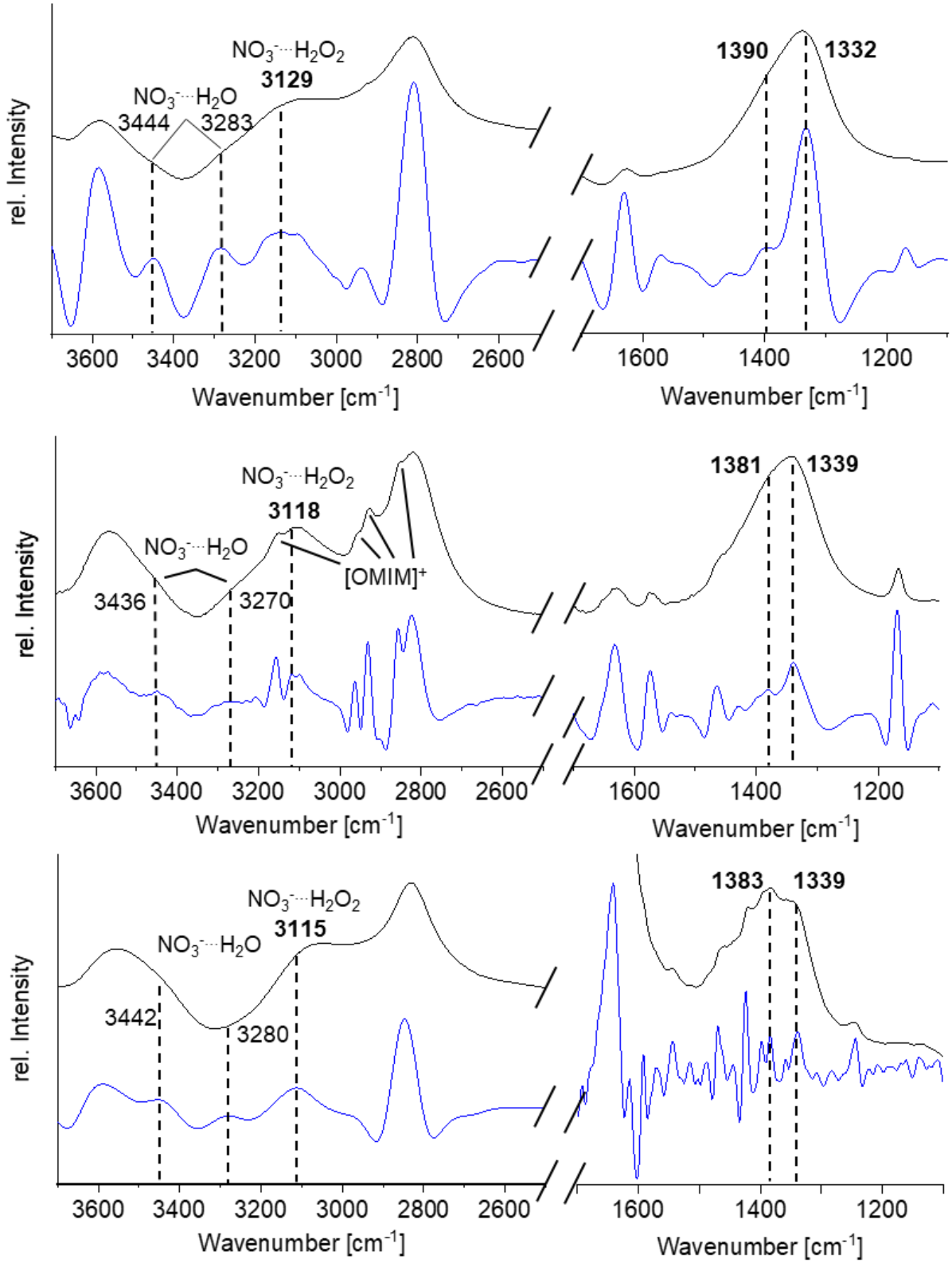

Figure 37: FTIR-spectra (black, subtracted by pure 50 wt.% H_2O_2) and second derivative spectra thereof (blue) of 357 mmol/L solutions of KNO_3 (top), [OMIM] [NO_3] (middle) and [OMMIM] [NO_3] (bottom) in 50 wt.% H_2O_2.

Concluding from this spectroscopic study it is feasible that the nitrate anion is able to activate hydrogen peroxide for its use in the catalytic epoxidation of olefins with the premise that the nitrate anion is part of a cationic micelle. The observed micellar effect on the nitrate anion is partial loss of its hydration shell, elucidated from the nitrate band splitting.

DFT calculations on the activation of hydrogen peroxide

The unique properties of the bonding situation of [OMIM] [NO_3] and H_2O_2 responsible for the activation by H-bonds was investigated by DFT. The calculations were conducted by Dr. Markus Drees. The functional M06[167] with the grimme dispersion GD3[168] and solvation model by density (SMD)[169] in water were used on a 6-311+G** level of theory.[170][171] In contrast to the simple nitrate salt KNO_3, [OMIM] [NO_3] forms shorter H-bonds in-between the H_2O_2 hydrogen atoms and the nitrate's oxo groups, resulting in a stronger activation (Figure 38). The *Lewis*-acidic imidazolium C2-proton additionally interacts with one of the H_2O_2 oxygen atoms, further decreasing the O-O bond order.

The influence of the C-2 imidazolium hydrogen atom was investigated *in silico* by substitution by a methyl group resulting in the $[OMMIM]^+$ cation. Spectroscopic investigations suggest a negligible difference in H_2O_2 activation. The DFT optimized structure similarly presents a small difference in H-bond lengths in-between nitrate and H_2O_2 (Figure 39). The missing supporting influence of the C-2 proton is compensated by H-bond formations with all imidazolium C_α methyl and methylene groups. The DFT calculations are in good agreement with the spectroscopic results and support a sufficiently strong activation of H_2O_2 for its use as oxidant in epoxidation reactions. Hence, the reactivity of micellar nitrates towards olefins is investigated in kinetic reactivity studies.

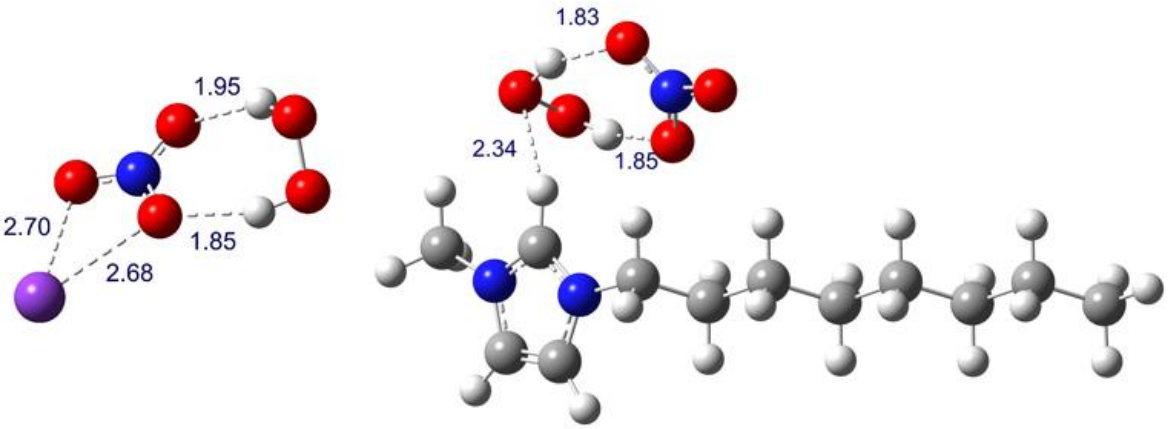

Figure 38: DFT-optimized structures of the interaction of KNO_3 (left) and [OMIM] [NO_3] with H_2O_2. M06/6-311+G** SMD (water) level of theory. H-bond lengths are given in Å.

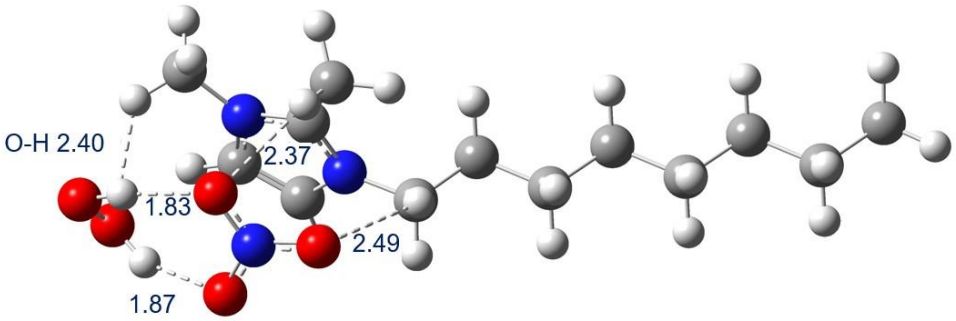

Figure 39: DFT-optimized structures of the interaction of [OMMIM] [NO_3] with H_2O_2. M06/6-311+G** SMD (water) level of theory. H-bond lengths are given in Å.

Catalytic epoxidation with micellar imidazolium nitrates

The synthesized micelle-forming imidazolium salts have been subjected to the catalytic epoxidation of the model substrate *cis*-cyclooctene in aqueous hydrogen peroxide (Scheme 8). 5 mol-% of the respective nitrate salt (vs. one equivalent of COE) were dissolved in 2.5 equivalents of 50 wt.% hydrogen peroxide (c = 357 mmol/L) and heated to 80 °C. Following, cyclooctene and the internal standard mesitylene were added and aliquots taken after certain time intervals from the supernatant organic phase. Upon dilution with deuterated chloroform, conversion of COE and yield of COO were determined by ^{1}H-NMR.

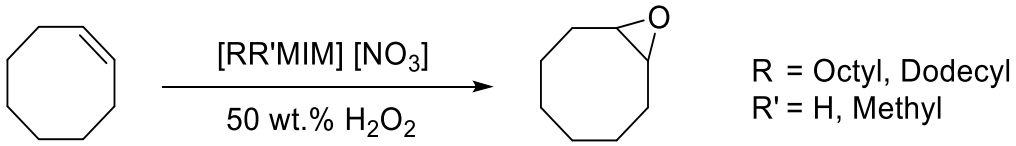

Scheme 8: Epoxidation of cyclooctene by surface-active imidazolium nitrates in 50 wt.% H_2O_2.

The first catalytic experiments were performed without any additive to investigate the intrinsic reactivity of [RMIM] [NO_3] as catalyst with H_2O_2 towards COE. Stirring of the aqueous hydrogen peroxide with COE for 24 hours at 80 °C results in a conversion of 6% and can be considered as the blind conversion, occurring independently and parallel to the investigated catalyst (Table 8, Entry 1). The use of 5 mol-% sodium nitrate vs. COE under equal conditions does not show any impact the conversion or epoxide selectivity. Hence, a catalytic activity of the homogeneously dissolved nitrate salt at 80 °C can be excluded. Upon application of 5 mol-% of the micelle-forming ionic liquid [OMIM] [NO_3], conversion of COE and yield of COO are 27% and 20%, respectively. This catalytic run confirms the predicted reactivity of imidazolium nitrates in the activation of hydrogen peroxide and allows for a catalytic use of nitrate in the epoxidation of COE. [DoMIM] [NO_3] has a little higher activity towards the activation of H_2O_2 which can be explained by the different CMC and hence the amount of catalyst assembled to micelles.

Table 8: Epoxidation of COE with 357 mmol/L nitrate salts in 50 wt.% aq. H_2O_2. Conditions: $[NO_3]^-$:COE:H_2O_2 = 5:100:250, 80 °C, 24

Entry	Catalyst	CMC	Micellar. Conc.	Conversion [%]	Yield [%]
1	None	---	0	6	5
2	$NaNO_3$	---	0	6	5
3	[OMIM] [NO_3]	115	242	27	20
4	[DoMIM] [NO_3]	4.7	352	40	29
5	[OMIM] [NO_3] + $NaNO_3$	n.d.	n.d.	26	18

Hence, a small CMC leads to a higher percentage of the catalyst to be aggregated. The respective micellar concentrations of [OMIM] [NO_3] and [DoMIM] [NO_3] are 242 mmol/L and 352 mmol/L (Table 8). The conversions subtracted by the blind conversion of 6% result in COE conversions of 21% and 34%. These activities in relation to their micellar catalyst concentration yield a very close intrinsic catalyst activity. Hence, the nitrate's intrinsic activity in micellar catalysis is independent of the surfactant's alkyl chain length. The addition of 5 mol-% $NaNO_3$ to the [OMIM] [NO_3] catalyst does not increase the overall nitrate activity. This experiment verifies the spectroscopic hypothesis that the nitrate anion is only active as part of a micelle and is inactive in case of a homogeneously dissolution in the aqueous phase (see Table 8, Entries 2 and 5). Tensiometry and conductivity studies of surface-active imidazolium ILs in water show that the methyl substituent at the imidazolium C2-position does not have a significant influence on the CMC.[172] Therefore, the micellar concentration of the active catalyst aggregated to micelles can be considered to be similar. The spectroscopic prediction, that the nitrate asymmetric stretching band splitting and H_2O_2 activation is similarly strong for the 1-alkyl-3-methylimidazolium and the 1-alkyl-2,3-dimethylimidazolium cation is supported by the catalytic application of the two respective C2-methyl substituted micellar catalysts (Figure 40). Here, the catalysts' difference in catalytic activity depends solely on the alkyl chain length and not on the imidazolium substitution pattern. As the substitution pattern of the imidazolium cations does not influence the catalytic activity, the necessity of the imidazolium motif is arguable. This was investigated by the application of synthesized cetyltrimethylammonium nitrate [CTA] [NO_3], which comes with several drawbacks. First, it is slightly soluble in the organic phase, leading to catalyst loss and product contamination and secondly, the activity is drastically reduced compared to the imidazolium-based catalysts. This is due to lack of sufficiently *Lewis*-acidic protons of the quaternary ammonium group for a strong H-bonding with the nitrate anions on the micellar surface. The tendency of lower reactivities is in good accordance with investigations of micellar perrhenate catalysts. The alkyltrimethylammonium perrhenates are likewise lower in activity compared to the imidazolium derivatives.[173]

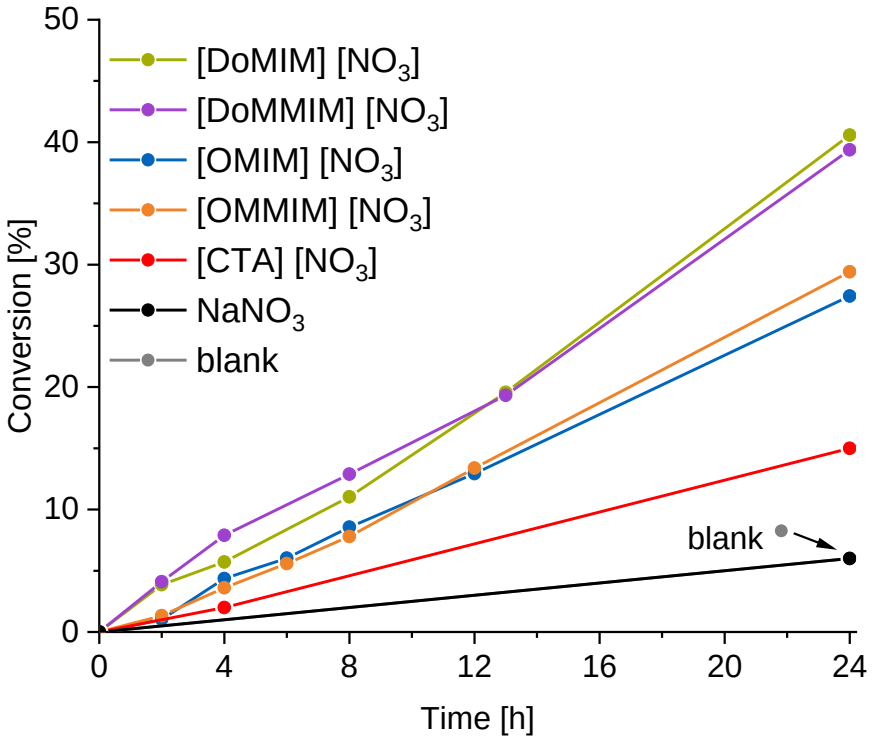

Figure 40: Conversion of COE by 357 mmol/L of various nitrate salts using 50 wt.% aqueous hydrogen peroxide. Conditions: Nitrate:COE:H_2O_2 = 5:100:250, 80° C.

To support these findings, the energetic profile of the catalytic cyclooctene epoxidation has been calculated by DFT. Starting from the optimized catalyst···H_2O_2 adduct geometries (Figure 38 and Figure 39), the interaction with the olefin and the transition state energies and were investigated (Scheme 9). Here, ethylene was exploited as a DFT model substrate for the M06/6-311+G** SMD (water) level of theory. The results show that starting from the nitrate/H_2O_2 adduct **A**, energetically being set to zero, the interaction with cyclooctene results in the slightly energetically demanding adduct **B** (Figure 41). Regarding the transition state **TS C**, both imidazolium catalysts show a decreased activation barrier compared to the KNO_3 salt (32.6 kcal/mol and 33.4 kcal/mol vs. 34.6 kcal/mol, Figure 41).

This energetic difference is the reason for the catalytic inactivity of simple nitrate salts. The micellar contribution and in particular the interaction with the imidazolium cation is detrimental for the activation of H_2O_2 by H-bonds. Additionally, it could be shown that the B3LYP/6-311+G** gas-phase level of theory is of sufficient accuracy to evaluate the micellar activation of hydrogen peroxide and the epoxidation mechanism within reasonable effort and time. The catalysts [OMIM] [NO_3] and [OMMIM] [NO_3] show a similar transition state energy for **TS C** of 36.4 kcal/mol. Nevertheless, simple alkali nitrate salts (e.g., $NaNO_3$, KNO_3) cannot be handled by the functional due to the lack of solvation of the cation, leading to unnaturally high *Lewis*-acidities, reducing the transition state energy drastically.

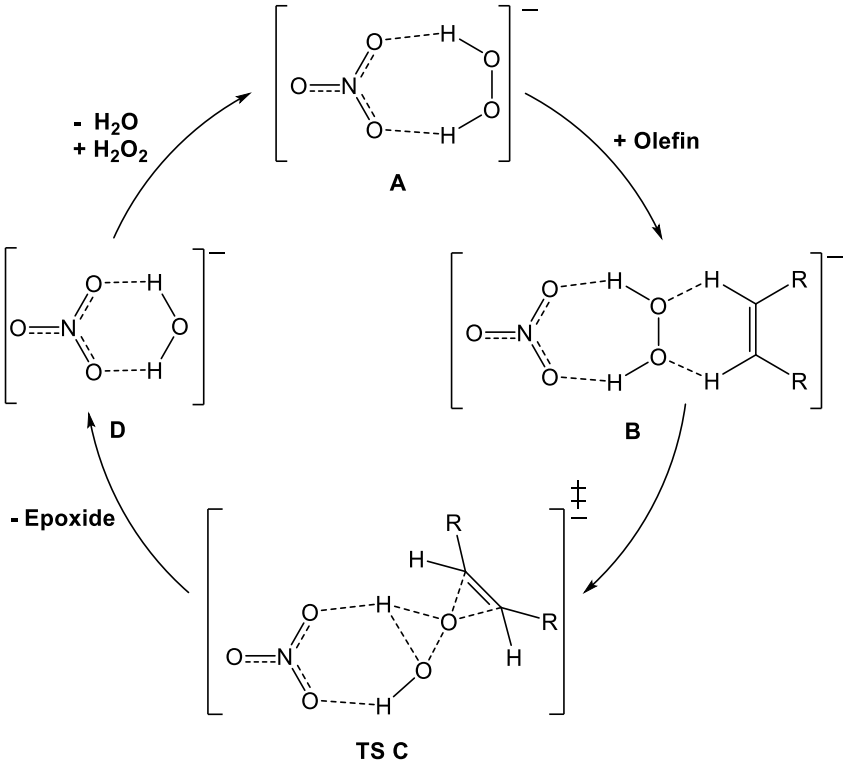

Scheme 9: Mechanistic cycle of the epoxidation of olefins via H_2O_2 H-bond activation by nitrate salts. The $[OMIM]^+$ cation is omitted for clarity.

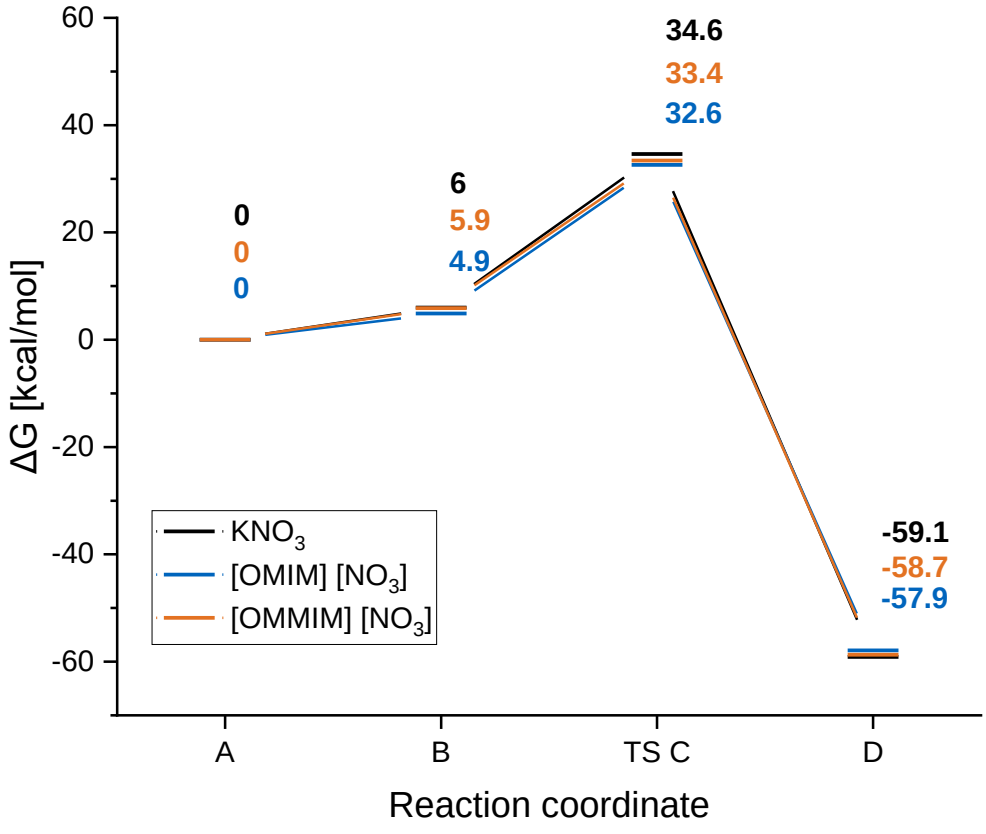

Figure 41: Energy profile for the epoxidation of ethylene by nitrate catalysts on the M06/6-311+G** SMD (water) level of theory.

Previous experiments have shown that additional amounts of $NaNO_3$ to the micellar catalyst [OMIM] [NO_3] have no influence on the catalytic activity of the COE epoxidation (Table 8). As the activation of hydrogen peroxide occurs via H-bonds, the influence of *Brønsted*-acidity was investigated. Hence, various amounts of nitric acid HNO_3 were added to the catalysis runs with 5 mol-% [OMIM] [NO_3] (Table 9). Even amounts as small as 1 mol-% HNO_3 vs. COE (c([OMIM] [NO_3]) = 5 mol-%) increase the reaction rate notably. This occurs to the fate of the produced epoxide, which is hydrolyzed to *trans*-1,2-cyclooctanediol by *Brønsted*-acid catalysis. Higher concentrations of acid further support the formation of the diol. Similarly, the addition of 1 mol-% NaOH results in a noteworthy increase of the reaction rate, leading to full conversion of COE and no yield of COO at all. This is explained by the nucleophilic character of the hydroxy groups, easily hydrolyzing the formed epoxide by nucleophilic attack. Therefore, the synthesis of the catalyst by anion exchange has to be carried out thoroughly as deviations of the imidazolium:nitrate = 1 ratio would lead to vastly lower product selectivities due to excess HNO_3 or hydroxides. Higher concentrations of NaOH lead to a rapid decomposition of the hydrogen peroxide at elevated temperature.

Table 9: Effects of various amounts of additives on the conversion of COE and yield of COO. Conditions: IL:COE:H_2O_2 = 5:100:250, 80 °C.

Additive	**mol-%**	**Conversion [%]**	**Yield [%]**	**Conversion [%]**	**Yield [%]**
		4 h		**24 h**	
HNO_3	0	4	3	27	20
	1	11	1	54	5
	2	24	1	72	4
	5	61	2	100	0
	10	91	1	100	0
NaOH	1	16	0	100	0

In order to optimize the reaction conditions of the catalytic runs with the pure [RMIM] [NO_3] (R = octyl, dodecyl) catalysts, the loading was varied to elucidate the most efficient catalyst concentration. [OMIM] [NO_3] and [DoMIM] [NO_3] with widely different CMCs were investigated towards activity of COE epoxidation after the subtraction of the blind conversion of 6% for easier comparison (Table 10). An experiment with 20 mol-% [DoMIM] [NO_3] did not phase-separate and can therefore not be considered a biphasic system and is not further considered. The obtained data were transferred to a conversion to catalyst-loading diagram presenting non-linear trends for both catalysts investigated (Figure 42). For [DoMIM] [NO_3], the activity to catalyst correlation rises strongly for the first two percent and then flattens progressively up to 10 mol-%. In contrast, [OMIM] [NO_3] shows a negligible conversion at 1 mol-% due to the

catalyst concentration being smaller than the CMC (71 mmol/L vs. 115 mmol/L) and hence the lack of micelles. Eventually, at higher catalyst loadings, the activity rises and then starts flattening. With the activity for small catalyst loadings being explained, the reason for this tendency is uncertain. As this phenomenon has to be a consequence of the micelle formation exclusively, conductometry experiments were performed with solutions of [OMIM] [NO_3] in aqueous hydrogen peroxide by Bastian Zehner. This is a powerful technique to investigate the surfactant aggregation beyond the CMC including changes of micellar phases. Here, the first bend of the trendlines indicates the CMC due to a decreased conductivity of micelles with aggregated ions compared to homogeneously dissolved ionic surfactant molecules (Figure 43, area **A**).

Table 10: Epoxidation of COE with various amounts imidazolium nitrates using 50 wt.% H_2O_2. Reaction Conditions: 24 h at 80 °C.

Entry	Catalyst	Loading [%]	Conc. [mmol/L]	Conv. [%]	Conv.[a] [%]
1	[OMIM] [NO_3]	1	71	8	2
2	[OMIM] [NO_3]	2	143	13	7
3	[OMIM] [NO_3]	5	357	27	20
4	[OMIM] [NO_3]	10	714	35	29
5	[OMIM] [NO_3]	20	1428	49	43
6	[DoMIM] [NO_3]	1	71	19	13
7	[DoMIM] [NO_3]	2	143	26	20
8	[DoMIM] [NO_3]	5	357	40	34
9	[DoMIM] [NO_3]	10	714	50	44

a: Conversion of COE subtracted by the blind conversion (6%).

The second trendline (area **B**) is not constant over the further concentration range but a second bend appears upon fitting with a third trend line (area **C**).This indicates a fundamental change of the shape of the surfactant assemblies. Unfortunately, DLS measurements at these high surfactant concentrations do not provide information on the aggregate size, but indicate the formation of polydisperse, large formations beyond 6 µm. Hence, the concentration of 5 mol-% has been shown to be the best micellar concentration (357 mmol/L, area **B**) in aqueous hydrogen peroxide. The conversion of COE with 5 mol-% [DoMIM] [NO_3] at 80 °C after 24 h is rather moderate with 40 %, so the catalytic activity is investigated at the higher temperatures 90 °C and 100 °C in order to further optimize the reaction conditions. The respective kinetic plots show that the activity is tripled and quadrupled within the first 12 h at 90 °C and 100 °C compared to the temperature of 80 °C (Figure 44). The small difference between the two higher temperatures is presumably due to the enormous CMC-increasing effect, leading to small concentrations of aggregated catalyst.

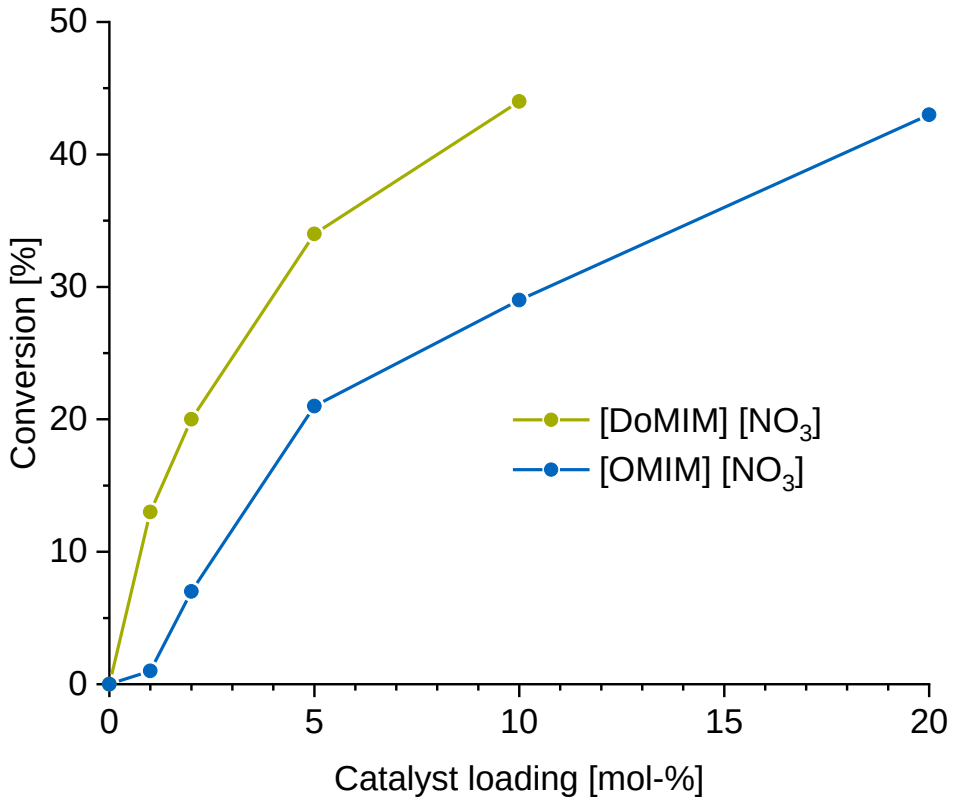

Figure 42: Conversion of the catalytic runs of [OMIM] [NO_3] (blue) and [DoMIM] [NO_3] (green) with various catalyst loadings, Conditions: COE: H_2O_2 = 1:2.5, 80 °C, 24 h.

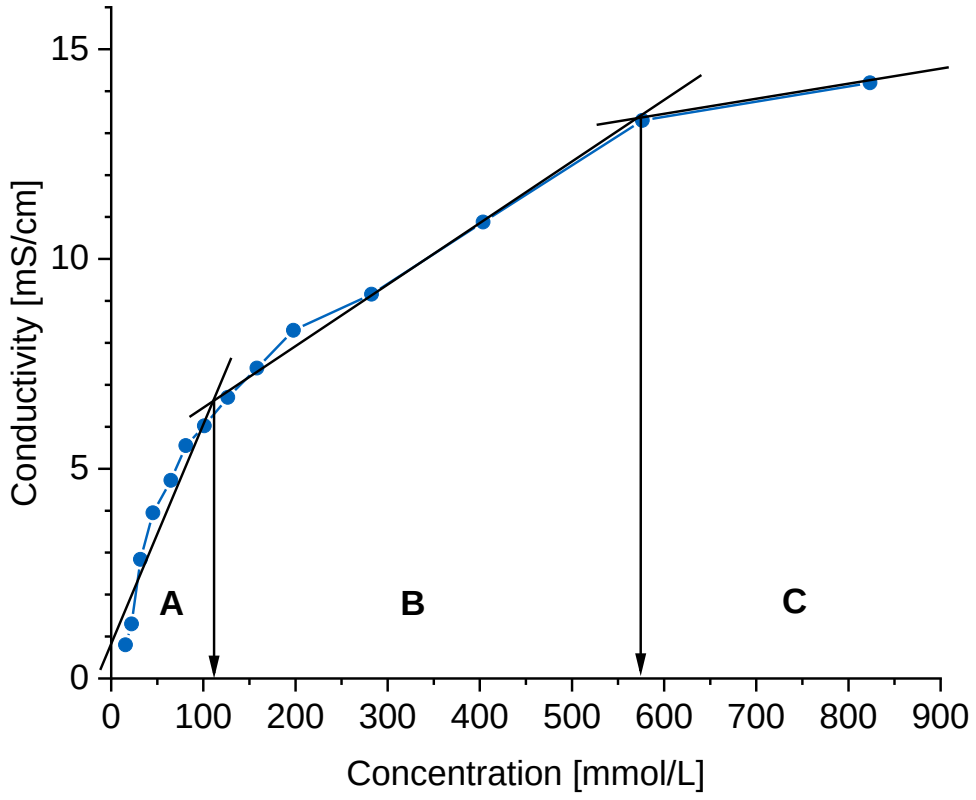

Figure 43: Conductometry of solutions of [OMIM] [NO_3] in 50 wt.% H_2O_2.

After 24 h, high conversions of COE and yields of COO are obtained. Interestingly, at 90 °C, the selectivity does not suffer from an increased epoxide hydrolyzation but is rather small compared to the 80 °C experiment. Hence, the activation energy of the epoxidation is smaller than the epoxide hydrolyzation, which is less influenced by the temperature.

The 90 °C experiment does indeed show the competitiveness of the imidazolium nitrate catalysts compared to classic homogeneous transition-metal catalyzed epoxidations with toxic organic oxidants. Nevertheless, the major advantage of the biphasic setup is the facile product separation and catalyst recovery. The reusability was shown for [DoMIM] [NO_3] as most efficient catalyst. Here, the organic phase is separated by decantation after each run and the residual organics solubilized in the aqueous phase by the micelles is extracted with toluene. Then, the hydrogen peroxide is decomposed using a platinum wire prior to removal of all volatiles in vacuo. The remaining catalyst is then dissolved in fresh aqueous hydrogen peroxide and cyclooctene added according to the standard catalysis procedure. The obtained data shows that the catalyst is recyclable for at least five times without any loss of activity (Figure 45). The perfect catalyst stability and the facile product separation paves the way for a continuous process, which can compensate the catalyst's low reactivity compared to homogeneous molecular catalysts.

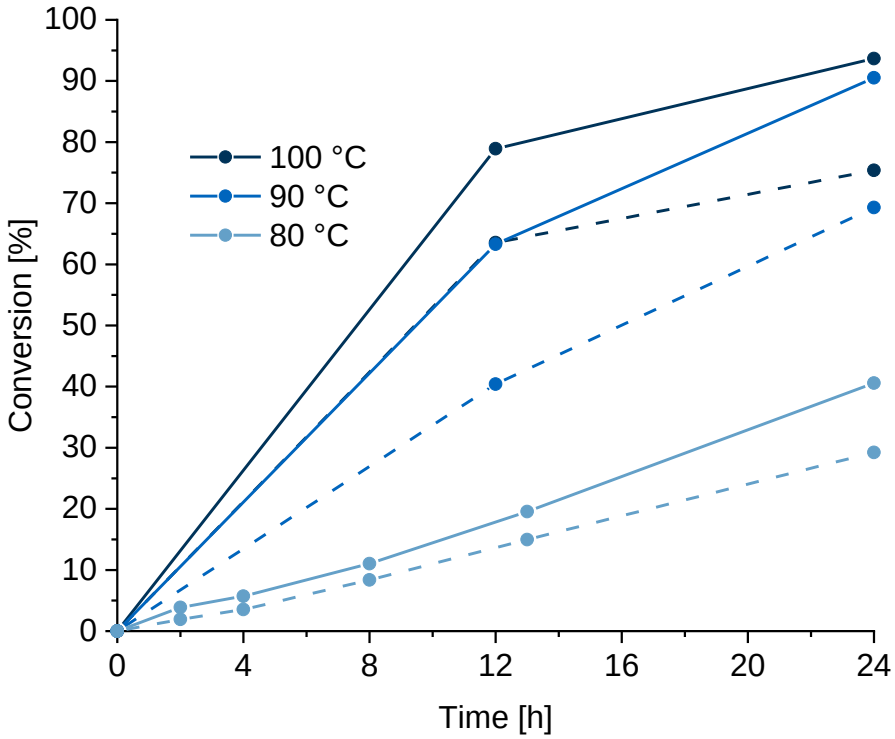

Figure 44: Conversion of COE (bold) and yield of COO (dashed) for the epoxidation with 5 mol-% [DoMIM] [NO_3] using 2.5 eq. H_2O_2 (50 wt.%) at various temperatures.

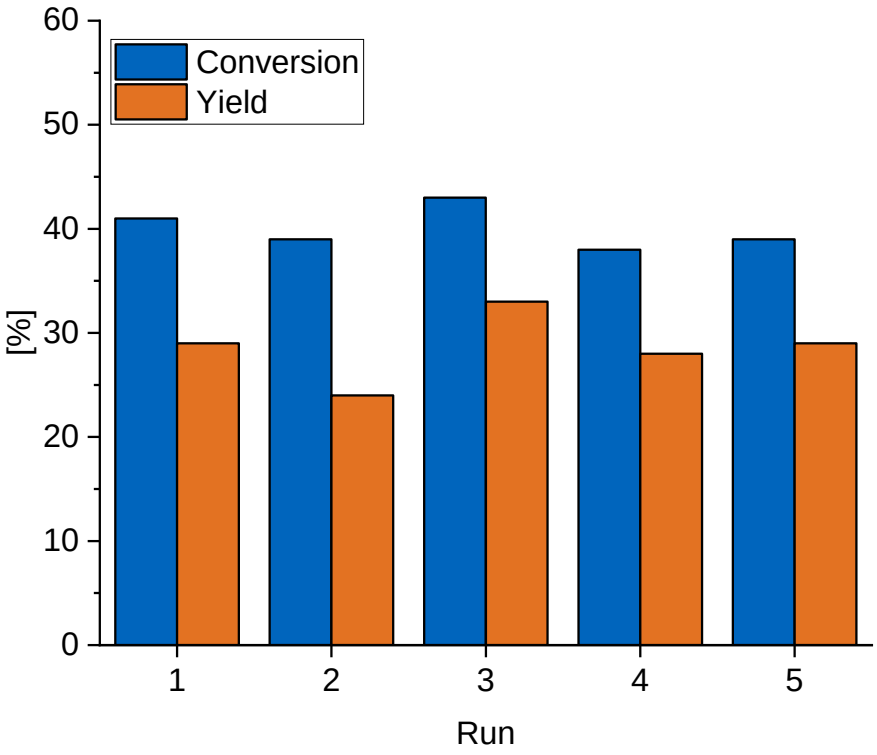

Figure 45: Recycling study with 5 mol-% [DoMIM] [NO_3]. Conversion of COE and yield of COO, respectively. Conditions: IL:COE:H_2O_2 = 5:100:250, 80 °C, 24 h.

Despite the atom-economic synthesis of the dialkylimidazolium nitrates, the necessity of the isolation of the catalyst is one of the major drawbacks of the herein discussed approach. Hence, the use of a commercially available imidazolium SAIL with the simple addition of co-catalytic amounts of a nitrate salt could lead in situ to the desired imidazolium nitrate in solution, without the need for a complicated catalyst synthesis and isolation procedure. Therefore, the common ionic liquids, [OMIM] Cl and [OMIM] [BF_4] were applied to form micelles in combination with equimolar amounts of sodium nitrate. At room temperature, the CMCs of the chloride (60 mmol/L) and tetrafluoroborate ionic liquids (48 mmol/L) are in the same order of magnitude as [OMIM] [NO_3] (31 mmol/L) in 50 wt.% aqueous hydrogen peroxide and a similar increase is expected at elevated temperatures.[121]

Due to the facile synthesis of [OMIM] Cl from 1-methylimidazole and octyl chloride, the combination of [OMIM] Cl with $NaNO_3$ is of high interest for a biphasic catalytic application. Here, the conversion of COE is slightly reduced compared to the pure [OMIM] [NO_3] catalyst (20% vs. 27%) (Table 11, Entries 1 and 2). The cross experiment [OMIM] [NO_3] in addition of NaCl leads to 18% conversion, proving the ion scrambling in solution. With chloride anions being involved, a severe oxygen evolution from the H_2O_2 decomposition is observed, leading to the question if the oxidant loss is responsible for the decrease in activity. Therefore, pure 50 wt.% H_2O_2 and two solutions of 357 mmol/L sodium salts ($NaNO_3$ and NaCl) were stirred for 24 h at 80 °C in absence of COE. It turned out that for the pure and the $NaNO_3$

solution 6% of the H_2O_2 is decomposed each. Surprisingly, NaCl decomposes 31% of the H_2O_2 within 24 h, resulting in a residual H_2O_2 concentration of approximately 35%. A use of 35% H_2O_2 in catalysis with 5 mol-% [OMIM] [NO_3] leads to a conversion of just 11% after 24 h. It has to be kept in mind that in this experiment the **initial** concentration of H_2O_2 was 35 wt.% while for [OMIM] Cl + $NaNO_3$ the **final** concentration after 24 h is 35%. Nevertheless, this chloride-induced oxidant decomposition is the reason for the decreased activity. Interestingly, the use of [OMIM] Cl only leads to a conversion of 21%. Hence, the chloride anion may also activate the hydrogen peroxide, likely via chloride oxidations, which are also responsible for the oxidant decomposition.[174] Conclusively, in the nitrate salt + [OMIM] Cl approach, the nitrate salt is homogeneously dissolved in solution without being part of the micelle. No catalytic activity may be attributed to the nitrate anion. This can be explained by the strong hydration of the anion, favouring its dissolution in the aqueous phase, while the chloride anions compensate the charges of the surfactant molecules on the surface of the cationic micelle. The application of pure imidazolium nitrate SAILs forces the anion to be part of the micellar assembly thus removing its hydration shell allowing for an activation of H_2O_2. Still, due to the high decomposition of valuable hydrogen peroxide, chloride-based cationic surfactants should not be used in catalysis as this would require additional amounts of valuable H_2O_2 and diminish the advantages of this ‘green’ and sustainable micellar approach. Hence, the combination of sodium nitrate and the commercially available IL [OMIM] [BF_4] was tested, as the $[BF_4]^-$ anion does not decompose hydrogen peroxide at elevated temperature. The run reveals a high conversion of 77% but a drastically reduced selectivity towards COO of only 33% compared to the experiment with [OMIM] [NO_3] with 27 and 74%, respectively (Table 11, Entries 5 and 2). The corresponding cross experiment, namely the use of [OMIM] [NO_3] with co-catalytic amounts of Na[BF_4] yields comparable conversions and selectivities. The low selectivity is due to the pronounced the formation of the by-product *trans*-1,2-cyclooctane diol similar to the experiments with additional nitric acid added to the catalytic run (Table 9) with the difference that the source of the *Brønsted* acid must be different. In literature, formation of fluorooxoboric acids upon hydrolysis of the $[BF_4]^-$ counterions of imidazolium ionic liquids is reported.[175] Hence, the stability of $[BF_4]^-$ under catalytic conditions is investigated by ^{11}B-NMR spectroscopy. After 24 h of stirring in 50 wt.% H_2O_2 a 13% decomposition of $[BF_4]^-$ to fluorooxoborates upon release of toxic HF is observed. This acidic contribution to the catalytic run is responsible for the low selectivity towards COO by epoxide hydrolyzation. The disadvantages of both common [OMIM]-ILs with the anions chloride and tetrafluoroborate make their use incompatible for micellar reactions in aqueous hydrogen peroxide. Therefore, the imidazolium nitrates must be isolated for best results in terms of selectivity and H_2O_2-efficiency.

Table 11: Epoxidation of COE using various imidazolium ionic liquids and additive salts with 50 wt.% H_2O_2. Conversion and Yield correspond to COE and COO, respectively. Reaction Conditions: 24h at 80 °C, Catalyst:COE:H_2O_2 = 5:100:250.

Entry	Catalyst	Conversion [%]	Selectivity [%]
1	[OMIM] Cl + $NaNO_3$	20	70
2	[OMIM] [NO_3]	27	74
3	[OMIM] [NO_3] + NaCl	18	73
4	[OMIM] Cl	21	71
5	[OMIM] [BF_4] + $NaNO_3$	77	30
6	[OMIM] [NO_3] + $NaBF_4$	71	35
7	[OMIM] [BF_4]	65	26

For a deeper understanding of the catalytic behavior, the reactivity towards other olefins was investigated. Various hydrocarbon-only olefins were tested under the optimized reaction conditions and analyzed towards yield and selectivity of epoxide formation (Table 12). Both, cyclohexene and 1-methycyclohexene have a *cis* double bond configuration, which is more reactive towards epoxidation due to the ring strain (see chapter 3.1). Despite the high reactivities, only negligible amounts of epoxide can be isolated after 24 h of reaction. The hydrolyzation of the product seems to be energetically preferred over the transfer of the oxygen atom to the olefin. The steric demand of the methyl group of 1-methylcyclohexene is insignificant and rather increases the reactivity by the electron-pushing nature of the substituent. The terminal olefin 1-octene shows a drastically reduced activity. Likely, the activation barrier is somewhat higher and the activation of H_2O_2 is barely sufficient for a small conversion. Internal olefins such as *cis*-2-octene and *trans*-2-octene without ring strain allow for higher conversions compared to the terminal derivative, attributed to the different substitution pattern of the C=C motif. Still, the epoxide hydrolysis plays a preferential role leading to low selectivities. The activated olefin β-*trans*-methylstyrene shows a very high conversion. Here, only a small amount of epoxide is found as it rather acts as an intermediate for the consecutive epoxide hydrolysis. The substrate variation experiments show that the activation of hydrogen peroxide by dialkylimidazolium nitrates is sufficient for the epoxidation of internal olefins. Mostly, the required high reaction temperatures and durations favor the hydrolysis of the epoxide towards diols.

Table 12: Epoxidation of various substrates with [OMIM][NO_3] using 50 wt.% H_2O_2. Conversion and yield of corresponding olefin and epoxide, respectively. Reaction conditions: 24h at 80 °C, [OMIM][NO_3]:olefin:H_2O_2 = 5:100:250.

Entry	Substrate	Conversion [%]	Yield [%]
1	*cis*-cyclooctene	27	20
2	cyclohexene	42	1
3	1-methylcyclohexene	100	0
4	1-octene	3	trace
5	*trans*-2-Octene	12	1
6	*cis*-2-octene	24	6
7	β-*trans*-methylstyrene	95	6

3.2.4 Conclusion

To date, the nitrate anion has never been considered as an active component in catalysis reactions in water as its hydration is responsible for the inactivity. The water molecules shield the negative charge and the *Lewis*-basic oxo-ligands from its surrounding. This does not allow for an activation of hydrogen peroxide by H-bonds due to the preferred and competing interaction with water molecules. Within this study, it is shown that the nitrate anion as part of a cationic micelle is less hydrated by water molecules, giving rise towards the H-bond activation of small molecules. This can be referred to two essential factors. On the one side, the hydrophobic effect by the micelle, for example exploited in cross-coupling catalysis with noble metal complexes in water,[24] leads similarly to an activation of the nitrate anion. On the other side, the strong H-bond interaction of the *Lewis*-acidic imidazolium protons with the nitrate anion further promotes its reactivity. In contrast, micelle-forming tetraalkylammonium cations reduce the nitrate's reactivity drastically and hence, a rate accelerating involvement of imidazolium H-bonds is apparent. Similar to the previously reported imidazolium tungstate ionic liquids,[128] the length of the imidazolium alkyl chain does not have an intrinsic influence on the activation by nitrate itself but determines the overall activity due to the amount of catalyst being assembled to micelles. The temperature and solvent-dependent CMC gives the concentration of the catalyst barely dissolved in the reaction medium without any catalytic contribution. Hence, a long alkyl-chain results in a low CMC and high amounts of the catalyst form micelles.

Moreover, this study shows that the concept of micellar activation of hydrogen peroxide by simple oxo-anions can be extended form the expensive perrhenate to cheap and abundant nitrate. The outer-spere mechanism can be considered to be similar to the perrhenate-catalyzed epoxidation, which occurs in ionic and micellar environments exclusively, albeit the perrhenate mechanism and the contribution of the surface-active cation has not been

investigated that deeply.[105] The higher reactivity of the perrhenate anion compared to nitrate is most probably due to the lower electronegativity, allowing for an increased electron density at the oxo-ligands. Additionally, the T_d symmetry of the perrhenate anion shows a tetrahedral geometry while the nitrate is trigonal planar and hence, might influence the H_2O_2-binding mode and angles by H-bonds.

In order to transfer the concept of the outer-sphere activation of H_2O_2 to other metal-free oxo-element anions, the related phosphate anion is a highly promising and interesting candidate. It has a triple negative charge allowing for a high electron density on its oxo-ligands and is likewise as simple and abundant as nitrate. A higher reactivity towards the activation of hydrogen peroxide can be expected and is thoroughly investigated in chapter 3.3.

3.3 Micellar Epoxidation with Imidazolium Phosphates

3.3.1 Introduction

The nitrate anion has been successfully applied as metal-free catalyst in the micellar epoxidation of olefins via formation of strong H-bonds for the activation of hydrogen peroxide. The micellar environment weakens the hydration shell allowing for a sufficiently strong interaction with hydrogen peroxide. Still, the reactivity of nitrate is somewhat lower compared to perrhenate despite the same nature of H_2O_2 activation, the outer-sphere mechanism. The different geometry of perrhenate and the lower electronegativity of the central atom has a major influence on the properties of the oxo-ligands and is beneficial for the H_2O_2-activation. Hence, the heavier pnictogen-oxide phosphate was investigated towards its reactivity towards hydrogen peroxide in micellar environments. Phosphate has the highest phosphorus oxidation state of +5 and is therefore stable towards oxidation, paving the way for its application under oxidative conditions. The bare phosphate anion has total triple negative charge and behaves alkaline in aqueous media due to the relatively high pK_a value of the corresponding hydrogenphosphate $[HPO_4]^{2-}$ of 12.4. This effect decreases the stability of H_2O_2 and hence leads to its decomposition resulting in a fast oxygen evolution at elevated temperature.[176] Moreover, a hypothetical $[RMIM]_3[PO_4]$ catalyst provides solely one phosphate anion per three surface-active cations leading to a lower anion concentration on the micellar surface. A one-on-one stoichiometry, combined with a circumvention of the basicity, is achieved by use of the dihydrogenphosphate $[(HO)_2PO_2]^-$ or esterification of two oxo-ligands with alcohols to diorganophosphates $[(RO)_2PO_2]^-$ (R = Alkyl, Aryl). Dialkylimidazolium dialkylphosphates are a renowned class of ionic liquids and are atom-economically synthesized by the reaction of alkylimidazoles with trialkylphosphates under solvent-free conditions. Surface-activity and micelle formation have been reported for long-chain derivatives and allow for a versatile tailoring towards the required application due to the wide functionalizability of the imidazolium cation as well as the anion.[177]

The activation of hydrogen peroxide by phosphate may arise via two different pathways, i) the outer-sphere activation via formation of H-bonds similar to the nitrate[148] or perrhenate[105] anions or ii) the formation of a peroxophosphate as a product of the reaction of the anion with H_2O_2 as in the case of tungstate.[128] Organic phosphoryl-species have been reported to strongly interact with hydrogen peroxide to form stable adducts.[178][179][180] This interaction could be sufficiently strong for the activation of hydrogen peroxide, especially for the herein proposed [OMIM] $[(RO)_2PO_2]$ SAILs, which bear an anionic phosphate species with a reasonably high electron density on the oxo-groups. Nevertheless, it has also been reported for the phosphate anion to react to peroxophosphate $[HPO_5]^{2-}$ in alkaline hydrogen

peroxide.[181] Hence, the formation of a diorganoperoxophosphate $[(RO)_2PO_3]^-$ may occur for micellar [OMIM] $[(RO)_2PO_2]$ solutions in aqueous hydrogen peroxide. Derived anionic peroxophosphorous species have been found to react with olefins according to the Prileschajev mechanism. However, the reported diaryl peroxophosphinates are synthesized prior to their use as stoichiometric oxidant from the respective chlorides or anhydrides in alkaline hydrogen peroxide.[182] In terms of sustainability and environmental aspects, the prevention of stoichiometric waste salt formation is an essential premise, as these species do not allow for a regeneration. The proposed activation of hydrogen peroxide by imidazolium diorganophosphates would in turn allow for a catalytic application of the SAILs in aqueous solution. The multifunctionality of the surface-active phosphates could fulfil the requirements of substrate transfer into the aqueous phase by formation of micelles, and the activation of hydrogen peroxide by the phosphate anions. Within this chapter, the micellar properties and the H_2O_2-activation mechanism are investigated by *in situ* analysis such as DLS and ^{31}P-VT-NMR spectroscopy with special regard to the diorganophosphate substitution pattern.

3.3.2 Results and Discussion

The dialkylphosphate-based ionic liquids [OMIM] $[(RO)_2PO_2]$ (R = Me, Et, ^{i}Pr) were synthesized in a one-step reaction by alkylation of *N*-octylimidazole with equimolar amounts of dialkylmethyl phosphate ($Alkyl_2MePO_4$) under solvent-free conditions (Scheme 10). The quantitatively obtained 1-methyl-3-octylimidazolium dialkylphosphates (Alkyl = Me, Et, ^{i}Pr) are further purified by evaporation of remaining volatiles and stored under argon atmosphere until application due to their high hygroscopicity.

For the synthesis of dihydrogen- and diarylphosphates (R = H, Ph, *p*-MeOPh), an anion exchange procedure was applied (Scheme 11). An aqueous solution of 1-octyl-3-methylimidazolium bromide [OMIM] Br is converted to [OMIM] [OH] by rinsing of a dilute solution over a freshly regenerated anion exchange resin and is subsequently converted to the SAIL by addition of one equivalent of the corresponding phosphoric acid. The quantitative removal of water in vacuo (10^{-6} mbar) yields the desired compounds [OMIM] $[(RO)_2PO_2]$ (R = H, Ph, MeOPh) on a multigram scale in excellent yields.

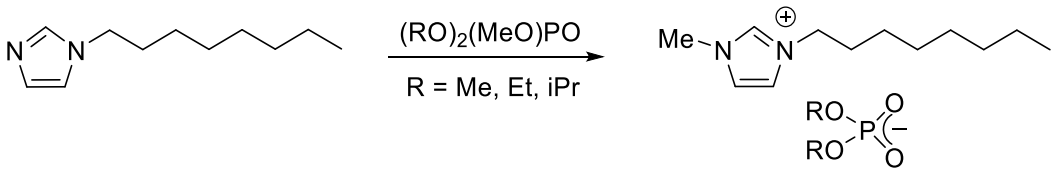

Scheme 10: Synthesis of [OMIM] $[(RO)_2PO_2]$ (R = Me, Et, ^{i}Pr) by methylation of N-octylimidazole.

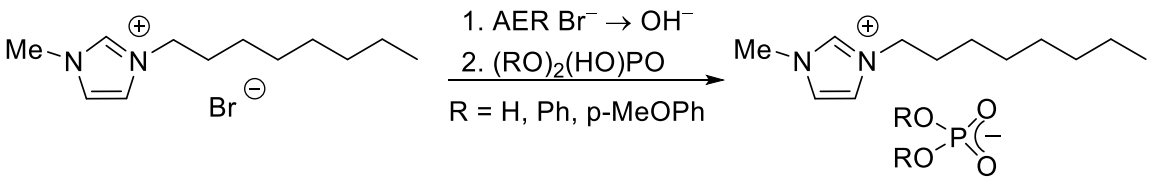

Scheme 11: Anion exchange procedure for the synthesis of [OMIM] $[(RO)_2PO_2]$ from [OMIM] Br via AER.

The synthesized ILs are highly soluble in water, aqueous hydrogen peroxide as well as chlorohydrocarbons but insoluble in nonpolar solvents such as hexane or toluene, paving the way for catalyst operation in the aqueous phase of an olefin/aq. H_2O_2 setup. All diorganophosphates are liquid at ambient temperature with increasing viscosity with the anion size. The 1-octyl-3-methylimidazolium dihydrogenphosphate [OMIM] $[(HO)_2PO_2]$ is a resinous solid with a melting point of ca. 120 °C, and hence not to be considered as an IL. For convenience, the surfactant is entitled as SAIL within this chapter.

Micelle characterization and solubility investigations

Water-soluble 1-octyl-3-methylimidazolium based ionic liquids are known for their surface activity and micelle formation above their respective critical micelle concentration (CMC), which is in the range of 25 mmol/L in water at room temperature.[177] The CMC is the surfactant-concentration that has to be exceeded for micelle formation and is dependent on the temperature[183] and the solvent mixture.[184][20] Recently, the formation of micelles by 1-octyl-3-methyl imidazolium ionic liquids was investigated by the collaboration partners of the University of Bayreuth and found that the choice of the anions barely influences the CMC in 50 wt.% aqueous hydrogen peroxide.[121] Therefore, a [OMIM] $[(RO)_2PO_2]$ surfactant concentration of 357 mmol/L (catalysis concentration, vide infra) is expected to be above the usual CMCs of approximately 100 mM in 50 wt.% aqueous H_2O_2 at 80 °C.

Dynamic light scattering (DLS) was exploited to study the aggregation of all [OMIM] $[(RO)_2PO_2]$ ILs in 50 wt.% aq. H_2O_2 at 80 °C with special regard to the organic phosphate substituents. DLS confirms the formation of supramolecular structures for all synthesized ionic liquids under catalytic conditions (Table 13). The [OMIM] $[(RO)_2PO_2]$ (R = H, alkyl) ILs show micelle formation of ca. 1 nm in size with larger diameters with increasing anion size, which is in good agreement with literature values for $[OMIM]^+$ based micelles in water.[185] The aryl derivatives show certainly larger aggregations, however, the shape of the micelle does not necessarily have to be spherical. For instance, diarylphosphates were reported to form vesicular bilayers in aqueous solution upon strong π-stacking, likely to influence the surfactant assembly.[186] To further reduce the size of the anion but maintain the aromatic substituent, an attempt was tried to synthesize a phenylene-derived catalyst.

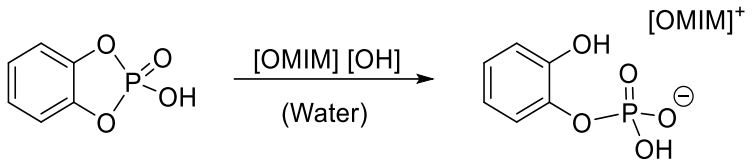

Scheme 12: The reaction of 1,2-phenylene phosphoric acid with basic reactants leads to hydrolysis of one ArylO-P bond.

Upon treatment of the corresponding 1,2-phenylenephosphoric acid with the freshly prepared [OMIM] [OH] solution, the anion hydrolyzes during synthesis (Scheme 12). Hence, the further investigations were performed with the presented compounds with phosphate-ILs of the general formula [OMIM] [$(RO)_2PO_2$] with two separate RO substituents. Upon addition of the supernatant *cis*-cyclooctene (COE) substrate phase to the catalyst in 50 wt.% hydrogen peroxide at 80 °C, a micelle swelling of the [OMIM] [$(RO)_2PO_2$] ILs is observed, confirming the uptake of the substrate (Table 13). The size for the [OMIM] [$(MeOPhO)_2PO_2$] aggregates with the largest anion maintains its size upon addition of COE, presumably due to a stronger interaction of the anion with the octyl chain of the imidazolium cation, leading to a non-spherical surfactant assembly, which cannot be elucidated by DLS. The uptake of COE was quantified by ^{1}H-NMR spectroscopy relative to the $[OMIM]^+$ cation and shows that all catalysts presented effectively solubilize fractions of the supernatant COE in the aqueous phase.

Table 13: Micellar COE uptake and micellar sizes of 357 mmol/L [OMIM] [$(RO)_2PO_2$] investigated by DLS at 80 °C in 50 wt.% aqueous hydrogen peroxide.

Catalyst	Micellar size without COE [nm]	Micellar size with COE [nm]	Uptake of COE (n_{COE}/n_{IL}) [a]
[OMIM] [$(HO)_2PO_2$]	0.693 ± 0.117	0.746 ± 0.164	0.27
[OMIM] [$(MeO)_2PO_2$]	0.751 ± 0.177	0.793 ± 0.167	0.13
[OMIM] [$(EtO)_2PO_2$]	0.959 ± 0.144	1.260 ± 0.223	0.63
[OMIM] [$(^iPrO)_2PO_2$]	0.995 ± 0.334	1.445 ± 0.201	0.94
[OMIM] [$(PhO)_2PO_2$]	3.908 ± 1.574	5.278 ± 1.017	0.36
[OMIM] [$(MeOPhO)_2PO_2$]	13.57 ± 3.04	13.12 ± 3.528	0.97

a: Determined by ^{1}H-NMR spectroscopy and referenced to the $[OMIM]^+$ cation proton signals.

SAIL interaction with hydrogen peroxide

The SAILs [OMIM] [$(RO)_2PO_2$] (R = H, Me, Ph, p-MeOPh) were investigated towards the interaction with 50 wt.% H_2O_2 by ^{31}P-NMR spectroscopy. Phosphorus is a mononuclidic element with a good gyromagnetic ratio and hence allows for a direct observation of the anion's central atom, which has been proven to be successful to elaborate the fundamental reactivity of tungstate in aqueous hydrogen peroxide. As the nitrate as well as the perrhenate anion are

inactive towards activation of hydrogen peroxide at room temperature, the interaction is analyzed at elevated temperatures (up to 80 °C). Solutions of 357 mmol/L [OMIM] [$(HO)_2PO_2$] and [OMIM] [$(MeO)_2PO_2$] in 50 wt.% H_2O_2 yield a single peak at approximately −1 ppm and 2 ppm, respectively, in-between RT and 80 °C (Figure 46 and Figure 47). A downfield peak shift can be observed at elevated temperatures, standing for a temperature-dependent influence of the chemical environment on the micellar bound phosphate anions. Such a downfield shift has previously been reported to be caused by interaction of the P=O species with hydrogen peroxide upon adduct formation.[178] Hence, this could support the theory that the strength of interaction is temperature-dependent. The higher the temperature, the stronger the H-bonding in-between phosphate and H_2O_2, which is required for its activation for epoxidation. From these experiments, the formation of a peroxophosphate can be excluded, as this would result in the formation of a second species or lead to a somewhat different P-resonance. A small ^{31}P-NMR chemical shift between the two species is reported for literature chemical shifts for diarylperoxophosphate and the diarylphosphate anions.[187] Unfortunately, peroxo-diarylphosphates cannot be isolated,[188] so an adapted literature protocol was applied to synthesize these species in situ to obtain the required NMR reference compounds.[182] Diphenylperoxophosphate and diethylperoxophosphate were synthesized from the respective diorganochlorophosphates in alkaline D_2O/H_2O_2 solution to allow for the ^{31}P-NMR shifts comparison to the respective organophosphates. The difference in-between the sharp signals of both species is observed as rather low with less than 1 ppm (Supplementary Figure 9 and Supplementary Figure 10). Still, the peak shift allows for a reliable distinguishment of the two species.

A first observation of the in situ formation of a second phosphate-species is presented by *in situ* ^{31}P-NMR-spectroscopy of [OMIM] [$(PhO)_2PO_2$] in aqueous H_2O_2. The distribution is highly dependent on the temperature, for which reason a variable-temperature (VT) NMR study in-between 0 °C and 80 °C was performed. (Figure 48). At low temperature, the majority of the phosphate is present in its usual diarylphosphate form. With increasing temperature, the amount of a second species is increased until at 80 °C it is exclusively present. After slow cooling to 20 °C, the distribution between the two species is back at its normal distribution, confirming a temperature- dependent equilibrium and excludes the decomposition of the diphenylphosphate.

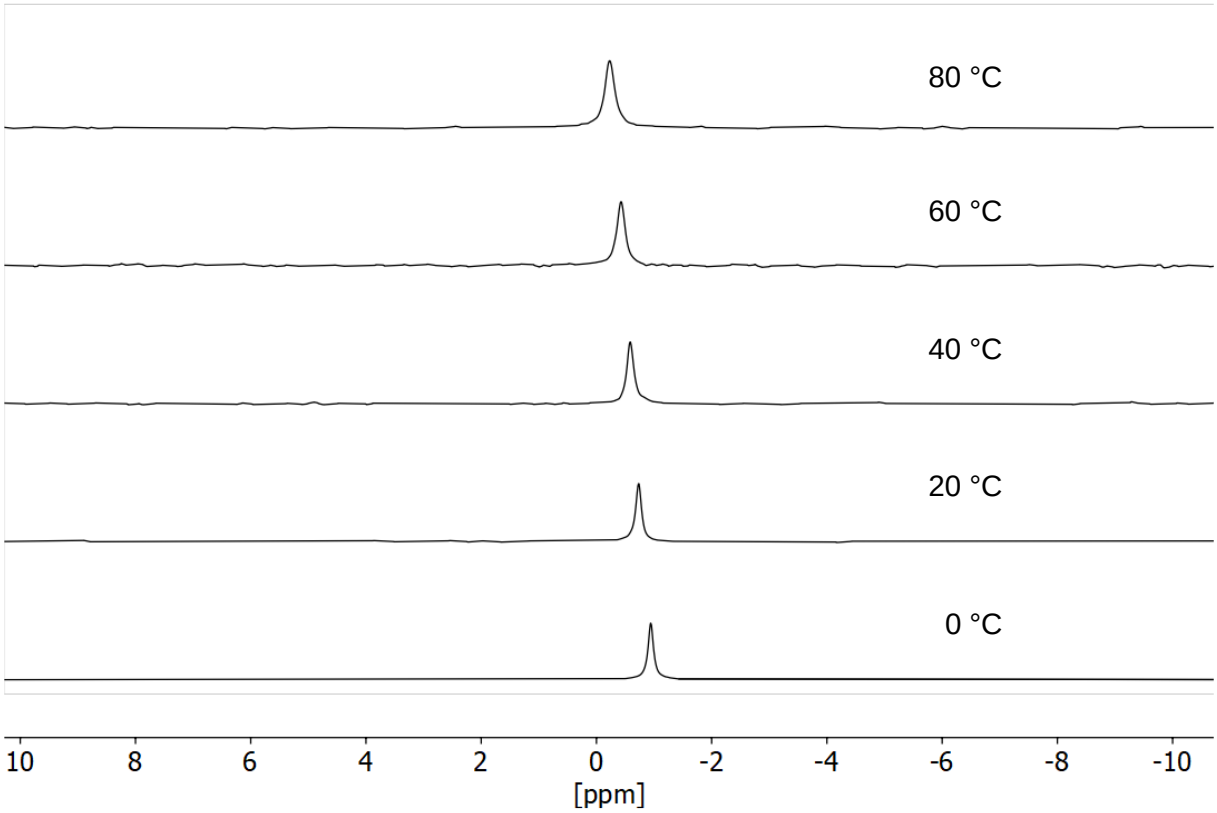

Figure 46: ^{31}P-VT-NMR spectra of 357 mmol/L [OMIM] [$(HO)_2PO_2$] at different temperatures in 50 wt.% H_2O_2.

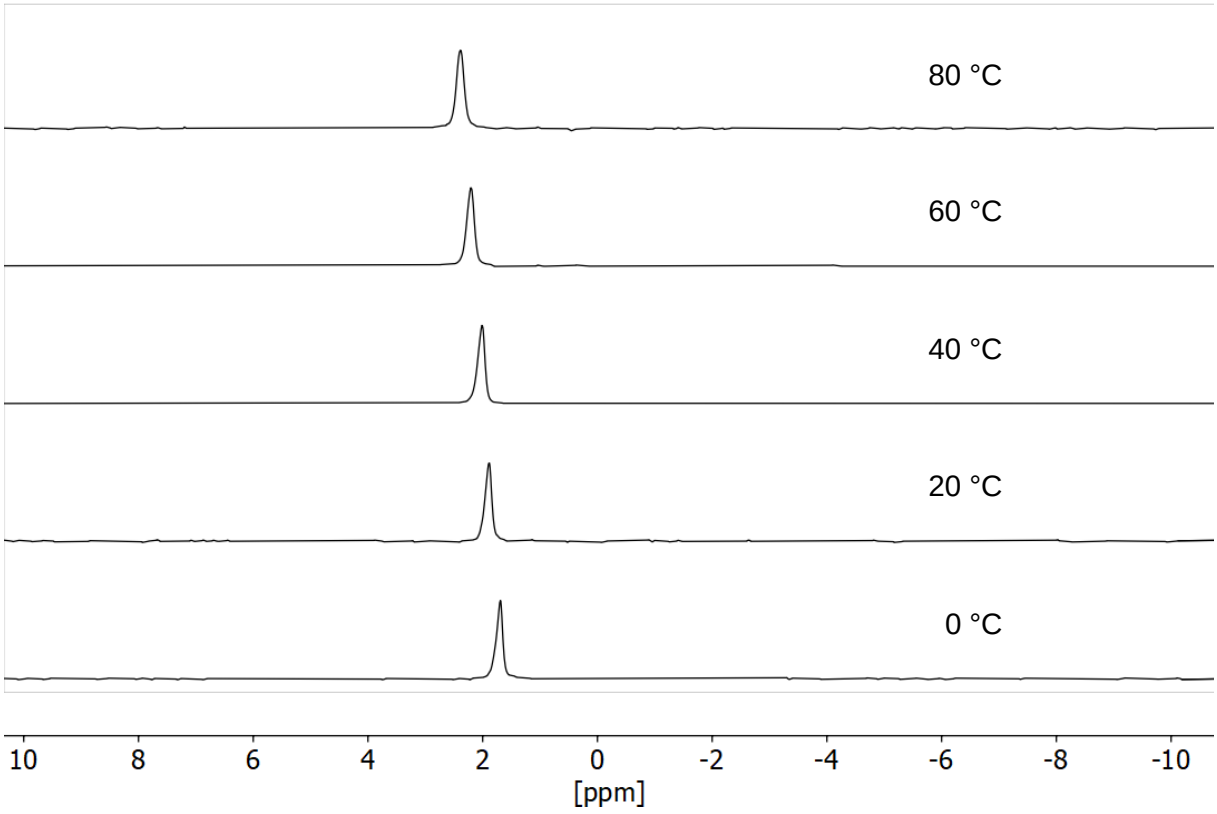

Figure 47: ^{31}P-VT-NMR spectra of 357 mmol/L [OMIM] [$(MeO)_2PO_2$] at different temperatures in 50 wt.% H_2O_2.

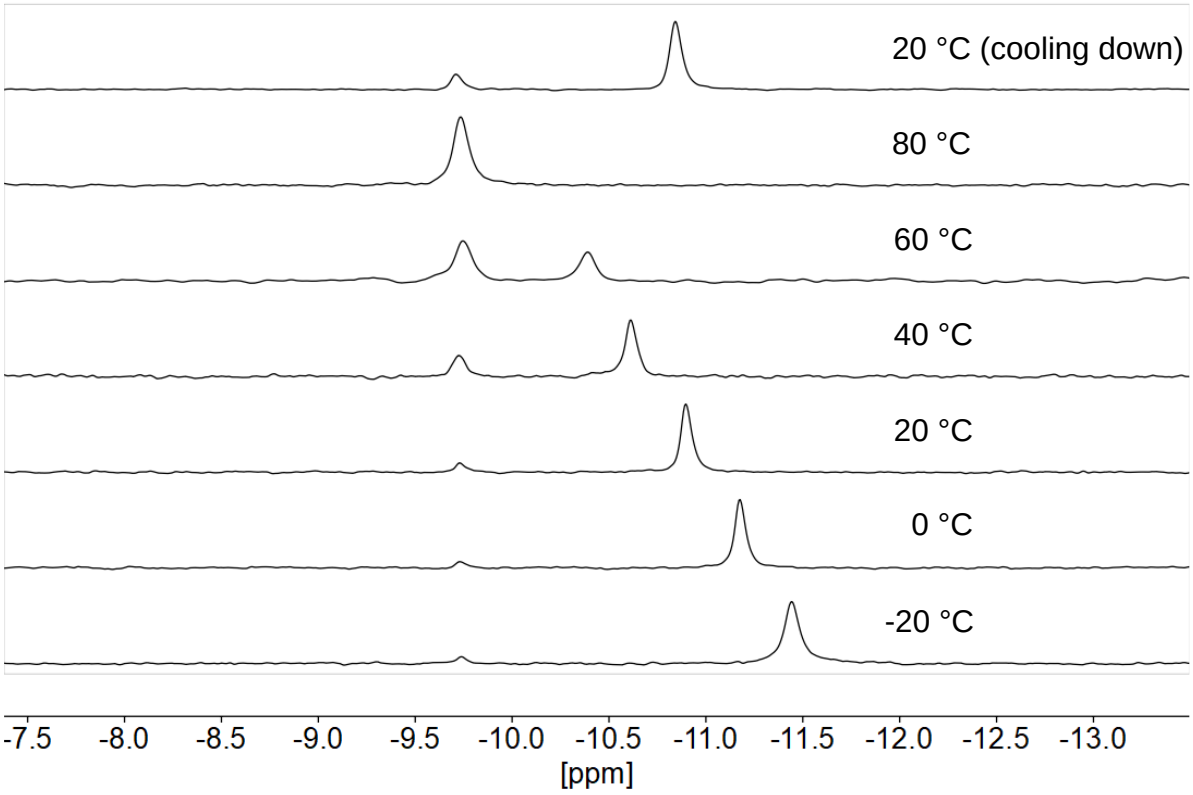

Figure 48: ^{31}P-VT-NMR spectra of 357 mmol/L [OMIM] [$(PhO)_2PO_2$] at different temperatures in 50 wt.% H_2O_2. Left signal: Diphenylperoxophosphate. Right signal: Diphenylphosphate.

The exact chemical shifts of the reference compounds sodium diphenylphosphate and sodium diphenylperoxyphosphate (Supplementary Figure 9) and the SAIL [OMIM] [$(PhO)_2PO_2$] (Figure 48) cannot be compared due to the influence of the different solvent (D_2O vs aq. H_2O_2) as well as the different cations with the resulting micellar environment. Nevertheless, the relative position of the chemical shift of the two species (phosphate and peroxophosphate) allows for an assignment of the two species. The formation of a peroxo-species from non-metal oxo-anions in aqueous hydrogen peroxide has been reported for carbonates[189][190] and carbonic acids.[191][192] A peroxophosphate formation is known for alkaline phosphate/H_2O_2 mixtures has not been reported for pH-neutral phosphate/H_2O_2 solutions so far.[181]

The *in situ* NMR experiments were similarly performed with [OMIM] [$(MeOPhO)_2PO_2$], which exhibits a higher electron at the phosphate's oxo-groups density due the *p*-methoxy electron pushing groups. At 80 °C, only 70% (in contrast to 100% for [OMIM] [$(PhO)_2PO_2$]) of the newly formed P-species is observed, suggesting a slightly energetically more demanding peroxo-phosphate formation than for [OMIM] [$(PhO)_2PO_2$] (Figure 49). This is presumably caused by the reduced phosphorus *Lewis*-acidity due to the electron-pushing effect of the *p*-methoxy phenyl substituents. For both [OMIM] [$(ArylO)_2PO_2$] ILs, a temperature-dependent peak shift for the non-reacted phosphate species can be observed, which is in accordance with the other SAILs investigated, hence supporting the peak assignment.

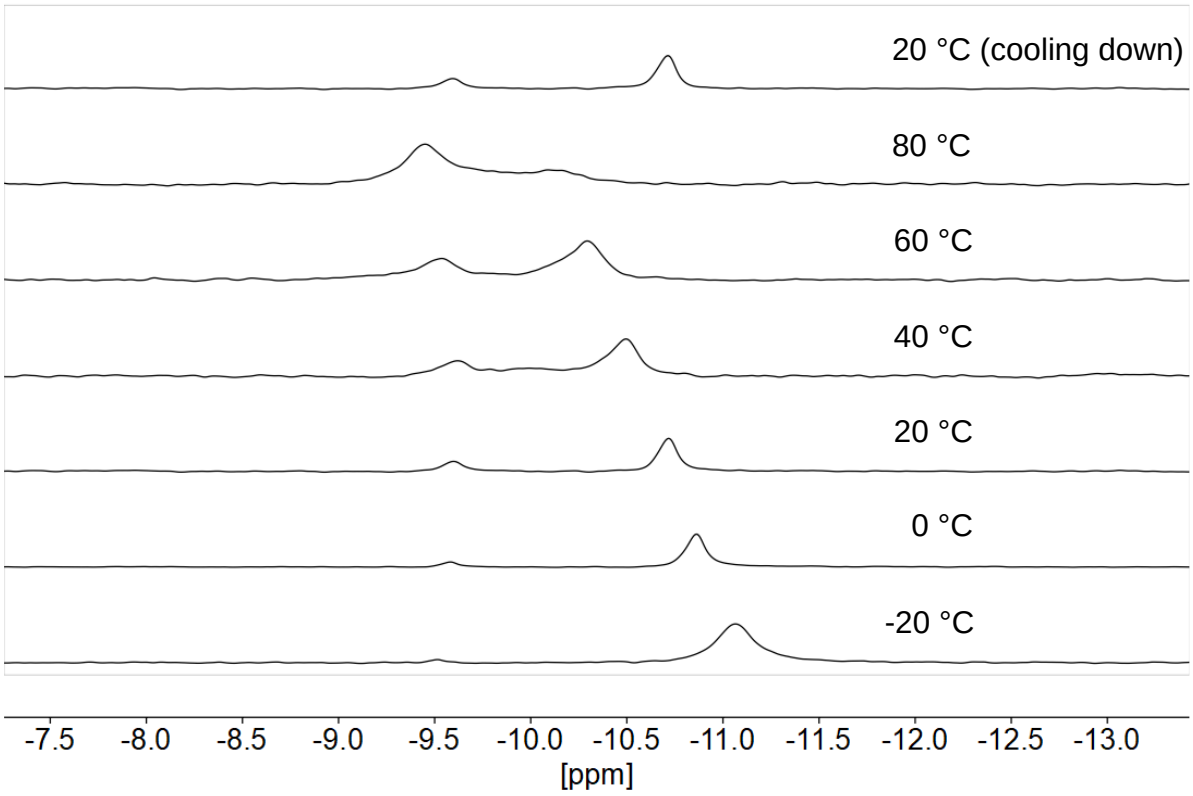

Figure 49: ^{31}P-VT-NMR spectra of 357 mmol/L [OMIM] [$(MeOPhO)_2PO_2$] at different temperatures in 50 wt.% H_2O_2. Left signal: Di(*p*-methoxyphenyl)peroxophosphate. Right signal: Di(*p*-methoxy-phenyl)phosphate.

The anticipated peroxophosphates are relatively independent on the chemical environment, as the species is already a product formed with H_2O_2.To investigate the impact of the micelles on the formation of a peroxophosphate species, a solution of the sodium salt Na[$(PhO_2)PO_2$] in 50 wt.% H_2O_2 was analyzed via ^{31}P-VT-NMR. In contrast to the micellar [OMIM] [$(PhO)_2PO_2$] solution, only the phosphate signal could be detected over the temperature range from 20 to 80 °C (Figure 50). This leads to the assumption, that a peroxophosphate species can only be formed if the anion is part of a cationic micelle, which is required for its stabilization. Moreover, the ^{31}P-NMR shift of the sodium salt is less influenced by the temperature, as it is homogeneously distributed and hence hydrated by water molecules, supressing interactions with the H_2O_2 molecules in solution as it is the case for e.g. nitrate and perrhenate.

Mechanistic DFT-calculations

To gain a better insight into the molecular mechanisms and the nature of possible peroxophosphates, the interaction of the micellar catalysts with hydrogen peroxide was investigated by DFT. The calculations were performed by Dr. Markus Drees using the functional B3LYP[193][194][195][196] on the 6-311+G** level of theory in the gas phase, which has shown to be sufficiently accurate to describe H-bond formations in a micellar environment (see chapter 3.2, activation of hydrogen peroxide by imidazolium nitrates).

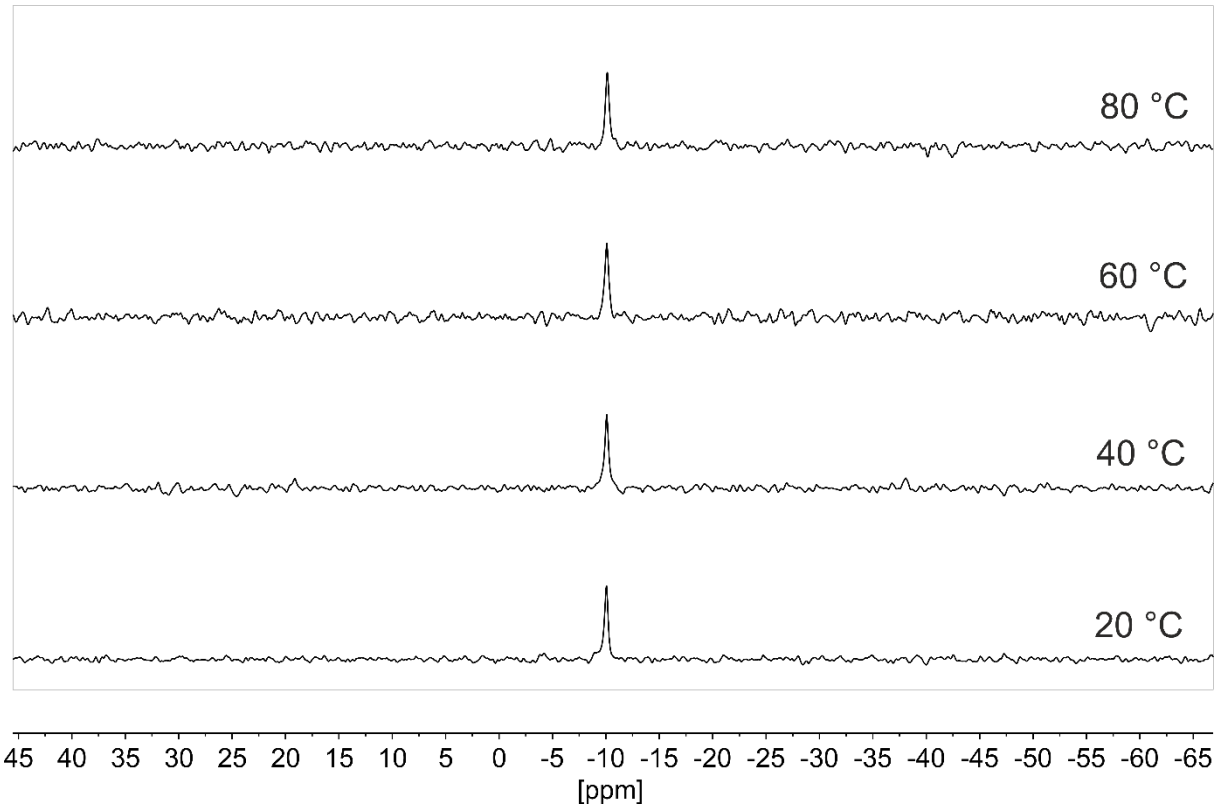

Figure 50: ^{31}P-VT-NMR spectroscopy of 357 mmol/L Na[$(PhO)_2PO_2$] at different temperatures in 50 wt.% H_2O_2.

The energy calculations reveal that the interaction of the catalyst with hydrogen peroxide forming a double bonded H-bond adduct is energetically preferred over the pure IL. This adduct [phosphate···H_2O_2]$^-$ is set as a zero-point for the further calculations (Scheme 13). According to the DFT calculations, the H_2O_2 molecule is not H-bonded via the two oxo groups but rather via one oxo group and one RO-substituent (Figure 51). The respective optimized structures reveal that this is due to the interaction of one oxo-group with the slightly acidic imidazolium C2-H. This is supported by the H-bond formed in-between the phosphate anion [$(RO)_2PO_2$]$^-$ and H_2O_2, which is shorter with 1.70 Å, 1.68 Å and 1.69 Å) for R = H, Me and Ph, respectively compared to [NO_3]$^-$···H_2O_2 with 1.80 Å.[148] Hence, the activation of hydrogen peroxide might be stronger for the phosphates than for nitrate, according to the B3LYP level of theory.

The investigation shows that a consecutive rearrangement reaction may occur upon nucleophilic attack of the H-bonded H_2O_2 molecule on the central phosphorous atom resulting in a five-bonded phosphorus species (**2R_is**; R = H, Me, Ph). The respective transition state energies are very close to the five-bonded intermediate and hence a dynamic equilibrium with the H-bonded complex can be expected. Depending on the substituent R, a rearrangement reaction may occur, which involves the insertion of a peroxo-oxygen into the P-OR bond. This results in an energetically favourable [peroxophosphate···H_2O]$^-$ adduct **3R_is**.

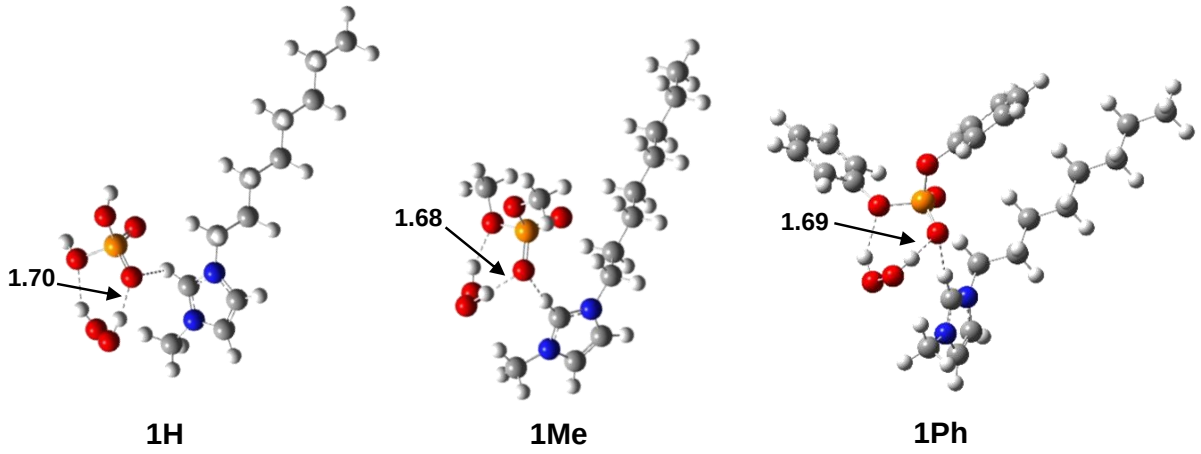

Figure 51: DFT-calculated structures of the SAIL/H_2O_2 adducts **1H**, **1Me** and **1Ph**. Bond lengths given in Å.

The respective transition state energy is rather high and hence the shift unlikely for R = Me and H with 50.2 kcal/mol but may occur for R = Ph with a reasonable low $\Delta G^{\#}$ of 38.2 kcal/mol. The major difference is the stabilization of the shifted group, with the aromatic phenyl ring contributing to delocalization of the negative charge. At elevated temperature, this rearrangement reaction appears to be very likely for [OMIM] $[(PhO)_2PO_2]$ and hence this species (**3R_is**) is possibly the peroxo-species detected in the ^{31}P-VT-NMR *in situ* investigation (Figure 48).

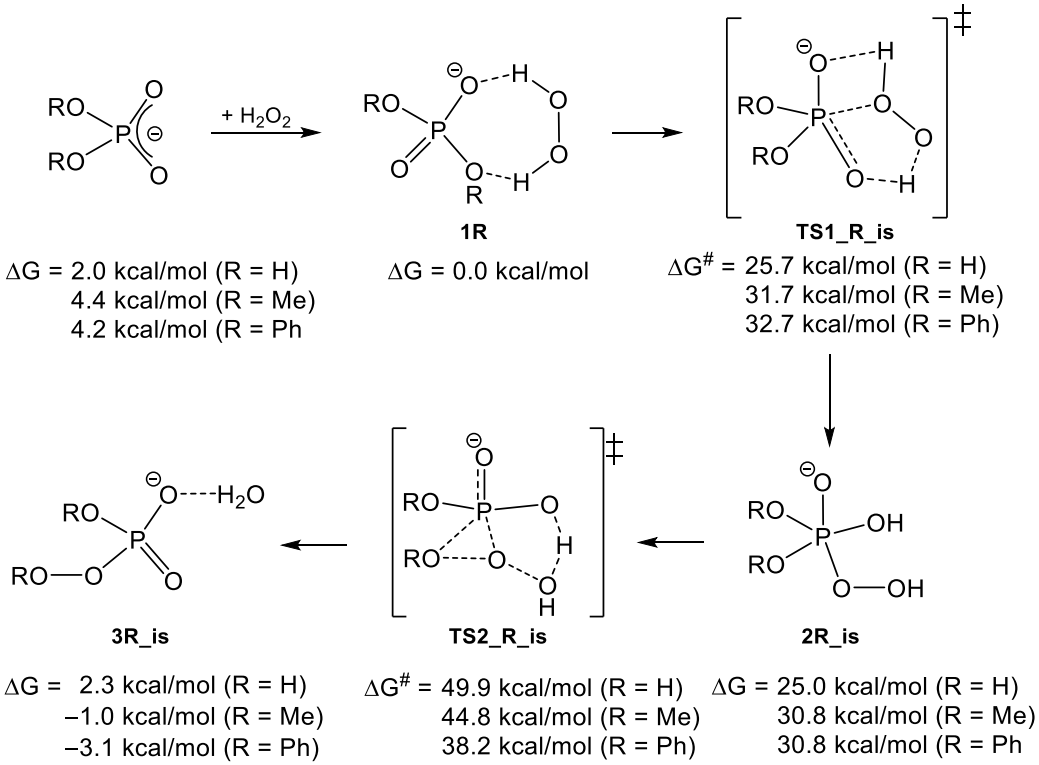

Scheme 13: Calculated mechanism and Energies for the interaction of various [OMIM] $[(RO)_2PO_2]$ ionic liquids with hydrogen peroxide. B3LYP/6-311+G** level of theory. The $[OMIM]^+$ cation is omitted for clarity.

Reactivity studies towards cis-cyclooctene (COE)

The activation of H_2O_2 by the phosphate anions under micellar conditions was tested for the epoxidation of *cis*-cyclooctene (COE) (Scheme 14). 1.0 eq. of cyclooctene, 2.5 eq. 50 wt.% hydrogen peroxide as well as the catalyst (5.0 mol-%, 357 mmol/L) were mixed at room temperature, resulting in a biphasic medium. The mixture was heated to 80 °C and stirred at 500 min^{-1} for defined time periods. After a certain time, the reaction vial was cooled down to room temperature and the organic media extracted with toluene. The conversion and selectivities were determined by GC-FID using mesitylene as internal standard.

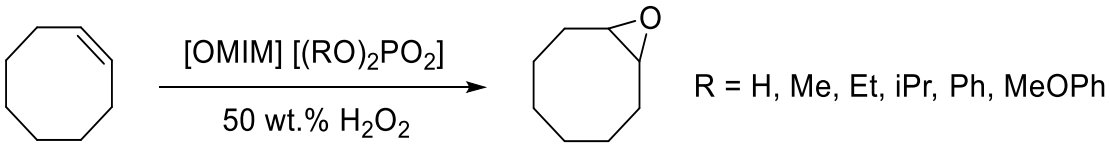

Scheme 14: Catalytic oxidation of cyclooctene using imidazolium diorganophosphates.

To exclude a reaction in the organic phase, the concentration of the catalyst in the supernatant organic overlayer is determined via ^{31}P-NMR spectroscopy with triphenylphosphine oxide as internal standard. Since no other phosphorus signals than the standard can be found down to the NMR detection limit, it can be expected that none of the presented catalysts is soluble in the organic medium under catalysis conditions. This indicates an exclusive catalyst operation in the aqueous phase. The kinetic investigation of all presented catalysts shows the anticipated activation of hydrogen peroxide and the corresponding epoxidation of COE. The reaction curves show a strong dependency of the phosphate substituents on the catalytic activity (Figure 52). The aromatic phosphate SAIL [OMIM] $[(MeOPhO)_2PO_2]$ shows the highest COE conversion of 72% after 48 h. The less electron-pushing derivative [OMIM] $[(PhO)_2PO_2]$ results in a slightly lower conversion at 66% despite a higher fraction of the diarylphosphate can be found by ^{31}P-NMR in the anticipated peroxo-state under similar conditions (Figure 48 and Figure 49). Remarkably, the latter catalyst shows the identical conversion with [OMIM] $[(EtO)_2PO_2]$ which is not expected to form a diethylperoxophosphate in solution (Table 14, Entries 3 and 5) as imidazolium dialkylphosphates have not been found by ^{31}P-NMR spectroscopy to react with hydrogen peroxide under catalysis conditions (Figure 47). This is in good agreement with the postulate, that the electron-push ability of the alkyl groups controls the interaction of the anion with H_2O_2 for an epoxidation via the H-bond outer-sphere mechanism. [OMIM] $[(^iPrO)_2PO_2]$ appears to be the least reactive catalyst despite it has the highest ability to push electron density to the phosphate group. Regarding the outer-sphere activation of the dialkyl- and dihydrogenphosphates, the strength of the H-bond is a function of the electron density on the phosphates oxo groups, which correlates with the pK_a value of the corresponding phosphoric acid.

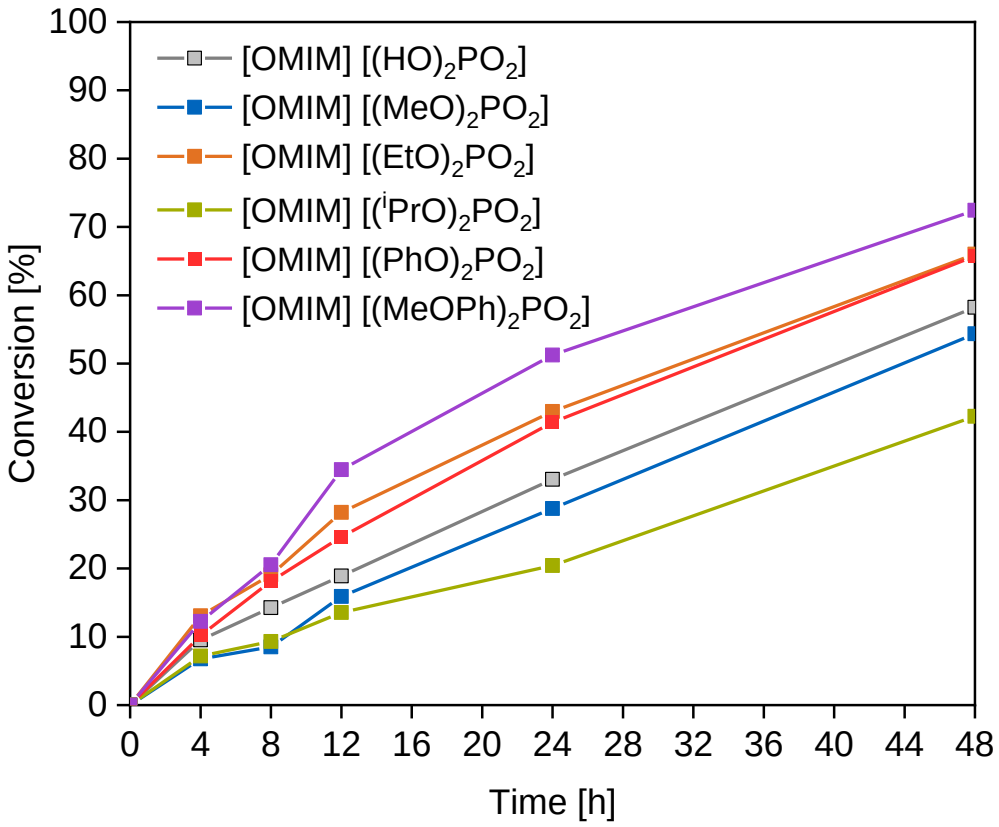

Figure 52: Conversion plots of the COE-epoxidation with 5 mol-% of various [OMIM][$(RO)_2PO_2$] ILs using 2.5 eq. aq. H_2O_2 (50 wt.% solution) at 80 °C.

This would lead to a reactivity order ^{i}Pr > Et > Me as electron-pushing substituents should result in a stronger H-bond to H_2O_2, hence a higher reactivity towards COE (Table 14). The correlation of the pK_a value of $[(HO)_2PO_2]^-$ within this series cannot be considered as it acts as an ampholyte, so in this case the pK_a is not a reliable measure for the electron density at the

Table 14. Epoxidation of COE using various [OMIM] [$(RO)_2PO_2$] with 2.5 eq. 50 wt.% H_2O_2. Conversion and selectivity correspond to COE and COO, respectively. Reaction Conditions: 5 mol% [OMIM] [$(RO)_2PO_2$] 24 h at 80 °C.

Entry	Catalyst	pKa[a]	Conversion [%]	Selectivity [%]
1	[OMIM] [$(HO)_2PO_2$]	1.97[197]	33	76
2	[OMIM] [$(MeO)_2PO_2$]	1.29[197]	27	65
3	[OMIM] [$(EtO)_2PO_2$]	1.39[197]	43	79
4	[OMIM] [$(^{i}PrO)_2PO_2$]	>1.59[b] [197]	26	54
5	[OMIM] [$(PhO)_2PO_2$]	1.9[198]	41	80
6	[OMIM] [$(MeOPhO)_2PO_2$]	---	51	55
7	None	---	7	70

a: pKa-values for the corresponding phosphoric acids in H_2O.

b: Reported pKa for $[n Pr_2PO_4]^-$; the value for $[i Pr_2PO_4]^-$ is expected to be slightly higher.

oxo groups. [OMIM] [(^{i}PrO)$_2$PO$_2$] shows the lowest catalytic activity compared to all other outer-sphere SAILs with 26% conversion after 24 h. As this finding cannot be assigned to electronic features, it must be caused by other effects. Hence, the stability of the catalysts was investigated after each run by ^{31}P-NMR spectroscopy revealing a severe decomposition for [OMIM] [(^{i}PrO)$_2$PO$_2$]. In fact, all diorganophosphates show hydrolysis according to Scheme 15 to organophosphate and phosphate after 24 h during the catalysis (Figure 53). Here, [OMIM] [(EtO)$_2$PO$_2$] shows the highest stability towards hydrolyzation of all catalysts, followed by the methyl derivative [OMIM] [(MeO)$_2$PO$_2$]. Both investigated [OMIM] [(ArylO)$_2$PO$_2$] tend to hydrolyze rapidly under the catalysis conditions (Figure 53). Their rate of decomposition can be correlated to the negative charge distribution of the phenolate leaving group. The diphenylphosphate [OMIM] [(PhO)$_2$PO$_2$] with the lowest electron density at the phosphorus atom is more prone to nucleophilic attack of water than dialkylphosphates and conclusively hydrolyzes to as much as 46% after 24 h. In comparison, the more electron-pushing *p*-methoxy group of [OMIM] [(MeOPhO)$_2$PO$_2$], limits hydrolysis to moderate 13% after 24 h. A remarkably high hydrolysis rate is observed for [OMIM] [(^{i}PrO)$_2$PO$_2$], which may explain the unexpectedly low reactivity among all 'outer-sphere SAILs'. Still, the low reactivity of the [OMIM] [(^{i}PrO)$_2$PO$_2$] catalyst cannot be explained by hydrolysis as the resulting [OMIM] [(HO)$_2$PO$_2$] catalyst has a higher reactivity towards COE (see Table 14, Entries 1 and 4). It has to be anticipated that the released isopropanol has a negative effect on the outer-sphere activation of H_2O_2, likely by formation of concurring H-bonds. It has been reported that phenol[109] and hexafluoroisopropanol[112] (HFIP) form strong H-bonds with hydrogen peroxide.

Computational investigation of the epoxidation mechanism

The initial mechanistic investigations on the adduct formation of the SAILs with hydrogen peroxide have shown that the mechanism is greatly dependent on the anion substitution pattern. Diarylphosphates favor the formation of diarylperoxophosphates which are most likely the catalytically active species. Dialkyl- and dihydrogenphosphates in contrast do not show any peroxophosphate formation under catalytic conditions, so the outer-sphere H-bond activation is expected. To support both hypothesis and to gain a deeper insight into the epoxidation mechanism, the respective catalytic cycles are calculated by DFT by Dr. Markus Drees. Both catalytic pathways are investigated for the substituent representatives R = H, Me and Ph. Ethylene was used as model substrate for all intermediates and transition states (Scheme 16).

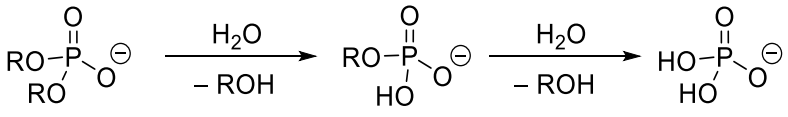

Scheme 15: Sequential hydrolysis pathway of diorganophosphate to dihydrogenphosphate.

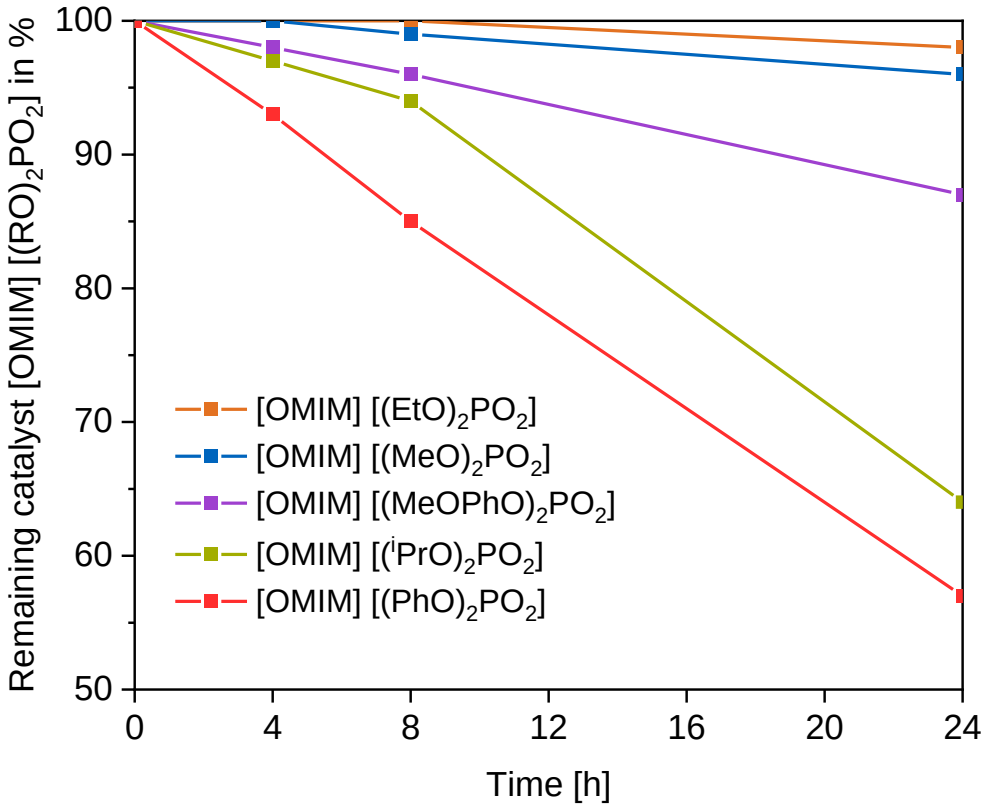

Figure 53: Hydrolysis trends of the diorganophosphate anions of [OMIM] [$(RO)_2PO_2$]. Conditions: 357 mM [OMIM] [$(RO)_2PO_2$] in 50 wt.% H_2O_2 at 80 °C.

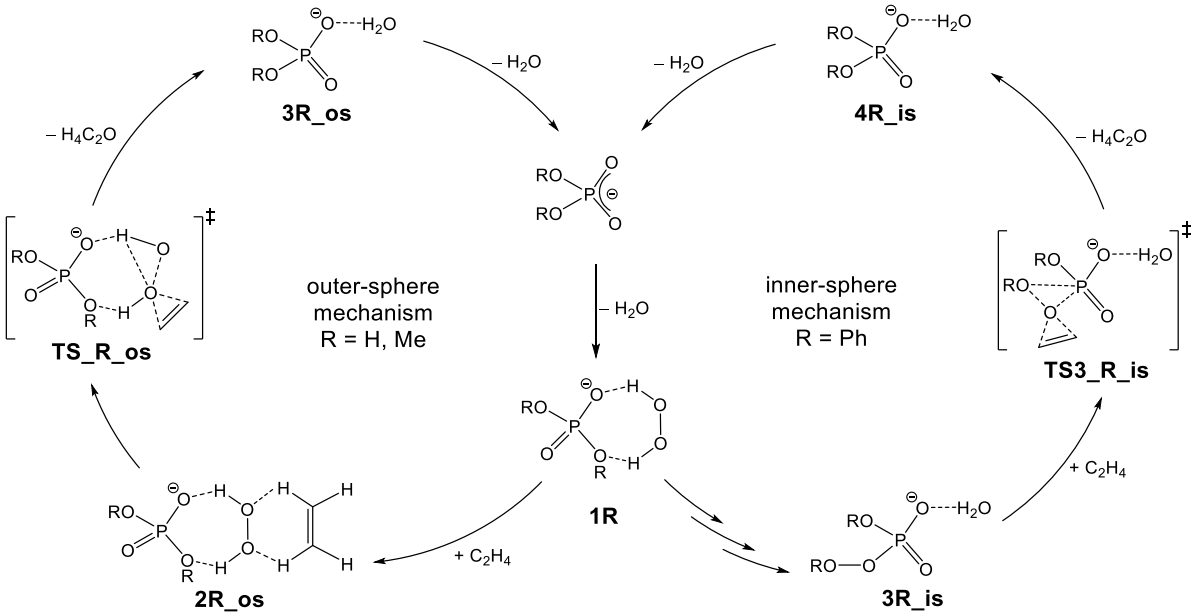

Scheme 16: The two possible mechanistic cycles of olefin epoxidation depending on the phosphate substitution pattern. Left: outer-sphere mechanism; right: inner-sphere mechanism. For details on the inner-sphere rearrangement mechanism to **3R_is**, see Scheme 13. The $[OMIM]^+$ cation is omitted for clarity.

The initial *in silico* catalyst interactions with H_2O_2 in absence of the substrate show that for R = Ph the formation of a peroxo-phosphate is likely (Scheme 13) and in good agreement with the *in situ* ^{31}P-VT-NMR spectra (Figure 48). The results show that the initial rearrangement reaction of [OMIM] [$(PhO)_2PO_2$] to **3Ph_is** has indeed the highest activation barrier, while the energetic barrier of the transfer of the oxygen atom to ethylene (**TS3_Ph_is**) is lower with only 18.3 kcal/mol. The inner-sphere transition state of the epoxidation step is rather high for [OMIM] [$(HO)_2PO_2$] and [OMIM] [$(MeO)_2PO_2$] with >50 kcal/mol and hence unlikely to occur at 80 °C (Table 15, column 'inner-sphere'). In contrast, the outer-sphere H-bond mechanism is energetically unfavoured for [OMIM] [$(PhO)_2PO_2$] with an activation barrier of 48.5 kcal/mol. A feasible activation barrier of 38.3 kcal/mol for **TS_Me_os** is obtained for [OMIM] [$(MeO)_2PO_2$] (Table 15, column 'outer-sphere'). Surprisingly, the activation energy is somewhat smaller for [OMIM] [$(HO)_2PO_2$] with 33.7 kcal/mol (**TS_H_os**) and not in agreement with the catalysis results (Figure 52). Despite the tendency towards the outer-sphere mechanism, the energy might be slightly underestimated by the functional B3LYP in the gas phase as the anion bears two hydrogen substituents which may form additional competitive H-bonds in a chemical environment to surrounding molecules. Thus, the real reactivity might be somewhat decreased and the energetic barrier higher than calculated. As already discussed, *in situ* ^{31}P-NMR investigations suggest that the micellar environment has a major impact on the reaction mechanism of the diarylphosphate catalysts as the micelle tends to stabilize the peroxophosphate species. To investigate the influence of the micelles on the activation of H_2O_2, the respective sodium salts of several phosphates were tested in epoxidation catalysis. Sodium dihydrogenphosphate shows the same conversion of COE after 24 h as the blank experiment (Table 14, Entry 7 and Table 16, Entry 1) and can therefore be regarded as inactive in H_2O_2 activation. Nevertheless, the selectivity drops from 70% for the blank experiment to 57% which shows some reactivity towards the formed epoxide by the ring opening consecutive reaction due to the slight acidity of $[H_2PO_4]^-$. In contrast, sodium dimethylphosphate yields 14% conversion and can therefore not be considered inactive in catalysis. Sodium diphenylphosphate with an even higher organic contribution shows 25% substrate conversion after 24 h, which is compared to 41% of the micellar diphenylphosphate remarkably high.

Table 15: Activation barriers for the epoxidation of ethylene calculated by DFT on the B3LYP/6-311G** level of theory.

Entry	Catalyst	Energy barrier $\Delta G^{\#}$ in kcal/mol	
		inner-sphere	outer-sphere
1	[OMIM] [$(HO)_2PO_2$]	53.3	33.7
2	[OMIM] [$(MeO)_2PO_2$]	52.3	38.3
3	[OMIM] [$(PhO)_2PO_2$]	38.2[a]	48.5

a: activation barrier for the rearrangement reaction; the enthalpy of the epoxidation **TS3_Ph_is** is 18.3 kcal/mol.

These experiments underline that the diorganophosphates are sufficiently low solvated by water molecules allowing for an interaction with hydrogen peroxide without the need of the hydrophobic effect of the micelles, as required for $[(HO)_2PO_2]^-$, $[NO_3]^-$ or $[ReO_4]^-$ Hence, sodium diphenylphosphate, not expected to form a peroxo-species under catalytic conditions (Figure 50), is able to activate hydrogen peroxide via the outer-sphere H-bond mechanism. DFT calculations with the sodium cation cannot be compared to the results with the catalyst [OMIM] $[(PhO)_2PO_2]$ due to the solvation of the cation, which is not sufficiently considered by the B3LYP calculations in the gas phase. For a detailed theoretical study, a more elaborate functional taking the dispersion energies into account and an adequate solvation model would be required.[148] This renders the computational effort for the *in silico* experiments inconveniently high for such large catalyst structures.

Dimethylimidazolium dimethylphosphate [MMIM] $[(MeO)_2PO_2]$ was synthesized to investigate the influence of the choice of cation on the activation of hydrogen peroxide (Table 16, Entry 4). The mechanistic imidazolium nitrate studies showed that the cation plays an essential role in the epoxidation mechanism by providing additional H-bond interactions from the imidazolium protons. In contrast, using the non-micellar catalyst [MMIM] $[(MeO)_2PO_2]$ does not differ distinctly from the reactivity of $Na[(MeO)_2PO_2]$ (Table 16, Entries 2 and 6). Hence, the imidazolium contribution to the activation of hydrogen peroxide might be less important compared to the imidazolium nitrates, which rely on distinct H-bonds. This might be supported by the calculated H_2O_2···phosphate adducts (Figure 51), which prefer formation of H-bonds via one less electron-dense RO-substituent over a oxo-groups.

The possibility to introduce various organic substituents does not only allow for the tuning of the electronic properties of the phosphate moiety but also for the introduction of organic substituents bearing chiral information. The esterification of the phosphate anion with two chiral alcohols, in combination with the micelle-forming $[OMIM]^+$ cation, would result in a chiral micellar catalyst for the asymmetric epoxidation of olefins. Essential works on the stereoselective epoxidation catalysis have thoroughly been investigated by Jacobsen[199][200], Shi[201][202] and Sharpless.[203][204] However, all catalytic approaches require large amounts of organic solvents and ecologically questionable oxidants such as *tert*-butylhydroperoxide,

Table 16: Epoxidation of COE using various phosphate salts with 2.5 eq. 50 wt.% H_2O_2. Conversion and selectivity correspond to COE and COO, respectively. Reaction Conditions: 5 mol% catalyst, 24 h, 80 °C

Entry	Catalyst	Conversion [%]	Selectivity [%]
1	NaH_2PO_4	7	57
2	$Na[(MeO)_2PO_2]$	14	86
3	$Na[(PhO)_2PO_2]$	25	56
4	[MMIM] $[(MeO)_2PO_2]$	13	77

peroxomonosulfates or hypochlorites and are limited to specific substrate substitution patterns. Recent works have shown that manganese-based catalysts with chiral chelating N-donor ligands allow for the use of hydrogen peroxide in the asymmetric epoxidation of olefins.[205][206][207] Disadvantageously, these catalysts operate in an organic homogeneous reaction mixture and catalyst recycling is not of interest due to the much higher value of the chiral epoxide product compared to the manganese catalyst. Non-chiral manganese porphyrin catalysts have been shown to be highly efficient in the epoxidation of olefins in micellar media, exploiting the micelle as a nanoreactor with the catalyst and olefin dissolved inside.[208][209] Micellar catalytic approaches towards the asymmetric epoxidation of olefins have not been published to date but are of high interest. The most renown chiral phosphoric acid esters are BINOL-derived and applied to various fields of catalysis as chiral ligands, *Brønsted*-acids or ion-pair components.[210] Hence, rendering the micelle-forming diorganophosphates chiral by introduction of enantiopure phosphate anions is plausible. The BINOL-derived phosphoric acid bears one acidic proton and is therefore prone to be deprotonated by imidazolium hydroxide obtained from an anion exchange of imidazolium bromides (Scheme 17). Initial investigations with the prepared racemic BINOL-derived catalyst show that the ionic liquid can be obtained via the proposed procedure. Unfortunately, due to the highly aromatic character, the IL shows a poor solubility in water. Upon heating, the solubility increases strongly, paving the way for an application in a biphasic setup. Prior to investigation of the micelle formation, the reactivity of the novel catalyst towards *cis*-cyclooctene was studied. A biphasic mixture of 50 wt.% H_2O_2 and *cis*-cyclooctene are stirred with catalytic amounts of [OMIM] [BINOL-PO_2] at 80 °C for 24 h. After this period, an exceptionally high conversion COE of 80% is observed, whereas the yield of COO is only 1%. The ^{31}P-NMR spectrum of an aliquot of the aqueous phase revealed that the catalyst is quantitatively decomposed by formation of phosphoric acid. Hence, the evolving acid leads to a rapid increase of the conversion while the selectivity drops remarkably. Accordingly, the ^{1}H-NMR spectrum does not show any traces of the initial anion but a series of aromatic signals which can be attributed to further side reactions besides the anion hydrolyzation. Radical decomposition mechanisms facilitated by the large π-system of the BINOL-derivative could contribute to the catalyst decomposition and COE-conversion. This is supported by the variety of COE molecules oxidized to hydroxides, carbonic acids, and ketones as well as a mixture thereof. Hence, this approach was not further considered for catalysis.

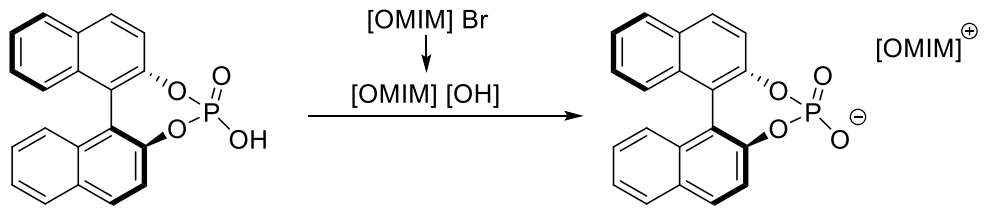

Scheme 17: Synthesis route towards chiral, surface-active BINOL-derived catalyst.

The catalyst stability study reveals that diorganophosphates esterified with alcohols are most stable towards hydrolysis. Henceforth, a chiral aliphatic alcohol bearing a stereocenter at the C-2 position with bulky substituents could be a simple building block for a chiral micellar catalyst. A simple chirality source could be enantiomerically pure 2-methylbutan-1-ol which would allow for the synthesis of the corresponding chiral dialkylphosphate anion. Still, the hydrolysis of this phosphate might be detrimental for an application, especially involving the recycling of the valuable chiral catalyst.

Recycling studies

The poor stability of the diorganophosphate catalysts due to the hydrolyzation does not allow for a catalyst recovery. However, the stable catalyst [OMIM] [$(HO)_2PO_2$] was tested in recycling experiments (Figure 54). After the first run, the activity of the recycled catalyst drops slightly but is constant for three more runs, which excludes catalyst loss by the recycling procedure. Starting from the sixth run, the activity appears to rise, while the selectivity towards the epoxide drops. Investigations show that the catalyst residue has gained in acidity, as aqueous solutions thereof changed from pH ≈ 5 to pH ≈ 4. A further buffering of the acidity (preferably with hydrogenphosphate $[HPO_4]^{2-}$) could prevent the loss in selectivity due to acidic epoxide ring opening and allow for use of the catalyst in a continuous process. There, the biphasic system is of great advantage as the substrate/product layer can easily be removed without any impurities or contaminations.

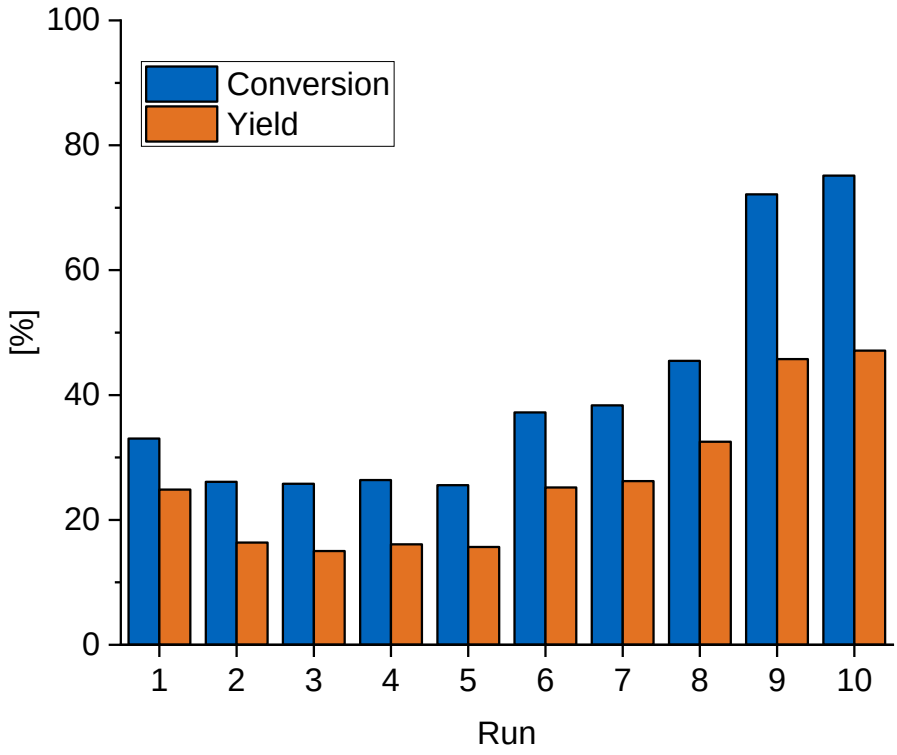

Figure 54: Recycling study with 5 mol-% [OMIM] [$(HO)_2PO_2$]. Conversion of COE and yield of COO, respectively. Conditions: IL:COE:H_2O_2 = 5:100:250, 80 °C, 24 h.

3.3.3 Conclusion

The simple phosphate anion $[PO_4]^{3-}$ which was expected to be suitable for the activation of hydrogen peroxide for olefin epoxidations but decomposes H_2O_2 catalytically due to the basic character. The functionalization of two oxo-ligands with organic substituents results in pH-neutral diorganophosphates which additionally offer the possibility to tailor the electronic properties of the phosphate moiety with electron-pushing or -withdrawing organic substituents. The outer-sphere H_2O_2 activation is proposed for dialkylphosphates and can be related to a high electron density at the phosphates oxo-ligands favouring H-bonding to H_2O_2. Electron-withdrawing aryl substituents increase the *Lewis*-acidic character of the P-atom and promote a nucleophilic attack by hydrogen peroxide to form a proposed peroxophosphate. Remarkably, this is exclusive to micelles formed by the [OMIM] $[(ArylO)_2PO_2]$ cation, whereas the corresponding sodium salts do not show a reaction with hydrogen peroxide. This is a further example of the superiority of supramolecular strategies in order to enable catalytic pathways which are not feasible in traditional approaches. It can be concluded that the catalytic boost of the micelles arises from the stabilization of the highly reactive peroxophosphate species. A major drawback of all diorganophosphates is the lack of stability under the catalysis conditions (e.g. 50 wt.% H_2O_2, 80 °C, 24 h) due to the anion hydrolysis leading to the formation of the highly polar dihydrogenphosphate. This $[H_2PO_4]^-$ anion does not, in contrast to $[PO_4]^{3-}$, decompose H_2O_2 and is merely slightly acidic in solution, which allows for its catalytic application without severe epoxide hydrolyzation. Homogeneously dissolved NaH_2PO_4 does not show any reactivity towards hydrogen peroxide, whereas the micellar derivative shows catalytic activity towards the epoxidation of COE due to the hydrophobic effect of the micelle in aqueous solutions. This is in accordance with the strong hydratization of the nitrate anion, which similarly sensitive to the cationic micelle.

The herein presented investigation represents another example of successful transfer of the concept of micellar hydrogen peroxide activation from tungstate via metal-free nitrate to anions of the constitution $[(RO)_2PO_2]$ (R = H, Alkyl, Aryl). The initially thought to be promising incompatible phosphate anion possesses a high electron density at its oxygen atoms, which would be beneficial for the H_2O_2 activation by H-bonds. The basicity in aqueous solution is detrimental for H_2O_2 stability. The abundant sulfate anion $[SO_4]^{2-}$ shows a similar tetragonal molecular symmetry, is double negative in charge, and behaving neutral in solution. Hence, this is another promising anion for the activation of hydrogen peroxide in micellar environments.

3.4 Sulfate-based Supramolecular Ions Pairs for Epoxidation Catalysis

3.4.1 Introduction

The nitrate and the dihydrogenphosphate anions do not show any reactivity towards hydrogen peroxide as simple sodium salts, which dissolve homogenously in aqueous solution. As counterions of a cationic micelle, the polar anions lose their hydration shell and form a H-bond adduct with hydrogen peroxide. This interaction is sufficiently strong for the activation of H_2O_2 for its use as oxidant in epoxidation reactions. The diorganophosphates are less hydrophilic in nature and show therefore reactivity towards hydrogen peroxide as sodium salts. The *in situ* formation of a diaryl peroxophosphate species, a potent oxidant, from diaryl phosphate and hydrogen peroxide in equilibrium is observed in micellar media. Similar to peroxophosphates, peroxomonosulfates are popular, strong oxidants and are commercially available as the triple-salt Oxone® ($KHSO_5 \cdot ½\ KHSO_4 \cdot ½\ K_2SO_4$). This stoichiometric oxidant is used to epoxidize olefins according to the Shi mechanism with ketones, generating large amounts of chemical waste, and requiring large amounts of acetonitrile or chlorohydrocarbon solvents.[211][212] Hence, for the use of one atom of active oxygen, large quantities of the salt have to be produced and in turn, disposed after the oxidation.

Based on this knowledge, it would be economically and -logically favourable to generate the peroxomonosulfate *in situ* from hydrogen peroxide and catalytical amounts of sulfate under neutral conditions to avoid side reactions during catalysis. The micellar approach of surface-active imidazolium sulfates has been thoroughly investigated by Jan Berger, concluding that the sulfate anion does not have sufficient reactivity towards hydrogen peroxide for its use as catalyst for the activation of hydrogen peroxide.[213] The catalytic application of the derived dialkylimidazolium hydrogensulfates results in a high conversion of cyclooctene, however, the high acidity of the anion leads instantly to epoxide hydrolyzation to yield diols. The functionalization of the sulfate with small alcohols in order to obtain a less hydrophilic anion was investigated therein. The pH-neutral 1-octyl-3-methylimidazolium alkylsulfates [OMIM] [RSO_4] (R = Me, Et) were synthesized and investigated as catalyst for the micellar epoxidation of olefins. Unfortunately, these ionic liquids hydrolyze rapidly to hydrogensulfate and the respective alcohol under reaction conditions, leading to instant formation of the diol from the formed epoxide. The bare sulfate anion as part of a cationic micelle has been shown to possess no reactivity towards olefins in hydrogen peroxide similar to the nitrate-based imidazolium catalysts. A high hydration energy of −1090 kJ/mol in water[214] results in a large hydration shell, avoiding the activation of weaker binding hydrogen peroxide. Nitrate (hydration energy −306 kJ/mol)[214] partly loses its water molecule shell by the influence of the imidazolium

cation, enabling an activation of H_2O_2, but the double negative charge of sulfate and the more polar character prevent this mechanism. It has been shown that the reactivity of highly polar ions can be increased drastically in an organic medium, which can be referred to the absence of a stabilizing hydration shell and the high anion polarity in a hydrophobic environment. This was shown by the transfer of the strong oxidant potassium permanganate into the organic phase by aid of crown ethers forming a supramolecular guest/host complex.[215] Sophisticated organic receptors have been synthesized to by Romanski et al. to selectively extract potassium sulfate into organic solvents by supramolecular assemblies.[216] These neutral molecules bear a crown ether functionality linked to a squaramide group, which bind strongly to potassium and sulfate, respectively. Nevertheless, the structural motif bears multiple functionalities, likely not to be compatible with hydrogen peroxide. Moreover, a potential application may rather be the accurate sensing of alkali sulfates in a mixture of various salts due to the high ion selectivity. A cationic receptor molecule could extract the sulfate anion more easily and may be simpler in constitution. Such organic cationic receptor molecules have been developed by Sole, Tasker et al. to extract metalchlorido and -oxo anions from the aqueous phase into an organic solvent.[106][107] These compounds contain an amidoamine motif which can be protonated in aqueous phase and confine the counterions by defined H-bond interactions inside the capsule of two aggregated receptor molecules. Supramolecular ion pairs (SIPs) have been exploited to activate hydrogen peroxide for olefin epoxidation by the perrhenate anion inside a hydrophobic capsule formed by organic receptor molecules.[108] These SIPs shuttle the perrhenate anion from the aqueous hydrogen peroxide to the substrate phase for the catalytic epoxidation of olefins under solvent-free conditions. The transfer of this SIP concept to the sulfate anion is therefore of high interest to exploit its reactivity in the organic phase without a restraining hydration shell. The sulfate-based ion pair approach to transfer the sulfate anion from the aqueous hydrogen peroxide into the organic substrate phase is studied in this chapter. Several sulfate-SIPs are synthesized and investigated towards their phase distribution and reactivity towards olefins with hydrogen peroxide. *In situ* analysis by DOSY-NMR, DLS and ESI-MS help to understand the assembly process and mechanistic pathways.

3.4.2 Results and Discussion

Synthesis Strategy of the SIPs

The three sulfate-based supramolecular ion pairs (SIPs) shown in Scheme 18 were synthesized by extraction of diluted sulfuric acid to the toluene phase with reported organic receptor molecules upon their protonation.[106][107] The herein presented receptor molecules were chosen to investigate the sulfate solubilization in organic media due to the different non-polar aromatic and aliphatic contribution.

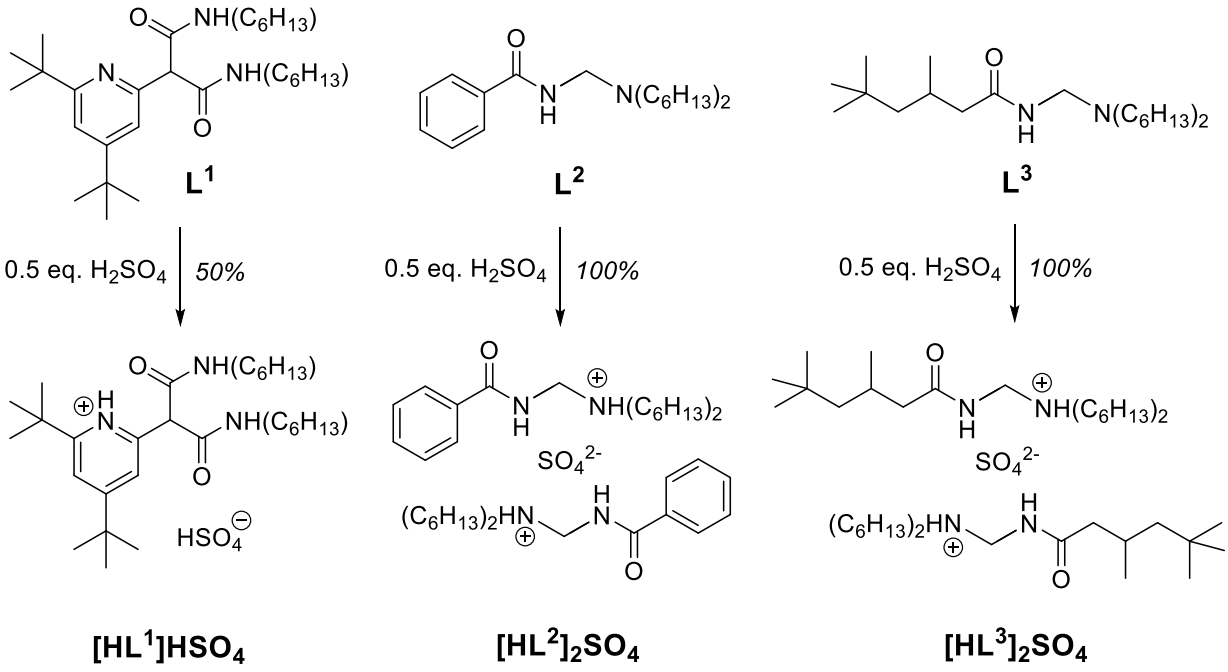

Scheme 18: Synthesis of the sulfate-based Supramolecular Ion Pairs (SIPs) from the pyridine or amidoamine receptor molecules L^{1-3}.

Equinormal amounts of the receptor and sulfuric acid were added to a biphasic mixture of water and toluene. After separation of the neutral aqueous phase and toluene evaporation under reduced pressure, the residues are investigated by ^{1}H-NMR and show a quantitative protonation for the receptor molecules L^2 and L^3. The receptor L^1 in contrast, only shows protonation of 50%, while consuming all of the sulfuric acid from the aqueous phase. In theory, this results in a proposed formation of the structure $[HL^1]HSO_4$ with a strongly acidic hydrogensulfate entrapped in the SIP. Elemental analysis supports the formation of the structures $[HL^1]HSO_4$ and $[HL^n]_2SO_4$ (n = 2, 3) due to the highly accurate elemental analysis ratio for C:H:N:S. It must be mentioned, that the two amidoammonium SIPs $[HL^n]_2SO_4$ (n = 2, 3) contain 1.5 equivalents H_2O each.

Crystal growth of $[HL^1]HSO_4$ by slow evaporation of the toluene solvent and subsequent structure analysis by single crystal X-ray diffraction performed by Stefan Burger shows the formation of two pyridine-based organic protonated receptor molecules $[HL^1]^+$ conjoined with a hydrogensulfate dimer (Figure 55). Similar to the reported $[ReO_4]^-$ derivative, the structure favours a dimeric constitution with two receptor molecules and two anion species.[108] The formed structure can be regarded as an organic capsule formed by the hydrophobic parts of the receptor containing the polar hydrogensulfate ions inside by connecting the receptor's polar functional groups by H-bonds. The pyridinium proton is part of a six-membered proton-chelate ring with one keto-function of the amide groups, while the amide hydrogen atoms are forming H-bonds to one hydrogensulfate each. Both hydrogensulfate anions exhibit H-bonds among themselves, as well with the pyridinic *meta*-proton. This highly polar and ionic domain is

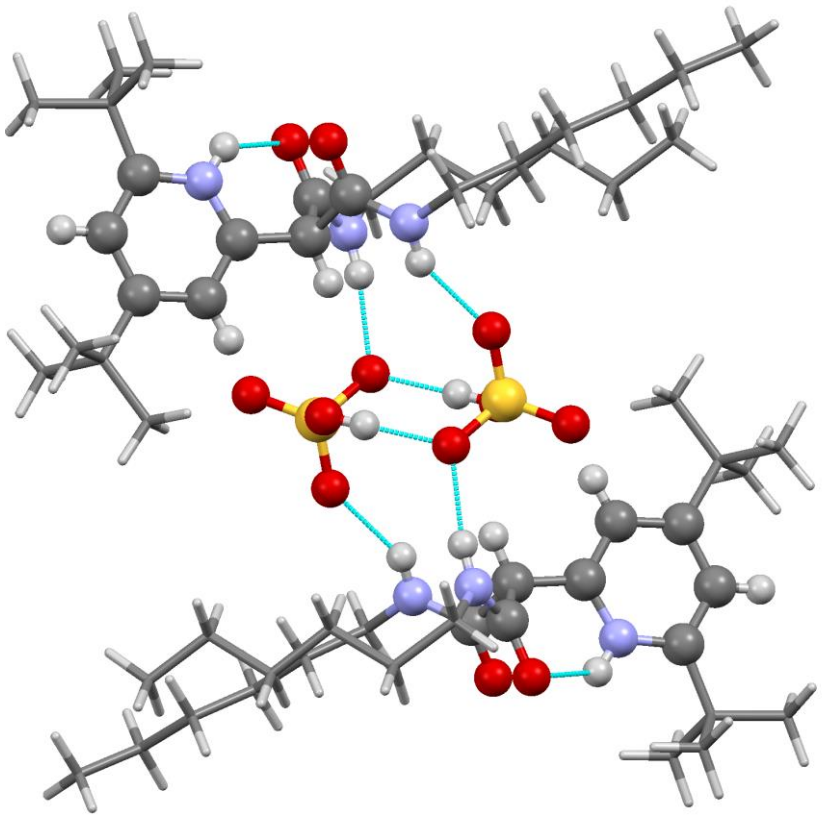

Figure 55: SCXRD structure of $[HL^1]HSO_4$. The *tert*-butyl and *n*-hexyl substituents are drawn as wireframes for clarity.

shielded by the non-polar hexyl and *tert*-butyl groups, enabling a high solubility in hydrocarbon solvents. Moreover, the high acidity of the hydrogensulfate ions is shielded from its environment, being the reason for the macroscopic pH-neutrality of the solution. The core/shell assembly $([HL^1]HSO_4)_2$ can be regarded as a supramolecular ion pair (SIP) with the non-covalent interactions keeping the structure stable. Concerning the ion pairs $[HL^n]_2SO_4$ (n = 2, 3), the formation of supramolecular assemblies is anticipated as well due to the sulfate solubilization in organic media. There, the intrinsic SIP stoichiometry is somewhat different for the receptor/sulfate ratio of 2:1, resulting in a dianionic sulfate species transferred to the organic phase by two receptor cations $[HL^n]^+$ (n = 2, 3). Unfortunately, single crystal growth was not successful for the amidoammonium sulfate SIPs due to the slow decomposition of the organic receptor (vide infra).

Catalytic olefin epoxidation experiments

The success of the sulfate transfer into the organic media and the loss of its catalytically restrictive hydration shell is one of the essential premises for the application of the SIPs in the epoxidation of olefins. The other requirement is the activation of hydrogen peroxide by the sulfate anion inside the receptor capsule. This was investigated by the reactivity of the SIPs

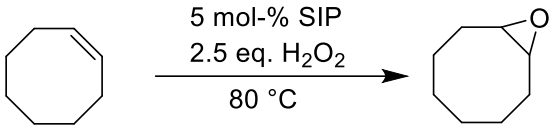

Scheme 19: Catalytic epoxidation of cyclooctene with 5 mol% SIP using 2.5 eq. 50 wt.% aqueous H_2O_2.

towards the epoxidation of the model substrate *cis*-cyclooctene (COE). The supramolecular ion pairs $[HL^1]HSO_4$ and $[HL^n]_2SO_4$ (n = 2, 3) were subjected to the catalytic epoxidation of COE at 80 °C with 5.0 mol-% SIP based on $[HSO_4]^-$ or $[SO_4]^{2-}$ using 2.5 eq. H_2O_2 (vs. COE; 50 wt.% solution in water) as oxidant (Scheme 19). The SIPs were dissolved in the biphasic mixture H_2O_2/cyclooctene at elevated temperature (80 °C) and stirred at 500 rpm during the course of the reaction. The conversion of COE and yield of COO were determined by taking of aliquots form the organic phase after certain time intervals and subsequently quantified by GC-FID with the standard mesitylene.

All tested SIPs show an epoxidation activity towards COE, with the highest conversion observed for the benzamide-derivative $[HL^2]SO_4$. (Figure 56). The catalytic performance of $[HL^2]SO_4$ and $[HL^3]SO_4$ can be regarded as rather similar, whereas the pyridinium-based SIP $[HL^1]HSO_4$ shows a somewhat decreased activity.

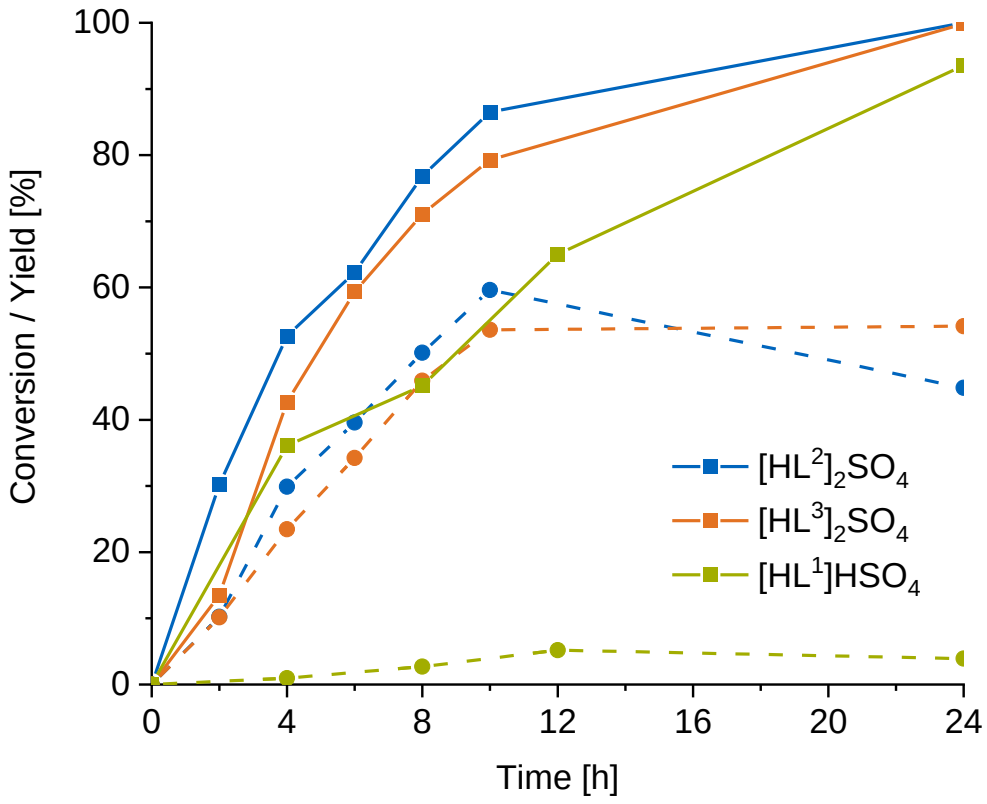

Figure 56: Epoxidation of COE to COO by 5 mol-% SIP (based on sulfate) at 80 °C using 2.5 eq. 50 wt.%. H_2O_2. Bold lines: conversion of COE, dashed lines: yield of COO.

This probably originates from the smaller amount of the organic receptor $[HL^1]^+$, which is deployed in a 1:1 ratio to hydrogensulfate, in contrast to the 2:1 ratio of $[HL^2]^+$ and $[HL^3]^+$ to $[SO_4]^{2-}$. The reason for the very low selectivity of $[HL^1]HSO_4$ towards cyclooctene oxide (COO) might be attributed to the acidic nature of the hydrogensulfate anions. Upon interaction of COE with the polar core of the SIP and subsequent epoxidation, the oxirane group is likely to be immediately hydrolyzed to *trans*-1,2-cyclooctane diol, which was found to be the only side-product. For the catalysts $[HL^2]SO_4$ and $[HL^3]SO_4$, the selectivities towards the formation of COO decrease significantly over time, owed to the same fate of the epoxide. This consecutive reaction is expected to be catalysed by the acidic nature of the SIP's ammonium functionalities inside the polar core. However, this is not observed for the literature-reported perrhenate derivatives, likely as the $[ReO_4]^-$-SIP's reactivities are at least three times higher at an even lower reaction temperature (70 vs. 80 °C).[108]

The effectiveness of the SIP as a transfer-agent for the sulfate into the organic phase under catalytic conditions is demonstrated by the catalytic application of simple sulfate salts, namely Na_2SO_4 or acidic $(NH_4)_2SO_4$, showing only a marginal conversion of 7 % after 24 h, equal to that of a pure solution of aq. H_2O_2 and cyclooctene (blank experiment). Hence, no catalytic activity can be attributed to the sulfate anion in the aqueous phase. These experiments clearly show that the reaction does not take place in the aqueous phase due to strong hydration of the sulfate by water. Thus, a supramolecular assembly is required for the phase-transfer and activation of H_2O_2 by absence of the sulfate's hydration shell.

Variations of the applied catalyst amount reveal the dependence of the selectivity on the acidity of the catalytic mixture, as the formation of the diol is further preferred by using catalyst concentrations higher than 2 mol-%. An increase of the SIP amount leads to a decreased intrinsic catalyst activity and also affects the selectivity, as a longer reaction time and therefore a longer product stirring in the mixture negatively affects the selectivity towards cyclooctene oxide (Table 17). The stability of the catalytically applied SIPs was investigated by ^{1}H-NMR, revealing that the SIP $[HL^1]HSO_4$ is still intact after full conversion of the substrate, while the SIPs $[HL^n]_2SO_4$ (n = 2, 3) are decomposed, indicated by the missing methylene proton signal of the hydrolytically sensitive amide and ammonium bridging CH_2-group. This is in good agreement with Saner Poplata's observations on the overall stability of amidoammonium receptors in aqueous hydrogen peroxide.[217] Stability tests herein on the sulfate-SIPs revealed that both protonated receptors $[HL^2]^+$ and $[HL^3]^+$ are rapidly disassembled within 20 min under catalytic conditions (80 °C, 50 wt.% H_2O_2) to the respective amide, formaldehyde and dihexylammonium sulfate (Scheme 20).

Table 17: Variation of the SIP amount of $[HL^n]_2SO_4$ (n= 2, 3) in the epoxidation of COE at 80°C using 2.5 eq. 50 wt.% H_2O_2.

SIP	mol-%	Time	Conversion [%]	Yield [%]	Selectivity [%]
$[HL^2]_2SO_4$	1	10 h	17	11	62
	1	24	33	23	70
	2	10 h	28	21	75
	2	24	53	39	74
	5	10 h	87	60	69
	5	24	100	45	45
	10	10 h	98	50	51
	10	24	100	45	45
$[HL^3]_2SO_4$	1	10 h	20	9	43
	1	24	38	21	56
	2	10 h	33	20	61
	2	24	63	44	70
	5	10 h	80	54	68
	5	24	100	54	54
	10	10 h	98	53	54
	10	24	100	39	39

Remarkably, the catalytic activities of both SIPs are retained over the full catalytic run and do not appear to cease in activity (Figure 56). The released co-catalytic amount of formaldehyde is slowly oxidized to formic acid, known to form performic acid in contact with hydrogen peroxide,[192] which is in turn is able to epoxidize olefins via the Prileschajev mechanism.[191] Hence, the catalytic activity is investigated by addition of the catalytic amounts of the SIP decomposition products organoamide, dihexylammonium sulfate and formaldehyde to the biphasic H_2O_2/COE system. The kinetic data show very similar curves compared to the activity of the pristine $[HL^n]_2SO_4$ (n = 2, 3) SIPs, albeit an initiation period of about 1-2 hours is observed (Figure 57).

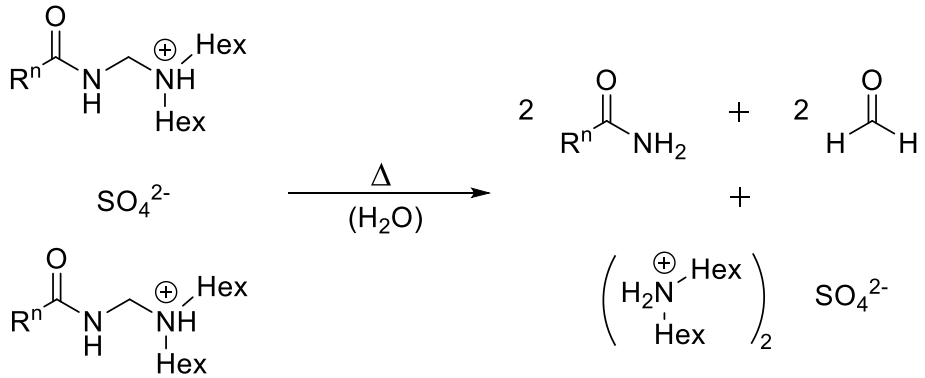

Scheme 20: Decomposition of the SIPs $[HL^n]SO_4$ (n = 2,3) to organoamide, formaldehyde and dihexylammonium sulfate. R^2 = phenyl, R^3 = 3,5,5-trimethylhexyl.

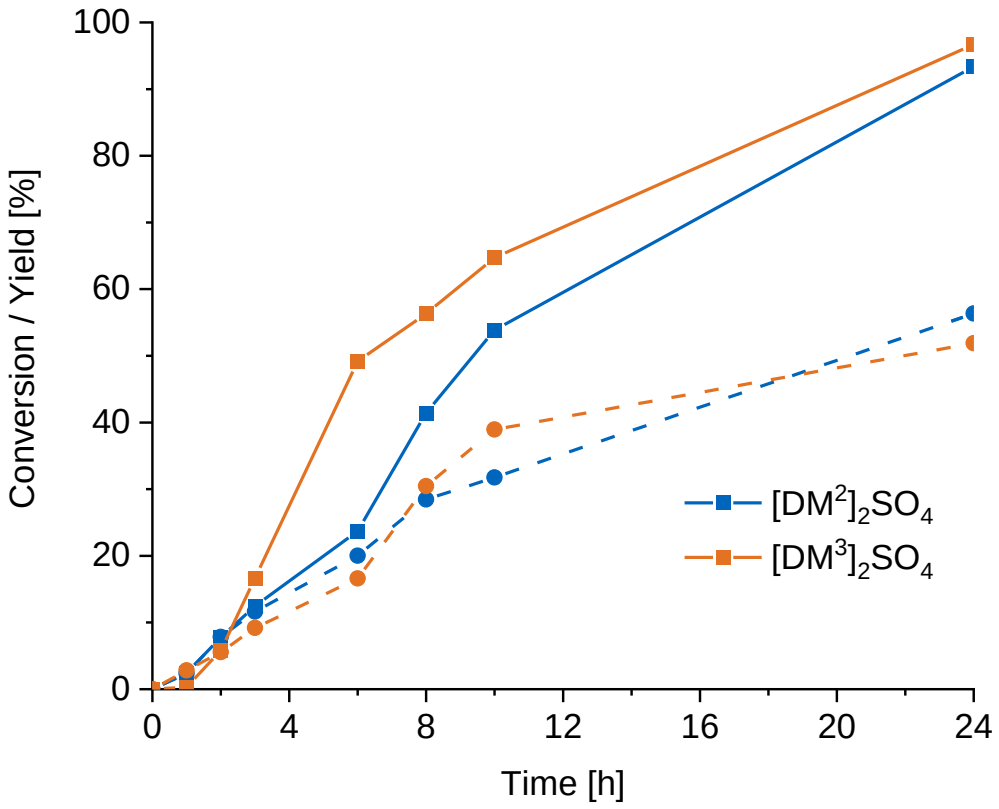

Figure 57: Epoxidation of COE to COO by 5 mol-% dihexylammonium sulfate and 10 mol-% organoamide and formaldehyde at 80 °C using 2.5 eq. 50 wt.%. H_2O_2. Bold lines: conversion of COE, dashed lines: yield of COO.

At this point it is still not clear if the catalytic activity arises from the formaldehyde only. Nevertheless, this hypothesis can be excluded with a closer look on the catalytic activity of the SIP $[HL^1]HSO_4$, which does not decompose and consequently release formaldehyde. Adding the exact co-catalytic amount of 10 mol-% of formaldehyde to a pure biphasic COE/H_2O_2 mixture results in a conversion of 23% COE, whereas the SIPs $[HL^n]_2SO_4$ (n = 2, 3) give full conversions after 24h each. Hence, a further catalytic process must occur parallel to the formaldehyde induced epoxidation. It can be concluded that the organoamide and dihexylammonium sulfate are responsible for the pronounced catalytic activity.

For a better understanding, the SIP components 10 mol-% benzamide or 3,3,5-trimethylhexylamide and 5 mol-% dihexylammonium sulfate (mixtures $[M^2]_2SO_4$ and $[M^3]_2SO_4$, Figure 58) -without any additional formaldehyde- were added to a biphasic mixture of H_2O_2/COE and heated to 80 °C. The catalytic activities are as predicted and only slightly decreased compared to the $[HL^n]_2SO_4$ (n = 2, 3) experiments by the catalytic formaldehyde contribution of 23% conversion after 24 h (Figure 59). These experiments highlight that the simple fine chemical precursors organoamide, dihexylamine and sulfuric acid are able to form a highly sophisticated metal-free catalyst for olefin epoxidation in a biphasic reaction mixture,

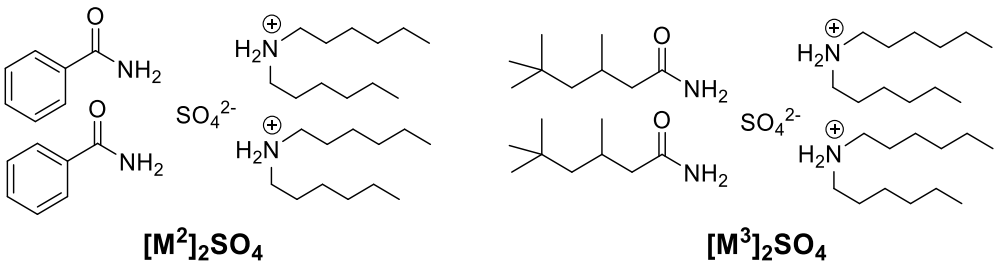

Figure 58: Molecular constitution of the SIP mixtures $[M^n]_2SO_4$ (n = 2, 3).

synergizing the effects of anion phase-transfer and H_2O_2 activation. Similar to the SIPs originating from the synthesized receptors L^n (n = 1, 2, 3), an application of 5 mol-% $[M^n]_2SO_4$ (n = 2, 3) is a good compromise of activity and selectivity (Table 18). The organoamide/dihexylammonium sulfate combination is expected to form a respective supramolecular assembly *in situ* even without the bridging methylene group due to the sulfate solubilization. This is supported by the co-crystallization of benzamide and dihexylammonium sulfate ($[M^2]_2SO_4$) from a toluene solution. Both precursors $(BA:(DHA)_2SO_4$ = 2:1) were dissolved in a water/toluene mixture at 80 °C and the separated toluene phase is slowly evaporated at room temperature.

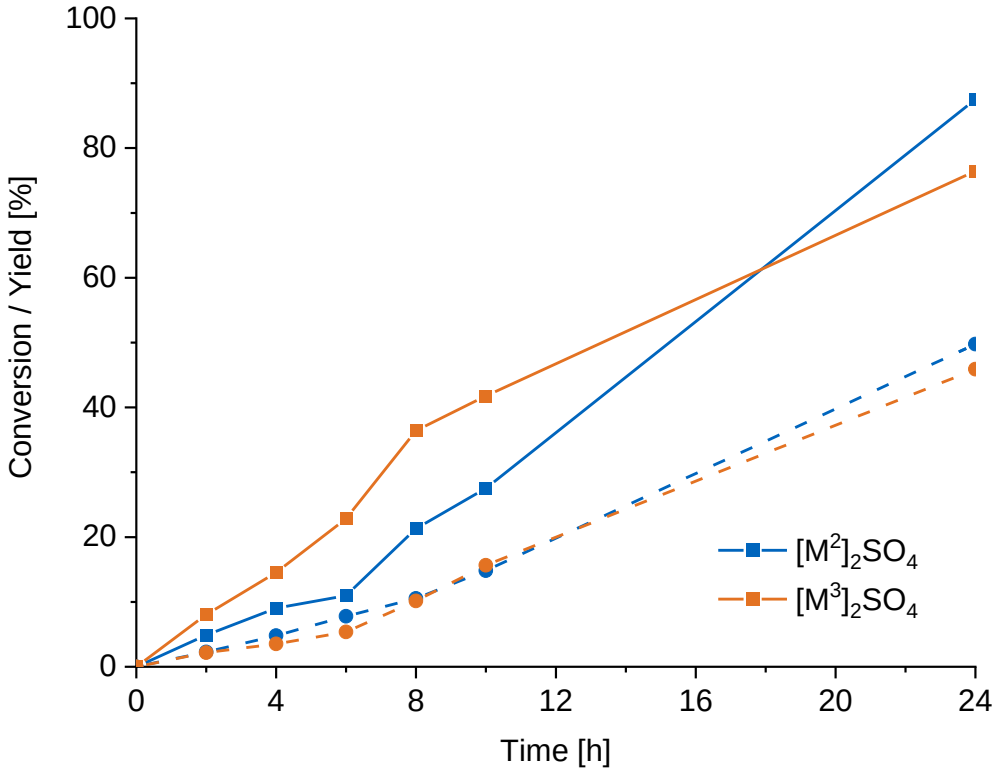

Figure 59: Epoxidation of COE to COO by 5 mol-% catalyst $[M^n]_2SO_4$ (based on sulfate) at 80 °C using 2.5 eq. 50 wt.%. H_2O_2. Bold lines: Conversion of COE, dashed lines: yield of COO.

Table 18: Variation of the catalyst amount of $[M^n]_2SO_4$ (n= 2, 3) in the epoxidation of COE at 80°C using 2.5 eq. 50 wt.% H_2O_2.

SIP	mol-%	Time	Conversion [%]	Yield [%]	Selectivity [%]
$[M^2]_2SO_4$	1	10 h	11	7	68
	1	24 h	24	19	79
	2	10 h	15	11	78
	2	24 h	35	31	88
	5	10 h	28	15	77
	5	24 h	88	50	57
	10	10 h	37	17	45
	10	24 h	97	41	42
$[M^3]_2SO_4$	1	10 h	17	7	40
	1	24 h	26	18	70
	2	10 h	26	11	42
	2	24 h	42	24	57
	5	10 h	46	20	43
	5	24 h	73	45	62
	10	10 h	65	23	35
	10	24 h	93	41	44

The formed crystals were investigated by single crystal X-ray diffraction presenting a supramolecular H-bond network of both components in the anticipated organoamide/dihexylammonium/sulfate ratio 2:2:1 in the crystal (Figure 60).

The single crystal XRD structure reveals an organic capsule formed by layers of dihexylammonium cations binding to the sulfate anion in-between via H-bonds. Moreover, the integrated benzamide molecules bind to the sulfate anion, further stabilizing the supramolecular SIP structure. Noteworthy, two molecules water per $[M^2]_2SO_4$ SIP unit are incorporated in the structure and is in good agreement with the elemental analysis of the constitutional analogue SIP $[HL^2]_2SO_4$, which supports the inclusion of 1.5 equivalents of water per SIP. However, due to the large distance of the amide and ammonium functional groups presented by the $[M^2]_2SO_4$ crystal structure, the SIPs $[HL^2]_2SO_4$ with the methylene bridge in between must be different in geometry with the respective influence on catalysis being unknown.

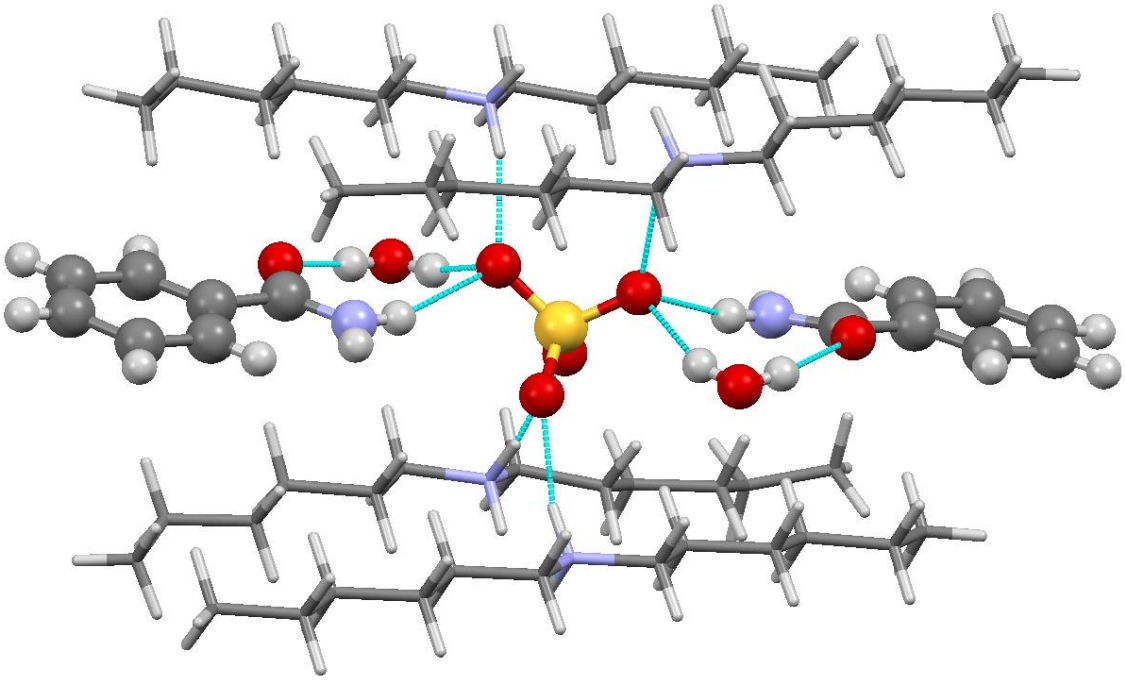

Figure 60: Cutout of the $[M^2]_2SO_4$ single crystal structure. The *n*-hexyl chains are drawn as wireframes for clarity. Note that the four dihexylammonium cations are shared with the adjacent SIP units.

Investigation of the SIP formation

In order to gain information on the SIP formation and constitution in solution, the sizes of the SIP assemblies of benzamide or 3,5,5-trimethylhexanamide and dihexylammonium sulfate, $[M^2]_2SO_4$ and $[M^3]_2SO_4$, are investigated by ^{1}H nuclear magnetic resonance diffusion ordered spectroscopy (DOSY) and dynamic light scattering (DLS). For the first method, the single components and the mixtures thereof were dissolved in benzene-d_6, stirred at 80 °C for one hour and then analyzed by DOSY-NMR, giving access to the diffusion coefficient of the species in solution, which correlates with the hydrodynamic radii of the solvated aggregates according to the *Stokes-Einstein* equation.

The analysis of pure benzamide or 3,3,5-trimethylhexanamide reveals as expected signals with rather small hydrodynamic radii of 2.79 Å and 2.93 Å, respectively. In contrast, the dihexylammonium sulfate solution shows larger assemblies with radii of 126 Å, indicating the formation of large supramolecular structures such as inverse micelles in the benzene solution (Figure 61 and Figure 62). Upon combination of the amides and dihexylammonium sulfate in the SIP ratio 2:1, assemblies of the size of 9.0 Å and 9.7 Å for $[M^2]_2SO_4$ and $[M^3]_2SO_4$, with an additional signal of SIP aggregates at 17.1 Å are detected. For comparison, the pure organic receptor L^1 shows a radius of 6.7 Å, which increases slightly to 9.0 Å upon protonation to the SIP $[HL^1]HSO_4$ by sulfuric acid (Supplementary Figure 11).

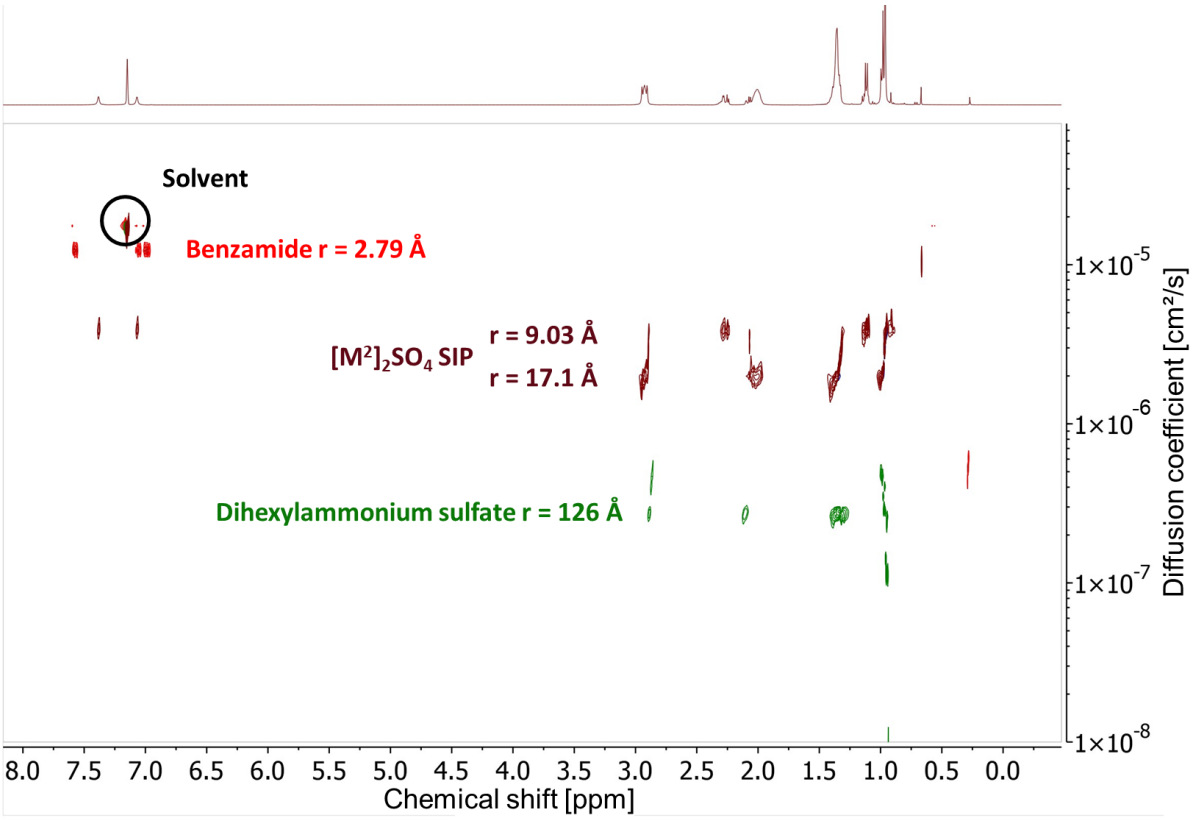

Figure 61: Stacked DOSY-NMR spectra of benzamide (red), $(DHA)_2SO_4$ (green) and $[M^2]_2SO_4$ (brown) in C_6D_6 at room temperature. The ^{1}H-NMR trace originates from the SIP experiment.

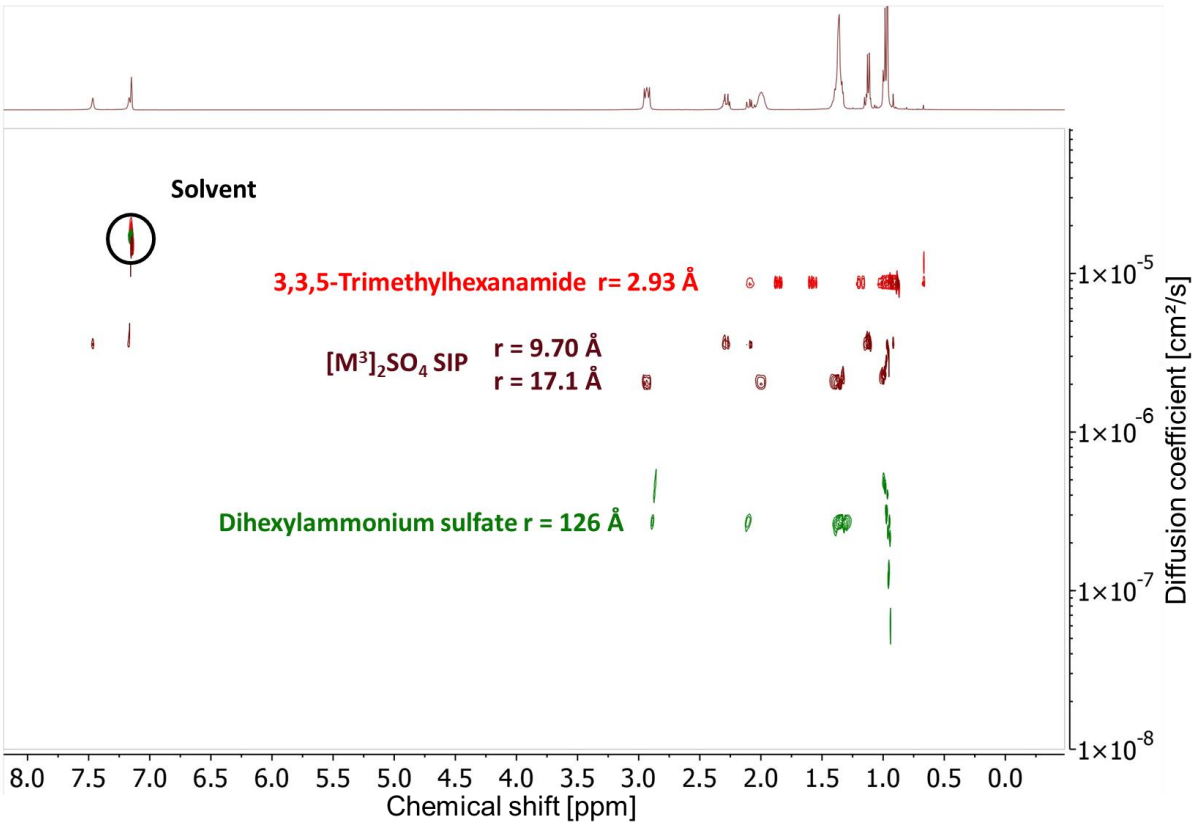

Figure 62: Stacked DOSY-NMR spectra of 3,3,5-trimethylhexanamide (red), $(DHA)_2SO_4$ (green) and $[M^3]_2SO_4$ (brown) in C_6D_6 at room temperature. The ^{1}H-NMR trace originates from the SIP experiment.

Additional DLS measurements are in agreement with the gained information by NMR on the SIP formation. The samples were prepared similarly to the DOSY-NMR approach with the difference that toluene is used as solvent and the solution is measured before and after heating to 80 °C in order to study the temperature-dependency of assembly formation. While the hydrodynamic radius of mixture $[M^2]_2SO_4$ decreases from 26.5 Å to and 11.9 Å after heating (which is in accordance with the DOSY-NMR analysis), the size of $[M^3]_2SO_4$ decreases rather slightly from 21.1 Å to 17.6 Å, indicating a preferred formation of the larger dynamic assembly as presented by DOSY-NMR (17.1 Å). This formation of a SIP-dimer may be explained by the preferred assembly of two sulfate anions, four amide and dihexylammonium cations each. This might also be influenced by the steric demand of the trimethylpentyl substituent on the amide, compared to rather small phenyl, allowing for a larger ionic cavity, in which two sulfate anions fit. In comparison, the DLS size of the SIP $[HL^1]HSO_4$ stays rather constant at 5.3 Å and 5.9 Å before and after heating and occurs to be slightly smaller in toluene than in benzene-d_6.

Comparison of the structural sizes of the SIPs in solution from DOSY-NMR and DLS measurements with the crystal structures are in good agreement and suggest a strong similarity of the structure in solution and in solid state. The radii of the crystal structures were calculated from the respective crystallographic SIP volumes in a simplified spherical approach. (Table 19).

Table 19: Radii of the three SIPs analyzed by various analytic methods.

SIP	DOSY (Å)	DLS (Å)	SCXRD (Å)
$[HL^1]HSO_4$	8.9	5.9	9.1
$[M^2]_2SO_4$	9.0 and 17.1	11.9	8.0
$[M^3]_2SO_4$	9.7 and 17.1	17.6	---
$(DHA)_2SO_4$	126	135	---

The DLS observations reveal that the formation of the crystallographically determined supramolecular structure of $[M^2]_2SO_4$ requires treating at elevated temperatures. To investigate a possible catalytic initiation period, the SIP mixture is stirred overnight in COE at 80 °C prior to addition of H_2O_2, eventually starting the reaction. Comparison of the catalytic activity with and without this pre-activation yields the same catalytic performances, supporting that the respective SIP is formed immediately in solution at 80 °C (Figure 59 and Figure 63).

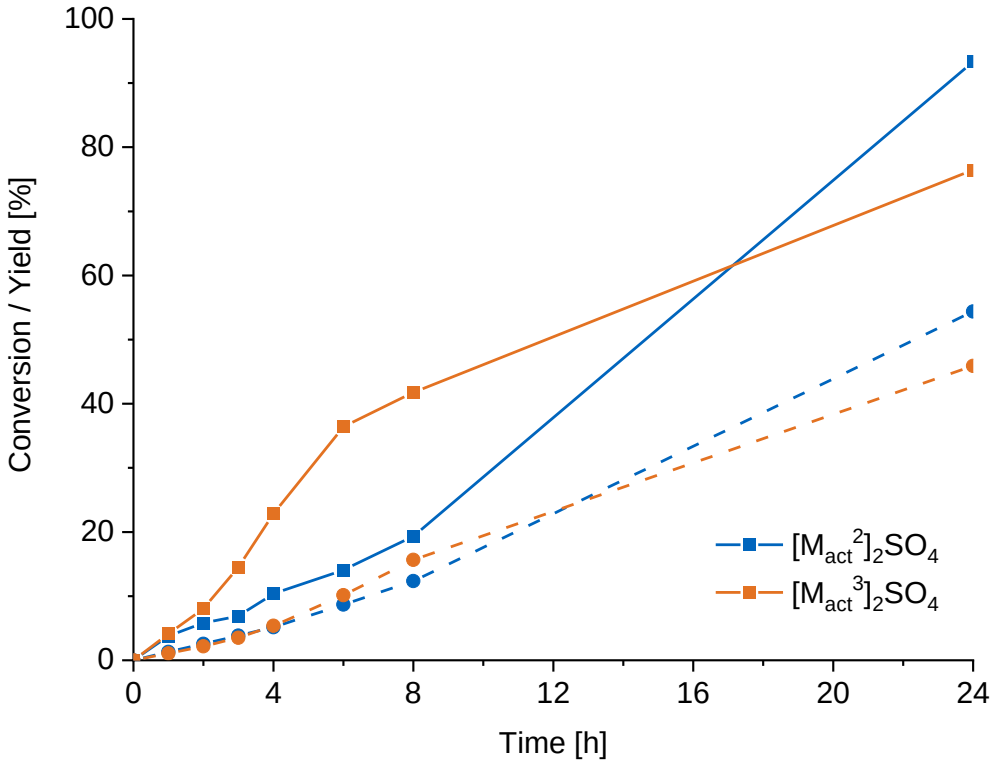

Figure 63: SIP- activation in COE for 18 h at 80 °C; Epoxidation of COE to COO by 5 mol-% SIP (based on sulfate) at 80 °C using 2.5 eq. 50 wt.%. H_2O_2. Bold lines: conversion of COE, dashed lines: yield of COO.

Mechanistic investigation

Elemental analysis and SCXRD investigations suggest a transfer of not only the sulfate anion but also water molecules into the organic phase, which indicates that also H_2O_2 might be transferred into the organic phase. The mechanism of the olefin epoxidation may proceed via the H-bond activation of H_2O_2 inside the polar SIP capsule or by the *in situ* formation of a peroxomonosulfate species. Albeit the formation of peroxomonosulfate from sulfate in aqueous hydrogen peroxide is known in literature for acidic solutions only,[218] the acidic capsule might indeed favour and stabilize the peroxo-species. The loss of the hydration shell of the sulfate inside the SIP might also allow for an H-bond activation similar to the nitrate anion.[148]

Björn Klimas investigated the potential peroxomonosulfate formation by negative mode ESI-MS to elucidate the epoxidation mechanism.[219] The SIP precursors were stirred in 50 wt.% aqueous hydrogen peroxide at 80 °C for five hours and were then extracted with toluene. After evaporation of the solvent, the residue is dissolved in acetonitrile and subjected to ESI-MS. The formation of peroxomonosulfate is observed by detection of two major peaks, namely 96.9 m/z (HSO_4^-) and 112.9 m/z (HSO_5^-) (Figure 64, top). Apparently, the ratio of monoanionic hydrogensulfate (97 m/z) to hydrogenperoxomonosulfate (113 m/z) does not change in case the treatment duration with hydrogen peroxide is shortened to 5 min, indicating a fast equilibrium between the sulfate and peroxomonosulfate species (Figure 64, bottom).

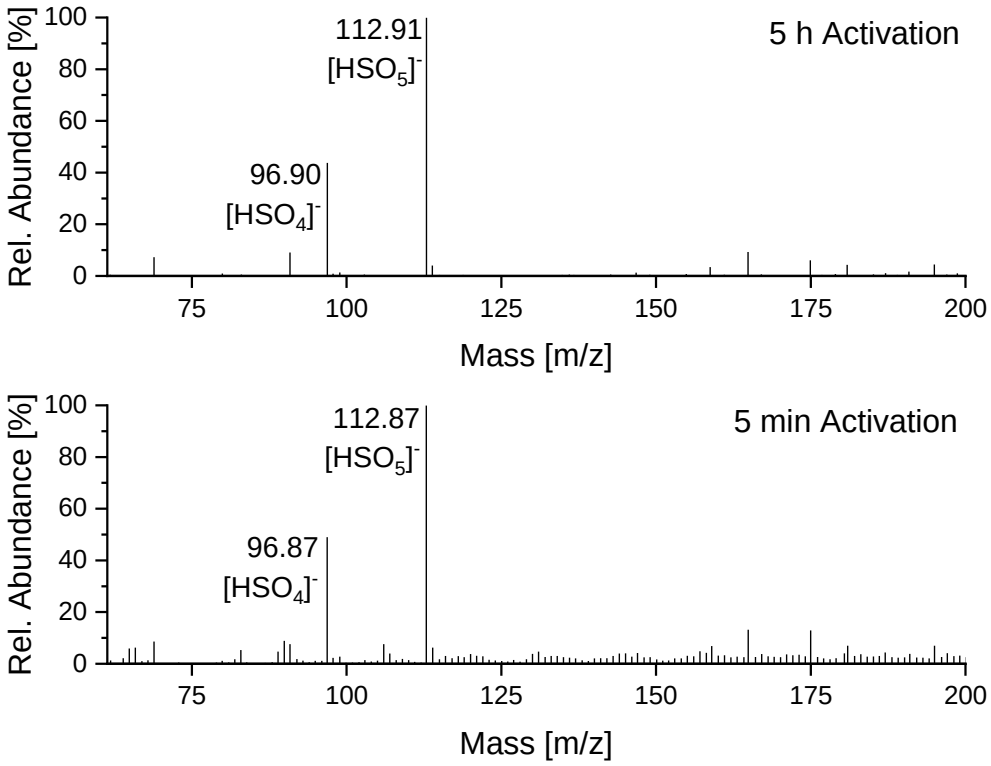

Figure 64: Negative mode ESI-MS spectra of $[M^2]_2SO_4$ treated with hydrogen peroxide, extracted with toluene and measured using acetonitrile as carrier.

Natural abundance *in situ* ^{33}S-NMR approaches to investigate the temperature-dependency of both species under catalysis conditions was not successful due to the quadrupolar moment of the ^{33}S nucleus leading to broad signals and an overlap of the signals due to the small chemical shift difference between the two species (0 ppm and −23 ppm for sulfate and peroxomonosulfate, respectively).[220]

The spectrometric data suggests that the peroxomonosulfate anion is formed upon contact of the SIP with H_2O_2 in the biphasic system and gets transferred to the substrate phase. There, the peroxomonosulfate epoxidizes the olefin and gets converted to the sulfate, restarting the catalytic cycle. In contrast to the enantioselective Shi-epoxidation using catalytic amounts of chiral ketones to form intermediate dioxiranes, peroxosulfates are directly able to epoxidize olefins.[221][222] To proof the peroxomonosulfate's ability to directly epoxidize olefins as part of the SIP in the organic phase, the commercially available and popular stoichiometric oxidant Oxone® was used for SIP formation. The high acidity of the triple-salt $KHSO_5 \cdot ½\ KHSO_4 \cdot ½\ K_2SO_4$ was buffered with stoichiometric amounts of dihexylamine in presence of benzamide, conveniently leading to formation of the peroxomonosulfate-SIP. Due to the required application of the SIP as stoichiometric oxidant, cyclooctane, which is expected to have no different influence on the SIP formation, is used to dilute the cyclooctene phase to maintain SIP-concentrations in the organic phase as investigated previously.

The mixture is stirred at 80 °C for 24 h under anhydrous conditions to avoid any H_2O_2 evolution. The resulting activity is similar to the catalytic application of the parent SIP $[M^2]_2SO_4$ in 50 wt.% H_2O_2 (Figure 65). This result proves two characteristics: i) peroxomonosulfate is the active species of the epoxidation and ii) Oxone® has no advantage as oxidant, as H_2O_2 is more convenient, similar in activity and much 'greener' due to the prevention of waste salts. Per gram of COE to be oxidized, three grams of Oxone® are required, compared to <0.5 mL H_2O_2 50 wt.%, which releases water and can easily be removed by decantation after the reaction. In addition, Oxone® has a higher acidity due to the release of strongly acidic $[HSO_4]^-$ from $[HSO_5]^-$ leading to lower epoxide selectivity with proceeding COE conversion and oxidant consumption.

Both essential premises, the solubilization of the (peroxomono)sulfate in the organic phase as well as the persulfate formation and the consecutive epoxidation are fulfilled. This is the first report on the catalytic application of simple sulfate anions in oxidation reactions. cheapness of the single SIP components could allow for the large-scale application beyond the laboratory scale. However, the model substrate COE is not of sufficient industrial relevance, so further olefins with different C=C double bond substitution- and configuration patterns were epoxidized with the most suitable SIP $[M^2]_2SO_4$ (Table 20).

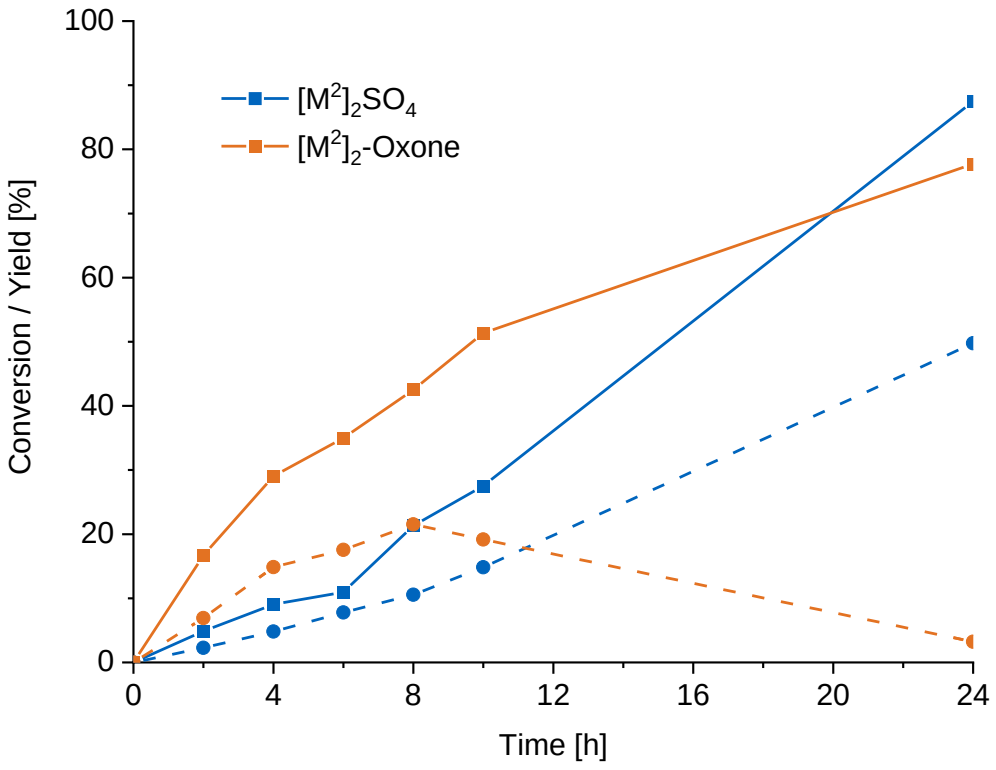

Figure 65: Comparison of the reactivities of $[M^2]_2$-Oxone® (orange) and $[M^2]_2SO_4$ plus hydrogen peroxide as oxidant (blue) in the epoxidation of cyclooctene at 80 °C. Bold lines: conversion of COE; dashed lines: yield of COO.

Similar to previous investigations, the highest reactivities show internal olefins with a *cis* substituent configuration, especially the ring-strained cyclic olefins cyclohexene and 1-methylcyclohexene. However, the acidic interior of the SIP leads to an instantaneous epoxide hydrolyzation and the corresponding epoxide cannot be isolated. *Cis*-2-octene has a higher reactivity than the *trans* derivative with 91% vs. 57% conversion after 24 h. The selectivity is rather low for both substrates due to the hydrolyzation of the epoxide. The terminal olefin 1-octene shows a high reactivity towards oxidation, but a low epoxide selectivity, caused by the facile epoxide hydrolysis. Styrene with a conjugated aromatic π-system, has the highest reactivity among the non-cyclic olefins which is also true for the epoxide, which is immediately hydrolyzed to 1,2-phenylethanediol. Additionally, traces of the side-products benzaldehyde and benzoic acid are detected, which arise from oxidative diol cleavage.

Table 20: Substrate Variation with 5 mol-% $[M^2]_2SO_4$ and 2.5 eq. H_2O_2.

Substrate	Time	Conversion [%]	Yield [%]	Selectivity [%][a]
Cyclooctene	24 h	88	50	63
Cyclohexene	4 h	91	traces	---
1-Methylcyclohexene	4 h	93	72	72
1-Octene	24 h	79	3	3
cis-2-octene	24 h	91	16	16
trans-2-octene	24 h	57	10	10
Styrene	12 h	73	0	0

a: GC-MS reveals that diols are the only side-product except for styrene, which forms traces of benzaldehyde and benzoic acid.

3.4.3 Conclusion

Inorganic peroxomonosulfates are used for decades as stoichiometric oxidants for the epoxidation of olefins. Especially the initial works by Shi on the enantioselective epoxidation of prochiral olefins with chiral ketones forming an intermediate dioxirane species lead to an academic popularity of the oxidant.[202][201] Due to the low active oxygen content of only 5 wt.%, the commercially available triple salt Oxone® releases large quantities of waste salts. Hence, its application beyond the laboratory scale is rather limited. The potassium peroxomonosulfate is produced by neutralization of Caro's acid H_2SO_5, which in turn is formed by addition of concentrated sulfuric acid to hydrogen peroxide. A formation of peroxomonosulfate from H_2O_2 and a sulfate salt in neutral solution is not reported to date in literature. This is the first report on the catalytic use of sulfates in oxidation reactions. The protonated organic receptor molecules L^{1-3} show a high affinity to sulfate and transfer the highly polar anion into the organic phase by formation of a sulfate-based SIP. Stability investigations show that the receptor L^{2-3}'s

amidoammonium group does not survive at elevated temperatures but decomposes rapidly. The ongoing conversion of the olefin to the epoxide cannot be completely attributed to the evolving formaldehyde and the sulfate remains dissolved in the organic phase. Hence, a SIP formation by the simple building blocks organic amide, dihexylamine and sulfuric acid is self-evident and shown by DLS and DOSY-NMR. The final information on the SIP's constitution was delivered by a SCXRD structure, showing the organic capsule motif with the sulfate entrapped inside. There, the sulfate anion is not completely surrounded by hydrating water molecules, as it would be the case for sulfate in aqueous solutions, where it is inactive in H_2O_2-activation. Upon transfer into the organic phase as SIP component, it loses the protecting water shell, giving rise to a direct interaction with H_2O_2. Negative-mode ESI-MS investigations reveal that an intermediate peroxomonosulfate is formed inside the SIP, which can act as a direct olefin oxidant at elevated temperature. Upon consumption of the catalytic peroxomonosulfate inside the SIP capsules, the sulfate is regenerated with the excess hydrogen peroxide in the aqueous phase, providing a route for the use of hydrogen peroxide in epoxidations in the organic phase without requirement of organic solvents.

Despite the *in situ* formation and cheapness of the catalyst, the recycling is somewhat intricate or rather impossible. The product can easily be separated from the aqueous hydrogen peroxide by decantation, but the catalyst is dissolved therein. A distillation or chromatographic separation is required to obtain the pure epoxide but decomposes the catalyst. Hence, the catalyst being solely soluble in the aqueous phase is advantageous for its recovery and reuse. Additionally, some problems arise such as the accumulation of the water by depletion of the oxidant and addition of new H_2O_2. Hence, a triphasic system would be required to separate the product as well as the catalyst from the aqueous phase. Temperature- or reaction-controlled micellar approaches in water could allow for such a process but are not developed to date. A special functionalization of the imidazolium cation is required to trigger such a responsiveness on external stimuli. The next chapter deals with the design and application of such catalytically active surfactants.

3.5 Temperature-responsive Micelles

3.5.1 Introduction

The previous chapters have shown that the epoxidation of olefins in the aqueous phase exploiting the solubilization by micelles is of great advantage in terms of product separation and catalyst recycling compared to the transfer of the catalytically active anion into the organic phase. The product phase is free of catalyst and water and can be separated by facile decantation, yielding the pure product. As advantageous this approach is, it accompanies two minor problems: Since the micelles are still present after the completed reaction, a fraction of the organic phase and hence the product is still solubilized inside the micelles and cannot be removed. An extraction procedure with organic solvents is required to separate the product from the aqueous phase. This diminishes the ‘green’ benefit of the use of aqueous hydrogen peroxide as reactant and solvent. Another drawback is the so-called ‘accumulating water problem’ and is related to catalysis involving hydrogen peroxide as oxidant. Upon depletion of the H_2O_2, the epoxidation inevitably stops due to the lack of oxidant. The addition of new oxidant leads to a further dilution of the catalyst until after certain runs, the total catalyst concentration is below the CMC. The water, due to its lower boiling point compared to hydrogen peroxide, could be distilled off for oxidant reconcentration but requires large amounts of thermal energy, questioning the green character of the micellar epoxidation.

Consequently, a targeted collapse of the micelles at the end of each catalysis run would be desirable to release the residual product, and a concomitant precipitation of the catalyst would allow for the separation of the reaction mixture into the three components product/water/catalyst. This concept requires a catalyst that, upon external stimuli, reduces its solubility in the aqueous phase and precipitates while still being immiscible with the organic phase. A suitable stimulus is the reaction temperature. The catalyst is only required to be soluble in aqueous hydrogen peroxide at the elevated temperature. Hence, a negligible solubility at low temperatures can be exploited to quantitatively separate the catalyst form the aqueous phase (Figure 66).

A class of organic compounds that show a wide temperature-depending solubility behavior are polyfluorinated surfactants. Those are considered amphiphobic as they are neither soluble in aqueous nor organic solvents and form a third phase. The degree of fluorination decreases their overall solubility and may be altered in order to adjust the catalyst solubilities.[223]

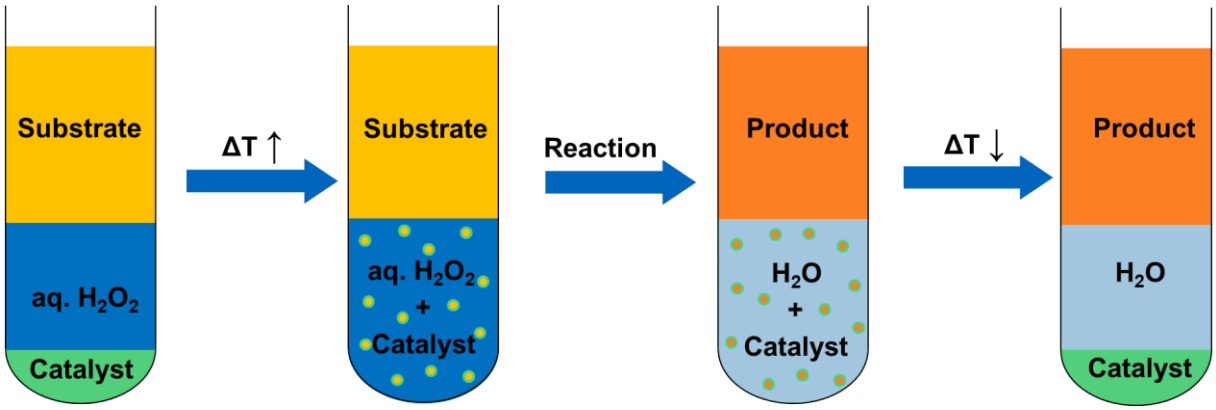

Figure 66: Schematic sequence of the temperature-responsive micellar epoxidation.

First reports by Neumann et al. on the controlled precipitation of a polyoxometalate-based epoxidation catalyst supported by fluorinated quaternary ammonium cations showed the potential for the temperature-controlled phase transfer epoxidation of olefins with H_2O_2.[82] At low temperatures, the catalyst consisting of twelve $[(CF_3(CF_2)_7(CH_2)_3]_3CH_3N^+$ cations surrounding the POM $[WZnM_2(H_2O)_2(ZnW_9O_{34})_2]^{12-}$ (M = Mn(II), Zn(II)) is insoluble in both, the aqueous and the organic phase. At an elevated temperature of 60-80 °C, is gains solubility and catalyses the epoxidation of olefins similarly to the initial POM-epoxidations by Venturello and Ishii.[74][77] After full conversion of the olefin, the reaction mixture is cooled to room temperature, the catalyst precipitates, and can be recovered from the aqueous phase by simple filtration. This approach allows for the separation of the three components water/product/catalyst by simple mechanic techniques. These temperature-controlled catalyst precipitations are very rare and show the difficulties to develop such a process.[71]

Regarding a temperature-controlled micellar epoxidation with surface-active imidazolium salts, a fluorinated structural motif offers a great opportunity to adjust the solubility of the catalyst. A suitable polyfluorinated substituent must therefore be covalently bound to the cation. While the octyl-group is required for the substrate interaction and formation of the micelle, the fluorinated group should be positioned to the opposite N-wingtip position of the imidazolium cation as this allows for a one-step synthesis procedure and the introduction of sterically demanding substituents. Hence, the *N*-methyl substituent is replaced by a polyfluorinated organic residue. Regarding the precipitation of the catalyst in cold media, a strong non-covalent interaction of the surfactant would be favourable as this can easily be overcome at elevated temperature for dissolution. In addition to the weak imidazolium π^+-π^+ interaction of aggregated molecules, the introduction of a further aromatic substituent could increase the intermolecular attraction and reduce the solubility.[224] 1-Alkyl-3-benzylimidazolium ionic liquids are easily synthesized and the methylene group bridging both aromatic system allows for a rotational freedom to facilitate micelle formation. A polyfluorination of the benzylic phenyl ring decreases the solubility in organic media sufficiently for an exclusive catalyst operation in the aqueous phase.

The solubility of the ionic liquid in water is dependent on the hydrophilicity of the cation as well as the hydratization of the anion. Besides the previously investigated diorganophosphate anions, the tungstate- and nitrate-based imidazolium ionic liquids show a very high, virtually unlimited solubility in water. Investigations by Cokoja et al. present the application of micellar imidazolium perrhenates or the biphasic epoxidation of olefins using hydrogen peroxide. There, some catalysts are barely sufficiently soluble in the aqueous phase with dependency on the imidazolium C-2 substituent.[118] For example, the catalyst [OMIM] [ReO_4] is perfectly soluble at 70 °C and at room temperature, whereas the 2-methyl derivative [OMMIM] [ReO_4] is barely soluble at 25 °C in the depleted H_2O_2 phase. Hence, perrhenate-based catalysts are of sufficient hydrophobicity to trigger the precipitation by the external stimulus temperature. The cation is designed towards amplification of the effect of the temperature on the solubility according to the proposed fluorination approach.

3.5.2 Results and Discussion

The fundamental reason of the catalyst precipitation in solutions of H_2O_2 is preferentially introduced by sufficiently strong intermolecular interactions, which are overcome at elevated temperature. Among the non-covalent interactions, π-π interactions are in the perfect range of the bond strength compared to other intermolecular interactions (Table 21).[225] Therefore, the introduction of a further aromatic system to the imidazolium cation could be beneficial for the temperature responsiveness. Nevertheless, the hydrophobicity might increase towards an immiscibility with water or even worse, solubility in the organic phase. Therefore, a fluorination of the benzylic moiety could increase the amphiphobicity. The resulting 1-(2',3',4',5',6'-fluorobenzyl)-2-R-3-octylimidazolium bromide precursors (R = H, Me) were synthesized by alkylation of 1-octylimidazole and consequently converted to the respective perrhenates via an anion exchange procedure (Scheme 21). Both catalysts with imidazolium C-2 = H and Me were synthesized to investigate the influence of the cation-anion interaction on the solubility.[226]

Table 21: Comparison of intermolecular interactions. Values taken from reference [225].

Interaction	Bond strength [kJ/mol]	Bond length [pm]	Directional
Ionic bond	5-200	Depends	No
Hydrogen bond	5-65	150-260	Yes
Van-der-Waals	2-4	Depends	No
π-π	4-8	330-380	Yes

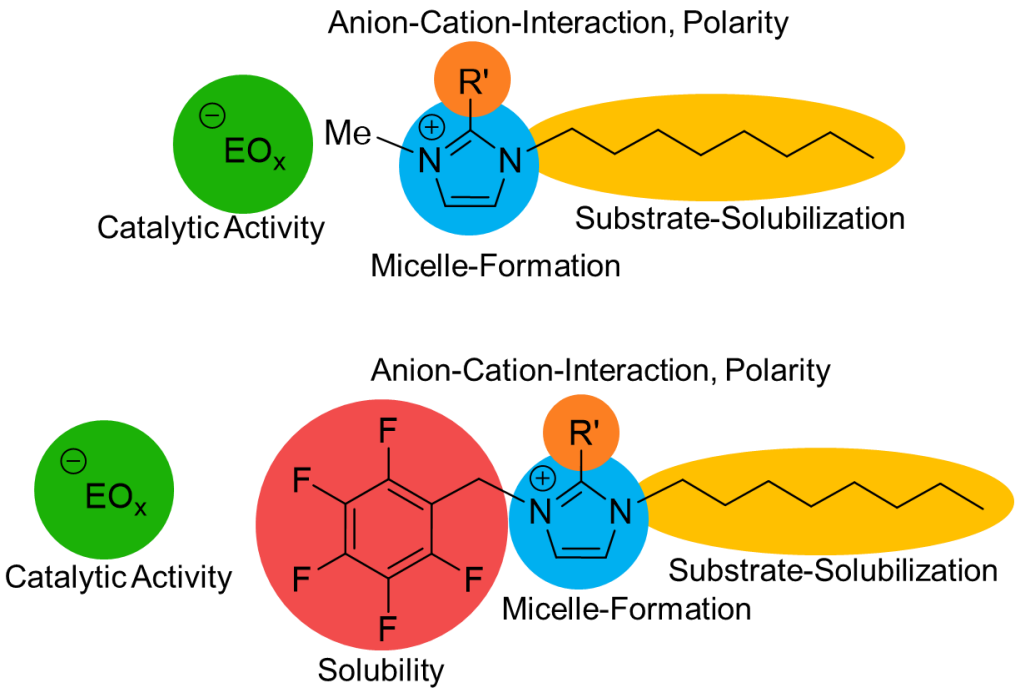

Figure 67: Structural motifs of imidazolium ionic liquids with task-specific functions. Top: Standard catalytically active SAIL. Bottom: Temperature-responsive SAIL.

The solubility of the obtained 1-(2',3',4',5',6'-fluorobenzyl)-2-R-3-octylimidazolium perrhenates, from now on called [^{F}BnOIM] [ReO_4] (for R = H) and [^{F}BnOMIM] [ReO_4] (for R = Me) (Figure 68), was investigated in water and 50 wt.% H_2O_2 at several temperatures (0 °C, 20 °C and 80 °C). It was found that the solubility is strongly dependent on the temperature reaching high values of several grams per liter at elevated temperature and dropping vastly at 0 °C (Table 22). In addition, the polarity of the solvent plays a crucial role as less polar H_2O_2 provides a higher solubility for the surfactant. In water, the temperature-dependent solubility differs by a factor of greater 20 between 0 °C and 80 °C for the less polar 2-methyl substituted IL. In general, aqueous hydrogen peroxide allows for a higher solubility of the perrhenate ILs than water. Regarding the epoxidation catalysis of olefins with the herein presented switchable ILs, both stimuli, the change in temperature and the depletion of the oxidant play a beneficial role for the collapse of the micelles. During the reaction, a high catalyst solubility is achieved at 80 °C, a reasonable temperature for perrhenate-catalyzed epoxidations (vide infra).

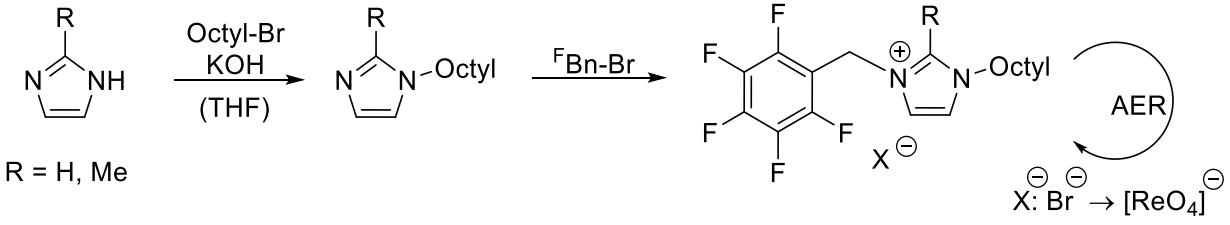

Scheme 21: Synthesis procedure towards pentafluorobenzylic imidazolium perrhenates.

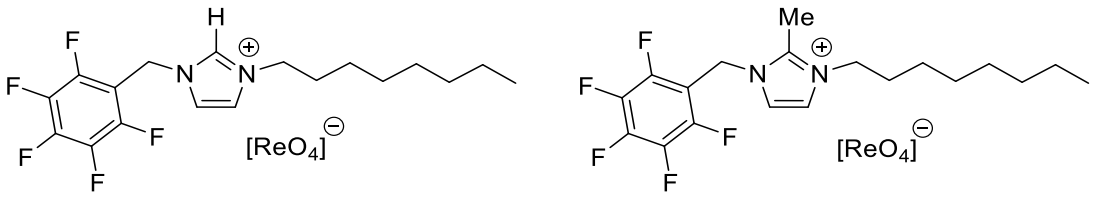

[^{F}BnOIM] [ReO_4] [^{F}BnOMIM] [ReO_4]

Figure 68: Structure of the perrhenate-based switchable catalysts.

Similarly, the H_2O_2 concentration decreases due to the consumption of the oxidant, increasing the polarity of the aqueous phase and further supporting the catalyst precipitation. The cooling of the reaction mixture decreases the solubility of the ILs by a factor of at least 70 but is limited to the detection limit of the NMR-based solubility quantification. Here, analytical techniques such as ICP-OES or ICP-MS would allow for an accurate rhenium determination down to a detection limit of ng/mL.[227]

In summary, the synthesized compounds (see Figure 68) show an adjustable solubility by i) the temperature of the reaction mixture and ii) the progress of the reaction by the residual H_2O_2-concentration. Additional DLS studies on the surface-activity and the olefin interaction confirm the presence of micelles and larger aggregates during catalysis and also a micelle collapse after cooling of the reaction mixture. The catalysts [^{F}BnOIM] [ReO_4]and [^{F}BnOMIM] [ReO_4] were dissolved in aqueous hydrogen peroxide and heated to 80 °C to obtain a saturated solution. Then, the clear solution is transferred into a quartz cuvette and equilibrated in the DLS instrument at 80 °C for 20 min. The detected aggregate sizes show that large aggregates with a diameter in the range of 100-200 nm and 200-300 nm are formed (Table 23). This is compared to all previously investigated micelles in the absence of an olefin rather large. In contrast, the micelles formed by the parent catalyst [OMIM] [ReO_4] without bearing the pentafluorobenzyl moiety are as expected in the rage of common micelle-forming [$OMIM]^+$ ionic liquids.[155]

Table 22: Solubility measurements of pentafluorobenzyl-substituted imidazolium perrhenates in various solvents and temperatures.

Surfactant	Solvent	0 °C		20 °C		80 °C	
		mmol/L	mg/L	mmol/L	mg/L	mmol/L	mg/L
[^{F}BnOIM] [ReO_4]	H_2O	2.7	1651	5.4	3303	19.8	12111
	50 wt.% H_2O_2	11.6	7095	15.5	9480	39.9	24403
[^{F}BnOMIM] [ReO_4]	H_2O	<0.5	<313	1.9	1189	10.3	6444
	50 wt.% H_2O_2	2.1	1314	6.6	4129	34.5	21583

Hence, the pentafluorobenzyl group cannot be considered innocent in micelle formation but triggers the formation of larger aggregates. Upon addition of excess *cis*-cyclooctene, the aggregates of [^{F}BnOIM] [ReO_4] and [OMIM] [ReO_4] swell slightly, speaking for an uptake of the hydrocarbon. The [^{F}BnOMIM] [ReO_4] aggregates in contrast decrease their diameter slightly upon contact with the olefin. An uptake of the olefin cannot be confirmed via DLS, but an influence of COE on the aggregates is observed. At 20 °C, the solubility drops and the collapse of the micelles can be observed: The respective aggregate sizes drop to 0.7 nm by precipitation of the surfactant. The residual measured scattering intensity may arise from surfactant molecules which are dissolved in solution due to the few mmol/L solubility at 20 °C (see Table 22). In contrast, the micelles formed by [OMIM] [ReO_4] are still present after cooling with a slightly increased aggregation number, pointing towards the containment of significant amounts of COE.

Table 23: DLS investigation of various imidazolium perrhenates in 50 wt.% H_2O_2.

Temperature	Additive	[^{F}BnOIM] [ReO_4]	[^{F}BnOMIM] [ReO_4]	[OMIM] [ReO_4]
80	---	122-159 nm	212-283 nm	1.64 nm
80	COE	142-234 nm	191-221 nm	1.85 nm
20	COE	0.78 nm	0.71 nm	2.59 nm

Due to the success of the temperature-responsive micellar concept, the catalytic performance of the designed catalysts was investigated and compared to the renown micellar catalyst [OMIM] [ReO_4], which presents a high COE conversion of 91% after 4 h at 80 °C, compared to 44% at 70 °C.[118] In comparison, the derived [^{F}BnOIM] [ReO_4] catalyst, which bears the pentafluorobenzyl group instead of the *N*-methyl substituent shows a reduced reactivity (Figure 69, blue and pink curves). In literature, [OMMIM] [ReO_4] is slightly more active than the C2-H derivative, likely due to a decreased cation-anion interaction.[118][226] Likewise, [^{F}BnOMIM] [ReO_4] is more active than [^{F}BnOIM] [ReO_4], comparable with [OMIM] [ReO_4] after 8h. For a better understanding of the effect of the benzyl substituent on the catalysis, the ILs 1-benzyl-3-methylimidazolium perrhenate [BnOIM] [ReO_4] and 1-(4'-fluorobenzyl)-3-methyimidazolium perrhenate [F-BnOIM] [ReO_4] were synthesized and tested towards their catalytic potential (see Figure 69, curves olive and red, respectively). Their catalytic activities in the epoxidation of COE are slightly higher than the pentafluorobenzyl-IL. Most presumably, this can be attributed to their severe solubility in the organic phase. Hence, the reactivity might be boosted by catalyst operation in the organic phase but this is the major criterion for the exclusion of these catalysts. In Addition, the non- or monofluorinated 1-benzyl-3-octylimidazolium perrhenates do not show a sufficient thermo-responsiveness in aqueous hydrogen peroxide and should therefore not be considered for catalysis.

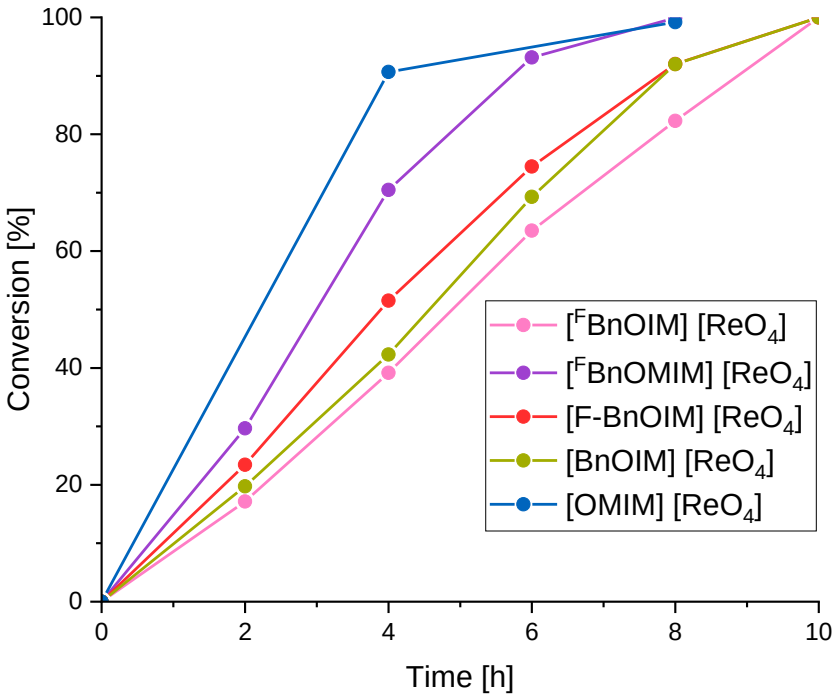

Figure 69: Epoxidation of COE with various imidazolium perrhenates using 50 wt.% H_2O_2. Reaction conditions: Catalyst:COE:H_2O_2 = 5:100:250, 80 °C.

4 Conclusion and Outlook

During the course of this thesis, supramolecular approaches towards the biphasic epoxidation of olefins with hydrogen peroxide have been investigated. Two classifications could be made according to the two possible reaction sites in a biphasic medium: i) the olefin being transferred into the aqueous catalyst solution or ii) the transfer of the catalyst into the supernatant substrate phase. Due to a targeted structural catalyst design and exploitation of supramolecular interactions of cationic surfactant or receptor molecules, the phase of operation can task-specifically be adjusted to the catalytic requirements.

In the first chapters, the focus lies on the application of surface-active imidazolium salts for the epoxidation of olefins. The solubilization of olefins in water is achieved with micelles, aggregates of surface-active compounds with a polar surface and a hydrophobic interior. Here, the use of cationic surfactants is of advantage due to the dynamic immobilization of catalytically active anions on the cationic micellar surface. This bifunctional cation-anion approach allows for the use of dialkylimidazolium cations, which are stable under oxidative conditions and structurally tuneable, in combination with catalytically active anions, which are required for the activation of hydrogen peroxide. Moreover, the catalysts can be tailored for the specific task by choice of the ion combination. The major advantage of surface-active imidazolium salts is the high uptake of olefin into the cationic micellar interior and the high anion density on the micellar interface in proximity to the olefin-saturated hydrophobic core. This leads to high reaction rates and a facile possibility of catalyst recycling due to the immiscibility with the supernatant organic phase.

The excellent recyclability of the micellar catalysts is presented for the epoxidation of olefins using novel surface-active imidazolium tungstates. This is the first report on the epoxidation of non-polar olefins with tungstate catalysts operating in the aqueous phase and additionally allowing for a facile product separation.[128] The catalysts are easily synthesized from cheap commercial precursors and allow for a large-scale production and application. Cryo-TEM imaging confirms the presence of micelles in aqueous hydrogen peroxide and the uptake of the substrate into the micelles. By application of a suitable ^{183}W-NMR experiment, the catalytically active species was found to be the tetra(peroxo)tungstate anion $[W(O_2)_4]^{2-}$, which is highly reactive towards olefins. The addition of organophosphonate additives boosts the reactivity of the catalyst by almost two orders of magnitude due to the additive coordination to the tungstate species, forming an even more reactive diperoxo tungstate adduct.[228] The covalent linkage of the phosphonate group to the surfactant cation results in a multi-task

catalyst with the tungstate anion coordinated to the micellar surface. Higher reaction rates than the single components dissolved in the reaction mixture are observed. In terms of activity, the micellar imidazolium tungstate approach in aqueous hydrogen peroxide can compete with traditional procedures, which solubilize the catalyst in the organic phase.

In order to transfer the perrhenate-derived concept of the outer-sphere H-bond mechanism to a metal-free micellar catalyst with more abundant anions, surface-active imidazolium nitrates were investigated for the activation of hydrogen peroxide. The nitrate anion does not react with hydrogen peroxide and has not been considered active in catalysis before but is able to activate hydrogen peroxide via H-bonds in a micellar environment.[148] As part of a cationic micelle, the nitrate anion is less hydrated according to the 'hydrophobic effect' and therefore prone to form H-bonds with the less polar hydrogen peroxide molecule. Hence, simple sodium salts which are homogeneously dissolved in solution, do not show reactivity towards hydrogen peroxide. Similar to the imidazolium tungstates, the nitrates are exclusively soluble in aqueous media and form micelles as shown by DLS measurements. The proven catalyst recovery procedure can be applied and allows for a reuse of the catalyst over multiple runs without decomposition or loss. In comparison to the somewhat more active tetragonal perrhenate anion,[118] the nitrate anion has a D_{3h} symmetry and a far more electronegative central atom. This forces the nitrate adduct with hydrogen peroxide into a weaker, energetically less favoured interaction. The nitrogen's electronegative character withdraws electron density from the three oxygen atoms, reducing the binding strength to H_2O_2 via H-bonds. This is most probably the reason for the lower reactivity of nitrate compared to perrhenate, which operates mechanistically similarly. Within this study, it could be shown that the concept of H_2O_2 activation via H-bonds can be transferred to simple nitrate, opening the field for further investigations on other oxo-anions.

The heavier pnictogen analogue, the phosphate anion, exhibits similar to perrhenate a T_d symmetry with four oxo-ligands and an even higher triple negative charge, prone for the activation of hydrogen peroxide by H-bonds. The basic character of phosphate can be circumvented by functionalization of two negatively charged oxygen atoms with organic substituents. The possibility to vary the organic phosphate residues allows for the investigation of the influence of the electronic and steric properties on the epoxidation mechanism. *In situ* ^{31}P-NMR spectroscopy suggests the formation of a diarylperoxophosphate intermediate in the presence of micelles exclusively. Dialkylphosphates in contrast, activate hydrogen peroxide *via* an outer-sphere H-bond mechanism as DFT investigations suggest. In contrast to the alkali nitrates, simple sodium diorganophosphates also activate hydrogen peroxide sufficiently as the organic substituents decrease the polarity and thereby the hydratization allowing for an increased interaction with hydrogen peroxide. Depending on the choice of substituents, a

negligible or fast hydrolyzation of the diorganophosphate may occur. The resulting 1-octyl-3-methylimidazolium dihydrogenphosphate [OMIM] [H_2PO_4] is stable, recyclable, does not decompose H_2O_2, and shows a slightly higher reactivity towards H_2O_2 than the nitrate anion. This highly polar $[H_2PO_4]^-$ anion does likewise not operate without the micellar environment due to its hydrophilicity and concomitant solvation shell and has shown to be suited for a recycling procedure due to the excellent stability of the catalyst.

As the basic phosphate anion is not compatible with aqueous hydrogen peroxide, a simple pH-neutral alternative, the sulfate anion was chosen to be studied towards its reactivity in the activation of H_2O_2. The highly polar sulfate anion is vastly hydrated and cannot be activated by the micellar influence in contrast to the nitrate anion. Hence, the activation of hydrogen peroxide is not sufficiently strong for its use in oxidation reactions. In absence of water, a strong H_2O_2-interaction would be possible. Therefore, the phase of operation was shifted from the aqueous to the organic phase by help of another supramolecular concept. Organic receptor molecules, which were developed by Tasker, Sole et al. for the extraction of inorganic metalates into the organic phase for wastewater treatment and purification processes seemed promising.[106][107] These amidoamine receptors were synthesized and treated with sulfuric acid to form sulfate-containing supramolecular ion pairs (SIPs) which can be regarded as shuttles for the sulfate anion into organic phase. It was found that these receptors decompose rapidly under the oxidative and slightly acidic conditions to the SIP's fundamental synthetic building blocks, namely an organoamide, bis(dihexylammonium)sulfate and formaldehyde. The reactivity does not decline upon SIP-decomposition and hence, a catalytically active species must be formed *in situ*. This allows for the catalytic use of the simple and commercially available commodity chemicals organoamide, dihexylamine and sulfuric acid. SCXRD structures along with DOSY-NMR and DLS investigations reveal the formation processes of supramolecular assemblies which have shown to be highly active in the epoxidation of olefins using hydrogen peroxide. ESI-MS studies suggest that the active species is peroxomonosulfate, which has not been reported to form in neutral solutions of sulfate and aqueous hydrogen peroxide. The SIPs transfer this oxidant into the organic phase for the reaction with the olefin. The sulfate is regenerated in the aqueous phase and can thereby be applied in catalytic amounts; in contrast to the commercially available oxidant Oxone®. Nevertheless, the epoxidation in the organic phase does not allow for a simple catalyst recycling and the product contains the catalyst species and has to be purified intricately.

The presented studies show that among both possible approaches, the epoxidation of olefins in the aqueous or organic phase, the micellar approach is advantageous and the only reasonable choice for catalyst recycling and product separation. Nevertheless, the partial solubilization of the supernatant organic phase in the aqueous hydrogen peroxide by the

micellar assemblies does not allow for the quantitative release of the product at the end of the reaction as the micelles are still present and contain the epoxide. Hence, the collapse of the micelles at the end of the reaction is highly desirable. Moreover, the consecutive removal of product and addition of fresh oxidant and substrate leads to the dilution of the catalyst, eventually below the CMC. This would result in a decrease of the catalytic activity due to the dissolution of the surfactant molecules. A catalyst precipitation supports the separation of the catalyst form the product as well as the residual water quantitatively.

This requirement was approached by design of a temperature-responsive micellar catalyst which allows for the catalyst separation from the two phases. On the basis of the previous gained information on structure-property relations of the imidazolium-based surfactants, especially on the polarity and phase-behavior in solution, the solubility was tailored for a catalyst precipitation upon cooling of the reaction mixture. Polyfluorinated imidazolium perrhenates have been shown to fulfil this requirement by their thermo-sensitive behavior. Intermolecular π-π interactions are exploited to increase the effect of the temperature on the solubility with the introduction of perfluorinated benzylic groups, diminishing the overall solubility in the aqueous hydrogen peroxide below room temperature. The perrhenate-based catalysts show an aggregation at elevated temperature and great reactivity towards *cis*-cyclooctene. Upon cooling of the reaction mixture, the catalyst precipitates and can be separated from the product as well as the aqueous medium due to the negligible solubility in both media. Perrhenate-based ILs were chosen as a model catalysts as their low polarity allow for a fine-tuning of the overall catalyst solubility by functionalization of the imidazolium motif. Hence, the influences of the polarity-decisive C-2 substituent on the phase behavior can be studied in detail. The results show that the methylation of the C-2 imidazolium position further spread the solubility range at different temperatures compared to the C2-H derivative. The thermo-responsive micellar catalysts are still based on the expensive perrhenate anion, that was successfully substituted with cheaper or even metal-free anions for $[OMIM]^+$-based catalysts during the course of this work. The herein gathered information on the structure-solubility and structure-responsiveness relations can help to design catalytically active catalysts with more abundant but catalytically highly active anions, such as tungstate.

A high reactivity towards the epoxidation of olefins can be expected from polyfluorinated imidazolium tungstates. The solubility of these ILs will be somewhat higher in water and aqueous hydrogen peroxide due to the much higher polarity of the tungstate counterion. Nevertheless, this could also be of advantage for the solubilization of olefins in the aqueous phase, which is higher for more polar $[OMIM]_2[WO_4]$ and [OMIM] $[NO_3]$ compared to [OMIM] $[ReO_4]$. To compensate for the anticipated loss of thermo-responsiveness due to high solubilities, the polarity of the anion could be matched with a lower hydrophilicity of the cation.

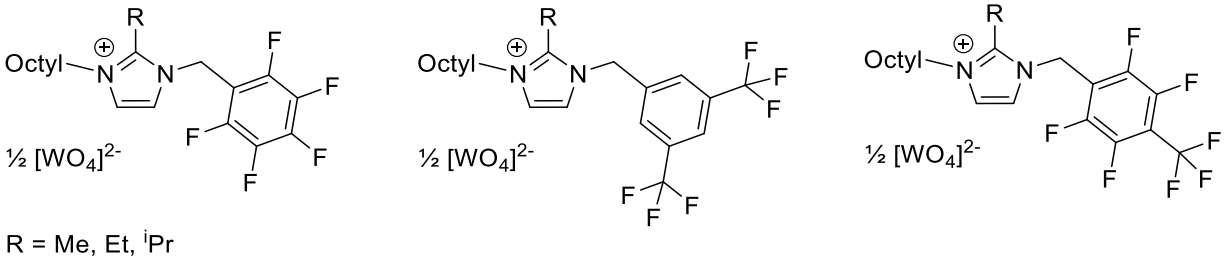

Figure 70: Proposed tungstate-based catalysts for a thermo-responsive micelle switching.

Here, an increase of the fluorine content by introduction of further fluorinated groups would be advantageous. Additionally, a decreased polarity could be achieved upon substitution of the imidazolium C2-H by an ethyl or even an isopropyl group (Figure 70).

Along the idea to replace the expensive perrhenate anion by abundant tungstate, supramolecular ions pairs (SIPs) could likewise be formed from the simple precursors tungstic acid, an organoamide and dihexylamine. Here, the tungstic acid is hardly soluble in aqueous media but an *in situ* formation of SIP assemblies and a consecutive transfer into the organic phase can be expected. Due to the structural similarity of tungstate and the herein investigated sulfate, a comparable SIP could form, despite the major difference of the active species (peroxomonosulfate vs. tetraperoxotungstate). The tungstate-based SIP could show tremendously high activities in the epoxidation of olefins in the organic phase; however, recycling would still be rather intricate. Hence, temperature-controlled catalyst precipitation as presented for the fluorinated imidazolium perrhenates would be favourable to separate the mixture into the components catalyst/water/epoxide. According to Neumann's strategy to create a temperature-sensitive catalyst by partial fluorination of the organic cations,[82] a fluorination of the SIP's dihexylammonium motif could likewise trigger a SIP precipitation upon cooling of the reaction mixture. To quantitatively recover the organoamide (benzamide or trimethylhexylamide), it should be covalently linked to the dihexylamine, else it would still be solubilized in solution and dissolve in the product phase. Due to the decomposition of the SIP receptor molecules under oxidative conditions, chemically more stable derivatives are required. The weak point, the amide-ammonium bridging methylene group hydrolyzes rapidly to formaldehyde, releasing the amide and the dihexylammonium sulfate. Hence, a chemically stable linker is required, which does not fundamentally change the constitution of the receptor. A simple ethylene bridge could fulfil this essential requirement and is synthetically easily introduced (Figure 71).

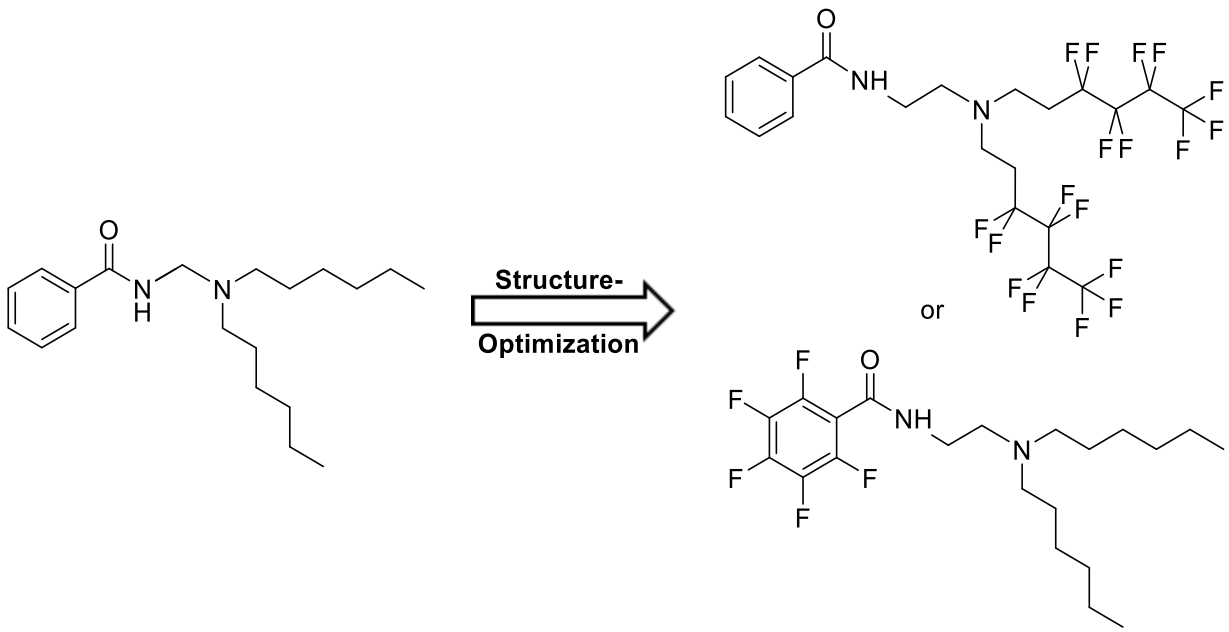

Figure 71: Proposed structure optimizations for the SIP receptor L^2 towards a promising temperature-controlled catalysis with SIPs.

In summary, supramolecular concepts have been exploited to design catalysts for the biphasic epoxidation of olefins with hydrogen peroxide. Supramolecular catalysis opens the field for novel catalytic approaches for the use of more atom-efficient and sustainable reactants, a contribution to a greener future of synthetic chemistry. The formed nano-sized assemblies interact with reactants of widely different polarities, the hydrophobic olefin as well as the polar oxidant hydrogen peroxide. According to the proposed principle to bring the reactants into contact in proximity of a catalytically active center, the micelles as well as the supramolecular ion pairs demonstrate unique reactivities beyond traditional homogeneous catalysis.

It could be demonstrated that the concept of the H-bond H_2O_2-activation by the perrhenate anion can perfectly be transferred to other element oxo-anions such as the simple and abundant nitrate anion as well as functionalized phosphate anions. Both anions have been considered inactive in catalysis and these are the first reports on their catalytic application. Moreover, it was shown comprehensively that the activation of hydrogen peroxide via H-bonds is dependent on the contribution of the organic cation. Hence, the close cation-anion contacts in the presented supramolecular assemblies are crucial for the use of hydrogen peroxide and explains the anion's inactivity in homogeneous solution or non-assembled states. The reactivities are not quite competitive with homogeneous epoxidation catalysts, but the perfect stability of imidazolium nitrates and imidazolium dihydrogenphosphate and their facile recyclability allow for applications in continuous processes.

For the most reactive catalysts, the micellar imidazolium tungstates, the influence of the cation and additives could be investigated thoroughly. Here, it was shown that the imidazolium cation

should ideally bear an aliphatic chain in the range of C_8 to C_{12}. Shorter derivatives lead to no or limited micellization, leaving the majority of the catalyst inactively homogeneously distributed in solution. This circumstance leads to a low overall reaction rate. The most important aspect of the olefin uptake and hence the micelle swelling is the combination of the cation and the anion. It has been shown that the micellar sizes and especially the sizes after saturation of the micelles with *cis*-cyclooctene is mostly influenced by the polarity of the anion. It must be concluded that the more polar the anions are, the larger the micellar swelling is. However, an influence of the aggregate size on the catalysis was not found as the micelles are in constant equilibrium with the supernatant substrate phase no phase transfer limitations are observed. The rection rate is therefore solely controlled by the anion's activity in H_2O_2-activation.

The micellar catalysts have been shown to be prone for a recycling procedure as they are stable and exclusively soluble in the aqueous phase, which can be obtained upon decantation of the supernatant organic phase. In this work, fundamental results for a large-scale application of micellar catalysts in biphasic media were gained. Here, a continuous process is prone for operation as the organic phase can continuously be withdrawn while the aqueous oxidant and catalyst phase is pumped in a loop. Steady addition of fresh oxidant is required, which in long term, dilutes the catalyst phase below its CMC. Hence, an energetically benign separation of the accumulation water must be conducted. Tailored imidazolium cations allow for a temperature-dependent switching of the catalyst solubility by structural introduction of a polyfluorinated substituent. This triggers catalyst precipitation upon cooling and hence allows for the separation of the catalytic mixture into the single components product, water and catalyst, which is highly attractive for application in a continuous process.

5 Experimental Section

5.1 General Information

All commercially available chemicals were purchased from the chemical suppliers abcr, Acros Organics, Sigma-Aldrich, TCI, VWR and, if not stated otherwise, used without further purification. Technical solvents were received from the central chemical store of the TUM faculty of chemistry and distilled prior to use. Dry solvents were obtained from a MBraun Solvent Purification System and stored over molecular sieves 3 Å under an argon atmosphere.

5.2 Analytical Methods

Dynamic Light Scattering

DLS measurements were performed on a Malvern Zetasizer Nano instrument using 10 mm quartz cuvettes in 173° angle backscattering mode. The compound is dissolved in 1.4 mL of the respective solvent and filtered into the cuvette through a 200 nm PTFE syringe filter. The cuvette is placed in the instrument and equilibrated at the desired temperature for 10 minutes prior to the measurement. Twelve measurement runs were averaged for one experiment to avoid statistical errors. The general-purpose method of the Malvern Zetasizer software is used for data analysis. In some experiments investigating the micelle-substrate interaction, 1.3 mL of cis-cyclooctene were added to form an organic overlayer. The biphasic system is shaken and allowed to separate prior to the measurement procedure. Then, the aqueous phase is used for the DLS investigation according to the standard protocol.

The dynamic viscosity of 50 wt.% H_2O_2 at 20 °C (1.17 mPas) and 80 °C (0.485 mPas) were determined with a Ubbelohde capillary viscosimeter, temperature-adjusted in a water bath.

Elemental Analysis

Elemental Analysis (determination of C, H, N and S) were conducted by Ulrike Ammari from the microanalytic laboratory of the Catalysis Research Center on a HEKAtech Euroanalysis instrument by flash combustion and subsequent chromatographic separation with an accuracy of <0.6% mass fraction. 1.5-2.5 mg of the sample are crimped into a tin foil under argon

atmosphere and stored in an air-tight screw neck glass vial. For the measurement, it is transferred rapidly into the sample injector.

The elements Re and W were determined by decomposition of 10-20 mg of the analyte by boiling in nitric acid. The solutions are then diluted with pure water and the anion concentration (perrhenate or tungstate) determined photometrically using a multi-point calibration curve.

Nuclear Magnetic Resonance Spectroscopy

NMR spectroscopy was performed on the Bruker instruments DRX 400, AVANCE-III 400-US, AVANCE Neo 400 at 400 MHz (^{1}H) and AVANCE 500-Cryo at 500 MHz (^{1}H). The sample is transferred into a 5 mm Deutero NMR tube und diluted with 500 µL of the respective solvent. Variable temperature experiments were performed on the Bruker DRX 400 exclusively and the sample allowed to equilibrate at the respective temperature for at least ten minutes.

Chemical shifts in [ppm] are reported relative to tetramethylsilane for ^{1}H and ^{13}C, 15% $BF_3{\cdot}OEt_2$ in $CDCl_3$ for ^{11}B, 85% H_3PO_4 for ^{31}P, $CFCl_3$ for ^{19}F and 2 M aq. Na_2WO_4 for ^{183}W detection. Data processing was performed using the MestreNova 12 software after baseline correction and FID apodization. The spectra were calibrated to the solvent proton and carbon signal.[229] Signal multiplicities were abbreviated as follows: s – singlet, d – duplet, t – triplet, q – quartet and p – pentet. For the standard experiments, the following number of scans were acquisitioned: ^{1}H – 16 scans, ^{11}B – 128 scans, ^{13}C – 1024 scans, ^{19}F – 16 scans, ^{31}P – 16 scans, ^{33}S – 8192 scans, ^{183}W – 4096 to 16.384 scans.

^{13}C and ^{31}P NMR experiments were recorded with ^{1}H decoupling.

Cryo-Transmission Electron Microscopy

Cryo-TEM measurements were carried out by Dr. Carsten Peters with a Jeol 1400 plus microscope at 120 kV equipped with a Ruby CCD detector. Blotting of the samples was performed with a FEI Vitrobot MK3 at 50 °C and >80% humidity on Quantifoil 1.2/1.3 grids (Cu 300 mesh). For this, a solution of the sample (3 µL) was deposited onto a TEM grid and blotted with two pieces of filter paper for approximately 4 s to form a solution thin film. Then, the grid was quickly dipped into a reservoir of liquid ethane (cooled by liquid nitrogen) and kept under liquid nitrogen until the transfer of the grid to a cryogenic sample holder.

Electrospray Ionisation Mass Spectrometry

ESI-MS measurements were performed on a Varian 500 LC/MS ion trap spectrometer using deionized water or 50 wt.% aqueous H_2O_2 as carrier at 20 µL/min solvent flow with ionisation at 50 °C in vacuo. The measurements were recorded after injection of 0.1 mL of the sample and averaged for a period of 30 seconds after the first substance detection.

Thermogravimetric Analysis coupled with Differential Scanning Calorimetry

The stability and melting point of the solid imidazolium catalysts is determined exploiting TGA-DSC by the measurement of the loss of weight and the temperature of melting enthalpy heat flow maximum, respectively. Approximately 4-5 mg of the sample is transferred into 5 mm aluminum oxide crucible under argon atmosphere and stored in air-tight screw neck vial until measurement. The crucible containing the sample is rapidly transferred into the Netzsch STA449 F5 Jupiter instrument and purged with an argon flow of 20 mL/min. The temperature is equilibrated at 30 °C for ten minutes until a heating ramp of 10 °C/min is applied till 800 °C. The heat flow to the sample is referenced to an empty crucible. The melting point is determined by the onset point of the respective DSC signal.

Tensiometry and Conductometry

Tensiometry and conductivity measurements were performed by Bastian Zehner, University of Bayreuth, chair of chemical engineering. Surface tensions were measured with a Krüss K11 tensiometer according to the Wilhelmy plate method with an accuracy of 0.01 N/m². For accurate determination of the surface tension, instead of platinum, 18 × 18 mm glass plates were used to avoid hydrogen peroxide decomposition. Prior to the measurements, the plates were washed with isopropyl alcohol and flame treated. Glass vessels were cleaned with water, acetone, and dichloromethane. Temperature adjustments were performed using an aluminum jacket with two electric heating cartridges.

Conductivity measurements were performed with a Metrohm 712 conductometer with a modified tin probe to avoid decomposition of hydrogen peroxide. The tin foil (99.99% purity) was cut to two 8 × 8 mm square plates and the cell constant of the electrode was determined by calibration with a 0.01 mol/L to 1.00 mol/L aqueous potassium chloride solution. The temperature of the sample was adjusted using a laboratory heater and measured by a PT100 thermo couple surrounded by a glass tube.

Gas Chromatography – Flame Ionization Detection

Cyclooctene and cyclooctene oxide concentrations were quantified on an *Agilent Technologies 7890B GC* System with a 30 m *HP-5 Ultra Inert* column and a flame ionization detector (FID) and referenced to the internal standard mesitylene. A seven-point calibration curve for both analytes *cis*-cyclooctene and cyclooctene oxide, referenced to mesitylene, was established. 1 µL of the analyte is injected into the liner pre-heated to 300 °C, vaporizing all components in a helium 5.0 flow of 25 mL/min using a split of 25:1. The column is initially heated to 70 °C, followed by a temperature ramp of 10 °C/min after sample injection. At 120 °C the ramp is increased to 15 °C/min and thereon to 50 °C/min after 150 °C reaching the final temperature of 270 °C. The eluated flow is injected into the FID detector burning 40 mL/min H_2 with 400 mL/min air.

Infrared Spectroscopy

Infrared spectroscopy was performed by Prof. János Mink on a Varian FTS-7000 infrared spectrometer equipped with a deuterated triglycine sulfate detector. Solids samples were recorded with a Varian FTS-2000 spectrometer, using a GladiATR diamond setup and a liquid nitrogen cooled mercury-cadmium-telluride detector. The spectra were ATR corrected and averaged from 256 scans with a resolution of 4 cm^{-1}.

Single-Crystal X-Ray Diffraction

SCXRD and consecutive structure refinement was performed by Stefan Burger. Single crystal X-Ray diffraction intensity data were collected on a *Bruker* “D8 Venture Duo IMS” diffractometer equipped with a IMS microsource anode for fine-focus with Mo-K_α radiation source (λ = 0.71073 Å), a CMOS plate detector (*Bruker* APEX III, κ-CMOS), a Helios optic monochromator and an Oxford Cryosystems cooling device by using the APEX3 software package.[230] Appropriate crystals were prepared and selected in perfluorinated ether oil, fixed on top of a *MiTeGen* Dual Thickness MicroMount sample holder, transferred to the diffractometer and frozen under a stream of cold nitrogen. A matrix scan (2 × 12) was used to determine the initial lattice parameters. Reflections were merged and corrected for Lorentz and polarization effects, scan speed, and background using SAINT.[231] Absorption corrections, including odd and even ordered spherical harmonics were performed using SADABS.[232] Space group assignments were based upon systematic absences, E-statistics, and successful refinement of the structures. Data reduction was performed with APEX3 and structure solution and refinement was performed by using SHELXL as integrated in Olex2.[233][234][235] Structures

were solved by direct methods with the aid of successive difference Fourier maps, and were refined against all data. Hydrogen atoms were placed in calculated positions and refined using a riding model. Non-hydrogen atoms were refined with anisotropic displacement parameters. Full-matrix least-squares refinements were carried out by minimizing $\Sigma w(F_o^2 F_c^2)^2$ with the SHELXL weighting scheme.[233] The images of the crystal structures were generated using VESTA 3.4.0.[236]

Manganometric Determination of Hydrogen Peroxide Concentration

A solutions of hydrogen peroxide in water (50 wt.%) were stirred for a determined time at a respective temperature. A 0.4 mL aliquot of the H_2O_2 solution was taken and diluted with 50 mL H_2O and acidified with 1 mL conc. H_2SO_4. Then, a 0.05 M $KMnO_4$ solution was added dropwise till a pinkish color remained for ten seconds. The volumetric consumption of the permanganate solution allows for the calculation of the hydrogen peroxide concentration and the respective decomposition.

5.3 Catalytic Investigations

5.3.1 Kinetic Investigations of Micellar Catalysts

In a standard experiment, 0.5 mmol of the catalyst are weighed into a 20 mL screw neck glass vial equipped under argon atmosphere and is dissolved therein in 1.40 mL H_2O_2 (50 wt.% aqueous solution, 25 mmol). A 20 mm PTFE stirring bar and 69 µL mesitylene is added as internal standard to the solution and heated to reaction temperature under stirring at 500 min^{-1} in a tight-fitting temperature-adjusted metal vial holder after closing with a PTFE sealed PP screw cap. Within two minutes, 1.36 mL *cis*-cyclooctene (10 mmol, 95% purity and 5% cyclooctane content) is added, starting the reaction. 10 µL aliquots of the organic phase were taken from the supernatant organic layer after distinct times, diluted in 500 mL $CDCl_3$ and conversion of COE and yield of COO determined by ^{1}H-NMR spectroscopy in reference to the mesitylene signal.

5.3.2 Kinetic Investigations of SIP Catalysts

In a standard experiment, the SIP catalysts or the component thereof were dissolved in 272 µL of COE (2.0 mml, 95% purity and 5% cyclooctane content) and stirred at 750 min^{-1} at 80 °C for 5 minutes in a 1.5 mL PTFE-sealed crimp vial equipped with an 8 mm stirring bar in a tight-

fitting metal vial holder. Then, 281 µL H_2O_2 (50 wt.% aqueous solution, 5.0 mmol) are added, starting the reaction. After one minute equilibration, a 9.0 µL aliquot is taken from the top organic phase and diluted in 4.0 mL toluene containing 1 mg/mL mesitylene as standard. 1.5 mL thereof are transferred into a 1.5 mL GC vial and measured by GC-FID according to the standard seven-point calibrated method. This run used as zero-point for the further data point taken similarly after distinct times. Conversions of COE and yields of COE were determined by integration of the FID signal at the compound-specific retention times and referenced to the mesitylene peak area.

5.4 Synthesis Procedures

5.4.1 Synthesis of Ionic Liquid Precursors

1-Octylimidazole

1-Octylimidazole was synthesized according to a literature protocol.[237] 10 g imidazole (147 mmol, 1.0 eq.) were dissolved in 50 mL THF and 13 g 50 wt% aq. NaOH (162 mmol, 1.1 eq.) were added. The solution is stirred under reflux for three days. Subsequently, 100 mL water was added and the aqueous phase extracted with DCM (3 × 50 mL). Evaporation of the solvent in vacuo yields a yellow oil which was further purified by vacuum distillation ($5*10^{-3}$ mbar) to yield 16.7 g of the product as a colorless liquid (93 mmol, 64%).

^{1}H-NMR (400 MHz, chloroform-d, 298 K) δ [ppm]: 7.39 (d, *J* = 1.2 Hz, 1H), 6.99 (d, *J* = 1.2 Hz, 1H), 6.84 (t, *J* = 1.2 Hz, 1H), 3.86 (t, *J* = 7.1 Hz, 2H), 1.70 (p, *J* = 6.9 Hz, *J* = 7.1Hz, 2H), 1.29 – 1.17 (m, 10H), 0.82 (t, *J* = 6.9 Hz, 3H).
^{13}C{^{1}H}-NMR (101 MHz, chloroform-d, 298 K) δ [ppm]: 137.02, 129.29, 118.74, 46.98, 31.67, 31.05, 29.05, 28.99, 26.50, 22.56, 14.02.

1-Octyl-2-methylimidazole

1-Octyl-2-methylimidazole was synthesized according to an adapted literature protocol.[237] 20 g 2-methylimidazole (244 mmol, 1.0 eq.) were dissolved in 150 mL THF and 23.4 g 50 wt% aq. NaOH (292 mmol, 1.2 eq.) were added. The solution is stirred under reflux for three days. Subsequently, 150 mL water was added and the aqueous phase extracted with DCM (2 × 100 mL). Evaporation of the solvent in vacuo yields a yellow oil which was further purified by vacuum distillation ($2*10^{-3}$ mbar) to yield 39.9 g of the product as a colorless liquid (205 mmol, 84%).

^{1}H-NMR (400 MHz, chloroform-d, 298 K) δ [ppm]: 6.87 (d, *J* = 1.3 Hz, 1H), 6.78 (d, *J* = 1.3 Hz, 1H), 3.86 – 3.70 (m, 2H), 2.34 (s, 3H), 1.68 (pseudo-p, *J* = 6.9 Hz, 1H), 1.30 – 1.18 (m, 10H), 0.85 (t, *J* = 7.0 Hz, 3H).
^{13}C{^{1}H}-NMR (101 MHz, chloroform-d, 298 K) δ [ppm]: 144.28, 126.96, 119.00, 46.04, 31.71, 30.75, 29.10 (s, 2C), 26.58, 22.58, 14.04, 13.04.

Diethylmethylphosphate

Diethylmethylphosphate was synthesized according to a literature procedure.[238] 4.7 mL diethylphosphite (5.0 g, 36.2 mmol) were mixed with 4.4 mL methanol (3.5 g, 109 mmol, 3.0 eq.) and 0.92 g iodine (3.6 mmol, 0.1 eq.). Under cooling to room temperature using a water bath, 2.3 mL 50 wt.% H_2O_2 (40 mmol, 1.1 eq.) were added dropwise over a period of 30 min and the mixture stirred for 4 h. After addition of 0.5 g sodium thiosulfate, the solvent was evaporated in vacuo and the residue distilled under vacuum (35 °C, $5*10^{-3}$ mbar, yielding in 3.81g (22.7 mmol, 63%) of a colorless liquid.

^{1}H-NMR (400 MHz, chloroform-d, 298 K) δ [ppm]: 4.08 (dq, J_{P-H} = 8.0 Hz, *J* = 7.1 Hz, 4H), 3.72 (d, J_{P-H} = 11.1 Hz, 3H), 1.30 (t, *J* = 7.1 Hz, 6H).
^{31}P{^{1}H}-NMR (162 MHz, chloroform-d, 298 K) δ [ppm]: 0.17.

Di*iso*propylmethylphosphate

Di*iso*propylmethylphosphate was synthesized according to an adapted literature procedure.[238] 5.0 mL diethylphosphite (5.0 g, 30.1 mmol) were mixed with 3.56 mL methanol (2.89 g, 90.3 mmol, 3.0 eq.) and 0.76 g iodine (3.0 mmol, 0.1 eq.). Under cooling to room temperature using a water bath, 1.9 mL 50 wt.% H_2O_2 (33 mmol, 1.1 eq.) were added dropwise over a period of 30 min and the mixture stirred for 4 h. After addition of 0.5 g sodium thiosulfate, the solvent was evaporated in vacuo and the residue distilled under vacuum (40 °C, $3*10^{-3}$ mbar, yielding in 2.69 g (13.7 mmol, 46%) of a colorless liquid.

^{1}H-NMR (400 MHz, chloroform-d, 298 K) δ [ppm]: 4.62 (dq, J_{P-H} = 12.7, *J* = 6.3 Hz, 1H), 3.71 (d, J_{P-H} = 11.2 Hz, 3H), 1.32 (d, *J* = 6.3 Hz, 6H).
^{31}P{^{1}H}-NMR (162 MHz, chloroform-d, 298 K) δ [ppm]: -1.53.

Diphenylphosphoric acid

To a solution of 2.0 g phenol (21.3 mmol, 2.0 eq.) and 1.7 mL pyridine (1.68 g, 21.3 mmol, 2.0 eq.) in 10 mL dry toluene, 0.97 mL phosphoryl chloride (1.63 g, 10.6 mmol, 1.0 eq.) are added dropwise under argon atmosphere at room temperature. The solution is stirred overnight at 80 °C and subsequently 20 mL water are added to the formed suspension. The

solid is filtered off and the organic phase is separated and washed with 1 M HCl (3 × 20 mL). The solution is dried over anhydrous Na_2SO_4 and the solvent is removed in vacuo, yielding 0.97 g of the product as a slightly yellowish solid (3.87 mmol, 36%).

^{1}H-NMR (400 MHz, D_2O, 298 K) δ [ppm]: 7.39 (dd, *J* = 7.9, 7.9 Hz, 4H), 7.25 – 7.16 (m, 6H).
^{31}P{^{1}H}-NMR (162 MHz, D_2O, 298 K) δ [ppm]: -8.83.

Di-(*p*-methoxyphenyl)phosphoric acid

To a solution of 2.0 g 4-methoxyphenol (16.1 mmol, 2.0 eq.) and 1.3 mL pyridine (1.27 g, 16.1 mmol, 2.0 eq.) in 10 mL dry toluene, 0.74 mL phosphoryl chloride (1.24 g, 8.1 mmol, 1.0 eq.) are added dropwise under argon atmosphere at room temperature. The solution is stirred overnight at 80 °C and subsequently 20 mL water added to the formed suspension. The solid is filtered off and the organic phase is separated and washed with 1 M HCl (3 × 20 mL). The solution is dried over anhydrous Na_2SO_4 and the solvent is removed in vacuo. After purification by column chromatography over silica (Et_2O, 12×5 cm), 1.95 g of the product were obtained as a white solid (6.3 mmol, 78%).

^{1}H-NMR (400 MHz, chloroform-d, 298 K) δ [ppm]: 7.22 (dd, *J* = 9.0, 1.8 Hz, 4H), 6.89 (dd, *J* = 9.2, 0.9 Hz, 4H), 3.81 (s, 6H).
^{31}P{^{1}H}-NMR (162 MHz, chloroform-d, 298 K) δ [ppm]: -3.73.

(*rac*)-1,1'-Binaphthyl-2,2'-diylphosphoric acid

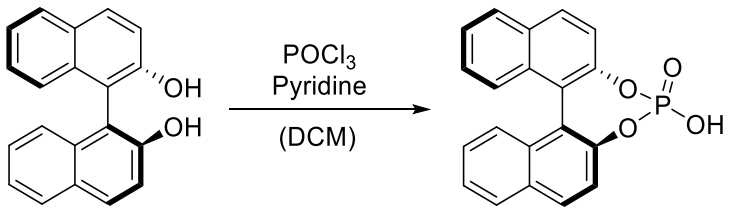

This compound was synthesized according to a modified literature procedure.[239]
1.0 g (*rac*)-1,1'-bi-2,2'-naphtol (3.49 mmol, 1.0 eq.) were filled in a 25 mL Schlenk flask and purged with argon. Then, 3 mL of pyridine and 5 mL of DCM were added and the resulting solution cooled to 0 °C using an ice bath. Under vigorous stirring, 400 µL phosphoryl chloride (0.67 g, 4.37 mmol, 1.25 eq.) were added dropwise. Then, the mixture is heated to reflux for three hours. All volatiles are removed in vacuo and the white residue is dissolved in 50 mL 0.5 M sodium carbonate solution. 0.5 g activated carbon are added and stirred under gentle boiling of the dispersion. The mixture is hot filtrated using filter paper to remove the activated carbon. The obtained colorless solution is cooled to 0 °C and slowly acidified to pH = 0 with concentrated hydrochloric acid. After stirring overnight, the white precipitate was filtered off

and dried in a vacuum to yield 287 mg (0.82 mmol, 23%) of the desired product as a white powder.

^{1}H-NMR (400 MHz, DMSO-d_6, 298 K) δ [ppm]: 8.16 – 8.04 (m, 4H), 7.58 – 7.45 (m, 4H), 7.35 (ddd, *J* = 8.4, 6.7, 1.4 Hz, 2H), 7.23 (d, *J* = 8.5 Hz, 2H).
^{31}P{^{1}H}-NMR (162 MHz, DMSO-d_6, 298 K) δ [ppm]: 3.59.

1,2-Phenylenephosphoric acid

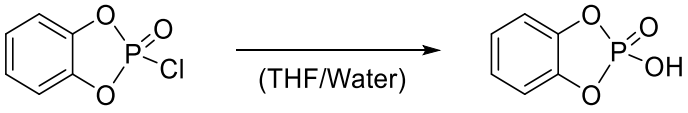

1.0 g 1,2-Phenylene chlorophosphate (5.3 mmol) is dissolved in 20 mL of a THF/water mixture (3:1) and stirred at room temperature for three days. Then, the THF is removed in vacuo and 30 mL 1M hydrochloric acid added. The product 1,2-phenylene phosphoric acid is extracted with DCM (3 × 10 mL) and obtained in 84% yield (761 mg, 4.4 mmol) as a grey powder after solvent evaporation.

^{1}H-NMR (400 MHz, DMSO-d_6, 298 K) δ [ppm]: 7.08 (ddd, *J* = 5.9, 3.5, 1.3 Hz, 2H), 6.97 (dd, *J* = 5.9, 3.4 Hz, 2H).

^{31}P{^{1}H}-NMR (162 MHz, DMSO-d_6, 298 K) δ [ppm]: -4.50 (s).

5.4.2 Synthesis of Phosphonate Additives

Diethyl-*p*-fluorophenylphosphonate

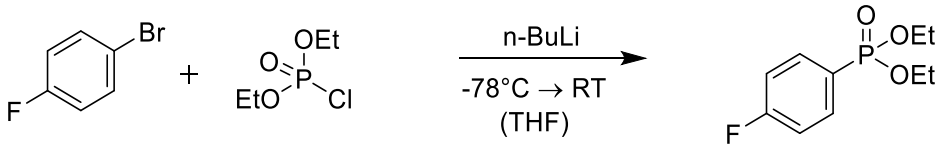

This compound was synthesized according to an adapted literature procedure.[240] (8.00 g 1-bromo-4-fluorobenzene (46 mmol, 1.0 eq.) dissolved in 250 mL anhydrous THF are cooled to -78 °C in a acetone/dry ice bath. Under vigorous stirring, 22.9 mL n-butyllithium (2.2 M, 3.22 g, 50 mmol, 1.1 eq.) are added dropwise. After ten minutes, 6.63 mL diethylchlorophosphate (7.89 g, 46 mmol, 1.0 eq.) are added carefully within one hour under vigorous stirring. Then, the mixture is slowly heated to room temperature and 100 mL diethylether and 100 mL water containing 1 g $NaHCO_3$ is added. The organic phase is

separated and concentrated resulting in an orange oil. Purification by column chromatography (silica, EtOAc:hexane = 1:1, 10 × 10 cm) results in 8.30 g diethyl-p-tolylphosphate (78%, 36 mmol) as a colorless crystalline solid.

R_f = 0.20 (EtOAc:hexane = 1:1, [UV])

^{1}H-NMR (400 MHz, $CDCl_3$, 298 K) δ [ppm]: 7.89 – 7.77 (m, 1H), 7.71 – 7.59 (m, 1H), 7.23 – 7.11 (m, 2H), 4.23 – 4.01 (m, 4H), 1.34 (qd, *J* = 7.0, 0.8 Hz, 6H).

^{19}F-NMR (376 MHz, $CDCl_3$, 298 K) δ [ppm]: −106.1 (s).

^{31}P{^{1}H}-NMR (162 MHz, $CDCl_3$, 298 K) δ [ppm]: 17.8 (s).

Diethyl-*p*-tolylphosphonate

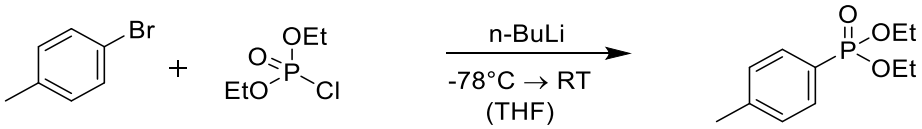

This compound was synthesized according to a literature procedure.[240] 7.50 g 1-bromo-4-methylbenzene (44 mmol, 1.0 eq.) dissolved in 250 mL anhydrous THF are cooled to -78 °C in a acetone/dry ice bath. Under stirring, 21.9 mL *n*-butyllithium (2.2 M, 3.09 g, 48 mmol, 1.1 eq.) are added dropwise. After ten minutes, 6.36 mL diethylchlorophosphate (7.57 g, 44 mmol, 1.0 eq.) are added carefully within one hour under vigorous stirring. Then, the mixture is slowly heated to room temperature and 100 mL diethylether and 100 mL water containing 1 g $NaHCO_3$ is added. The organic phase is separated and concentrated resulting in an orange oil. Purification by column chromatography (silica, EtOAc:hexane = 1:1, 12 × 10 cm) results in 4.60 g diethyl-p-tolylphosphate (46%, 20 mmol) as a colorless liquid.

R_f = 0.25 (EtOAc:hexane = 1:1, [UV])

^{1}H-NMR (400 MHz, $CDCl_3$, 298 K) δ [ppm]: 7.72 (dd, *J* = 13.2, 7.90 Hz, 2H), 7.34 – 7.21 (m, 2H), 4.27-3.94 (m, 4H), 2.42 (s, 3H), 1.33 (t, *J* = 7.05 Hz, 6H).

^{31}P{^{1}H}-NMR (162 MHz, $CDCl_3$, 298 K) δ [ppm]: 19.6 (s).

_p_-Fluorophenylphosphonic acid

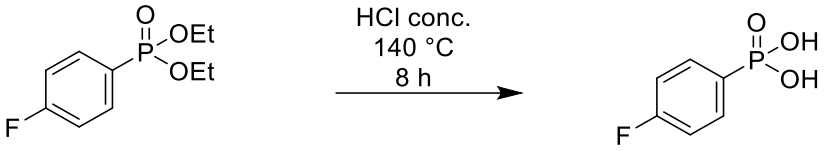

p-Fluorophenylphosphonic acid was synthesized according to an adapted literature procedure.[241]

8.3 g diethyl-*p*-fluorophenylphosphonate (35.8 mmol) was suspended in 50 mL conc. HCl and stirred under reflux for 8 h. Afterwards, the solution was washed with dichloromethane (2 × 50 mL) and the aqueous phase concentrated in vacuo and diluted with 3 × 10 mL H_2O, resulting in 4.29 g (24.4 mmol) *p*-fluorophenylphosphonic acid in 68% yield.

^{1}H-NMR (400 MHz, D_2O, 298 K) δ [ppm]: 7.08 (m, 2H), 7.62 (m, 2H).

^{13}C{^{1}H}-NMR (101 MHz, D_2O, 298 K) δ [ppm]: 115.70 (dd, $J_{C\text{-}F}$ = 21.6, 16.1 Hz), 126.86 (d, $J_{C\text{-}F}$ = 185.7 Hz), 133.07 (t, J = 10.6 Hz), 164.78 (d, $J_{C\text{-}F}$ = 251.5 Hz).

^{19}F-NMR (376 MHz, D_2O, 298 K) δ [ppm]: −107.8 (s).

^{31}P{^{1}H}-NMR (162 MHz, D_2O, 298 K) δ [ppm]: 15.9 (s).

_p_-Tolylphosphonic acid

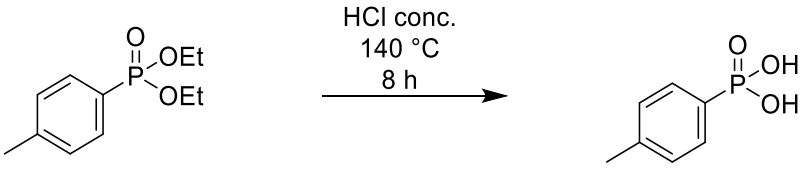

p-Tolylphosphonic acid was synthesized according to an adapted literature procedure.[241]

1.5 g diethyl-*p*-tolylphosphonate (6.57 mmol) was suspended in 10 mL conc. HCl and stirred under reflux for 8 h. Afterwards, the solution was washed with dichloromethane (2 × 10 mL) and the aqueous phase was concentrated in vacuo and diluted with 3 x 2 mL H_2O, resulting in 950 mg (5.52 mmol) *p*-tolylphosphonic acid in 84% yield.

^{1}H-NMR (400 MHz, D_2O, 298 K) δ [ppm]: 2.26 (s, 1H), 7.24 (dd, J = 8.0, 3.7 Hz, 1H), 7.54 (dd, J = 13.2, 8.1 Hz, 1H).

^{13}C{^{1}H}-NMR (101 MHz, D_2O, 298 K) δ [ppm]: 20.58 (s), 127.85 (d, J = 184.3 Hz), 129.19 (d, J = 15.1 Hz), 130.44 (d, J = 10.7 Hz), 142.95 (s).

^{31}P{^{1}H}-NMR (162 MHz, D_2O, 298 K) δ [ppm]: 17.0 (s).

Diethyl (4-bromomethyl)phenylphosphonate

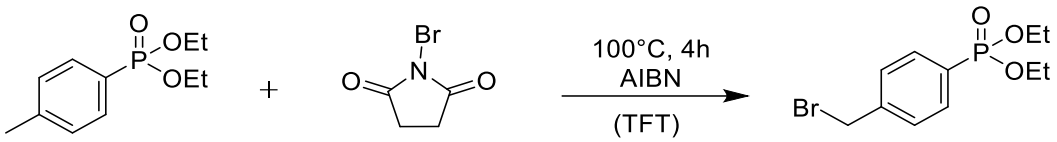

Diethyl (4-bromomethyl)phenylphosphonate was synthesized according to an adapted literature procedure.[240] 3.00 diethyl p-tolylphosphonate (13.1 mmol, 1.0 eq.), 2.57 g freshly recrystallized N-bromosuccinimide (14.5 mmol, 1.1 eq.) and 86 mg azoisobutyronitrile (AIBN, 0.53 mmol, 4 mol-%) are suspended in 50 mL α,α,α-trifluorotoluene and refluxed at 100 °C for 4 hours. The mixture is then cooled to 0 °C and the precipitated succinimide filtered off. The filtrate is washed with 50 mL water, 50 mL brine and dried over anhydrous Na_2SO_4. The solvent is evaporated in vacuo and the residue is purified by column chromatography (silica, EtOAc:hexane = 1:2, 15 ×8 cm). The product is obtained as a colorless oil in 78% yield (3.15 g, 10.3 mmol).

^{1}H-NMR (400 MHz, $CDCl_3$, 298 K) δ [ppm]: 7.71 (dd, *J* = 13.1, 8.0 Hz, 2H), 7.40 – 7.13 (m, 2H), 4.49 – 3.73 (m, 4H), 2.41 (s, 2H), 1.63 – 1.14 (m, 6H).

^{31}P{^{1}H}-NMR (162 MHz, $CDCl_3$, 298 K) δ [ppm]: 19.6 (s).

Diethyl 2-bromoethylphosphonate

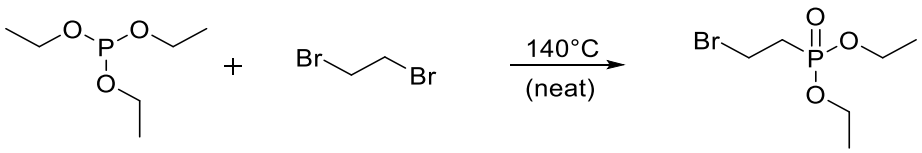

This synthesis was carried out according to a literature protocol.[242] 11.5 mL triethylphosphite (11.1 g, 66.5 mmol, 1.0 eq.) and 23.0 mL 1,2-dibromoethane (50.0 g, 266 mmol, 4.0 eq.) are heated to 140 °C under vigorous stirring for three hours. The evolving bromoethane is continuously distilled off. Then, residual dibromoethane product are separated by fractional distillation under fine vacuum, yielding 10.9 g diethyl 2-bromoethylphosphonate (67%, 45.0 mmol) as a colorless liquid.

^{1}H-NMR (400 MHz, $CDCl_3$, 298 K) δ [ppm]: 4.16 – 3.98 (m, 4H), 3.53 – 3.42 (m, 2H), 2.40 – 2.26 (m, 2H), 1.28 (t, *J* = 7.1 Hz, 6H).

^{31}P{^{1}H}-NMR (162 MHz, $CDCl_3$, 298 K) δ [ppm]: 25.5 (s).

Synthesis of Zwitterion-1[128]

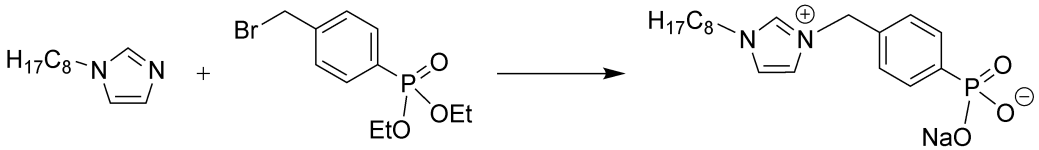

Zwitterion **1**

1.54 mL 1-octylimidazole (1.40 g, 7.75 mmol, 1.0 eq.) and 2.38 g diethyl-4-bromomethyl-phenylphosphonate (7.75 mmol, 1.0 eq.) were slowly heated to 100 °C from 0 °C within 2 h and then all volatiles removed under reduced pressure at 100 °C for 4 h. Afterwards, 10 mL 48 wt.% aq. HBr was added and stirred for 4 h under reflux. After cooling to room temperature, HBr is evaporated and the residue dissolved in 20 mL water. The solution is neutralised with aq. Na_2CO_3. The water was removed and the residue extracted with 30 mL MeOH/EtOAc (1:1 mixture). The crude product was purified by column chromatography (silica gel 60, MeOH/EtOAc 1:1 → MeOH, 3 × 10 cm). Halide-free fractions (tested with aq. $AgNO_3$) were combined and the solvent evaporated, resulting in 1.79 g (62% yield) of zwitterion-**1**.

^{1}H-NMR (400 MHz, D_2O, 298 K) δ [ppm]: 0.80–0.88 (m, 3H), 1.20–1.30 (m, 10H), 1.84 (t, *J* = 7.1 Hz, 2H), 4.15 (t, *J* = 7.1 Hz, 2H), 5.37 (s, 2H), 7.34 (d, J = 2.4 Hz, 1H), 7.36 (d, *J* = 2.6 Hz, 1H), 7.48 (q, *J* = 2.1 Hz, 2H), 7.69–7.78 (m, 2H). 8.84 (s, 1H).

^{13}C{^{1}H}-NMR (101 MHz, D_2O, 298 K) δ [ppm]: 13.42, 21.97, 25.27, 27.97, 28.18, 29.09, 30.97, 49.67, 52.55, 122.55, 122.59, 127.98 (d, $J_{C–P}$ = 13.9 Hz), 131.06 (d, $J_{C–P}$ = 9.8 Hz), 135.20 (d, $J_{C–P}$ = 3.1 Hz), 135.39, 137.78 (d, $J_{C–P}$ = 174.4 Hz).

^{31}P{^{1}H}-NMR (162 MHz, D_2O, 298 K) δ [ppm]: 10.33 (s).

ESI-MS (negative mode, H_2O): measured: 349.6 m/z; calculated: [**1**−Na]$^-$ = 349.2 m/z.

Synthesis of Zwitterion-2[128]

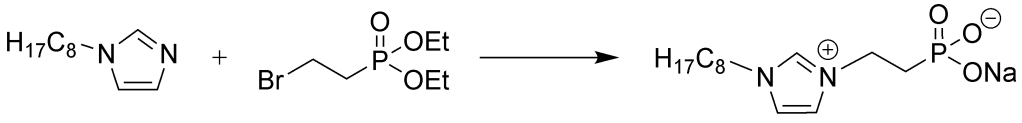

Zwitterion **2**

3.00 mL 1-octylimidazole (2.72 g, 11.1 mmol, 1.0 eq.) and 2.00 g diethyl-2-bromoethyl-phosphonate (11.1 mmol, 1.0 eq.) were heated to 50 °C for 24 h and then all volatiles removed at 60 °C for 4 h using a turbomolecular pump. Afterwards, 10 mL 48% aq. HBr was added and stirred for 4 h under reflux. After cooling to room temperature, HBr was evaporated, and the residue dissolved in 20 mL water. The solution was neutralized with aq. Na_2CO_3. The water was removed, and the residue extracted with 30 mL MeOH/EtOAc 1:1. The crude product was purified by column chromatography (silica gel 60, MeOH, 3 × 10 cm). Halide-free fractions

(tested with aq. $AgNO_3$) were combined and the solvent evaporated, resulting in 1.00 g (30 % yield) of zwitterion-**2**.

^{1}H-NMR (400 MHz, D_2O, 298 K) δ [ppm]: 0.72 – 0.79 (m, 3H), 1.13 – 1.24 (m, 10H), 1.78 (q, J = 7.1 Hz, 2H), 1.96 – 2.09 (m, 2H), 4.09 (t, J = 7.1 Hz, 2H), 4.21 – 4.32 (m, 2H), 7.37 (t, J = 1.9 Hz, 1H), 7.44 (t, J = 1.9 Hz, 1H), 8.72 (s, 1H).

^{13}C{^{1}H}-NMR (101 MHz, D_2O, 298 K) δ [ppm]: 13.33, 21.92, 25.24, 27.94, 28.12, 29.06, 29.80 (d, J = 127.9 Hz), 30.93, 45.94, 49.58, 122.11, 122.22, 135.09.

^{31}P{^{1}H}-NMR (162 MHz, D_2O, 298 K) δ [ppm]: 16.41.

ESI-MS (negative mode, H_2O): Measured: 287.3 m/z; calculated: [**2**−Na]$^-$ = 287.2 m/z.

Ethylphosphonic acid

2.5 g Diethyl ethylphosphonate (15.1 mmol, 1.0 eq.) are dissolved in 5 mL concentrated hydrochloric acid and stirred for 24 h at 100 °C. Then, the product is extracted with ethyl ether (3 × 10 mL) and dried over anhydrous Na_2SO_4. The solvent is evaporated in vacuo, yielding 1.32 g ethylphosphonic acid (80%, 12.0 mmol) as a slightly brownish discolored oil.

^{1}H-NMR (400 MHz, D_2O, 298 K) δ [ppm]: 1.66 (dq, $J_{P\text{-}H}$ = 17.8 Hz, J = 7.7 Hz, 2H), 1.01 (dt, $J_{P\text{-}H}$ = 20.3 Hz, J = 7.7 Hz, 3H).

^{31}P{^{1}H}-NMR (162 MHz, D_2O, 298 K) δ [ppm]: 33.65.

Octylphosphonic acid

This synthesis was carried out according to a literature protocol.[243] 4.46 mL 1-bromooctane (5.00 g, 25.9 mmol, 1.0 eq.) and 4.48 mL triethylphosphite (4.30 g, 25.9 mmol, 1.0 eq.) are stirred at 110 °C for 24 hours with the forming bromoethane continuously distilled off into another vessel connected via a hose. The residue is then distilled under fine vacuum to give 4.7 g diethyl octylphosphonate as a colorless oil. This intermediate is then mixed with 20 mL concentrated hydrochloric acid and stirred at 100 °C for 24 hours. The product is then extracted with ethyl ether (3 × 20 mL) and dried over anhydrous Na_2SO_4. The solvent is evaporated in vacuo, yielding 3.9 g of a slightly brownish solid. After recrystallization from diethyl ether, 2.0 g octylphosphonic acid (40%, 10.3 mmol) are obtained as colorless crystals.

^{1}H-NMR (400 MHz, $CDCl_3$, 298 K) δ [ppm]: 8.65 (s, 2H, O*H*), 1.74 (dd, $J_{P\text{-}H}$ = 18.0 Hz, J = 8.2 Hz, 2H), 1.66 – 1.55 (m, 2H), 1.43 – 1.34 (m, 2H), 1.34 – 1.21 (m, 8H), 0.88 (t, J = 6.8 Hz, 3H).

^{31}P{^{1}H}-NMR (162 MHz, $CDCl_3$, 298 K) δ [ppm]: 37.75.

5.4.3 Synthesis of Imidazolium Halides

Imidazolium halide ionic liquids [RR'MIM] X (R = Butyl, Octyl, Decyl, Dodecyl; R' = H, Me; X = Cl, Br) were synthesized in 30 g scales by addition of 1.05 eq. of alkylhalide (R-X) to 1.00 eq. of (di)methylimidazole. After degassing under fine vacuum and argon purging for three times, the solution was heated for 24 h (RBr: 60°C, RCl; 80 °C) under gentle stirring. Purification was performed by removing volatile impurities and excess educts under high vacuum using a turbomolecular pump, yielding the ionic liquids in quantitative yields in excellent purities (by NMR) and colorless appearances.

Analytic Data of the Imidazolium Halides

1-Octyl-3-methylimidazolium chloride [OMIM] Cl

^{1}H-NMR (400 MHz, $CDCl_3$, 298 K) δ [ppm]: 10.69 (d, *J* = 1.7 Hz, 1H), 7.60 (t, *J* = 1.8 Hz, 1H), 7.39 (t, *J* = 1.8 Hz, 1H), 4.26 (t, *J* = 7.4 Hz, 2H), 4.08 (s, 3H), 1.86 (q, *J* = 7.3 Hz, 2H), 1.40 – 1.10 (m, 10H), 0.86 – 0.77 (m, 3H).

^{13}C{^{1}H}-NMR (101 MHz, $CDCl_3$, 298 K) δ [ppm]: 138.09, 123.60, 121.75, 50.06, 36.53, 31.61, 30.30, 28.96, 28.90, 26.21, 22.52, 14.01.

1-Octyl-2,3-dimethylimidazolium chloride [OMMIM] Cl

^{1}H-NMR (400 MHz, $CDCl_3$, 298 K) δ [ppm]: 7.82 (d, *J* = 2.1 Hz, 1H), 7.45 (d, *J* = 2.1 Hz, 1H), 4.15 (t, *J* = 7.5 Hz, 2H), 4.00 (s, 3H), 2.76 (s, 3H), 1.75 (pseudo-p, *J* = 7.3 Hz, 2H), 1.32 – 1.12 (m, 10H), 0.81 (t, *J* = 6.7 Hz, 3H).

^{13}C{^{1}H}-NMR (101 MHz, $CDCl_3$, 298 K) δ [ppm]: 143.25, 123.11, 121.09, 48.68, 35.71, 31.40, 29.72, 28.75 (s, 2C), 26.08, 22.29, 13.82, 10.30.

Elemental analysis for $C_{13}H_{25}N_2Cl$ calc. (%): C 63.78, H 10.29, N 11.44, Cl 14.48; found: C 63.46, H 9.86, N 11.36.

1-Butyl-3-methylimidazolium bromide [BMIM] Br

^{1}H-NMR (400 MHz, $CDCl_3$, 298 K) δ [ppm]: 10.20 – 10.15 (m, 1H), 7.61 (s, 1H), 7.49 (s, 1H), 4.22 (t, *J* = 7.4 Hz, 2H), 3.99 (s, 3H), 1.84 – 1.72 (m, 2H), 1.24 (pseudo-h, *J* = 7.5 Hz, 2H), 0.81 (t, *J* = 7.3 Hz, 3H).

^{13}C{^{1}H}-NMR (101 MHz, $CDCl_3$, 298 K) δ [ppm]: 137.42, 123.78, 122.18, 49.89, 36.77, 32.20, 19.49, 13.45.

1-Octyl-3-methylimidazolium bromide [OMIM] Br

^{1}H-NMR (400 MHz, $CDCl_3$, 298 K) δ [ppm]: 10.31 (s, 1H), 7.61 (s, 1H), 7.43 (s, 1H), 4.26 (t, *J* = 7.4 Hz, 2H), 4.07 (s, 3H), 1.85 (pseudo-p, *J* = 7.3 Hz, 2H), 1.37 – 1.06 (m, 10H), 0.80 (t, *J* = 6.6 Hz, 3H).

^{13}C{^{1}H}-NMR (101 MHz, $CDCl_3$, 298 K) δ [ppm]: 137.34, 123.78, 122.02, 50.13, 36.72, 31.64, 30.32, 28.99, 28.92, 26.23, 22.55, 14.04.

Elemental analysis for $C_{12}H_{23}N_2Br$ calc. (%): C 52.37, H 8.42, N 10.18, Br 29.03; found: C 52.24, H 8.66, N 9.99.

1-Octyl-2,3-dimethylimidazolium bromide [OMMIM] Br

^{1}H-NMR (400 MHz, $CDCl_3$, 298 K) δ [ppm]: 7.70 (d, *J* = 2.1 Hz, 1H), 7.42 (d, *J* = 2.1 Hz, 1H), 4.17 (t, *J* = 7.5 Hz, 2H), 4.02 (s, 3H), 2.80 (s, 3H), 1.81 (s, 2H), 1.36 – 1.21 (m, 10H), 0.86 (t, *J* = 6.6 Hz, 3H).

^{13}C{^{1}H}-NMR (101 MHz, $CDCl_3$, 298 K) δ [ppm]: 143.95, 123.23, 121.09, 49.19, 36.38, 31.78, 29.95, 29.13, 29.10, 26.51, 22.68, 14.16, 11.18.

Elemental analysis for $C_{13}H_{25}N_2Br$ calc. (%): C 53.89, H 8.71, N 9.68, Br 27.62; found: C 53.30, H 8.73, N 9.54.

1-Decyl-3-methylimidazolium bromide [DeMIM] Br

^{1}H-NMR (400 MHz, $CDCl_3$, 298 K) δ [ppm]: 10.25 (s, 1H), 7.65 (d, *J* = 1.8 Hz, 1H), 7.45 (d, *J* = 1.9 Hz, 1H), 4.24 (t, *J* = 7.4 Hz, 2H), 4.05 (s, 3H), 1.83 (pseudo-p, *J* = 7.2 Hz, 2H), 1.28 – 1.13 (m, 14H), 0.78 (t, *J* = 6.8 Hz, 3H).

^{13}C{^{1}H}-NMR (101 MHz, $CDCl_3$, 298 K) δ [ppm]: 137.16, 123.84, 122.06, 50.03, 36.71, 31.73, 30.27, 29.35, 29.28, 29.14, 28.91, 26.16, 22.56, 14.03.

1-Dodecyl-3-methylimidazolium bromide [DoMIM] Br

^{1}H-NMR (400 MHz, $CDCl_3$, 298 K) δ [ppm]: 10.23 (s, 1H), 7.63 (t, *J* = 1.8 Hz, 1H), 7.42 (t, *J* = 1.8 Hz, 1H), 4.21 (t, *J* = 7.5 Hz, 2H), 4.03 (s, 3H), 1.80 (pseudo-p, *J* = 7.4 Hz, 2H), 1.31 – 1.07 (m, 18H), 0.76 (t, *J* = 6.8 Hz, 3H).

^{13}C{^{1}H}-NMR (101 MHz, $CDCl_3$, 298 K) δ [ppm]: 137.13, 123.83, 122.04, 50.03, 36.64, 31.79, 30.27, 29.49 (s, 2C), 29.41, 29.29, 29.22, 28.92, 26.17, 22.57, 14.03.

1-Dodecyl-2,3-dimethylimidazolium bromide [DoMMIM] Br

^{1}H-NMR (400 MHz, $CDCl_3$, 298 K) δ [ppm]: 7.73 (d, *J* = 2.1 Hz, 1H), 7.45 (d, *J* = 2.2 Hz, 1H), 4.13 (t, *J* = 7.5 Hz, 2H), 3.96 (s, 3H), 2.74 (s, 3H), 1.73 (pseudo-p, *J* = 7.4 Hz, 2H), 1.30 – 1.14 (m, 18H), 0.78 (t, *J* = 6.7 Hz, 3H).

^{13}C{^{1}H}-NMR (101 MHz, $CDCl_3$, 298 K) δ [ppm]: 143.61, 123.12, 121.10, 48.99, 36.22, 31.81, 29.86, 29.51 (s, 2C), 29.44, 29.32, 29.24, 29.00, 26.32, 22.60, 14.05, 11.01.

5.4.4 Synthesis of Imidazolium Nitrates

The ionic liquids [RR'MIM] [NO_3] (R = octyl, dodecyl, R' = H, Me) are prepared using by an anion exchange procedure.[148] 30 mmol, 1.0 eq. of the corresponding [RR'MIM] Br ionic liquids are dissolved in 800 mL (Millipore grade, resistance 18.2 MΩ·cm) water and rinsed over 120 g freshly regenerated Amberlite IRA 402 (OH) anion exchange resin within four hours. The basic eluate was neutralized to pH = 7.0 by addition of 2 wt.% aqueous HNO_3 monitored with a calibrated pH meter. After removal of the water and drying under fine vacuum at 80 °C with a turbomolecular pump, the colorless ionic liquids are obtained in yields >95%. The absence of residual bromide contaminations was ensured by titration by Mohr down to a detection limit of 13 ppm using a literature procedure.[153]

Analytic Data of the Imidazolium Nitrates:

1-Octyl-3-methylimidazolium nitrate [OMIM] [NO_3]

Melting range: −40 - −35 °C

^{1}H-NMR (400 MHz, $CDCl_3$, 298 K) δ [ppm]: 9.51 (s, 1H), 7.42 (t, *J* = 1.8 Hz, 1H), 7.34 (t, *J* = 1.8 Hz, 1H), 4.08 (t, ^{3}J = 7.4 Hz, 2H), 3.86 (s, 3H), 1.73 (dd, ^{3}J = 7.4, ^{3}J = 7.1 Hz, 2H), 1.23 – 1.03 (m, 10H), 0.70 (t, ^{3}J = 7.1 Hz, 3H).

^{13}C{^{1}H}-NMR (101 MHz, $CDCl_3$, 298 K) δ [ppm]: 137.10, 123.59, 122.08, 49.80, 35.94, 31.38, 29.93, 28.72, 28.61, 25.93, 22.28, 13.78.

Elemental analysis calcd. (%) for $C_{12}H_{23}N_3O_3$: C 56.01, H 9.01, N 16.33, O 18.65; found: C 55.62, H 9.13, N 16.02.

1-Octyl-2,3-dimethylimidazolium nitrate [OMMIM] [NO_3]

Melting point: 56 °C

^{1}H-NMR (400 MHz, $CDCl_3$, 298 K) δ [ppm]: 7.45 (d, *J* = 2.2 Hz, 1H), 7.31 (d, *J* = 2.2 Hz, 1H), 4.07 (t, ^3J = 7.6 Hz, 2H), 3.85 (s, 3H), 2.64 (s, 3H), 1.76 (dd, ^3J = 7.6 Hz, ^3J = 7.7 Hz, 2H), 1.33 – 1.18 (m, 10H), 0.83 (t, ^3J = 6.8 Hz 3H).

^{13}C{^{1}H}-NMR (101 MHz, $CDCl_3$, 298 K) δ [ppm]: 143.84, 122.98, 121.07, 48.84, 35.37, 31.72, 29.83, 29.07, 29.03, 26.41, 22.61, 14.10, 9.66.

Elemental analysis calcd. (%) for $C_{13}H_{25}N_3O_3$: C 57.54, H 9.29, N 15.49, O 17.69; found: C 57.33, H 9.45, N 15.65.

1-Dodecyl-3-methylimidazolium nitrate [DoMIM] [NO_3]

Melting point: 43 °C

^{1}H-NMR (400 MHz, $CDCl_3$, 298 K) δ [ppm]: 9.74 (s, 1H), 7.50 (t, *J* = 1.9 Hz, 1H), 7.38 (t, *J* = 1.9 Hz, 1H), 4.15 (t, ^3J = 7.4 Hz, 2H), 3.94 (s, 3H), 1.80 (dd, ^3J = 7.4 Hz, ^3J = 6.8 Hz, 2H), 1.26 – 1.14 (m, 18H), 0.80 (t, ^3J = 6.6 Hz, 3H).

^{13}C{^{1}H}-NMR (101 MHz, $CDCl_3$, 298 K) δ [ppm]: 137.65, 123.78, 122.16, 50.05, 36.21, 31.84, 30.21, 29.54, 29.46, 29.34, 29.27, 28.94, 26.21, 22.62, 14.07.

Elemental analysis calcd. (%) for $C_{16}H_{31}N_3O_3$: C 61.31, H 9.97, N 13.41, O 15.31; found: C 61.11, H 10.17, N 13.23.

1-Dodecyl-2,3-dimethylimidazolium nitrate [DoMMIM] [NO_3]

Melting point: 65 °C

^{1}H-NMR (400 MHz, $CDCl_3$, 298 K) δ [ppm]: 7.53 (s, 1H), 7.34 (s, 1H), 4.10 (t, ^3J = 7.6 Hz, 2H), 3.90 (s, 3H), 2.69 (s, 3H), 1.78 (dd, ^3J = 7.6 Hz, ^3J = 7.2 Hz, 2H), 1.33 – 1.20 (m, 18H), 0.85 (t, ^3J = 6.7 Hz, 4H).

^{13}C{^{1}H}-NMR (101 MHz, $CDCl_3$, 298 K) δ [ppm]: 143.90, 123.10, 121.07, 48.92, 35.59, 31.99, 29.91, 29.68, 29.61, 29.49, 29.42, 29.15, 26.49, 22.77, 14.21, 9.97.

Elemental analysis calcd. (%) for $C_{17}H_{33}N_3O_3$: C 62.35, H 10.16, N 12.83, O 14.66; found: C 61.82, H 10.11, N 12.33.

5.4.5 Synthesis of Imidazolium Tungstates

The imidazolium tungstates were synthesized according to an anion exchange procedure from the corresponding imidazolium bromides.[128] 20.0 mmol (2.00 eq.) [RMIM] Br (R = butyl, octyl, decyl, dodecyl) were dissolved in 800 mL deionized water and subsequently rinsed over 120 g freshly regenerated Amberlite 402 (OH). The basic fractions of the eluted [RMIM] [OH] were collected and 2.62 g tungstic acid (H_2WO_4, 10.5 mmol, 1.05 eq.) were added. The dispersion was stirred for one hour until pH = 7 was reached. Then, the excess tungstic acid is filtered off and the water evaporated under reduced pressure. The resulting solid was further dried overnight at 10^{-6} mbar and 80 °C using a turbomolecular pump. The resulting colorless resins were obtained in very high yields (>95%, >9.5 mmol) and stored under an argon atmosphere due to the high hygroscopy.

Analytic Data of the Imidazolium Tungstates:

1-Butyl-3-methylimidazolium tungstate $[BMIM]_2[WO_4]$

^{1}H-NMR* (400 MHz, D_2O, 298 K) δ [ppm]: 7.40 (d, *J* = 2.0 Hz, 1H), 7.35 (d, *J* = 2.0 Hz, 1H), 4.12 (t, *J* = 7.1 Hz, 2H), 3.82 (s, 3H), 1.77 (pseudo-p, *J* = 7.3 Hz, 2H), 1.24 (pseudo-h, *J* = 7.4 Hz, 2H), 0.85 (t, *J* = 7.4 Hz, 3H).

^{13}C{^{1}H}-NMR (101 MHz, D_2O, 298 K) δ [ppm]: 135.59 (t, $J_{D\text{-}C}$ = 34.0 Hz), 123.40, 122.13, 49.22, 35.55, 31.22, 18.72, 12.59.

Elemental analysis calcd. (%) for $C_{16}H_{30}N_4O_4W{\cdot}H_2O$: C 35.31, H 5.93, N 10.29, O 14.70, W 33.78; found: C 34.60, H 5.75, N 10.01.

1-Octyl-3-methylimidazolium tungstate $[OMIM]_2[WO_4]$

^{1}H-NMR* (400 MHz, D_2O, 298K) δ [ppm]: 7.43 (s, 1H), 7.41 (s, 1H), 4.14 (t, *J* = 7.2 Hz, 2H), 3.85 (s, 2H), 1.78 (pseudo-p, *J* = 7.2 Hz, 4H), 1.26 – 1.09 (m, 10H), 0.75 (t, *J* = 6.9 Hz, 3H).

^{13}C{^{1}H}-NMR (101 MHz, D_2O, 298K) δ [ppm]: 135.65 (t, $J_{D\text{-}C}$ = 33.4 Hz), 123.64, 122.11, 49.51, 35.72, 31.30, 29.44, 28.55, 28.41, 25.61, 22.20, 13.59.

^{183}W-NMR (16.6 MHz, D_2O, 298K) δ [ppm]: − 6.01.

Elemental analysis calcd. (%) for $C_{24}H_{46}N_4O_4W$: C 45.15, H 7.26, N 8.77, O 10.02, W 28.79; found: C 44.65, H 7.95, N 8.64.

1-Decyl-3-methylimidazolium tungstate $[DeMIM]_2[WO_4]$

^{1}H-NMR* (400 MHz, D_2O, 298 K) δ [ppm]: 7.45 (d, *J* = 2.0 Hz, 1H), 7.41 (d, *J* = 1.9 Hz, 1H), 4.15 (t, *J* = 7.2 Hz, 2H), 3.86 (s, 3H), 1.87 – 1.69 (m, 2H), 1.29 – 1.01 (m, 14H), 0.75 (t, *J* = 6.6 Hz, 3H).

^{13}C{^{1}H}-NMR (101 MHz, D_2O, 298 K) δ [ppm]: 135.75 (t, $J_{D\text{-}C}$ = 32.6 Hz), 123.73, 122.07, 49.51, 35.77, 31.61, 29.58, 29.21, 29.09, 28.99, 28.66, 25.79, 22.37, 13.66.

Elemental analysis calcd. (%) for $C_{28}H_{54}N_4O_4W$: C 48.42, H 7.84, N 8.07, O 9.21, W 26.47; found: C 48.40, H 8.38, N 8.14.

1-Dodecyl-3-methylimidazolium tungstate $[DoMIM]_2[WO_4]$

^{1}H-NMR* (400 MHz, D_2O, 298 K) δ [ppm]: 7.59 (d, *J* = 2.0 Hz, 1H), 7.51 (d, *J* = 2.0 Hz, 1H), 4.26 (t, *J* = 7.3 Hz, 2H), 3.97 (s, 3H), 2.00 – 1.78 (m, 2H), 1.44 – 1.15 (m, 18H), 0.85 (t, *J* = 6.7 Hz, 3H).

^{13}C{^{1}H}-NMR (101 MHz, D_2O, 298K) δ [ppm]: 135.88 (t, $J_{D\text{-}C}$ = 31.2 Hz), 123.87, 122.01, 49.49, 35.89, 31.90, 29.85, 29.75, 29.71 (s, 2C), 29.52, 29.39, 29.09, 26.12, 22.57, 13.78.

Elemental analysis calcd. (%) for $C_{32}H_{62}N_4O_4W \cdot H_2O$: C 50.00, H 8.39, N 7.29, O 10.41, W 23.91; found: C 50.07, H 8.61, N 7.29.

*C2 proton is not detectable due to a fast H/D exchange in D_2O.

5.4.6 Synthesis of Imidazolium Phosphates

1,3-Dimethylimidazolium dimethylphosphate [MMIM] $[(MeO)_2PO_2]$

0.91 mL freshly under distilled 1-methylimidazole (1.00 g, 12.2 mmol, 1.0 eq.) and 1.41 mL degassed and dried trimethylphosphate (1.71 g, 12.2 mmol, 1.0 eq.) are filled into a 20 mL air-tight screw neck vial in an inert gas glove box. The mixture is then heated to 120 °C under gentle stirring within one hour and kept at the final temperature for another hour. Then, fine vacuum is applied to the vessel for one hour and all volatiles evaporated, giving 2.71 g of the pure desired ionic liquid in quantitative yield (12.2 mmol, 100%).

^{1}H-NMR (400 MHz, chloroform-d, 298 K) δ [ppm]: 10.26 (s, 1H), 7.44 (t, *J* = 1.3 Hz, 2H), 3.85 (s, 6H), 3.39 (d, $J_{P\text{-}H}$ = 10.5 Hz, 6H).

$^{13}C\{^{1}H\}$-NMR (100 MHz, chloroform-d, 298 K) δ [ppm]: 139.23, 123.34 (s, 2C), 52.17 (d, J_{P-C} = 6.2 Hz, 2C), 35.92 (s, 2C).

$^{31}P\{^{1}H\}$-NMR (162 MHz, chloroform-d, 298 K) δ [ppm]: 2.49.

Elemental analysis for $C_7H_{15}N_2O_4P$ calc. (%): C 37.84, H 6.81, N 12.61, O 28.80, P 13.94; found: C 37.49, H 7.26, N 12.40.

Synthesis of 1-Octyl-3-methylimidazolium dialkylphosphates

1.0 g *N*-octylimidazole (5.6 mmol, 1.0 eq.) and 5.6 mmol dialkylmethylphosphate R_2MePO_4 (R = Me, Et, iPr, 1.0 eq.) are stirred under an argon atmosphere at 80 °C for 1 hour. Then, the temperature was increased to 120 °C and the mixture stirred for 4 more hours. After cooling to room temperature, volatile impurities are removed under high vacuum ($5*10^{-6}$ mbar) using a turbomolecular pump. The resulting ionic liquids are obtained in >98% yield and stored under an argon atmosphere until further use.

Analytic data of the imidazolium dialkylphosphates:

1-Octyl-3-methylimidazolium dimethylphosphate [OMIM] [$(MeO)_2PO_2$]

^{1}H-NMR (400 MHz, chloroform-d, 298 K) δ [ppm]: 10.62 (s, 1H), 7.47 (s, 1H), 7.29 (s, 1H), 4.21 (t, *J* = 7.4 Hz, 2H), 4.01 (s, 3H), 3.54 (d, J_{P-H} = 10.5 Hz, 6H), 1.82 (td, *J* = 10.7, 9.1, 5.7 Hz, 2H), 1.31 – 1.12 (m, 10H), 0.81 (t, *J* = 6.9 Hz, 3H).

$^{13}C\{^{1}H\}$-NMR (101 MHz, chloroform-d, 298 K) δ [ppm]: 138.13, 123.73, 121.65, 52.34 (d, J_{P-C} = 6.0 Hz), 49.69, 36.20, 31.59, 30.20, 28.96, 28.93, 26.18, 22.47, 13.93.

$^{31}P\{^{1}H\}$-NMR (162 MHz, chloroform-d, 298 K) δ [ppm]: 2.63.

Elemental analysis calcd. (%) for $C_{14}H_{29}N_2O_4P \cdot H_2O$: C 49.69, H 9.23, N 8.28, O 23.64, P 9.15; found: C 49.82, H 9.14, N 8.22.

1-Octyl-3-methylimidazolium diethylphosphate [OMIM] [$(EtO)_2PO_2$]

^{1}H-NMR (400 MHz, chloroform-d, 298 K) δ [ppm]: 10.85 (s, 1H), 7.34 (t, *J* = 1.8 Hz, 1H), 7.19 (t, *J* = 1.8 Hz, 1H), 4.23 (t, *J* = 7.5 Hz, 2H), 4.03 (s, 3H), 3.90 (dq, J_{P-H} = 7.0Hz, *J* = 7.0 Hz, 4H), 1.83 (pseudo-p, *J* = 7.4 Hz, 2H), 1.33 – 1.22 (m, 6H), 1.22 – 1.15 (m, 10H), 0.82 (t, *J* = 6.6 Hz, 3H).

$^{13}C\{^{1}H\}$-NMR (101 MHz, chloroform-d, 298 K) δ [ppm]: 140.22, 123.01, 121.16, 60.64 (d, J_{P-C} = 5.5 Hz), 49.91, 36.38, 31.63, 30.26, 28.96, 26.23, 22.52, 16.72, 16.69 (d, J_{P-C} = 6.8 Hz), 13.99.

$^{31}P\{^{1}H\}$-NMR (162 MHz, chloroform-d, 298 K) δ [ppm]:0.54.

Elemental analysis calcd. (%) for $C_{16}H_{33}N_2O_4P \cdot H_2O$: C 52.44, H 9.63, N 7.64, O 21.83, P 8.45; found: C 51.98, H 9.52, N 7.64.

1-Octyl-3-methylimidazolium diisopropylphosphate [OMIM] [(^{i}PrO)$_2$PO$_2$]

^{1}H-NMR (400 MHz, chloroform-d, 298 K) δ [ppm]: 11.07 (d, J = 1.7 Hz, 1H), 7.23 (t, *J* = 1.8 Hz, 1H), 7.13 (t, *J* = 1.8 Hz, 1H), 4.45 (dh, J_{P-H} = 7.9, 6.2 Hz, 2H), 4.26 (t, *J* = 7.5 Hz, 2H), 4.06 (s, 3H), 1.85 (pseudo-p, *J* = 7.4 Hz, 2H), 1.36 – 1.25 (m, 10H), 1.23 (d, J_{P-H} = 6.2 Hz, 12H), 0.84 (t, *J* = 6.8 Hz, 3H).

$^{13}C\{^{1}H\}$-NMR (101 MHz, chloroform-d, 298 K) δ [ppm]: 140.52, 123.10, 121.18, 67.75 (d, J_{P-C} = 5.9 Hz), 49.96, 36.48, 31.70, 30.34, 29.06, 29.03, 26.32, 24.44 (d, J_{P-C} = 4.6 Hz), 22.60, 14.07.

$^{31}P\{^{1}H\}$-NMR (162 MHz, chloroform-d, 298 K) δ [ppm]: -0.86.

Elemental analysis calcd. (%) for $C_{18}H_{37}N_2O_4P \cdot 0.5\ H_2O$: C 56.08, H 9.94, N 7.27, O 18.68, P 8.04; found: C 56.26, H 10.08, N 7.65.

Synthesis of 1-Octyl-3-methylimidazolium dihydrogen/diarylphosphates

1 g 1-octyl-3-methylimidazolium bromide ([OMIM] Br, 3.63 mmol, 1.0 eq.) is dissolved in 200 mL deionized water (Millipore grade, resistance 18.2 MΩ·cm) and rinsed over a column (20 × 1 cm) with 25 g freshly regenerated Amberlite IRA 402 (OH) anion exchange resin within one hour. The collected basic fraction of the eluate is collected and neutralized by addition of 3.63 mmol the desired phosphoric acid HR_2PO_4 (R = H, Ph, p-MeOPh, 1.0 eq.). The water is evaporated in vacuo and the resulting ionic liquid dried under high vacuum ($8 \cdot 10^{-6}$ mbar) using a turbomolecular pump, giving the products in >96% yield. The absence of residual bromide contaminations was ensured by titration by Mohr down to a detection limit of 13 ppm according to a literature procedure.[153]

1-Octyl-3-methylimidazolium dihydrogenphosphate [OMIM] [$(HO)_2PO_2$]

^{1}H-NMR (400 MHz, D_2O, 298 K) δ [ppm]: 8.61 (s, 1H), 7.36 (t, *J* = 1.9 Hz, 1H), 7.34 (t, *J* = 2.0 Hz, 1H), 4.08 (t, *J* = 7.0 Hz, 2H), 3.78 (s, 3H), 1.74 (pseudo-h, *J* = 6.9 Hz, 2H), 1.23 – 1.05 (m, 10H), 0.72 (t, *J* = 6.7 Hz, 3H).

^{13}C{^{1}H}-NMR (101 MHz, D_2O, 298 K) δ [ppm]: 135.76, 123.51, 122.17, 49.51, 35.59, 30.98, 29.16, 28.20, 28.03, 25.29, 21.96, 13.38.

^{31}P{^{1}H}-NMR (162 MHz, D_2O, 298 K) δ [ppm]: -0.03.

Elemental analysis calcd. (%) for $C_{12}H_{25}N_2O_4P \cdot 0.5\ H_2O$: C 47.83, H 8.70, N 9.30, O 23.89, P 10.28; found: C 48.04, H 8.64, N 9.25.

1-Octyl-3-methylimidazolium diphenylphosphate [OMIM] [$(PhO)_2PO_2$]

^{1}H-NMR (400 MHz, chloroform-d, 298 K) δ [ppm]: 9.91 (s, 1H), 7.36 – 7.13 (m, 9H), 6.99 (t, *J* = 7.2 Hz, 2H), 4.00 (t, *J* = 7.4 Hz, 2H), 3.79 (s, 3H), 1.70 (pseudo-p, *J* = 7.6 Hz, 2H), 1.36 – 1.11 (m, 10H), 0.89 (t, *J* = 7.0 Hz, 3H).

^{13}C{^{1}H}-NMR (101 MHz, chloroform-d, 298 K) δ [ppm]: 153.52, 138.05, 129.07, 123.49, 122.73, 121.52, 120.29 (d, $J_{P\text{-}C}$ = 5.1 Hz), 49.69, 36.06, 31.64, 30.08, 28.99, 28.91, 26.15, 22.54, 14.03.

^{31}P{^{1}H}-NMR (162 MHz, chloroform-d, 298 K) δ [ppm]: -10.05.

Elemental analysis calcd. (%) for $C_{24}H_{33}N_2O_4P \cdot H_2O$: C 62.32, H 7.63, N 6.06, O 17.30, P 6.70; found: C 62.27, H 7.66, N 6.22.

1-Octyl-3-methylimidazolium di(*p*-methoxyphenyl)phosphate [OMIM] [$(MeOPhO)_2PO_2$]

^{1}H-NMR (400 MHz, chloroform-d, 298 K) δ [ppm]: 9.73 (s, 1H), 7.29 (s, 1H), 7.12 (s, 1H), 7.10 (m, J = 9.0 Hz, 4H), 6.69 (d, J = 9.0 Hz, 4H), 3.96 (t, J = 7.5 Hz, 2H), 3.77 (s, 3H), 3.67 (s, 6H), 1.64 (p, J = 7.5 Hz, 2H), 1.31 – 1.04 (m, 10H), 0.82 (t, J = 7.0 Hz, 3H)

^{13}C{^{1}H}-NMR (101 MHz, Chloroform-d, 298 K) δ [ppm]: 155.06, 147.30 (d, $J_{P\text{-}C}$ = 7.3 Hz), 137.91, 123.53, 121.55, 121.01 (d, $J_{P\text{-}C}$ = 4.8 Hz), 114.07, 55.54, 49.67, 36.06, 31.64, 30.09, 29.00, 28.93, 26.17, 22.53, 14.01.

^{31}P{^{1}H}-NMR (162 MHz, chloroform-d, 298 K) δ [ppm]: -9.25

Elemental analysis calcd. (%) for $C_{26}H_{37}N_2O_6P \cdot 0.5\ H_2O$: C 60.81, H 7.46, N 5.45, O 20.25, P 6.03; found: C 60.56, H 7.50, N 5.41.

Attempt to synthesize [OMIM] [1,2-phenylenephosphate]

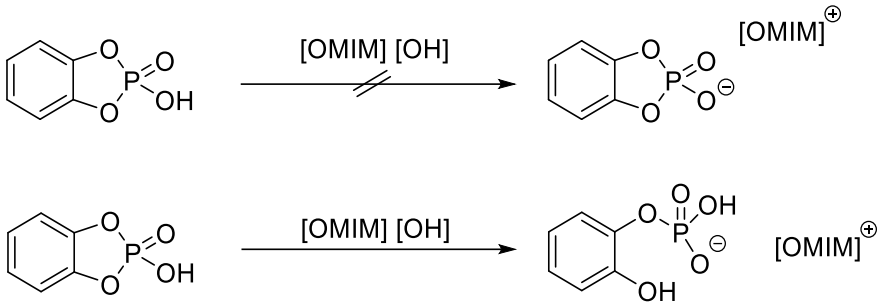

200 mg phosphoric acid o-phenylenediester (1.16 mmol, 1.0 eq.) are added to 41.5 mL of a solution of [OMIM] [OH] in water (28 mM, 263 mg, 1.16 mmol, 1.0 eq.) and stirred for 3 h at room temperature prior to removal of water in vacuo. 486 mg of a colorless resin (110% of theoretic yield) are obtained. NMR spectroscopy reveals a hydrolyzation of the desired product to a catechol phosphoric acid monoester.

^{1}H-NMR (400 MHz, DMSO-d_6, 298 K) δ [ppm]: 9.26 (s, 1H), 7.80 (t, *J* = 1.8 Hz, 1H), 7.73 (t, *J* = 1.8 Hz, 1H), 7.14 (dt, *J* = 7.9, 1.4 Hz, 1H), 6.98 – 6.89 (m, 1H), 6.89 (dd, *J* = 8.1, 2.0 Hz, 1H), 6.73 (ddd, *J* = 8.0, 7.0, 2.0 Hz, 1H), 4.16 (t, *J* = 7.2 Hz, 2H), 3.86 (s, 3H), 1.78 (pseudo-p, *J* = 7.3 Hz, 2H), 1.34 – 1.17 (m, 10H), 0.86 (t, *J* = 7.1 Hz, 3H).

^{13}C{^{1}H}-NMR (101 MHz, DMSO-d_6, 298 K) δ [ppm]: 148.54 (d, $J_{P\text{-}C}$ = 5.1 Hz), 139.67 (d, $J_{P\text{-}C}$ = 6.6 Hz), 136.57, 124.51, 123.59, 122.26, 121.36 (d, $J_{P\text{-}C}$ = 3.3 Hz), 119.02, 117.39, 48.74, 35.73, 31.16, 29.39, 28.47, 28.34, 25.50, 22.05, 13.94.

^{31}P{^{1}H}-NMR (162 MHz, DMSO-d_6, 298 K) δ [ppm]: -4.29

[OMIM] [(*rac*)-1,1'-binaphtyl-2,2'-diylphosphate]

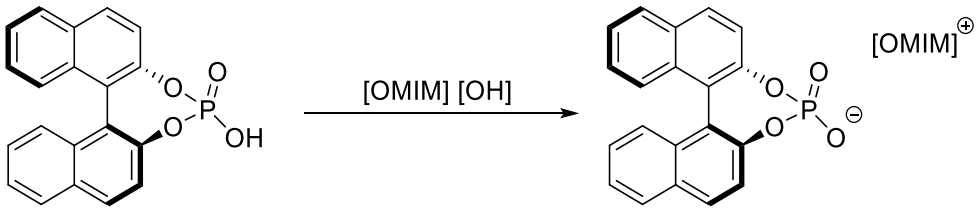

70.0 mg *rac*-1,10-binaphthalene-2,2'-diylphosphoric acid (201µmol, 1.0 eq.) are dissolved in 8.0 mL of a freshly prepared solution of [OMIM] [OH] (25 mM, 45.5 mg, 201 µmol, 1.0 eq.) and stirred at 60 °C for 3 h prior to removal of water in vacuo. 108 mg (194 µmol, 96%) of the product are obtained as a colorless resin. A slight hydrolyzation of the anion to rac-BINOL is observed by NMR-spectroscopy.

^{1}H-NMR (400 MHz, DMSO-d_6, 298 K) δ [ppm]: 9.25 (s, 1H), 8.06 (dd, *J* = 15.9, 7.9 Hz, 4H), 7.77 (t, *J* = 1.8 Hz, 1H), 7.70 (t, *J* = 1.8 Hz, 1H), 7.51 – 7.44 (m, 4H), 7.32 (ddd, *J* = 8.1, 6.7, 1.4 Hz, 2H), 7.22 (d, *J* = 8.5 Hz, 2H), 4.12 (t, *J* = 7.2 Hz, 2H), 3.83 (s, 3H), 1.74 (pseudo-p, *J* = 7.3 Hz, 3H), 1.23 (s, 10H), 0.85 (t, *J* = 6.7 Hz, 3H).

^{13}C{^{1}H}-NMR (101 MHz, DMSO-d_6, 298 K) δ [ppm]: 149.37 (d, $J_{P\text{-}C}$ = 9.2 Hz), 143.98, 136.57, 131.84 (2C), 130.49 (2C), 130.06 (2C), 128.44 (2C), 126.26 (2C), 126.17, 126.02 (2C), 124.70, 123.54, 122.21 (3C), 121.53 (d, $J_{P\text{-}C}$ = 2.4 Hz, 2C) 48.69, 35.68, 31.14, 29.36, 28.46, 28.31, 25.47, 22.03, 13.92.

^{31}P{^{1}H}-NMR (162 MHz, DMSO-d_6, 298 K) δ [ppm]: 4.34

5.4.7 Synthesis of SIP Precursors

Dimethyl-(4,6-di-*tert*-butylpyridin-2-yl)malonate

Synthesis of the organic receptor L^{1} precursor according to an adapted literature procedure.[106]

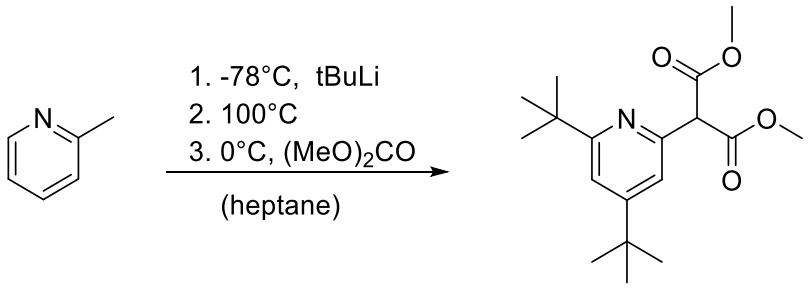

1.4 mL 2-picoline (1.30 g, 14 mmol, 1.0 eq.) in dry *n*-heptane (70 mL) was cooled under argon atmosphere to −78°C. *tert*-Butyllithium in *n*-pentane (1.6 M, 41 mL, 70 mmol, 5.0 eq.) was added to the stirred solution under argon atmosphere over 1 h using a syringe pump, resulting in the colorless solution turning yellow. The *n*-pentane was carefully evaporated in vacuo and the solution was refluxed for 1 h, during which the color changed from yellow to deep red. The reaction solution was cooled in an ice bath to 0°C, and then 5.9 mL dimethyl carbonate (6.3 g, 70 mmol, 5.0 eq.) were added dropwise. The resulting suspension was re-dissolved in Et_2O at 0 °C (150 mL), and 5 g ammonium chloride followed by 50 g ice were added portion wise. The organic layer was separated, and the aqueous layer was extracted with ethyl acetate (3 × 50 mL). The combined organic solutions were dried over anhydrous Na_2SO_4, filtered and the solvent was removed in vacuo. The crude product was purified by column chromatography on silica with Et_2O/hexane (10:90 → 50:50) as eluent to give dimethyl(4,6-di-*tert*-butylpyridin-2-yl)malonate 4 (2.10 g, 6.5 mmol, 47%) as a bright yellow crystalline solid.

^{1}H-NMR (400 MHz, chloroform-*d*, 298 K) δ [ppm]: 7.24 (s, 1H, py-*H*), 7.17 (s, 1H, py-*H*), 4.94 (s, 1H, -C*H*-(COOMe)$_2$), 3.78 (s, 6H, COOC*H*$_3$), 1.32 (s, 9H, C(C*H*$_3$)$_3$), 1.30 (s, 9H, C(C*H*$_3$)$_3$).

^{13}C{^{1}H}-NMR (101 MHz, chloroform-*d*, 298 K) δ [ppm]: 168.85, 168.54, 160.70, 151.35, 117.51, 115.04, 60.54, 52.82, 37.59, 35.08, 30.81, 30.29.

2-(4,6-di-*tert*-butylpyridin-2-yl)-N,N'-dihexylmalonamide

Synthesis of the organic receptor L^1 according to a adapted literature procedure.[106]

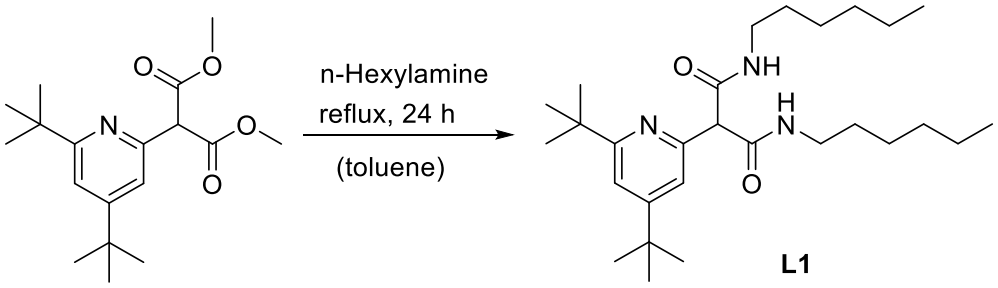

Dimethyl(4,6-di-*tert*-butylpyridin-2-yl)malonate (2.00 g, 6.2 mmol, 1.0 eq.) and 2.5 mL *n*-hexylamine (1,89 g, 18.7 mmol, 3.0 eq.) in 150 mL toluene were refluxed for 24 h. After cooling to room temperature, the solvent was removed in vacuo and the residual resin dried under fine vacuum at 50 °C for two hours. The resulting dark orange solid was then purified by column chromatography over silica using EtOAc/hexane (50:50 → 80:20) as eluent. The last fraction (determined by TLC under UV light) was concentrated to give 2-(4,6-di-*tert*-butylpyridin-2-yl)-dihexylmalonamide (L1) (2.41 g, 5.2 mmol, 84%) as an orange solid.

^{1}H-NMR (400 MHz, chloroform-*d*, 298 K) δ [ppm]: 7.94 (s, 2H, CON*H*-), 7.25 (s, 1H, py-*H*), 7.04 (s, 1H, py-*H*), 4.53 (s, 1H, -C*H*-(CONH-)$_2$), 3.34 – 3.15 (m, 4H, NH-C*H*$_2$-), 1.55 – 1.44 (m, 4H, NH-CH$_2$-C*H*$_2$-), 1.37 (s, 9H, C(C*H*$_3$)$_3$), 1.28 (s, 9H, C(C*H*$_3$)$_3$), 1.29 – 1.20 (m, 12H, H$_3$C-C*H*$_2$-C*H*$_2$-C*H*$_2$-), 0.85 (t, J = 6.8 Hz, 6H, CH$_2$-C*H*$_3$).

^{13}C{^{1}H}-NMR (101 MHz, chloroform-*d*, 298 K) δ [ppm]: 168.24, 167.80, 161.90, 153.42, 118.86, 115.15, 61.86, 39.87, 37.69, 35.12, 31.56, 30.70, 30.40, 29.50, 26.73, 22.64, 14.10.

Elemental analysis for $C_{28}H_{49}N_3O_2$ calc. (%): C 73.16, H 10.74, N 9.14, O 6.96; found: C 73.13, H 10.87, N 9.13.

N-[(Di-*n*-hexylamino)methyl]benzamide

Synthesis of organic receptor L^2 according to a adapted literature procedure.[107]

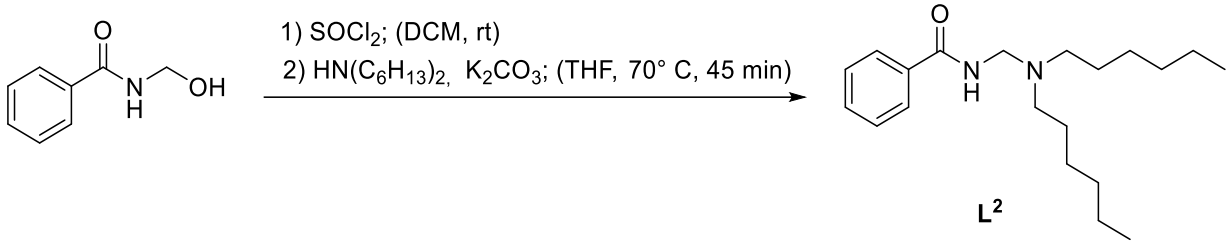

10.0 g of hydroxymethyl benzamide (1.0 eq., 66.2 mmol) were dissolved in 70 mL dry DCM under argon atmosphere and stirred using a magnetic stirring bar. 14.4 mL of thionyl chloride (23.6 g, 198 mmol, 3.0 eq.) were carefully added within one hour. After addition, the reaction mixture was stirred for one more hour and mixed with 150 mL of *n*-hexane, leading to the precipitation of a yellow solid. The solvent mixture was filtered off under argon atmosphere and the obtained solid was washed with *n*-hexane (2 × 5 mL) and dried *in vacuo*. The solid was then dissolved in 100 mL of dry acetone and mixed with 15.9 mL dihexylamine (12.6 g, 66.2 mmol, 1.0 eq.) and 7.00 g potassium carbonate (50.6 mmol, 0.77 eq.). The reaction mixture was heated to refluxed for 45 min under argon atmosphere. Then, the solvent was removed *in vacuo* and the obtained solid was extracted with 20 mL DCM and washed with a saturated sodium carbonate solution (2 × 10 mL). The combined organic solutions were then dried over anhydrous $MgSO_4$ and purified by column chromatography over silica with eluent pentane/EtOAc (1:1), collecting the fastest fraction (determined by TLC under UV light). The product (L^2) was obtained as yellowish oil in 61% yield (13.0 g, 40.7 mmol).

Rf-value: 0.90

^{1}H-NMR (400 MHz, chloroform-*d*, 298 K) δ [ppm]: 7.76 (d, *J* = 7.1 Hz, 2H, Ar-*H*), 7.55 – 7.47 (m, 1H, Ar-*H*), 7.46 – 7.39 (m, 2H, Ar-*H*), 6.35 (s, 1H, N-*H*), 4.40 (d, *J* = 5.8 Hz 2H, N-C*H*$_2$-N), 2.59 – 2.47 (m, 4H, N(-C*H*$_2$-CH$_2$-)$_2$), 1.56 – 1.45 (m, 4H, N(-CH$_2$-C*H*$_2$-)$_2$), 1.37 – 1.22 (m, 12H, N(-(CH$_2$)$_2$-(C*H*$_2$)$_3$-CH$_3$)$_2$), 0.99 – 0.63 (t, *J* = 6.6 Hz, 6H, N(-(CH$_2$)$_5$-C*H*$_3$)$_2$).

^{13}C{^{1}H}-NMR (101 MHz, chloroform-*d*, 298 K) δ [ppm]:167.94, 134.80, 131.51, 128.62, 126.99, 58.84, 52.24, 31.85, 27.81, 27.23, 22.75, 14.14.

Elemental analysis for $C_{20}H_{34}N_2O$ calc. (%): C 75.42, H 10.76, N 8.80, O 5.02: found: C 75.34, H 10.85, N 8.85.

Synthesis of 3,3,5-trimethylhexanamide

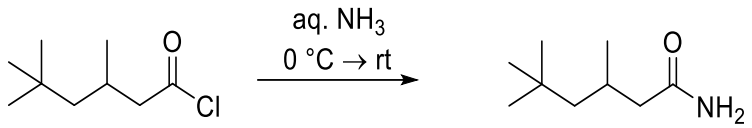

83 mL NH_3 (28 wt.% aq. solution, 1.3 mol, 13 eq.) are cooled to 0 °C using an ice bath and 19.0 mL 3,5,5-trimethylhexanoyl chloride (17.7 g, 100 mmol, 1.0 eq.) are carefully added under vigorous stirring. After complete addition within a half hour, the mixture is allowed to warm up and stirred overnight at room temperature. The supernatant organic layer is then extracted with dichloromethane (3 × 50 mL). The combined organic solutions are washed with water (2 × 100 mL) and the solvent is removed in vacuo yielding 13.3 g 3,5,5-trimethylhexanamide (84.7 mmol, 85%) as a white powder.

^{1}H-NMR (400 MHz, chloroform-*d*, 298 K) δ [ppm]: 6.09 (s, 1H, N*H*), 5.65 (s, 1H, N*H*), 2.26 – 2.17 (m, 1H, CH_2-CO), 2.07 – 2.01 (m, 1H, CO-CH_2-C*H*(CH_3)-), 2.00 – 1.92 (m, 1H, CH_2-CO), 1.23 (dd, *J* = 14.1, 3.7 Hz, 1H, C(CH_3)$_3$-CH_2-CH(CH_3)-), 1.15 – 1.05 (m, 1H, C(CH_3)$_3$-CH_2-CH(CH_3)-), 0.98 (d, *J* = 6.4 Hz, 3H, CH-CH_3), 0.89 (s, 9H, C-(CH_3)$_3$).

^{13}C{^{1}H}-NMR (101 MHz, chloroform-*d*, 298 K) δ [ppm]: 175.55, 50.79, 45.93, 31.15, 30.11, 27.40, 22.64.

***N*-[(Di-*n*-hexylamino)methyl]-3,5,5-trimethylhexanamide**

Synthesis of the organic receptor L^3 was conducted according to an adapted literature procedure.[107]

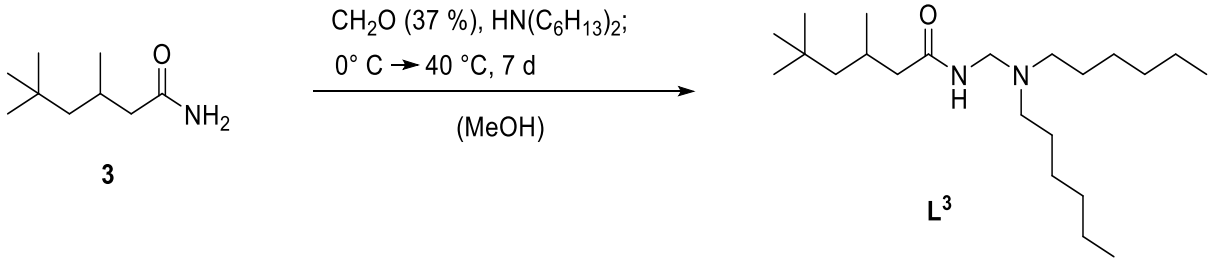

3.93 g of 3,5,5-trimethylhexylamide (25.0 mmol, 1.0 eq.) were dissolved in 2 mL MeOH by vigorous stirring and then cooled in an ice bath. To the stirring solution, 2.03 g formaldehyde (37 wt.% in water, 25.0 mmol, 1.0 eq.) and then 6.0 mL dihexylamine (4.36 g, 25.0 mmol, 1.0 eq.) were added dropwise. After complete addition the reaction was warmed to 40 °C and stirred for seven days. Then, the remaining solvent and other volatile components were removed *in vacuo* an the collected solid was purified by column chromatography over silica with eluent mixture EtOAc/pentane (40:60), collecting the fastest fraction (determined with TLC

using a $KMnO_4$ solution). After solvent removal the product was obtained as yellow oil in 74 % yield (6.58 g, 18.6 mmol).

Rf-value: 0.60

^{1}H-NMR (400 MHz, chloroform-*d*, 298 K) δ [ppm]: 5.62 (s, 1H, N-*H*), 4.19 (d, *J* = 6.0 Hz, 2H, N-C*H*$_2$-N), 2.49 – 2.40 (m, 4H, N(-C*H*$_2$-CH$_2$-)$_2$), 2.20 (dd, *J* = 13.6, 5.8 Hz, 1H, CO-C*H*$_2$-CH(CH$_3$)-), 2.12 – 2.02 (m, 1H, CO-CH$_2$-C*H*(CH$_3$)-), 1.94 (dd, *J* = 13.6, 8.3 Hz, 1H, CO-C*H*$_2$-CH(CH$_3$)-), 1.52 – 1.39 (m, 4H, N(-CH$_2$-C*H*$_2$-)$_2$), 1.34 – 1.24 (m, 12H, N(-(CH$_2$)$_2$-(C*H*$_2$)$_3$-CH$_3$)$_2$), 1.20 – 1.25 (m, 1H, C(CH$_3$)$_3$-C*H*$_2$-CH(CH$_3$)-), 1.10 (dd, *J* = 13.9, 6.6 Hz, 1H, C(CH$_3$)$_3$-C*H*$_2$-CH(CH$_3$)-), 0.98 (d, *J* = 6.5 Hz, 3H, C(CH$_3$)$_3$-CH$_2$-CH(C*H*$_3$)-), 0.91 (s, 9H, C(C*H*$_3$)$_3$-CH$_2$-), 0.88 (t, *J* = 6.7 Hz, 6H, N(-(CH$_2$)$_5$-C*H*$_3$)$_2$).

^{13}C{^{1}H}-NMR (101 MHz, chloroform-*d*, 298 K) δ [ppm]: 172.88, 58.01, 52.18, 50.84, 47.07, 31.88, 31.17, 30.16, 27.77, 27.37, 27.26, 22.77, 22.68, 14.17.

Elemental analysis for $C_{22}H_{46}N_2O$ calc. (%): C 74.51, H 13.08, N 7.90, O 4.51; found: C 75.03, H 12.94, N 7.99.

5.4.8 Synthesis of Sulfate-based Supramolecular Ion Pairs

Synthesis of [HL^1]HSO$_4$

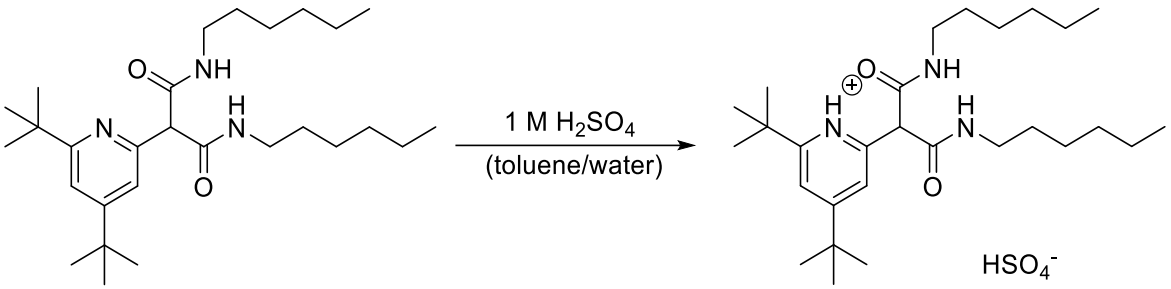

500 mg of 2-(4,6-di-*tert*-butylpyridin-2-yl)-dihexylmalonamide (1.1 mmol, 1.0 eq.) are dissolved in 20 mL toluene. 20 mL water and 1.1 mL H_2SO_4 (1M in H_2O, 1.1 mmol, 1.0 eq.) are added and stirred for 30 min at room temperature. Afterwards, the aqueous phase is removed, and the toluene phase washed with water (2 × 10 mL) and concentrated under reduced pressure. The oily residue is dried under fine vacuum, yielding 602 mg of [HL^1]HSO$_4$ as a colorless solid (1.1 mmol, 99%). The use of 0.5 eq. H_2SO_4 results in the formation of a 50:50 mixture of [HL^1]HSO$_4$ and L^1. In this case, short path column chromatography over silica (toluene → EtOAc) allows for the separation of L^1 (yellow toluene fraction, 42% recovery) and [HL^1]HSO$_4$ (colorless EtOAc fraction, 28% yield).

^{1}H-NMR (400 MHz, benzene-d_6, 298 K) δ [ppm]: 9.25 (t, *J* = 5.6 Hz, 2H, -CON*H*-), 8.78 (s, 1H, py-*H*), 7.04 (d, *J* = 1.8 Hz, 1H, py-*H*), 6.29 (s, 1H, C*H*-(CONH)$_2$-), 3.48 (dq, *J* = 13.4, 6.9 Hz, 2H, -CONH-C*H*$_2$-), 3.34 (dq, *J* = 13.0, 6.9 Hz, 2H, -CONH-C*H*$_2$-), 1.80 – 1.61 (m, 4H, -NCH$_2$-C*H*$_2$-), 1.39 – 1.14 (m, 12H, H$_3$C-C*H*$_2$-C*H*$_2$-C*H*$_2$-), 1.21 (s, 9H, C(C*H*$_3$)$_3$), 1.02 (s, 9H, C(C*H*$_3$)$_3$), 0.85 (t, *J* = 6.9 Hz, 6H, CH$_2$-C*H*$_3$).

^{13}C{^{1}H}-NMR (101 MHz, benzene-d_6, 298 K) δ [ppm]: 172.18, 165.98, 149.59, 138.52, 123.99, 117.64, 58.72, 41.01, 36.95, 36.11, 31.81, 30.10, 29.40, 28.69, 26.93, 22.97, 14.32.

Elemental analysis for $C_{28}H_{51}N_3O_6S$ calc. (%): C 60.29, H 9.22, N 7.53, O 17.21, S 5.75; found: C 60.44, H 9.29, N 7.54, S 5.76.

Synthesis of $[HL^2]_2SO_4$

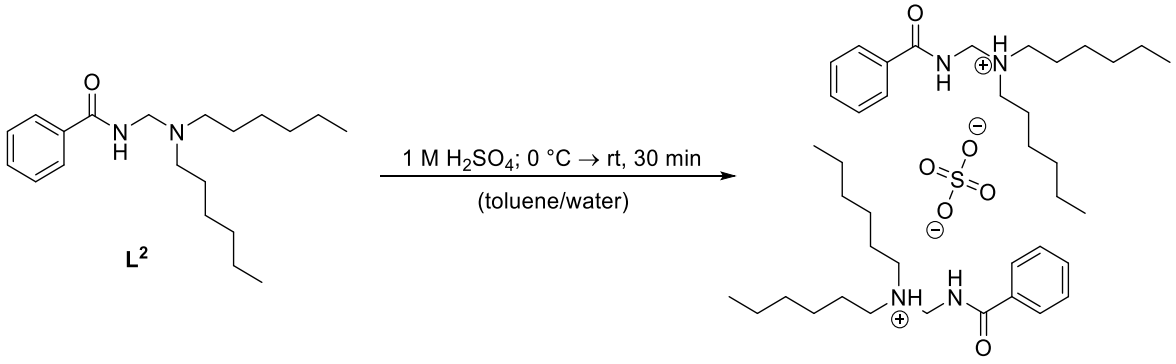

1.00 g L^2 (3.14 mmol, 2.0 eq.) in 20 mL toluene and 1.57 mL of 1 M sulfuric acid (1.57 mmol, 1.0 eq.) are combined at 0 °C under vigorous stirring. After 30 min at 0 °C, the mixture is allowed to warm to room temperature. After the separation of the aqueous phase, the organic phase was washed with deionized water (2 × 5 mL) and dried over anhydrous $MgSO_4$ for the following removal of toluene in vacuo at 50 °C maximum to avoid decomposition. The resulting product $[HL^2]_2SO_4$ was obtained as yellowish, highly viscous oil in 67 % yield (0.78 g, 1.06 mmol).

^{1}H-NMR (400 MHz, chloroform-*d*, 298 K) δ [ppm]: 8.07 (d, *J* = 7.5 Hz, 2H, Ar-*H*), 7.42 – 7.39 (m, 1H, Ar-*H*), 7.36 – 7.28 (m, 2H, Ar-*H*), 4.79 (d, J = 6.6 Hz, 2H, N-C*H*$_2$-N), 3.05 – 2.90 (m, 4H, N(-C*H*$_2$-CH$_2$-)$_2$), 1.77 – 1.63 (m, 4H, N(-CH$_2$-C*H*$_2$-)$_2$), 1.35 – 1.14 (m, 12H, N(-(CH$_2$)$_2$-(C*H*$_2$)$_3$-CH$_3$)$_2$), 0.90 – 0.75 (m, 6H, N(-(CH$_2$)$_5$-C*H*$_3$)$_2$).

^{13}C{^{1}H}-NMR (101 MHz, chloroform-*d*, 298 K) δ [ppm]: 132.26, 128.56, 128.21, 49.20, 31.25, 26.66, 23.32, 22.50, 13.97.

Elemental analysis for $C_{40}H_{70}N_4O_6S \cdot 1.5\ H_2O$ calc. (%): C 63.04, H 9.65, N 7.35, O 15.75, S 4.21; found: C 63.21, H 9.82, N 7.44, S 3.86.

Synthesis of $[HL^3]_2SO_4$

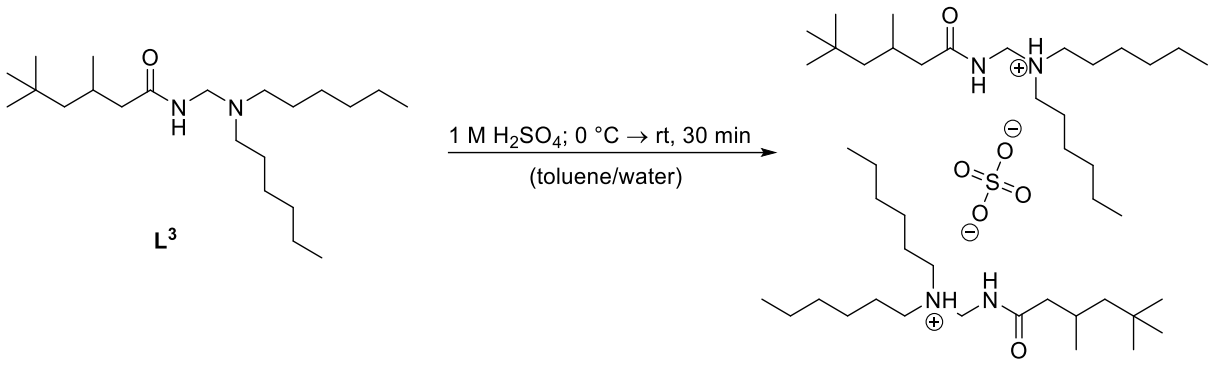

1.00 g L^3 (2.82 mmol, 2.0 eq.,) in 20 mL toluene and 1.41 mL of 1 M sulfuric acid (1.0 eq., 1.41 mmol) are combined at 0 °C under vigorous stirring. After 30 min at 0 °C, the mixture is allowed to warm to room temperature. After the separation of the aqueous phase, the organic phase was washed with deionized water (2 × 5 mL) and dried over anhydrous $MgSO_4$ for the following removal of toluene in vacuo at 50 °C maximum to avoid decomposition. The resulting product $[HL^3]_2SO_4$ was obtained as yellowish, highly viscous oil in 78 % yield (0.89 g, 1.10 mmol).

^{1}H-NMR (400 MHz, chloroform-*d*, 298 K) δ [ppm]: 4.51 (d, *J* = 6.7 Hz, 2H, N-C*H*$_2$-N), 3.00 – 2.81 (m, 4H, N(-C*H*$_2$-CH$_2$-)$_2$), 2.33 – 2.06 (m, 2H, CO-C*H*$_2$-CH(CH$_3$)-), 1.75 – 1.59 (m, 4H, N(-CH$_2$-C*H*$_2$-)$_2$), 1.27 (s, 12H, N(-(CH$_2$)$_2$-(C*H*$_2$)$_3$-CH$_3$)$_2$), 1.25 – 1.05 (m, 2H, C(CH$_3$)$_3$-C*H*$_2$-CH(CH$_3$)-), 0.94 (d, *J* = 6.2 Hz, 3H, C(CH$_3$)$_3$-CH$_2$-CH(C*H*$_3$)-), 0.88 (s, 9H, C(C*H*$_3$)$_3$-CH$_2$-), 0.91 – 0.84 (m, 6H, N(-(CH$_2$)$_5$-C*H*$_3$)$_2$).

^{13}C{^{1}H}-NMR (101 MHz, chloroform-*d*, 298 K) δ [ppm]: 57.23, 50.78, 50.69, 31.27, 30.09, 26.64, 22.53, 13.98.

Elemental analysis for $C_{44}H_{94}N_4O_6S \cdot 1.5\ H_2O$ calc. (%): C 63.34, H 11.72, N 6.72, O 14.38, S 3.84; found: C 63.58, H 11.90, N 6.81, S 3.62.

5.4.9 Synthesis of 1-Benzyl-3-octylimidazolium Bromides

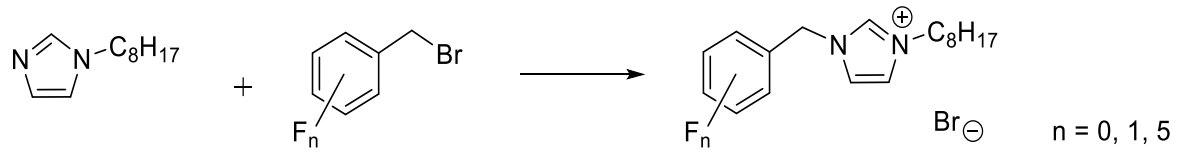

1.1 mL freshly distilled 1-ocytylimidzole (1.0 g, 5.6 mmol, 1.0 eq.) is cooled to -20 °C under an argon atmosphere and stirred gently. 5.6 mmol (1.0 eq.) of the precooled and degassed benzylbromide derivative are added rapidly. The mixture is allowed to warm-up to room temperature within one hour. Subsequently, the mixture is heated to 80 °C stepwise within two hours. Then, all volatiles are removed under fine vacuum at the elevated temperature overnight. The desired white solids are obtained in >98% yield and stored under an argon atmosphere until further use.

1-Benzyl-3-octylimidazolium bromide [BnOIM] Br

^{1}H-NMR (400 MHz, $CDCl_3$, 298 K) δ [ppm]: 10.53 (s, 1H), 7.51 – 7.43 (m, 3H), 7.44 (d, *J* = 1.8 Hz, 1H), 7.33 – 7.27 (m, 2H), 7.28 (d, *J* = 2.8 Hz, 1H), 5.57 (s, 2H), 4.22 (t, *J* = 7.5 Hz, 2H), 1.84 (pseudo-p, *J* = 7.5 Hz, 1H), 1.30 – 1.07 (m, 10H), 0.79 (t, *J* = 7.1 Hz, 3H).

^{13}C{^{1}H}-NMR (101 MHz, $CDCl_3$, 298K) δ [ppm]: 136.68, 133.23, 129.38, 129.34 (2C), 129.01 (2C), 122.26, 122.14, 53.09, 50.16, 31.59, 30.21, 28.96, 28.86, 26.20, 22.52, 14.02.

1-(4'-Fluorobenzyl)-3-octylimidazolium bromide [F-BnOIM] Br

^{1}H-NMR (400 MHz, $CDCl_3$, 298 K) δ [ppm]: 10.51 (s, 1H), 7.63 – 7.53 (m, 3H), 7.39 (t, *J* = 1.8 Hz, 1H), 7.02 – 6.92 (m, 2H), 5.61 (s, 2H), 4.20 (t, *J* = 7.5 Hz, 2H), 1.89 – 1.77 (m, 2H), 1.29 – 1.08 (m, 10H), 0.78 (t, *J* = 7.1 Hz, 3H).

^{13}C{^{1}H}-NMR (101 MHz, $CDCl_3$, 298K) δ [ppm]: 163.13 (d, $J_{F\text{-}C}$ = 249.4 Hz), 136.56, 131.31 (d, $J_{F\text{-}C}$ = 8.4 Hz), 129.39 (d, $J_{F\text{-}C}$ = 3.4 Hz), 122.30, 122.10, 116.30 (d, $J_{F\text{-}C}$ = 21.9 Hz), 52.15, 50.19, 31.57, 30.16, 28.95, 28.84, 26.20, 22.50, 14.00.

^{19}F-NMR (376 MHz, $CDCl_3$, 298K) δ [ppm]: -111.42 – -111.59 (m).

1-(2',3',4',5',6'-Pentafluorobenzyl)-3-octylimidazolium bromide [^{F}BnOIM] Br

^{1}H-NMR (400 MHz, $CDCl_3$, 298 K) δ [ppm]: 10.60 (s, 1H), 7.56 (d, *J* = 1.7 Hz, 1H), 7.55 (d, *J* = 1.9 Hz, 1H), 5.87 (s, 2H), 4.32 (t, *J* = 7.5 Hz, 2H), 1.90 (pseudo-p, *J* = 7.3 Hz, 2H), 1.35 – 1.14 (m, 11H), 0.83 (t, *J* = 6.8 Hz, 3H).

^{13}C{^{1}H}-NMR (101 MHz, $CDCl_3$, 298K) δ [ppm]: 137.68, 122.92, 122.26, 50.57, 41.11, 31.70, 30.28, 29.07, 28.97, 26.28, 22.63, 14.09. The phenylic carbon atoms are not detectable due to a strong multipletation by coupling to fluorine.

^{19}F-NMR (376 MHz, $CDCl_3$, 298K) δ [ppm]: -140.14 – -140.92 (m, 2F), -149.59 (t, J_{F-F} = 21.0 Hz, 1F), -159.02 – -159.36 (m, 2F).

1-(2',3',4',5',6'-Pentafluorobenzyl)-2-methyl-3-octylimidazolium bromide [^{F}BnOMIM] Br

Synthesis according to 1-(2,3,4,5,6-Pentafluorobenzyl)-3-methylimidazolium bromide but 15.4 mmol 1-octyl-2-methylimidazolium and 2.3 mL 2,3,4,5,6-pentafluorobenzyl bromide (4.03 g, 15.4 mmol, 1.0 eq.) were used. Due to the high melting point, the product was heated to 100 °C for evaporation of volatiles using a turbomolecular pump, where the color turned slightly beige. The product is obtained in 97% yield and stored under an argon atmosphere until further use. A slightly smaller scheduled quantity is recommended.

^{1}H-NMR (400 MHz, $CDCl_3$, 298 K) δ [ppm]: 7.61 (d, *J* = 2.2 Hz, 1H), 7.55 (d, *J* = 2.2 Hz, 1H), 5.78 (s, 22H), 4.20 (t, *J* = 7.6 Hz, 2H), 2.90 (s, 3H), 1.80 (pseudo-p, *J* = 8.0 Hz, 2H), 1.41 – 1.14 (m, 10H), 0.83 (t, *J* = 6.9 Hz, 3H).

^{13}C{^{1}H}-NMR (101 MHz, $CDCl_3$, 298K) δ [ppm]: 144.56, 122.24, 122.00, 49.41, 40.88, 31.70, 29.82, 29.04 (2C), 26.41, 22.61, 14.08, 11.32. The phenylic carbon atoms are not detectable due to a strong multipletation by coupling to fluorine.

^{19}F-NMR (376 MHz, $CDCl_3$, 298K) δ [ppm]: -140.20 – -140.78 (m, 2F), -149.86 (t, J_{F-F} = 20.8 Hz, 1F), -158.76 – -159.72 (m, 2F).

5.4.10 Synthesis of 1-Benzyl-3-octylimidazolium Perrhenates

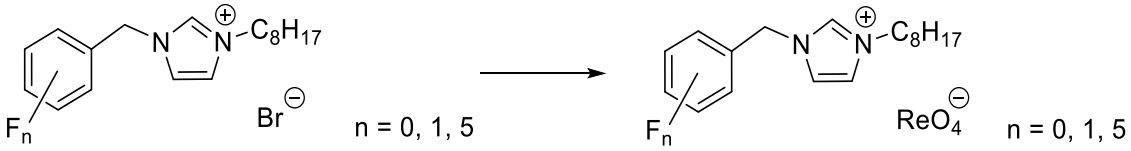

1.0 g of the respective benzylic octylimidazolium bromide (2.2-2.9 mmol, 1.0 eq.) is dissolved in 100 mL water and slowly rinsed over a thin column containing 25 g freshly regenerated Amberlite IRA 402 (OH) anion exchange resin within one hour. The basic fraction is collected, 1.2 eq. NH_4ReO_4 added and stirred for two hours at 60 °C. Then, the solution concentrated in vacuo. The remaining solution (ca. 40 mL) is extracted with DCM (3 × 50 mL). The organic solution is concentrated to 20 mL and filtered. The resulting white solid is dried in vacuo using a turbomolecular pump for 4 h at elevated temperature (60 -80 °C). The desired imidazolium perrhenates are obtained in >97 yield.

1-Benzyl-3-octylimidazolium perrhenate [BnOIM] [ReO_4]

^{1}H-NMR (400 MHz, $CDCl_3$, 298 K) δ [ppm]: 8.88 (s, 1H), 7.38 – 7.24 (m, 5H), 7.29 (s, 1H), 7.27 (s, 1H), 5.31 (s, 2H), 4.13 (t, *J* = 7.5 Hz, 2H), 1.81 (pseudo-p, *J* = 7.3 Hz, 2H), 1.28 – 1.14 (m, 10H), 0.79 (t, *J* = 6.7 Hz, 3H).

^{13}C{^{1}H}-NMR (101 MHz, $CDCl_3$, 298K) δ [ppm]: 135.54, 132.60, 129.70, 129.62 (s, 2C), 129.00 (s, 2C), 122.56, 122.46, 53.83, 50.55, 31.63, 30.08, 28.98, 28.85, 26.25, 22.57, 14.07.

1-(4'-Fluorobenzyl)-3-octylimidazolium perrhenate [F-BnOIM] [ReO_4]

^{1}H-NMR (400 MHz, $CDCl_3$, 298 K) δ [ppm]: 8.97 (s, 1H), 7.50 – 7.41 (m, 2H), 7.32 (d, *J* = 1.8 Hz, 1H), 7.30 (d, *J* = 1.8 Hz, 1H), 7.09 (t, *J* = 8.5 Hz, 2H), 5.39 (s, 2H), 4.20 (t, *J* = 7.5 Hz, 2H), 1.88 (pseudo-p, *J* = 7.5 Hz, 2H), 1.36 – 1.17 (m, 10H), 0.85 (t, *J* = 6.8 Hz, 3H).

^{13}C{^{1}H}-NMR (101 MHz, $CDCl_3$, 298K) δ [ppm]: 163.36 (d, $J_{C\text{-}F}$ = 249.8 Hz), 135.70, 131.25 (d, $J_{C\text{-}F}$ = 8.6 Hz, 2C), 128.49, 122.43, 122.28, 116.71 (d, $J_{C\text{-}F}$ = 22.0 Hz, 2C), 53.10, 50.62, 31.64, 30.06, 28.99, 28.86, 26.28, 22.57, 14.06.

^{19}F-NMR (376 MHz, $CDCl_3$, 298K) δ [ppm]: -110.81.

1-(2',3',4',5',6'-Pentafluorobenzyl)-3-octylimidazolium perrhenate [^{F}BnOIM] [ReO_4]

^{1}H-NMR (400 MHz, $CDCl_3$, 298 K) δ [ppm]: 9.03 (s, 1H), 7.44 (t, *J* = 1.8 Hz, 1H), 7.41 (t, *J* = 1.8 Hz, 1H), 5.63 (s, 2H), 4.24 (t, *J* = 7.5 Hz, 2H), 1.90 (pseudo-p, *J* = 7.0 Hz, 2H), 1.39 – 1.17 (m, 10H), 0.85 (t, *J* = 6.7 Hz, 3H).

^{13}C{^{1}H}-NMR (101 MHz, $CDCl_3$, 298K) δ [ppm]: 136.54, 123.14, 122.69, 77.48, 77.16, 76.84, 50.93, 40.80, 31.75, 30.12, 29.10, 28.98, 26.36, 22.68, 14.14. The phenylic carbon atoms are not detectable due to a strong multiplettation by coupling to fluorine.

^{19}F-NMR (376 MHz, $CDCl_3$, 298K) δ [ppm]: -141.02 – -141.52 (m, 2F), -149.34 (tt, J_{F-F} = 21.1, 3.3 Hz, 1F), -158.84 – -159.60 (m, 2F).

1-(2',3',4',5',6'-Pentafluorobenzyl)-2-methyl-3-octylimidazolium perrhenate [^{F}BnOMIM] [ReO_4]

^{1}H-NMR (400 MHz, $CDCl_3$, 298 K) δ [ppm]: 7.35 (d, *J* = 2.2 Hz, 1H), 7.31 (d, *J* = 2.2 Hz, 1H), 5.49 (s, 2H), 4.09 (t, *J* = 7.7 Hz, 2H), 2.75 (s, 3H), 1.82 (p, *J* = 7.4 Hz, 2H), 1.38 – 1.19 (m, 10H), 0.85 (t, *J* = 7.0 Hz, 3H).

^{13}C{^{1}H}-NMR (101 MHz, $CDCl_3$, 298K) δ [ppm]: 144.41, 121.93, 121.85, 49.25, 39.51, 31.74, 29.59, 29.09, 29.04, 26.46, 22.66, 14.12, 9.58. The phenylic carbon atoms are not detectable due to a strong multipletation by coupling to fluorine.

^{19}F-NMR (376 MHz, $CDCl_3$, 298K) δ [ppm]: -140.30 – -141.24 (m, 2F), -149.85 (t, J_{F-F} = 20.8 Hz, 1F), -158.89 – -160.08 (m, 2F).

5.4.11 Miscellaneous Compounds

Synthesis of 1-Octyl-(2,)3-(di)methylimidazolium perrhenate according to an adapted literature protocol.[105]

29 mmol of the corresponding bromide IL ([OMIM] Br and [OMMIM] Br, 1.0 eq.) were dissolved in 400 mL water and slowly rinsed over a column filled with 120 g freshly regenerated Amberlite IRA 402 (OH) anion exchange resin within four hours and rinsed with water until the eluate was pH neutral. The basic fraction was collected and 32 mmol NH_4ReO_4 (8.58 g, 1.1 eq.) were added before the solution is stirred for 2 h at 70 °C. Then, the water was removed in vacuo, the liquid residue dissolved in 50 mL DCM and filtrated. The solvent was removed and the products dried under fine vacuum at 70 °C. The desired perrhenate ILs obtained as a colorless liquid ([OMIM] [ReO_4]) or solid ([OMMIM] [ReO_4]) in >96% yield.

1-Octyl-3-methylimidazolium perrhenate [OMIM] [ReO_4]

^{1}H-NMR (400 MHz, $CDCl_3$, 298 K) δ [ppm]: 8.70 (t, *J* = 1.8 Hz, 1H), 7.37 (t, *J* = 1.8 Hz, 1H), 7.34 (t, *J* = 1.8 Hz, 1H), 4.12 (t, *J* = 7.4 Hz, 2H), 3.90 (s, 3H), 1.80 (pseudo-p, *J* = 7.3 Hz, 2H), 1.30 – 1.12 (m, 10H), 0.75 (t, *J* = 7.0 Hz, 2H).

^{13}C{^{1}H}-NMR (101 MHz, $CDCl_3$, 298K) δ [ppm]: 135.83, 123.75, 122.32, 50.18, 36.27, 31.42, 29.93, 28.75, 28.65, 26.02, 22.34, 13.86.

Elemental analysis for $C_{12}H_{23}N_2O_4Re$ calc. (%): C 32.35, H 5.20, N 6.29, O 14.36, Re 41.79; found: C 32.26, H 5.27, N 6.42, Re 41.34.

1-Octyl-2,3-dimethylimidazolium perrhenate [OMMIM] [ReO_4]

^{1}H-NMR (400 MHz, $CDCl_3$, 298 K) δ [ppm]: 7.31 (d, *J* = 2.1 Hz, 1H), 7.24 (d, *J* = 2.1 Hz, 1H), 4.07 (t, *J* = 7.5 Hz, 2H), 3.85 (s, 3H), 2.65 (s, 3H), 1.80 (pseudo-p, *J* = 7.5 Hz, 2H), 1.37 – 1.21 (m, 10H), 0.85 (t, *J* = 6.8 Hz, 3H).

^{13}C{^{1}H}-NMR (101 MHz, $CDCl_3$, 298K) δ [ppm]: 143.82, 122.81, 121.05, 48.97, 35.37, 31.73, 29.77, 29.08, 29.04, 26.44, 22.63, 14.13, 9.56.

Elemental analysis for $C_{13}H_{25}N_2O_4Re$ calc. (%): C 33.98, H 5.48, N 6.10, O 13.93, Re 40.52; found: C 33.60, H 5.73, N 6.26, Re 40.14.

1-Octyl-3-methylimidazolium tetrafluoroborate [OMIM] [BF_4]

[OMIM] [BF_4] was synthesized by equimolar addition of 6.92 g [OMIM] Cl (30 mmol, 1.0 eq.) and 3.29 g Na[BF_4] (30 mmol, 1.0 eq.) to 200 mL water. The solution was stirred for 24 h at room temperature and extracted with dichloromethane (3 × 100 mL). The organic phases were combined and washed with water (2 × 50 mL) prior to evaporation of the solvent under reduced pressure. After drying under high vacuum (10^{-6} mbar), 8.23 g (29 mmol) of the ionic liquid [OMIM] [BF_4] were obtained in 97% yield and stored under argon until use.

^{1}H-NMR (400 MHz, $CDCl_3$, 298 K) δ [ppm]: 8.70 (s, 1H), 7.33 (s, 1H), 7.26 (s, 1H), 4.10 (t, *J* = 6.6 Hz, 2H), 3.87 (s, 3H), 1.84 – 1.76 (m, 2H), 1.27 – 1-16 (m, 10H), 0.80 (t, *J* = 6.9 Hz, 3H).

^{11}B-NMR (128 MHz, $CDCl_3$, 298 K) δ [ppm]: − 0.99.

^{13}C{^{1}H}-NMR (101 MHz, $CDCl_3$, 298K) δ [ppm]: 136.29, 123.75, 122.11, 50.09, 36.23, 31.65, 30.03, 28.98, 28.87, 26.17, 22.55, 14.02.

^{19}F-NMR (376 MHz, $CDCl_3$, 298K) δ [ppm]: −151.

1-Octyl-3-methylimidazolium tetraphenylborate [OMIM] [BPh_4]

941 mg [OMIM] Cl (4.1 mmol, 1.0 eq.) and 1.40 g sodium tetraphenylborate (4.1 mmol, 1.0 eq.) are stirred in 4 mL acetone for 48 h. The insoluble sodium chloride is filtered off over celite and the solvent is evaporated. 1.65 g [OMIM] [BPh_4] (79%, 3.2 mmol) are obtained as a white solid.

^{1}H-NMR (400 MHz, DMSO-d_6, 298 K) δ [ppm]: 9.06 (s, 1H), 7.74 (d, J = 1.9 Hz, 1H), 7.67 (d, J = 1.8 Hz, 1H), 7.18 (t, J = 5.9 Hz, 8H), 6.92 (t, J = 7.3 Hz, 8H), 6.79 (t, J = 7.2 Hz, 4H), 4.12 (t, J = 7.2 Hz, 2H), 3.82 (s, 3H), 1.76 (pseudo-p, J = 7.3 Hz, 2H), 1.32 – 1.18 (m, 10H), 0.86 (t, J = 6.5 Hz, 3H).

^{11}B-NMR (128 MHz, DMSO-d_6, 298 K) δ [ppm]: −6.67 (m).

^{13}C{^{1}H}-NMR (101 MHz, DMSO-d_6) δ [ppm]: 163.34 (q, $J_{B\text{-}C}$ = 49.2 Hz, 4C), 136.43, 135.51 (s, 8C), 125.26 (s, 8C), 123.59, 122.24, 121.49 (s, 4C), 48.75, 35.73, 31.15, 29.36, 28.46, 28.32, 25.48, 22.05, 13.94.

Elemental Analysis for $C_{36}H_{43}BN_2$ calc. (%): C 84.03, H 8.42, B 2.10, N 5.44; found: C 83.61, H 8.68, N 5.52.

1-Octyl-2,3-dimethylimidazolium tetraphenylborate [OMMIM] [BPh_4]

572 mg [OMMIM] Cl (2.3 mmol, 1.0 eq.) and 800 mg sodium tetraphenylborate (2.3 mmol, 1.0 eq.) are stirred in 2 mL acetone for 48 hours. The insoluble sodium chloride is filtered off over celite and the solvent is evaporated. 1.17 g [OMMIM] [BPh_4] (95%, 2.2 mmol) are obtained as a white solid.

^{1}H-NMR (400 MHz, DMSO-d_6, 298 K) δ [ppm]: 7.58 (d, J = 2.1 Hz, 1H), 7.54 (d, J = 2.1 Hz, 1H), 7.22 (td, J = 6.1, 2.9 Hz, 8H), 6.95 (t, J = 7.3 Hz, 8H), 6.81 (t, J = 7.1 Hz, 4H), 4.03 (t, J = 7.4 Hz, 2H), 3.67 (s, 3H), 3.45 (s, 1H), 2.54 – 2.48 (m, 5H), 2.49 (s, 4H), 1.68 (p, J = 7.2 Hz, 2H), 1.34 – 1.22 (m, 10H), 0.88 (t, J = 6.6 Hz, 3H).

^{11}B-NMR (128 MHz, DMSO-d_6, 298 K) δ [ppm]: −6.64 (m).

^{13}C{^{1}H}-NMR (101 MHz, DMSO-d_6, 298 K) δ [ppm]: 163.39 (q, $J_{B\text{-}C}$ = 49.5 Hz, 4C), 144.09, 135.56 (q, $J_{B\text{-}C}$ = 1.3 Hz, 8C), 125.32 (q, $J_{B\text{-}C}$ = 2.8 Hz, 8C), 122.25, 121.53 (s, 4C), 120.81, 47.48, 34.60, 31.19, 29.18, 28.55, 28.47, 25.60, 22.08, 13.96, 9.04.

Cetyltrimethylammonium nitrate [CTA] [NO_3]

2.00 g cetyltrimethylammonium bromide (CTAB, 5.5 mmol) were dissolved in 500 mL pure water and slowly rinsed over a column filled with 120 g freshly regenerated Amberlite IRA 402 (OH) anion exchange resin. The basic eluate is collected and neutralized with 2% nitric acid to pH = 7.0 using a calibrated pH-meter. The water is carefully evaporated under reduced pressure at 80 °C due to the vast foaming of the solution. The residual colorless liquid is further dried under high vacuum using a turbomolecular pump (10^{-6} mbar) and stored under argon until further use. 1.82 g cetyltrimethylammonium nitrate ([CTA] [NO_3], 96%, 5.3 mmol) are obtained as a white solid.

^{1}H-NMR (400 MHz, $CDCl_3$, 298 K) δ [ppm]: 3.40 – 3.31 (m, 2H), 3.21 (s, 9H), 1.76 (pseudo-dq, *J* = 8.6, 5.4, 4.1 Hz, 2H), 1.40 – 1.25 (m, 4H), 1.26 (s, 22H), 0.88 (t, *J* = 7.1 Hz, 3H).

^{13}C{^{1}H}-NMR (101 MHz, $CDCl_3$, 298 K) δ [ppm]: 67.27, 53.27 (s, 3C), 31.91, 30.00 – 28.84 (m, 10C), 26.12, 23.11, 22.69, 14.11.

5.5 Supplementary Data

5.5.1 Imidazolium Tungstates

Kinetic Investigations and Arrhenius Plot

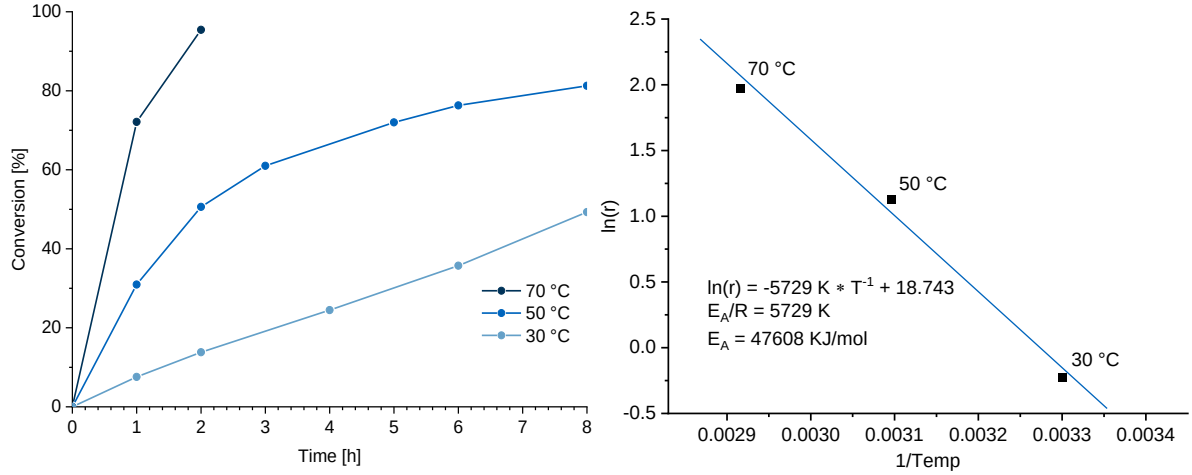

Supplementary Figure 1: Kinetic plots of the epoxidation of COE with $[OMIM]_2[WO_4]$ at various temperatures (left) and Arrhenius plot of the respective maximum reaction rates (right). Conditions: $[OMIM]_2[WO_4]$:COE:H_2O_2 = 5:100:250. The rate was determined from the first hour section.

Tensiometric Data

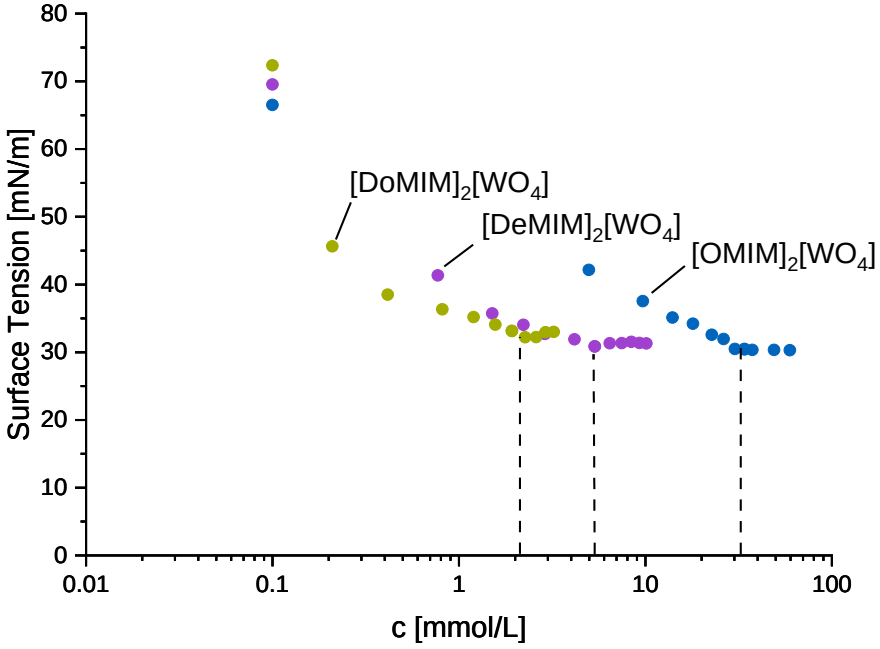

Supplementary Figure 2: Tensiometry measurement of various $[RMIM]_2[WO_4]$ ILs in 50 wt.% H_2O_2 at 50 °C. The respective CMCs are indicated by the dashed lines.

5.5.2 Imidazolium Phosphates

DLS Measurements

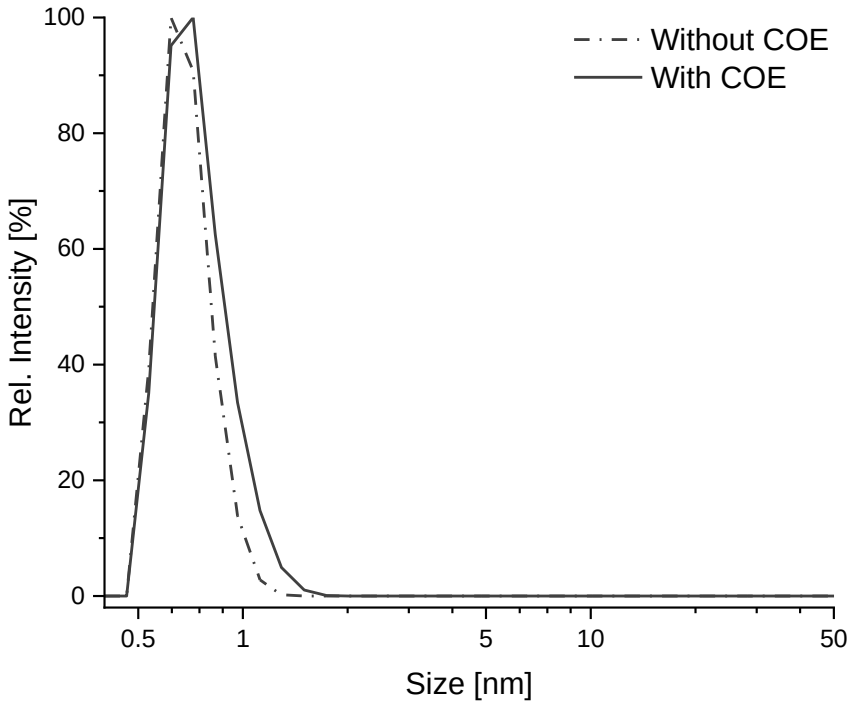

Supplementary Figure 3: DLS measurement of 357 mmol/L [OMIM] [$(HO)_2PO_2$] in 50 wt.% H_2O_2 at 80 °C prior (dashed) and after (bold) addition of excess COE.

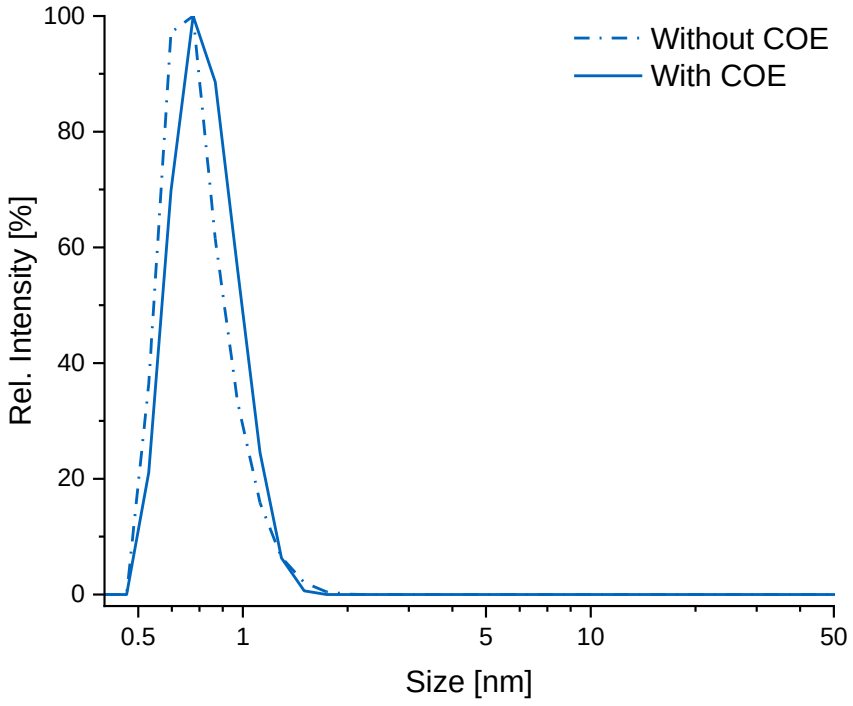

Supplementary Figure 4: DLS measurement of 357 mmol/L [OMIM] [$(MeO)_2PO_2$] in 50 wt.% H_2O_2 at 80 °C prior (dashed) and after (bold) addition of excess COE.

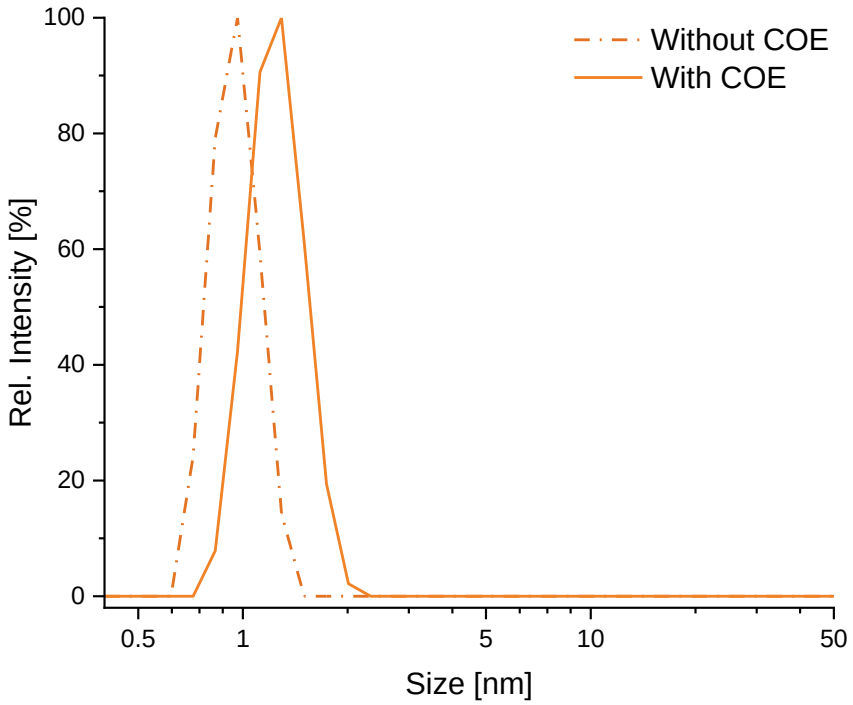

Supplementary Figure 5: DLS measurement of 357 mmol/L [OMIM] [$(EtO)_2PO_2$] in 50 wt.% H_2O_2 at 80 °C prior (dashed) and after (bold) addition of excess COE.

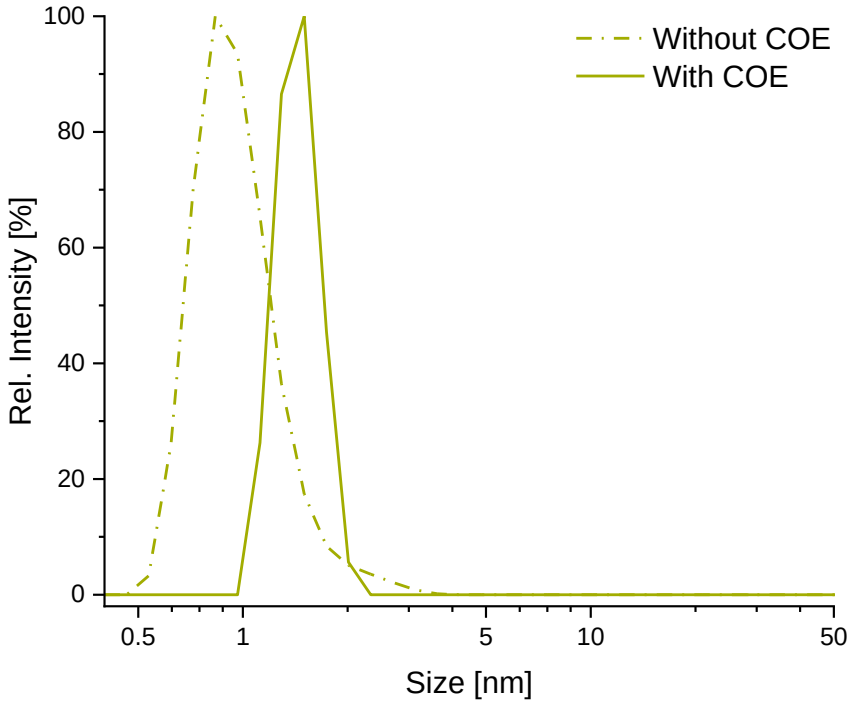

Supplementary Figure 6: DLS measurement of 357 mmol/L [OMIM] [$(^iPrO)_2PO_2$] in 50 wt.% H_2O_2 at 80 °C prior (dashed) and after (bold) addition of excess COE.

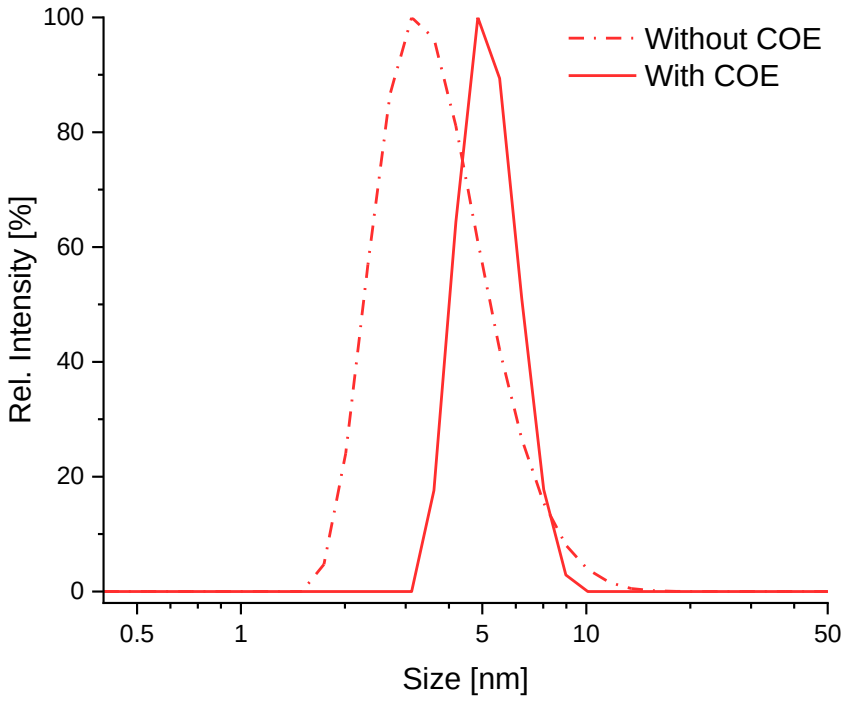

Supplementary Figure 7: DLS measurement of 357 mmol/L [OMIM] [$(PhO)_2PO_2$] in 50 wt.% H_2O_2 at 80 °C prior (dashed) and after (bold) addition of excess COE.

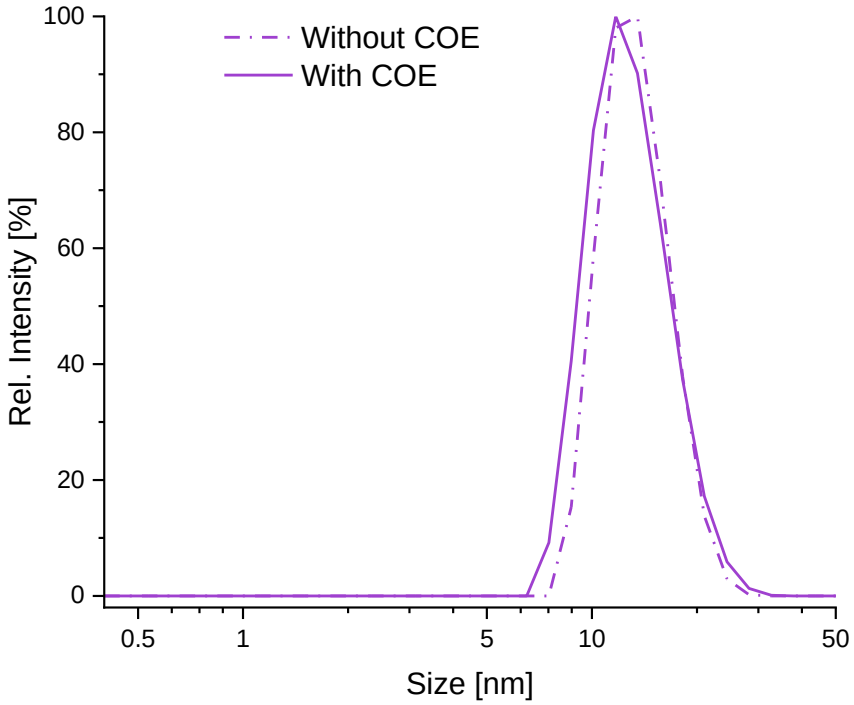

Supplementary Figure 8: DLS measurement of 357 mmol/L [OMIM] [$(MeOPhO)_2PO_2$] in 50 wt.% H_2O_2 at 80 °C prior (dashed) and after (bold) addition of excess COE.

Spectra of ^{31}P-NMR reference compounds.

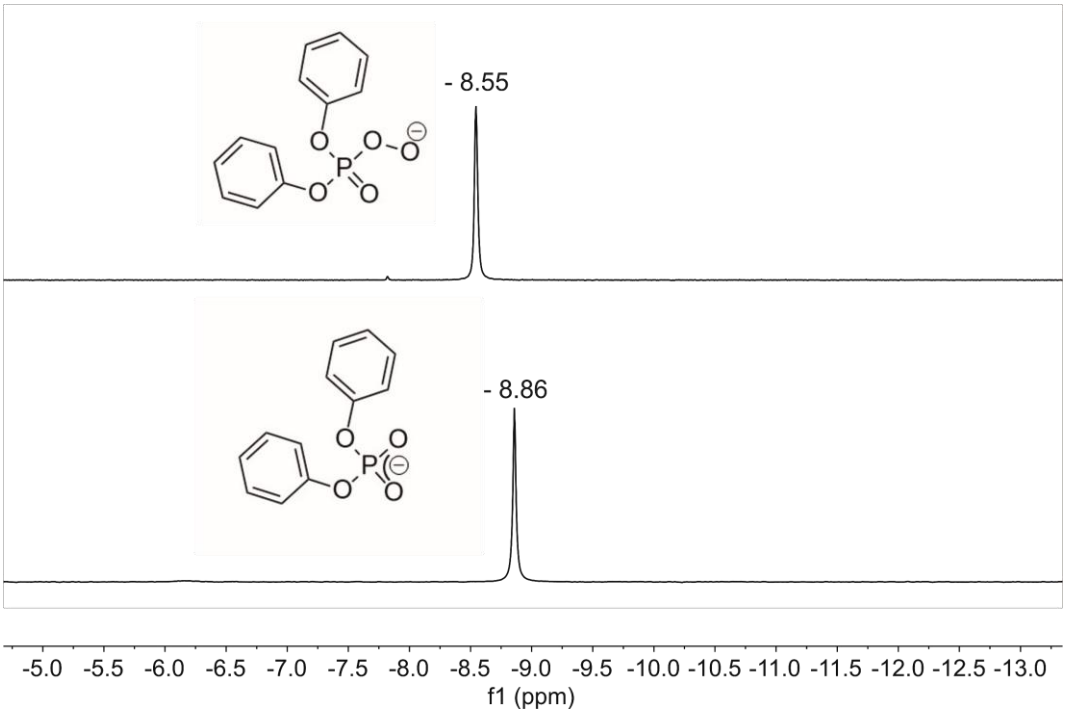

Supplementary Figure 9: ^{31}P-NMR shift comparison of sodium diphenylperoxophosphate (top) and sodium diphenylphosphate (bottom) in D_2O at room temperature.

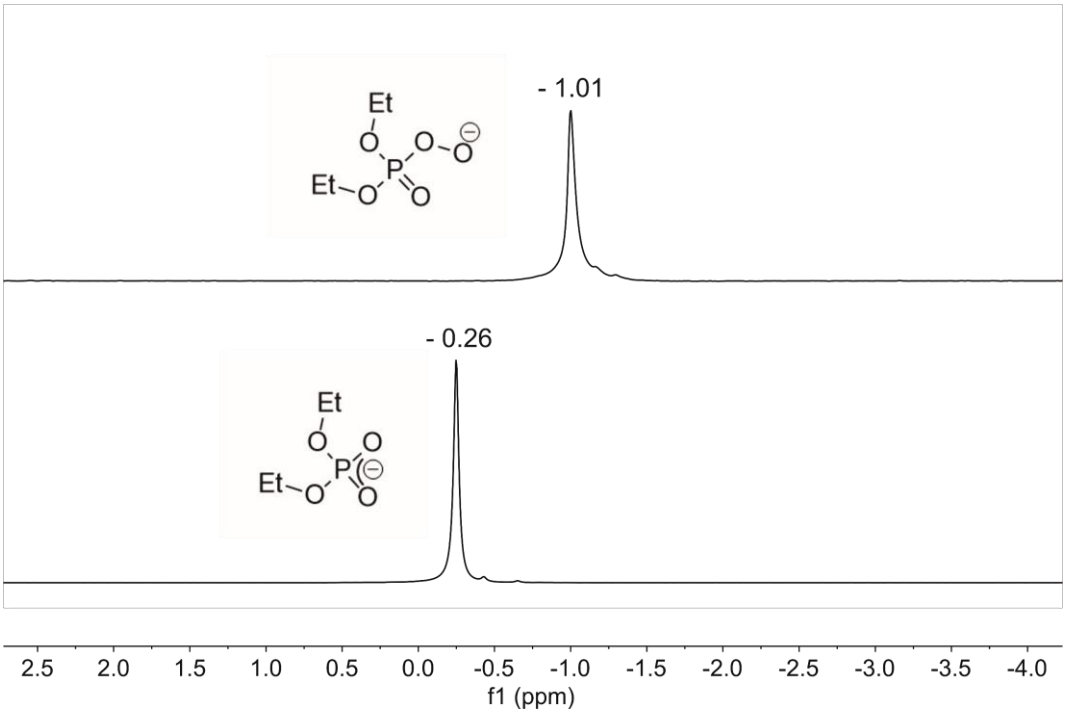

Supplementary Figure 10: ^{31}P-NMR shift comparison of sodium diethylperoxophosphate (top) and sodium diethylphosphate (bottom) in D_2O at room temperature.

5.5.3 Sulfate-based SIPs

DOSY-NMR investigation of L^1 and $[HL^1][HSO_4]$

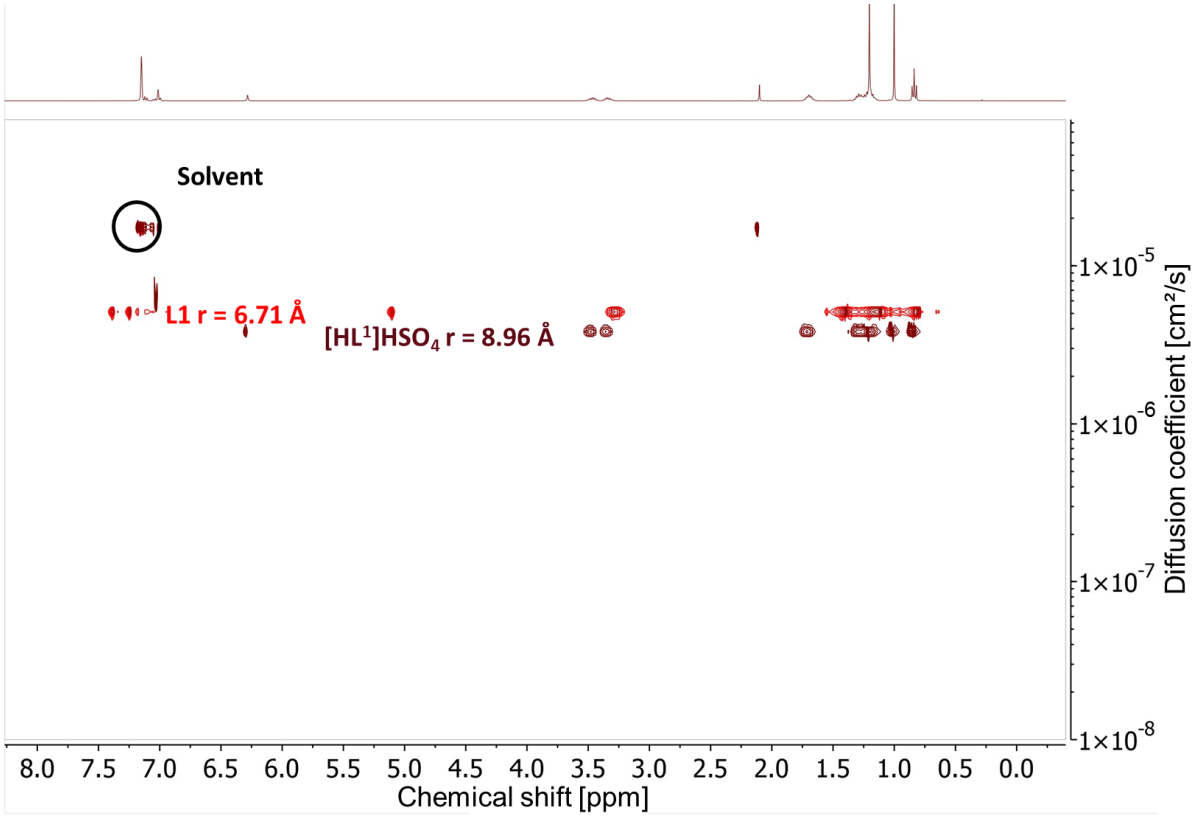

Supplementary Figure 11: Stacked DOSY-NMR spectra of L1 (red) and $[HL^1]HSO_4$ (dark red) in C_6D_6 at room temperature. The ^{1}H-NMR trace originates from the SIP experiment.

Single-Crystal X-Ray Diffraction

Supplementary Table 1: Crystallographic data of $[HL^1][HSO_4]$ and $[M^2]_2SO_4$, collected at 100 K.

Compound	**$C_{28}H_{51}N_3O_6S$**	**$C_{114}H_{218}N_{12}O_{22}S_3$**
Alias	$[HL^1][HSO_4]$	$[M^2]_2[SO_4]$
Empirical formula	$C_{28}H_{51}N_3O_6S$	$C_{114}H_{218}N_{12}O_{22}S_3$
Formula weight / $gmol^{-1}$	557.77	2205.17
Temperature / K	100.0	100.0
Crystal system	monoclinic	triclinic
Space group	$P2_1/c$	P-1
a / Å	12.6609(14)	18.986(3)
b / Å	23.926(3)	19.657(3)
c / Å	10.7098(12)	20.362(3)
α / °	90	67.784(4)
β / °	104.423(3)	68.760(5)
γ / °	90	74.819(4)
Volume / $Å^3$	3142.1(6)	6488.2(15)
Z	4	2
ρ_{calc} / gcm^{-3}	1.179	1.129
μ / mm^{-1}	0.145	0.123
F (000)	1216.0	2420.0
Crystal size / mm^{-3}	0.539 × 0.289 × 0.144	0.273 × 0.231 × 0.072
Radiation	$MoK_α$ (λ = 0.71073)	$MoK_α$ (λ = 0.71073)
2θ range for data collection / °	3.732 to 51.36	4.1 to 52.744
Index ranges	-15 ≤ h ≤ 15	-23 ≤ h ≤ 23
	-29 ≤ k ≤ 29	-24 ≤ k ≤ 24
	-13 ≤ l ≤ 13	-25 ≤ l ≤ 25
Reflections collected	105051	372834
Independent reflections	5969 [R_{int} = 0.0653]	26540 [R_{int} = 0.0713]
	[R_{sigma} = 0.0256]	[R_{sigma} = 0.0267]
Data/restraints/parameters	5969/0/356	26540/0/1385
Goodness of fit on F^2	1.258	1.091
Final R indexes [I > 2σ (I)]	R_1 = 0.0664, wR_2 = 0.1270	R_1 = 0.0499, wR_2 = 0.1084
Final R indexes [all data]	R_1 = 0.0703, wR_2 = 0.1287	R_1 = 0.0605, wR_2 = 0.1133
Largest diff. peak/hole / e $Å^{-3}$	0.44/-0.42	0.35/-0.46

5.5.4 Temperature-responsive Catalysts

DLS Measurements

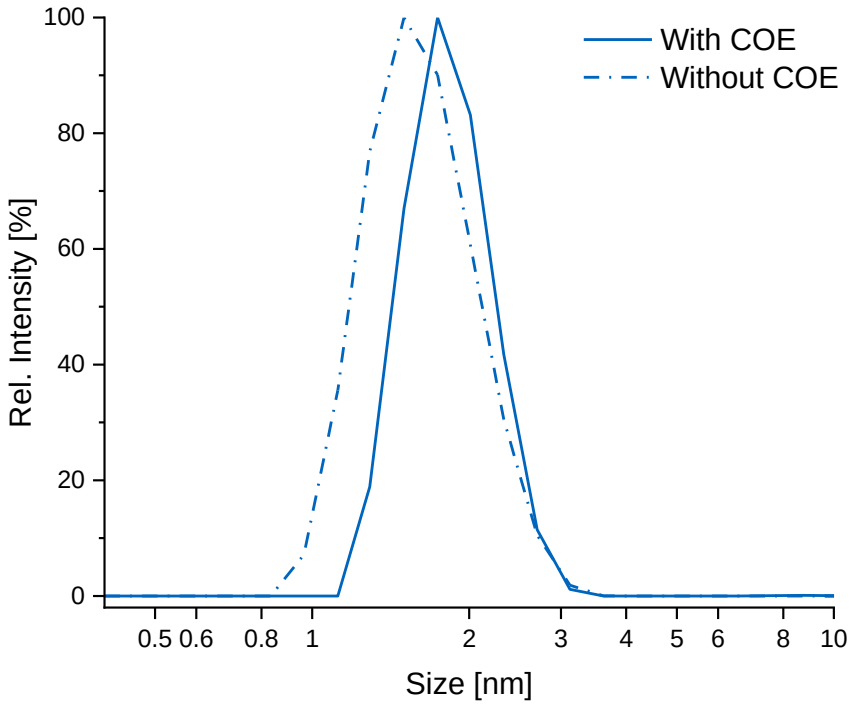

Supplementary Figure 12: DLS Measurement of a 357 mmol/L solution of [OMIM] [ReO_4] in 50 wt.% H_2O_2 at 80 °C prior (dashed) and after (bold) addition of excess COE.

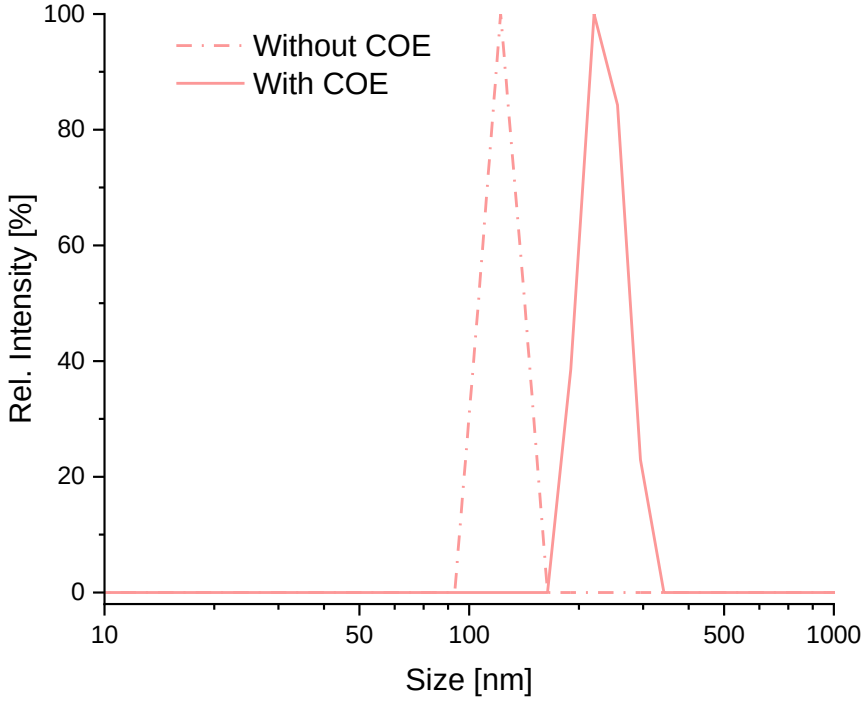

Supplementary Figure 13: DLS Measurement of a saturated solution of [^{F}BnOIM] [ReO_4] in 50 wt.% H_2O_2 at 80 °C prior (dashed) and after (bold) addition of excess COE.

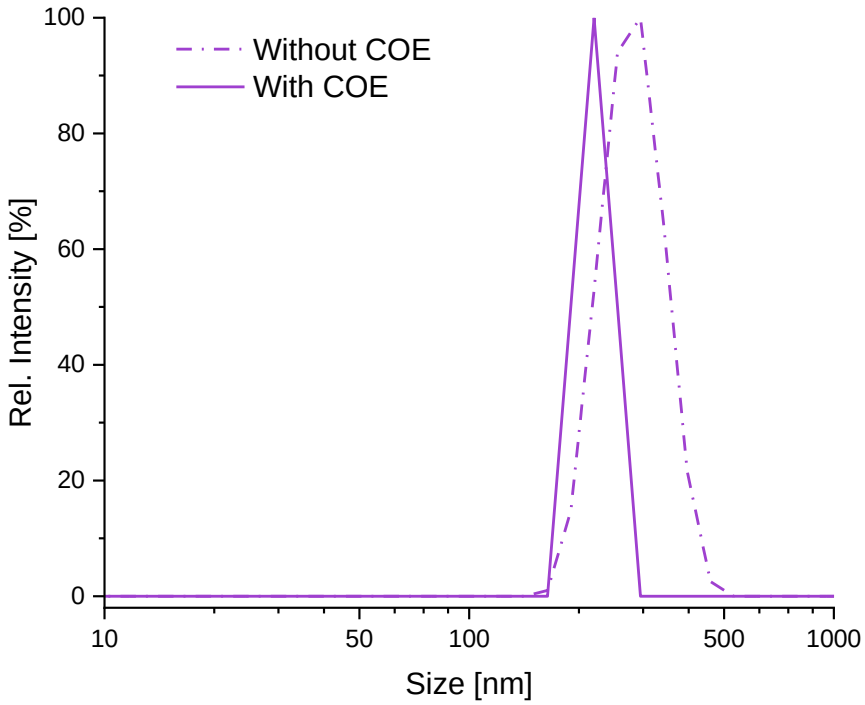

Supplementary Figure 14: DLS Measurement of a saturated solution of [^{F}BnOMIM] [ReO_4] in 50 wt.% H_2O_2 at 80 °C prior (dashed) and after (bold) addition of excess COE.

6 References

[1] J. M. Lehn, *Acc. Chem. Res.* **1978**, *11*, 49.

[2] J. W. Steed, J. L. Atwood, P. A. Gale in *Definition and Emergence of Supramolecular ChemistryAdapted in part from Supramolecular Chemistry , J. W. Steed and J. L. Atwood, Wiley: Chichester, 2nd Ed., 2009* (Eds.: J. W. Steed, J. L. Atwood, P. A. Gale), John Wiley & Sons, Ltd, Chichester, UK, **2012**.

[3] P. J. Cragg, *Supramolecular Chemistry*, Springer Netherlands, Dordrecht, **2010**.

[4] Lindoy, Leonard F., Atkinson, Ian M., *Self Assembly in Supramolecular Systems*, Royal Society of Chemistry, Cambridge, **2007**.

[5] A. J. Savyasachi, O. Kotova, S. Shanmugaraju, S. J. Bradberry, G. M. Ó'Máille, T. Gunnlaugsson, *Chem* **2017**, *3*, 764.

[6] G. T. Williams, C. J. E. Haynes, M. Fares, C. Caltagirone, J. R. Hiscock, P. A. Gale, *Chem. Soc. Rev.* **2021**, *50*, 2737.

[7] J.-M. Lehn, *Chem. Soc. Rev.* **2017**, *46*, 2378.

[8] K. L. Wolf, H. Prahm, H. Harms, *Z. Phys. Chem.* **1937**, *36B*, 237.

[9] J. D. Watson, F. H. Crick, *Nature* **1953**, *171*, 737.

[10] W. C. de Vries, B. J. Ravoo, *Vesicles and Micelles; in: Supramolecular Chemistry in Water (S. Kubik Ed.)*, Wiley-VCH, Weinheim, **2019**.

[11] C. J. Pedersen, *J. Am. Chem. Soc.* **1967**, *89*, 7017.

[12] P. B. Smith, J. L. Dye, J. Cheney, J. M. Lehn, *J. Am. Chem. Soc.* **1981**, *103*, 6044.

[13] T. J. Haverlock, P. V. Bonnesen, R. A. Sachleben, B. A. Moyer, *J. Inclusion Phenom. Macrocyclic Chem.* **2000**, *36*, 21.

[14] T. Le Minh, T. Lengyel, *J. Radioanal. Nucl. Chem.* **1989**, *135*, 403.

[15] T. Gunnlaugsson, M. Nieuwenhuyzen, L. Richard, V. Thoss, *Tetrahedron Lett.* **2001**, *42*, 4725.

[16] C. J. Ward, P. R. Ashton, T. D. James, P. Patel, *Chem. Commun.* **2000**, 229.

[17] P. W. N. M. van Leeuwen, *Supramolecular Catalysis*, Wiley-VCH, Weinheim, **2008**.

[18] E. Anslyn, R. Breslow, *J. Am. Chem. Soc.* **1989**, *111*, 8931.

[19] R. Breslow, C. Schmuck, *J. Am. Chem. Soc.* **1996**, *118*, 6601.

[20] K. Shirahama, T. Kashiwabara, *J. Colloid Interface Sci.* **1971**, *36*, 65.

[21] N. Muller, *Langmuir* **1993**, *9*, 96.

[22] T. Lorenzetto, G. Berton, F. Fabris, A. Scarso, *Catal. Sci. Technol.* **2020**, *10*, 4492.

[23] P. Anastas, N. Eghbali, *Chem. Soc. Rev.* **2010**, *39*, 301.

[24] B. H. Lipshutz, S. Ghorai, M. Cortes-Clerget, *Chem. Eur. J.* **2018**, *24*, 6672.

[25] G. La Sorella, G. Strukul, A. Scarso, *Green Chem.* **2015**, *17*, 644.

[26] S. Ebnesajjad, *Surface Tension and Its Measurement, in: Handbook of Adhesives and Surface Preparation*. *Surface Tension and Its Measurement*, William Andrew Publishing, Norwich, NY, **2011**.

[27] B. Aveyard, *Surfactants*. *In Solution, at Interfaces and in Colloidal Dispersions*, Oxford University Press, Oxford, **2019**.

[28] K. Lunkenheimer, K.-D. Wantke, *Colloid. Polym. Sci.* **1981**, *259*, 354.

[29] C. Della Volpe, S. Siboni, *Surf. Innovations* **2018**, *6*, 120.

[30] I. Mukherjee, S. P. Moulik, A. K. Rakshit, *J. Colloid Interface Sci.* **2013**, *394*, 329.

[31] D. Stigter, *J. Phys. Chem.* **1975**, *79*, 1008.

[32] B. Andersson, G. Olofsson, *J. Chem. Soc., Faraday Trans. 1* **1988**, *84*, 4087.

[33] T. L. Greaves, C. J. Drummond, *Chem. Soc. Rev.* **2008**, *37*, 1709.

[34] C. Tanford, *J. Phys. Chem.* **1972**, *76*, 3020.

[35] J. N. Israelachvili, D. J. Mitchell, B. W. Ninham, *J. Chem. Soc., Faraday Trans. 2* **1976**, *72*, 1525.

[36] A. R. Bhat, F. A. Wani, K. A. Alzahrani, A. A. Alshehri, M. A. Malik, R. Patel, *J. Mol. Liq.* **2019**, *292*, 111347.

[37] B. Dong, N. Li, L. Zheng, L. Yu, T. Inoue, *Langmuir* **2007**, *23*, 4178.

[38] X. Wang, L. Yu, J. Jiao, H. Zhang, R. Wang, H. Chen, *J. Mol. Liq.* **2012**, *173*, 103.

[39] C. Tanford, *PNAS* **1974**, *71*, 1811.

[40] R. C. Oliver, J. Lipfert, D. A. Fox, R. H. Lo, S. Doniach, L. Columbus, *PloS one* **2013**, *8*, e62488.

[41] S. Weisenburger, V. Sandoghdar, *Contemporary Physics* **2015**, *56*, 123.

[42] C. A. Gracia, S. Gómez-Barreiro, A. González-Pérez, J. Nimo, J. R. Rodríguez, *J. Colloid Interface Sci.* **2004**, *276*, 408.

[43] J. Lipfert, L. Columbus, V. B. Chu, S. A. Lesley, S. Doniach, *J. Phys. Chem. B* **2007**, *111*, 12427.

[44] J. N. Israelachvili, *Thermodynamic Principles of Self-Assembly*, Academic Press, Cambridge, MA, **2011**.

[45] P. Becher, *Encyclopedia of emulsion technology*, Dekker, New York, NY, **1996**.

[46] W. D. Bancroft, *J. Phys. Chem.* **1913**, *17*, 501.

[47] W. D. Bancroft, *J. Phys. Chem.* **1915**, *19*, 275.

[48] J. Sjoblom, *Encyclopedic Handbook of Emulsion Technology*, CRC Press, Boca Ranton, **2001**.

[49] V. Lutz-Bueno, S. Isabettini, F. Walker, S. Kuster, M. Liebi, P. Fischer, *Phys. Chem. Chem. Phys.* **2017**, *19*, 21869.

[50] H. B. Klevens, *Chem. Rev.* **1950**, *47*, 1.

[51] J. W. McBain, P. H. Richards, *Ind. Eng. Chem.* **1946**, *38*, 642.

[52] T. Dwars, E. Paetzold, G. Oehme, *Angew. Chem. Int. Ed.* **2005**, *44*, 7174.

[53] A. K. Yatsimirski, K. Martinek, I. V. Berezin, *Tetrahedron* **1971**, *27*, 2855.

[54] S. Otto, J. B. F. N. Engberts, J. C. T. Kwak, *J. Am. Chem. Soc.* **1998**, *120*, 9517.

[55] P. Mukerjee, K. L. Mittal, *Solubilization in Aqueous Micellar Systems; in: Solution Chemistry of Surfactants*, Springer New York, Boston, MA, **1979**.

[56] Sienel, G., Rieth, R. and Rowbottom, K.T., *Epoxides. In Ullmann's Encyclopedia of Industrial Chemistry*, Wiley-VCH, Weinheim, **2000**.

[57] A. K. Yudin, *Aziridines and Epoxides in Organic Synthesis*, Wiley, Weinheim, **2006**.

[58] W. H. Faveere, S. van Praet, B. Vermeeren, K. N. R. Dumoleijn, K. Moonen, E. Taarning, B. F. Sels, *Angew. Chem. Int. Ed.* **2021**, *60*, 12204.

[59] Rebsdat, S., Mayer, D., *Ethylene Oxide. In Ullmann's Encyclopedia of Industrial Chemistry*, Wiley-VCH, Weinheim, **2001**.

[60] Baer, H., Bergamo, M., Forlin, A., Pottenger, L.H. and Lindner, J., *Propylene Oxide. In Ullmann's Encyclopedia of Industrial Chemistry*, Wiley-VCH, Weinheim, **2012**.

[61] M. Dusi, T. Mallat, A. Baiker, *Catal. Rev.* **2000**, *42*, 213.

[62] G. de Faveri, G. Ilyashenko, M. Watkinson, *Chem. Soc. Rev.* **2011**, *40*, 1722.

[63] M. O. Özbek, R. A. van Santen, *Catal. Letters* **2013**, *143*, 131.

[64] T. Punniyamurthy, S. Velusamy, J. Iqbal, *Chem. Rev.* **2005**, *105*, 2329.

[65] J. García-Serna, T. Moreno, P. Biasi, M. J. Cocero, J.-P. Mikkola, T. O. Salmi, *Green Chem.* **2014**, *16*, 2320.

[66] G. Grigoropoulou, J. H. Clark, J. A. Elings, *Green Chem.* **2003**, *5*, 1.

[67] F. Schmidt, M. Cokoja, *Green Chem.* **2021**, *23*, 708.

[68] B. H. Lipshutz, S. Ghorai, *Green Chem.* **2014**, *16*, 3660.

[69] S.-S. Wang, G.-Y. Yang, *Chem. Rev.* **2015**, *115*, 4893.

[70] G. Grigoropoulou, J. H. Clark, J. A. Elings, *Green Chem.* **2003**, *5*, 1.

[71] Y. Zhou, Z. Guo, W. Hou, Q. Wang, J. Wang, *Catal. Sci. Technol.* **2015**, *5*, 4324.

[72] Wu, Lixin, Samahe Sadjadi, *Organically Encapsulated Polyoxometalate Catalysts: Supramolecular Composition and Synergistic Catalysis, in: Encapsulated Catalysts*, Academic Press, Cambridge, Massachusets, **2017**.

[73] W. Qi, Y. Wang, W. Li, L. Wu, *Chemistry* **2010**, *16*, 1068.

[74] C. Venturello, E. Alneri, M. Ricci, *J. Org. Chem.* **1983**, *48*, 3831.

[75] C. Venturello, R. D'Aloisio, J. C. Bart, M. Ricci, *J. Mol. Catal.* **1985**, *32*, 107.

[76] C. Venturello, R. D'Aloisio, *J. Org. Chem.* **1988**, *53*, 1553.

[77] Y. Ishii, K. Yamawaki, T. Ura, H. Yamada, T. Yoshida, M. Ogawa, *J. Org. Chem.* **1988**, *53*, 3587.

[78] Y. Ishii, K. Yamawaki, T. Yoshida, T. Ura, M. Ogawa, *J. Org. Chem.* **1987**, *52*, 1868.

[79] C. Aubry, G. Chottard, N. Platzer, J. M. Bregeault, R. Thouvenot, F. Chauveau, C. Huet, H. Ledon, *Inorg. Chem.* **1991**, *30*, 4409.

[80] D. C. Duncan, R. C. Chambers, E. Hecht, C. L. Hill, *J. Am. Chem. Soc.* **1995**, *117*, 681.

[81] J. Gao, Y. Chen, B. Han, Z. Feng, C. Li, N. Zhou, S. Gao, Z. Xi, *J. Mol. Catal. A: Chem.* **2004**, *210*, 197.

[82] G. Maayan, R. H. Fish, R. Neumann, *Org. Lett.* **2003**, *5*, 3547.

[83] H. Hamamoto, Y. Suzuki, Y. M. A. Yamada, H. Tabata, H. Takahashi, S. Ikegami, *Angew. Chem. Int. Ed.* **2005**, *44*, 4536.

[84] L. Hua, J. Chen, C. Chen, W. Zhu, Y. Yu, R. Zhang, L. Guo, B. Song, H. Gan, Z. Hou, *New J. Chem.* **2014**, *38*, 3953.

[85] Xi Zuwei, Zhou Ning, Sun Yu, Li Kunlan, *Science* **2001**, *292*, 1139.

[86] S. S. Lele, R. R. Bhave, M. M. Sharma, *Chem. Eng. Sci.* **1983**, *38*, 765.

[87] R. Neumann, A. M. Khenkin, *J. Org. Chem.* **1994**, *59*, 7577.

[88] T.-H. H. Maw-Ling Wang, *React. Kinet. Catal. Lett.* **2003**, *78*, 275.

[89] K. Kamata, K. Yonehara, Y. Sumida, K. Yamaguchi, S. Hikichi, N. Mizuno, *Science* **2003**, *300*, 964.

[90] B. Ma, W. Zhao, F. Zhang, Y. Zhang, S. Wu, Y. Ding, *RSC Adv.* **2014**, *4*, 32054.

[91] D. G. Kurth, P. Lehmann, D. Volkmer, H. Cölfen, M. J. Koop, A. Müller, A. Du Chesne, *Chem. Eur. J.* **2000**, *6*, 385.

[92] A. Nisar, J. Zhuang, X. Wang, *Chem. Mater.* **2009**, *21*, 3745.

[93] A. Nisar, Y. Lu, J. Zhuang, X. Wang, *Angew. Chem. Int. Ed.* **2011**, *50*, 3187.

[94] H. Li, H. Sun, W. Qi, M. Xu, L. Wu, *Angew. Chem. Int. Ed.* **2007**, *46*, 1300.

[95] P. T. Witte, P. L. Alsters, W. Jary, R. Müllner, P. Pöchlauer, D. Sloboda-Rozner, R. Neumann, *Org. Process Res. Dev.* **2004**, *8*, 524.

[96] P. T. Witte, S. R. Chowdhury, J. E. ten Elshof, D. Sloboda-Rozner, R. Neumann, P. L. Alsters, *Chem. Commun.* **2005**, 1206.

[97] Y. Qiao, Z. Hou, H. Li, Y. Hu, B. Feng, X. Wang, L. Hua, Q. Huang, *Green Chem.* **2009**, *11*, 1955.

[98] A. Lambert, P. Plucinski, I. V. Kozhevnikov, *Chem. Commun.* **2003**, 714.

[99] K. Sato, M. Aoki, M. Ogawa, T. Hashimoto, R. Noyori, *J. Org. Chem.* **1996**, *61*, 8310.

[100] D. E. de Vos, B. F. Sels, P. A. Jacobs in *Adv. Catal.*, pp. 1–87.

[101] K. Yamaguchi, C. Yoshida, S. Uchida, N. Mizuno, *J. Am. Chem. Soc.* **2005**, *127*, 530.

[102] W. Qi, Y. Wang, W. Li, L. Wu, *Chem. Eur. J.* **2010**, *16*, 1068.

[103] C. J. Münchmeyer, L. R. Graser, I. I. E. Markovits, M. Cokoja, F. E. Kühn in *Topics in Organometallic Chemistry* (Eds.: J. Dupont, L. Kollár), Springer, Berlin, Heidelberg, **2015**, pp. 185–235.

[104] B. J. Hofmann, S. Huber, R. M. Reich, M. Drees, F. E. Kühn, *J. Organomet. Chem.* **2019**, *885*, 32.

[105] I. I. E. Markovits, W. A. Eger, S. Yue, M. Cokoja, C. J. Münchmeyer, B. Zhang, M.-D. Zhou, A. Genest, J. Mink, S.-L. Zang et al., *Chem. Eur. J.* **2013**, *19*, 5972.

[106] R. J. Ellis, J. Chartres, D. K. Henderson, R. Cabot, P. R. Richardson, F. J. White, M. Schröder, J. R. Turkington, P. A. Tasker, K. C. Sole, *Chem. Eur. J.* **2012**, *18*, 7715.

[107] J. R. Turkington, V. Cocalia, K. Kendall, C. A. Morrison, P. Richardson, T. Sassi, P. A. Tasker, P. J. Bailey, K. C. Sole, *Inorg. Chem.* **2012**, *51*, 12805.

[108] M. Cokoja, I. I. E. Markovits, M. H. Anthofer, S. Poplata, A. Pöthig, D. S. Morris, P. A. Tasker, W. A. Herrmann, F. E. Kühn, J. B. Love, *Chem. Commun.* **2015**, *51*, 3399.

[109] J. Wahlen, D. E. de Vos, P. A. Jacobs, *Org. Lett.* **2003**, *5*, 1777.

[110] K. Neimann, R. Neumann, *Org. Lett.* **2000**, *2*, 2861.

[111] A. Berkessel, J. A. Adrio, *J. Am. Chem. Soc.* **2006**, *128*, 13412.

[112] O. Hollóczki, A. Berkessel, J. Mars, M. Mezger, A. Wiebe, S. R. Waldvogel, B. Kirchner, *ACS Catal.* **2017**, *7*, 1846.

[113] A. Berkessel, J. Krämer, F. Mummy, J.-M. Neudörfl, R. Haag, *Angew. Chem. Int. Ed.* **2013**, *52*, 739.

[114] D. Monti, P. Tagliatesta, G. Mancini, T. Boschi, *Angew. Chem.* **1998**, *110*, 1154.

[115] D. Monti, A. Pastorini, G. Mancini, S. Borocci, P. Tagliatesta, *J. Mol. Catal. A: Chem.* **2002**, *179*, 125.

[116] J. Heijnen, V. de Bruijn, L. van den Broeke, J. Keurentjes, *Chem. Eng. Process* **2003**, *42*, 223.

[117] P. W. N. M. van Leeuwen, M. Raynal, *Supramolecular Catalysis in Water, in: Supramolecular Catalysis in Water (S. Kubik, Ed.)*, Wiley, Weinheim, **2019**.

[118] M. Cokoja, R. M. Reich, M. E. Wilhelm, M. Kaposi, J. Schäffer, D. S. Morris, C. J. Münchmeyer, M. H. Anthofer, I. I. E. Markovits, F. E. Kühn et al., *ChemSusChem* **2016**, *9*, 1773.

[119] J. Schäffer, M. Alber, W. Korth, M. Cokoja, A. Jess, *ChemistrySelect* **2017**, *2*, 11891.

[120] Q. Q. Baltazar, J. Chandawalla, K. Sawyer, J. L. Anderson, *Colloids Surf., A* **2007**, *302*, 150.

[121] B. Zehner, F. Schmidt, W. Korth, M. Cokoja, A. Jess, *Langmuir* **2019**, *35*, 16297.

[122] S. Dorbritz, W. Ruth, U. Kragl, *Adv. Synth. Catal.* **2005**, *347*, 1273.

[123] J. Łuczak, C. Jungnickel, M. Markiewicz, J. Hupka, *J. Phys. Chem. B* **2013**, *117*, 5653.

[124] D. Bethell, R. E. Fessey, E. Namwindwa, D. W. Roberts, *J. Chem. Soc., Perkin Trans. 2* **2001**, 1489.

[125] M. Blesic, M. H. Marques, N. V. Plechkova, K. R. Seddon, L. P. N. Rebelo, A. Lopes, *Green Chem.* **2007**, *9*, 481.

[126] B. Dong, X. Zhao, L. Zheng, J. Zhang, N. Li, T. Inoue, *Colloids Surf., A* **2008**, *317*, 666.

[127] P. D. Galgano, O. A. El Seoud (Eds.) *Ionic Liquid-Based Surfactants*.

[128] F. Schmidt, B. Zehner, W. Korth, A. Jess, M. Cokoja, *Catal. Sci. Technol.* **2020**, *10*, 4448.

[129] S. A. Hauser, M. Cokoja, F. E. Kühn, *Catal. Sci. Technol.* **2013**, *3*, 552.

[130] S. Huber, M. Cokoja, F. E. Kühn, *J. Organomet. Chem.* **2014**, *751*, 25.

[131] J.-M. Brégeault, M. Vennat, L. Salles, J.-Y. Piquemal, Y. Mahha, E. Briot, P. C. Bakala, A. Atlamsani, R. Thouvenot, *J. Mol. Catal. A: Chem.* **2006**, *250*, 177.

[132] E. Alcalde, I. Dinarès, A. Ibáñez, N. Mesquida, *Molecules* **2012**, *17*, 4007.

[133] A. Cognigni, P. Gaertner, R. Zirbs, H. Peterlik, K. Prochazka, C. Schröder, K. Bica, *Phys. Chem. Chem. Phys.* **2016**, *18*, 13375.

[134] S. Friesen, T. Buchecker, A. Cognigni, K. Bica, R. Buchner, *Langmuir* **2017**, *33*, 9844.

[135] G. Mao, A. Zhu, *Iran. J. Chem. Chem. Eng.* **2013**, *32*, 77.

[136] S. de Carlo, J. R. Harris, *Micron (Oxford, England : 1993)* **2011**, *42*, 117.

[137] M. J. Deery, O. W. Howarth, K. R. Jennings, *J. Chem. Soc., Dalton Trans.* **1997**, 4783.

[138] Y.-G. Chen, J. Gong, L.-Y. Qu, *Coord. Chem. Rev.* **2004**, *248*, 245.

[139] V. Nardello, J. Marko, G. Vermeersch, J. M. Aubry, *Inorg. Chem.* **1998**, *37*, 5418.

[140] R. Stomberg, *J. Less-Common Met.* **1988**, *143*, 363.

[141] K. Sato, M. Aoki, M. Ogawa, T. Hashimoto, D. Panyella, R. Noyori, *Bull. Chem. Soc. Jpn.* **1997**, *70*, 905.

[142] P. U. Maheswari, X. Tang, R. Hage, P. Gamez, J. Reedijk, *J. Mol. Catal. A: Chem.* **2006**, *258*, 295.

[143] G. S. Kim, K. S. Hagen, C. L. Hill, *Inorg. Chem.* **1992**, *31*, 5316.

[144] P. U. Maheswari, P. de Hoog, R. Hage, P. Gamez, J. Reedijk, *Adv. Synth. Catal.* **2005**, *347*, 1759.

[145] J. Zajac, C. Chorro, M. Lindheimer, S. Partyka, *Langmuir* **1997**, *13*, 1486.

[146] A. P. Gerola, P. F. Costa, F. Nome, F. Quina, *Curr. Opin. Colloid Interface Sci.* **2017**, *32*, 48.

[147] B. Zehner, W. Korth, F. Schmidt, M. Cokoja, A. Jess, *Chem. Eng. Technol.* **2021**, *44*, 2374.

[148] F. Schmidt, B. Zehner, M. Kaposi, M. Drees, J. Mink, W. Korth, A. Jess, M. Cokoja, *Green Chem.* **2021**, *23*, 1965.

[149] W. A. Herrmann, R. W. Fischer, W. Scherer, M. U. Rauch, *Angew. Chem. Int. Ed.* **1993**, *32*, 1157.

[150] F. E. Kühn, A. M. Santos, W. A. Herrmann, *Dalton Trans.* **2005**, 2483.

[151] S. Warwel, M. R. gen. Klaas, M. Sojka, *J. Chem. Soc., Chem. Commun.* **1991**, 1578.

[152] T. Nijhuis, S. Musch, M. Makkee, J. Moulijn, *Appl. Catal., A* **2000**, *196*, 217.

[153] A. R. Toral, A. P. de los Ríos, F. J. Hernández, M. H. Janssen, R. Schoevaart, F. van Rantwijk, R. A. Sheldon, *Enzyme Microb. Technol.* **2007**, *40*, 1095.

[154] E. Sutherland, S. M. Mercer, M. Everist, D. G. Leaist, *J. Chem. Eng. Data* **2009**, *54*, 272.

[155] I. Goodchild, L. Collier, S. L. Millar, I. Prokes, J. C. D. Lord, C. P. Butts, J. Bowers, J. R. P. Webster, R. K. Heenan, *J. Colloid Interface Sci.* **2007**, *307*, 455.

[156] J. Wang, H. Wang, S. Zhang, H. Zhang, Y. Zhao, *J. Phys. Chem. B* **2007**, *111*, 6181.

[157] S. G. Ramesh, S. Re, J. Boisson, J. T. Hynes, *J. Phys. Chem. A* **2010**, *114*, 1255.

[158] M. R. Waterland, D. Stockwell, A. M. Kelley, *J. Chem. Phys.* **2001**, *114*, 6249.

[159] M. R. Whitbeck, *Appl. Spectrosc.* **1981**, *35*, 93.

[160] M. A. Czarnecki, *Appl. Spectrosc.* **2015**, *69*, 67.

[161] A. Wulf, K. Fumino, R. Ludwig, *Angew. Chem. Int. Ed.* **2010**, *49*, 449.

[162] A. M. Fernandes, M. A. A. Rocha, M. G. Freire, I. M. Marrucho, J. A. P. Coutinho, L. M. N. B. F. Santos, *J. Phys. Chem. B* **2011**, *115*, 4033.

[163] K. Nakamoto, *Infrared and Raman Spectra of Inorganic and Coordination Compounds*, John Wiley & Sons Inc., Hoboken, NJ, USA, **2008**.

[164] W. C. Oelfke, W. Gordy, *J. Chem. Phys.* **1969**, *51*, 5336.

[165] E. B. Wilson, J. C. Decius, P. C. Cross, *Molecular vibrations*. *The theory of infrared and Raman vibrational spectra*, Dover Publications, New York, NY, **1980**.

[166] J. Mink, L. M. Mink (Eds.) *Computer Program for Vibrational Analysis of Polyatomic Molecules (in Lahey-Fujitsu Fortran Win32, available from the authors)*, **2004**.

[167] Y. Zhao, D. G. Truhlar, *Theor. Chem. Acc.* **2008**, *120*, 215.

[168] S. Grimme, J. Antony, S. Ehrlich, H. Krieg, *J. Chem. Phys.* **2010**, *132*, 154104.

[169] A. V. Marenich, C. J. Cramer, D. G. Truhlar, *J. Phys. Chem. B* **2009**, *113*, 6378.

[170] A. D. McLean, G. S. Chandler, *J. Chem. Phys.* **1980**, *72*, 5639.

[171] R. Krishnan, J. S. Binkley, R. Seeger, J. A. Pople, *J. Chem. Phys.* **1980**, *72*, 650.

[172] S. L. I. Toh, J. McFarlane, C. Tsouris, D. W. DePaoli, H. Luo, S. Dai, *Solvent Extr. Ion Exch.* **2006**, *24*, 33.

[173] M. Cokoja, R. M. Reich, F. E. Kühn, *Catal. Commun.* **2017**, *100*, 103.

[174] A. Podgorsek, M. Zupan, J. Iskra, *Angew. Chem. Int. Ed.* **2009**, *48*, 8424.

[175] R. E. Mesmer, K. M. Palen, C. F. Baes Jr., *Inorg. Chem.* **1973**, 89.

[176] W. D. Nicoll, A. F. Smith, *Ind. Eng. Chem.* **1955**, *47*, 2548.

[177] M. Tariq, M. G. Freire, B. Saramago, J. A. P. Coutinho, J. N. C. Lopes, L. P. N. Rebelo, *Chem. Soc. Rev.* **2012**, *41*, 829.

[178] S. H. Ahn, K. J. Cluff, N. Bhuvanesh, J. Blümel, *Angew. Chem. Int. Ed.* **2015**, *54*, 13341.

[179] F. F. Arp, S. H. Ahn, N. Bhuvanesh, J. Blümel, *New J. Chem.* **2019**, *43*, 17174.

[180] F. F. Arp, N. Bhuvanesh, J. Blümel, *Dalton Trans.* **2019**, *48*, 14312.

[181] B. Yang, J. J. Pignatello, D. Qu, B. Xing, *Environ. Eng. Sci.* **2016**, *33*, 193.

[182] A. S. Kende, P. Delair, B. E. Blass, *Tetrahedron Lett.* **1994**, *35*, 8123.

[183] O. Naderi, R. Sadeghi, *J. Chem. Thermodyn.* **2016**, *102*, 68.

[184] B. D. Flockhart, *J. Colloid Sci.* **1957**, *12*, 557.

[185] J. Bowers, C. P. Butts, P. J. Martin, M. C. Vergara-Gutierrez, R. K. Heenan, *Langmuir* **2004**, *20*, 2191.

[186] T. Dorn, A.-C. Chamayou, C. Janiak, *New J. Chem.* **2006**, *30*, 156.

[187] A. Mori, M. Abe, M. Nojima, *J. Org. Chem.* **2001**, *66*, 3548.

[188] S. Xu, Z. Wang, Y. Li, X. Zhang, H. Wang, K. Ding, *Chem. Eur. J.* **2010**, *16*, 3021.

[189] H. Yao, D. E. Richardson, *J. Am. Chem. Soc.* **2003**, *125*, 6211.

[190] E. V. Bakhmutova-Albert, H. Yao, D. E. Denevan, D. E. Richardson, *Inorg. Chem.* **2010**, *49*, 11287.

[191] D. Swern, *Chem. Rev.* **1949**, *45*, 1.

[192] E. Santacesaria, V. Russo, R. Tesser, R. Turco, M. Di Serio, *Ind. Eng. Chem. Res.* **2017**, *56*, 12940.

[193] A. D. Becke, *J. Chem. Phys.* **1993**, *98*, 5648.

[194] Lee C., Yang W., Parr R. G., *Phys. Rev. B Condens. Matter* **1988**, *37*, 785.

[195] S. H. Vosko, L. Wilk, M. Nusair, *Can. J. Phys.* **1980**, *58*, 1200.

[196] P. J. Stephens, F. J. Devlin, C. F. Chabalowski, M. J. Frisch, *J. Phys. Chem.* **1994**, *98*, 11623.

[197] W. D. Kumler, J. J. Eiler, *J. Am. Chem. Soc.* **1943**, *65*, 2355.

[198] T. Mutai, Y. Abe, K. Araki, *J. Chem. Soc., Perkin Trans. 2* **1997**, 1805.

[199] W. Zhang, J. L. Loebach, S. R. Wilson, E. N. Jacobsen, *J. Am. Chem. Soc.* **1990**, *112*, 2801.

[200] E. N. Jacobsen, W. Zhang, A. R. Muci, J. R. Ecker, L. Deng, *J. Am. Chem. Soc.* **1991**, *113*, 7063.

[201] Z.-X. Wang, Y. Tu, M. Frohn, J.-R. Zhang, Y. Shi, *J. Am. Chem. Soc.* **1997**, *119*, 11224.

[202] Y. Tu, Z.-X. Wang, Y. Shi, *J. Am. Chem. Soc.* **1996**, *118*, 9806.

[203] T. Katsuki, K. B. Sharpless, *J. Am. Chem. Soc.* **1980**, *102*, 5974.

[204] Y. Gao, J. M. Klunder, R. M. Hanson, H. Masamune, S. Y. Ko, K. B. Sharpless, *J. Am. Chem. Soc.* **1987**, *109*, 5765.

[205] R. V. Ottenbacher, K. P. Bryliakov, E. P. Talsi, *Adv. Synth. Catal.* **2011**, *353*, 885.

[206] I. Garcia-Bosch, L. Gómez, A. Polo, X. Ribas, M. Costas, *Adv. Synth. Catal.* **2012**, *354*, 65.

[207] O. Cussó, I. Garcia-Bosch, D. Font, X. Ribas, J. Lloret-Fillol, M. Costas, *Org. Lett.* **2013**, *15*, 6158.

[208] J. Heijnen, V. de Bruijn, L. van den Broeke, J. Keurentjes, *Chem. Eng. Process.* **2003**, *42*, 223.

[209] T. Omagari, A. Suzuki, M. Akita, M. Yoshizawa, *J. Am. Chem. Soc.* **2016**, *138*, 499.

[210] D. Parmar, E. Sugiono, S. Raja, M. Rueping, *Chem. Rev.* **2014**, *114*, 9047.

[211] D. Yang, *Acc. Chem. Res.* **2004**, *37*, 497.

[212] H. Hussain, I. R. Green, I. Ahmed, *Chem. Rev.* **2013**, *113*, 3329.

[213] Jan Berger, *Master's Thesis*, Technische Universität München, **2018**.

[214] Y. Marcus, *Ion properties*, M. Dekker, New York, Basel, Hong Kong, **1997**.

[215] K. Nakamura, S. Nishiyama, S. Tsuruya, M. Masai, *J. Mol. Catal.* **1994**, *93*, 195.

[216] D. Jagleniec, Ł. Dobrzycki, M. Karbarz, J. Romański, *Chem. Sci.* **2019**, *10*, 9542.

[217] S. Poplata, *Master's Thesis*, Technische Universität München, **2014**.

[218] J. M. Monger, O. Redlich, *J. Phys. Chem.* **1956**, *60*, 797.

[219] B. Klimas, *Master's Thesis*, Technische Universität München, **2016**.

[220] R. A. Aitken, S. Arumugam, S. T. E. Mesher, F. G. Riddell, *J. Chem. Soc., Perkin Trans. 2* **2002**, 225.

[221] R. Bloch, J. Abecassis, D. Hassan, *J. Org. Chem.* **1985**, *50*, 1544.

[222] W. Zhu, W. T. Ford, *J. Org. Chem.* **1991**, *56*, 7022.

[223] Q. Jochyms, E. Mignard, J.-M. Vincent, *J. Fluorine Chem.* **2015**, *177*, 11.

[224] R. P. Matthews, T. Welton, P. A. Hunt, *Phys. Chem. Chem. Phys.* **2015**, *17*, 14437.

[225] X. Zhang, *Electrostatic Supra-Amphiphiles, in: Supramolecular Amphiphiles*, Royal Society of Chemistry, Cambridge, **2017**.

[226] R. M. Reich, M. Cokoja, I. I. E. Markovits, C. J. Münchmeyer, M. Kaposi, A. Pöthig, W. A. Herrmann, F. E. Kühn, *Dalton Trans.* **2015**, *44*, 8669.

[227] O. V. Evdokimova, N. V. Pechishcheva, K. Y. Shunyaev, *J. Anal. Chem.* **2012**, *67*, 741.

[228] R. Noyori, M. Aoki, K. Sato, *Chem. Commun.* **2003**, 1977.

[229] G. R. Fulmer, A. J. M. Miller, N. H. Sherden, H. E. Gottlieb, A. Nudelman, B. M. Stoltz, J. E. Bercaw, K. I. Goldberg, *Organometallics* **2010**, *29*, 2176.

[230] APEX suite for crystallographic software, APEX 3 Version 2015-5.2, Bruker AXS Inc., Madison, Wisconsin, USA, **2015**.

[231] SAINT Version 8.34A, Bruker AXS Inc., Madison, Wisconsin, USA, **2014**.

[232] SADABS Version 2014/5, Bruker AXS Inc., Madison, Wisconsin, USA, **2014**.

[233] G. M. Sheldrick, *Acta Crystallogr., Sect. A: Found. Crystallogr.* **2015**, *71*, 3.

[234] G. M. Sheldrick, *Acta Crystallogr., Sect. C: Cryst. Struct. Commun.* **2015**, *71*, 3.

[235] O. V. Dolomanov, L. J. Bourhis, R. J. Gildea, J. A. K. Howard, H. Puschmann, *J. Appl. Crystallogr.* **2009**, *42*, 339.

[236] K. Momma, F. Izumi, *J. Appl. Crystallogr.* **2011**, *44*, 1272.

[237] M. Lee, U. H. Choi, S. Wi, C. Slebodnick, R. H. Colby, H. W. Gibson, *J. Mater. Chem.* **2011**, *21*, 12280.

[238] J. Dhineshkumar, K. R. Prabhu, *Org. Lett.* **2013**, *15*, 6062.

[239] T. Dorn, A.-C. Chamayou, C. Janiak, *New J. Chem.* **2006**, *30*, 156.

[240] Y. Ha, J. D. Emery, M. J. Bedzyk, H. Usta, A. Facchetti, T. J. Marks, *J. Am. Chem. Soc.* **2011**, *133*, 10239.

[241] G. Keglevich, A. Grün, A. Bölcskei, L. Drahos, M. Kraszni, G. T. Balogh, *Heteroat. Chem.* **2012**, *23*, 574.

[242] X. Tang, Q. Zhong, J. Xu, H. Li, S. Xu, X. Cui, B. Wei, Y. Ma, R. Yuan, *Inorg. Chim. Acta* **2016**, *442*, 195.

[243] S.-Y. Wu, J. E. Casida, *Phosphorus, Sulfur Relat. Elem.* **1995**, *102*, 177.

7 List of Publications and Conference Contributions

7.1 Publications as First Author

1) **F. Schmidt**, B. Zehner, W. Korth, A. Jess, M. Cokoja, Ionic liquid surfactants as multitasking micellar catalysts for epoxidations in water, *Catal. Sci. Technol.* **2020**, *10*, 4448-4457.
2) **F. Schmidt** and M. Cokoja, Supramolecular concepts for the biphasic epoxidation of olefins using aqueous hydrogen peroxide, *Green Chem.* **2021**, *23*, 708-722.
3) **F. Schmidt**, B. Zehner, M. Kaposi, M. Drees, J. Mink, W. Korth, A. Jess, M. Cokoja, Activation of hydrogen peroxide by the nitrate anion in micellar media, *Green Chem.* **2021**, *23*, 1965-1971.

7.2 Contributions as Co-Author in the Frame of the Project

1) B. Zehner, **F. Schmidt**, W. Korth, M. Cokoja and A. Jess, Determination of the Critical Micelle Concentration of Imidazolium Ionic Liquids in Aqueous Hydrogen Peroxide, *Langmuir* **2019**, *35*, 16297–16303.
2) B. Zehner, W. Korth, **F. Schmidt**, M. Cokoja and A. Jess, Kinetics of Epoxidation of Cyclooctene with Ionic Liquids Containing Tungstate as Micellar Catalyst, *Chem. Eng. Technol.* **2021**, *44*, 2374-2381.

7.3 Conference Contributions

1) **F. Schmidt**, B. Zehner, W. Korth, A. Jess, M. Cokoja, Epoxidation of Cyclooctene using Imidazolium Nitrate Catalysts in aqueous Hydrogen Peroxide, 21st International Symposium of Homogeneous Catalysis, Amsterdam, 08.-13. July 2018.
2) **F. Schmidt**, B. Zehner, W. Korth, A. Jess, M. Cokoja, Epoxidation of olefins using surface-active imidazolium tungstates, 52. Katalytikertreffen, Weimar, 13.-15. March 2019.
3) **F. Schmidt**, B. Zehner, W. Korth, A. Jess, M. Cokoja, Micellar approaches towards mild biphasic catalytic epoxidation of olefins with hydrogen peroxide, ACS Fall 2019 National Meeting, San Diego (USA), 25.-29. August 2019.

7.4 Summer and Winter School Participations

1) Winter School '*Innovative Catalysis and Sustainability'*, Bardonecchia (Italy), January 2018.
2) EFCATS Sommer School '*Engineering Materials for Catalysis'*, Portoroz (Slovenia), September 2020.

8 Eidesstattliche Erklärung

Ich Fabian Schmidt erkläre des Eides statt, dass ich die bei der promotionsführenden Einrichtung Fakultät für Chemie der TUM zur Promotionsprüfung vorgelegten Arbeit mit dem Titel:

Design of Supramolecular Nanocatalysts for the Biphasic Epoxidation of Olefins

am Lehrstuhl für Anorganische und Metallorganische Chemie unter Anleitung und Betreuung durch Prof. Dr. Roland A. Fischer ohne sonstige Hilfe erstellt und bei der Abfassung nur die gemäß §6 Ab. 6 und 7 PromO angebotenen Hilfsmittel benutzt habe.

Ich habe keine Organisation eingeschaltet, die gegen Entgelt Betreuerinnen und Betreuer für die Anfertigung von Dissertationen sucht, oder die mir obliegenden Pflichten hinsichtlich der Prüfungsleistungen für mich ganz oder teilweise erledigt.

Ich habe die Dissertation in dieser oder ähnlicher Form in keinem anderen Prüfungsverfahren als Prüfungsleistung vorgelegt.

Ich habe den angestrebten Doktorgrad noch nicht erworben und bin nicht in einem früheren Promotionsverfahren für den angestrebten Doktorgrad endgültig gescheitert.

Ich habe keine Kenntnis über ein strafrechtliches Ermittlungsverfahren in Bezug auf wissenschaftsbezogene Straftaten gegen mich oder eine rechtskräftige strafrechtliche Verurteilung mit Wissenschaftsbezug.

Die öffentlich zugängliche Promotionsordnung sowie die Richtlinien zur Sicherung guter wissenschaftlicher Praxis und für den Umgang mit wissenschaftlichem Fehlverhalten der TUM sind mir bekannt, insbesondere habe ich die Bedeutung von § 27 PromO (Nichtigkeit der Promotion) und § 28 PromO (Entzug des Doktorgrades) zur Kenntnis genommen. Ich bin mir der Konsequenzen einer falschen Eidesstattlichen Erklärung bewusst.